ACTIVATION OF JNK1β1 BY PHOSPHORYLATION: IMPLICATIONS FOR ITS FUNCTION, STABILITY, AND DYNAMICS

Gavin Ray Owen

A thesis submitted to the Faculty of Science, University of the Witwatersrand, Johannesburg in fulfilment of the requirements for the degree of Doctor of Philosophy

October 2014

DECLARATION

I, Gavin Ray Owen (Student number: 0705702K), am a student registered for the degree of Doctor of Philosophy (PhD) in the academic year 2014.

I hereby declare the following:

- I am aware that plagiarism (the use of someone else's work without their permission and/or without acknowledging the original source) is wrong.
- I confirm that the work submitted for assessment for the above degree is my own unaided work except where explicitly indicated otherwise.
- I have followed the required conventions in referencing the thoughts and ideas of others.
- I understand that the University of the Witwatersrand may take disciplinary action against me if there is a belief that this is not my own unaided work or that I have failed to acknowledge the source of the ideas or words in my writing.

Gavin Ray Owen

28 October 2014

Supervisor: Prof. Heini W. Dirr

Co-supervisor: Dr Ikechukwu A. Achilonu

– To my family and friends –

“It is what you learn after you know it all that counts.”

~ John Wooden

ABSTRACT

The c-Jun N-terminal kinases (JNKs) are mitogen-activated protein kinases (MAPKs) that are activated by the dual phosphorylation of a canonical threonine and tyrosine residue. While it is well known that the activation of JNK mediates many important cellular processes such as differentiation, proliferation, and apoptosis, the mechanisms by which phosphorylation induces its activation are not known. An understanding of the structural and biophysical basis for the activation of JNK is highly desirable however, as dysregulation of the kinase has been implicated in numerous prominent diseases. Aiming first to improve upon the previously reported inadequacies in acquiring active JNK, this work describes a novel method for the purification of large yields of pure and phosphorylated JNK1β1, the most abundant JNK isoform. Using codon harmonization as a precautionary measure toward increasing the soluble overexpression of the kinase raised unique questions about the role of translation kinetics in both the heterologous and natural co-translational modification of kinases. After purifying the upstream activating kinases of JNK, phosphorylation of JNK1β1 was achieved by reconstituting the MEKK1 → MKK4 → JNK MAPK activation cascade *in vitro*. Activated JNK1β1 was thereafter able to phosphorylate its substrate, ATF2, with high catalytic efficiency. Characterising the nature of JNK1β1 modification by MKK4, mass spectrometry revealed that the latter kinase phosphorylates JNK1β1 not only at its activation residues (T183 and Y185), but also at a recognised yet uncharacterised phospho-site (S377) as well as two novel phospho-residues (T228 and S284) whose phosphorylation appear to have functional significance. Unfolding studies and amide hydrogen-deuterium exchange (HX) mass spectrometry (MS) were then used to investigate the changes to the stability and structure/conformational dynamics of JNK1β1 induced by phosphorylation and nucleotide substrate binding. Increased flexibility detected at the hinge between the N- and C-terminal domains upon phosphorylation suggested that activation may require interdomain closure. Patterns of solvent protection by the ATP analogue, AMP-PNP, reflected a novel mode of nucleotide binding to the C-terminal domain of a destabilised and open domain conformation of inactive JNK1β1. HX protection at both domains following AMP-PNP binding to active JNK1β1 revealed that the domains close around nucleotide upon phosphorylation, simultaneously stabilising the kinase. This reveals that phosphorylation activates JNK1β1 in part by enhancing the flexibility of the hinge to enable interdomain closure and the formation of a functional active site. This work thus offers novel insight into the unique molecular mechanisms by which JNK1β1 is regulated by nucleotide binding and phosphorylation by MKK4, and by the complex interplay that exists between them.

RESEARCH OUTPUTS

ORIGINAL PUBLICATIONS

Publications forming part of PhD thesis

Owen, G. R., Achilonu, I. and Dirr, H. W. (2013) High yield purification of JNK1β1 and activation by *in vitro* reconstitution of the MEKK1 → MKK4 → JNK MAPK phosphorylation cascade, *Protein Expr Purif 87*, 87-99.

Owen, G. R., Stoychev, S., Achilonu, I. and Dirr, H. W. (2013) JNK1β1 is phosphorylated during expression in *E. coli* and *in vitro* by MKK4 at three identical novel sites, *Biochem Biophys Res Commun 432*, 638-688.

Owen, G. R., Stoychev, S., Achilonu, I. and Dirr, H. W. (2014) Phosphorylation- and nucleotide-binding-induced changes to the stability and hydrogen exchange patterns of JNK1β1 provide insight into its mechanisms of activation, *J Mol Biol 426*, 3569-3589.

Other publications

Owen, G. R. and Brenner, E. A. (2012) Mapping molecular memory: navigating the cellular pathways of learning, *Cell Mol Neurobiol 32*, 919-941.

CONFERENCE PRESENTATIONS

2nd Molecular Biosciences Research Thrust research day 2011

Poster presentation

Title: Phosphorylation of JNK1 by a constitutively active phosphomimetic form of its upstream kinase MKK4

Authors: Gavin R. Owen, Ikechukwu Achilonu, Heini W. Dirr

23rd South African Society for Biochemistry and Molecular Biology conference 2012

Poster presentation

Title: Over-expression and purification of codon harmonised c-Jun N-terminal Kinase 1

Authors: Gavin R. Owen, Ikechukwu Achilonu, Heini W. Dirr

3rd South African Proteomics Symposium 2012

Oral presentation

Title: Activation of JNK1 by *in vitro* reconstitution of the MEKK1 → MKK4 → JNK MAPK phosphorylation cascade

Authors: Gavin R. Owen, Ikechukwu Achilonu, Heini W. Dirr

University of the Witwatersrand 4th Cross-Faculty Postgraduate Symposium 2012

Poster presentation

Title: Purification of JNK1β1 and activation by *in vitro* reconstitution of the MEKK1 → MKK4 → JNK phosphorylation cascade

Authors: Gavin R. Owen, Ikechukwu Achilonu, Heini W. Dirr

3rd Molecular Biosciences Research Thrust research day 2012

Poster presentation

Title: Purification of JNK1β1 and activation by *in vitro* reconstitution of the MEKK1 → MKK4 → JNK phosphorylation cascade

Authors: Gavin R. Owen, Ikechukwu Achilonu, Heini W. Dirr

Awarded: 2nd Prize Poster Presentation

27th Annual Symposium of the Protein Society 2013

Poster presentation

Title: JNK1β1 is phosphorylated at three novel sites upon activation by *in vitro* reconstitution of the MEKK1 → MKK4 → JNK phosphorylation cascade

Authors: Gavin R. Owen, Ikechukwu Achilonu, Heini W. Dirr

University of the Witwatersrand 5th Cross-Faculty Postgraduate Symposium 2013

Oral presentation

Title: JNK1β1 is phosphorylated at three novel sites upon activation by *in vitro* reconstitution of the MEKK1 → MKK4 → JNK phosphorylation cascade

Authors: Gavin R. Owen, Ikechukwu Achilonu, Heini W. Dirr

4th Molecular Biosciences Research Thrust research day 2013

Poster presentation

Title: JNK1β1 is phosphorylated at three novel sites upon activation by *in vitro* reconstitution of the MEKK1 → MKK4 → JNK phosphorylation cascade

Authors: Gavin R. Owen, Ikechukwu Achilonu, Heini W. Dirr

ACKNOWLEDGEMENTS

To my supervisors, Professor Heini Dirr and Doctor Ikechukwu Achilonu, thank you for your support, guidance, and faith throughout my postgraduate career. Your passion, dedication, and expertise could not have provided me with more inspiration. It has been an honour to work with and learn from you.

To my friends and colleagues that I have had the privilege to work alongside at the Protein Structure-Function Research Unit over all the years, thank you for the many laughs, invaluable help, and stimulating discussions. It has been a pleasure.

To Nishal Parbhoo and David Balchin, a special thank you for not only your friendships, but for your tireless assistance with many of the practical and theoretical aspects of this work. I appreciate all of your time and effort.

I am also immensely grateful to Prof. Heini Dirr, the University of the Witwatersrand, and the South African National Research Foundation for their generous financial support that has enabled both my studies and this research.

And lastly, to my close friends and family, it is difficult to express the proper amount of thanks and appreciation owed to you all, but you know not how your love has sustained me – Thank you.

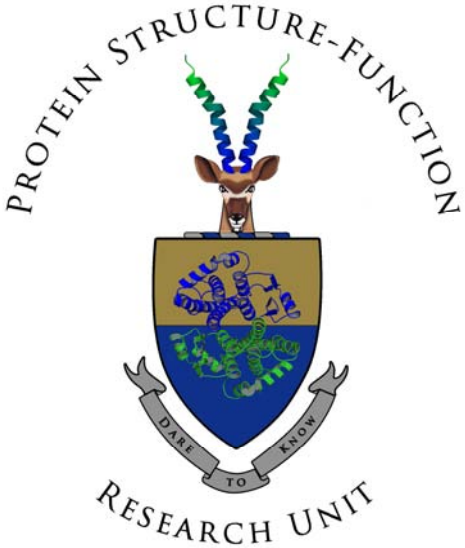

TABLE OF CONTENTS

LIST OF ABBREVIATIONS

ADP	adenosine diphosphate
AMP-PNP	adenosine 5′-(β,γ-imido)triphosphate
AP-1	activator protein-1
ATF2	activating transcription factor 2
ATP	adenosine triphosphate
cAMP	3′-5′-cyclic adenosine monophosphate
ERK	extracellular signal-regulated kinase
GST	glutathione transferase
HX	hydrogen-deuterium exchange
JNK	c-Jun N-terminal protein kinase gene
JNK	c-Jun N-terminal protein kinase protein
MAPK	mitogen-activated protein kinase
MEKK	mitogen-activated ERK-regulating kinase kinase
MKK	mitogen-activated protein kinase kinase
MS	mass spectrometry
PKA	cAMP-dependent protein kinase
UV	ultraviolet

The IUPAC-IUBMB one- and three-letter abbreviations for the 20 standard amino acids were used throughout.

LIST OF FIGURES

CHAPTER 1

INTRODUCTION

Cells respond to external stimuli and variations in the chemical and physical properties of their environment. These responses are induced partly by the cooperation of many intracellular signalling pathways that serve to transmit, integrate, and amplify a variety of signals, resulting finally in alterations in genomic and physiological activity. The mitogen-activated protein kinase signalling cascade is one of the major pathways that relay extracellular signals into cells, and like most signalling pathways, employ protein phosphorylation as its means of signal propagation.

1.1. Protein phosphorylation

Protein phosphorylation is the addition of a phosphate group (PO_4^{2-}) to a protein, a modification that elicits a change in the activity of the target protein by modifying enzyme function, interaction with other proteins, or cellular location [1]. Protein phosphorylation is enzymatically catalysed by protein kinases, a diverse range of enzymes that are employed widely to transduce signals and mediate complex cellular processes. These enzymes transfer a single phosphoryl group from a nucleoside triphosphate (commonly the γ-phosphate of ATP or GTP) and covalently attach it to the free hydroxyl group of one of three amino acids (Figure 1). Many kinases act upon both serine and threonine residues, others act on the phenolic group of tyrosine, and many others act on all three (dual-specificity kinases) [2,3].

Protein phosphorylation and dephosphorylation are regarded as two of the most significant post-translational protein modifications since they play roles in the regulation of nearly all cellular systems, and are the major intracellular mechanisms by which cells respond to extracellular stimuli [4]. Intermediary metabolism, DNA transcription and replication, RNA splicing, trafficking of organelles, cell cycle control, and cell differentiation are just a few of the numerous biological processes controlled by protein phosphorylation [5]. It has been proposed that up to 30% of all human proteins are subject to reversible phosphorylation, mediated by the at least 518 different kinases that have been identified in humans by cataloguing the protein kinase complement of the genome using genomic, complementary DNA, and expressed sequence tag sequences [6,7].

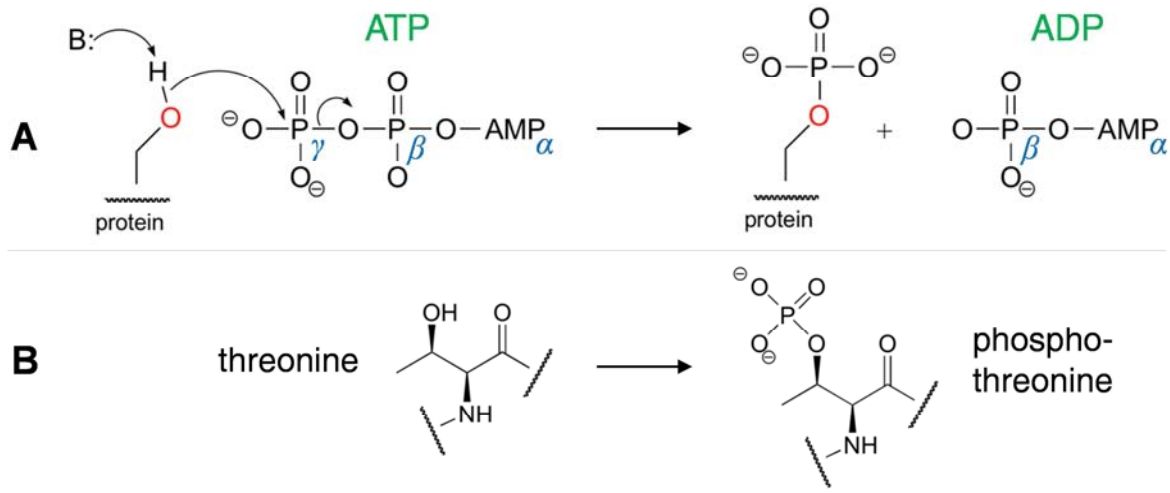

Figure 1. Generic protein phosphorylation reaction. (A) Kinases catalyse the transfer of the gamma-phosphate of ATP to the hydroxyl group of specific serine, threonine, or tyrosine residues of their protein substrates, producing a phospho-residue and ADP. An example of the chemistry that can take place during phospho-transfer is indicated. (B) Threonine is used as an example of the resulting phospho-residue, illustrating that since the phosphorylation reaction does not involve any bonds to the two carbon stereocenters, the stereochemical configuration of the residue does not change.

Reversible phosphorylation of proteins is therefore a critical regulatory mechanism during signal transduction in both prokaryotes and eukaryotes, where its ready reversibility makes it ideal for the controlled and rapid responses required in the internal cellular response pathways [8].

As protein kinases have significant effects on the functioning of a cell, their functioning is highly controlled. Not only are they themselves activated or deactivated through phosphorylation (which may be performed by the kinase itself through *cis*-phosphorylation/ autophosphorylation), but also by interacting with regulatory proteins, or by controlling their location within the cell relative to their target molecules [8-10]. Their enormous diversity and the fact that almost every known signalling pathway eventually impinges on a protein kinase, also makes them potentially important targets for therapeutic drugs. Kinases are thus avidly studied for their ability to control the many phosphorylation-dependant processes, whose dysfunction may cause an extensive array of diseases ranging from cancer to diabetes [11].

1.2. The mitogen-activated protein kinases

The mitogen activated protein kinases (MAPK) are an important group of enzymes conserved in fungi, plants and mammals that regulate cell proliferation in response to mitogen signalling [12,13]. The MAPK pathway involves a tiered cascade containing at least three protein kinases in series. Specific stimuli trigger the activation of MAPK kinase kinases (MAP3Ks),

which then phosphorylate and activate the downstream MAPK kinases (MAP2Ks), which in turn phosphorylate and activate MAPKs (Figure 2) [12]. These MAPKs have been shown to control gene expression by catalysing the phosphorylative activation of several transcription factors [14]. In mammals there are three main subfamilies of MAPK classified according to their sequence homology. These include the kinases of the extracellular signal-regulated kinase (ERK) subfamily that mediate all signalling pathways initiated by polypeptide mitogens, and the stress-activated protein kinases of p38 and c-Jun N-terminal kinase (JNK) [5]. JNK and p38 therefore mediate the central pathways activated in response to inflammatory cytokines and extra-cellular environmental stresses such as UV irradiation, heat and osmotic shock, and the deprivation of growth factors [12].

The members of all three families are serine/threonine-specific kinases that require dual phosphorylation for full activation, entailing the addition of a phosphate to both the well-conserved threonine residue located in the activation lip of all kinases, as well as on a tyrosine residue conserved in all MAP kinases [10]. These sites conform to the consensus tripeptide sequence Thr-X-Tyr, where X corresponds to Glu, Gly, and Pro, in ERK, JNK and p38 respectively [10].

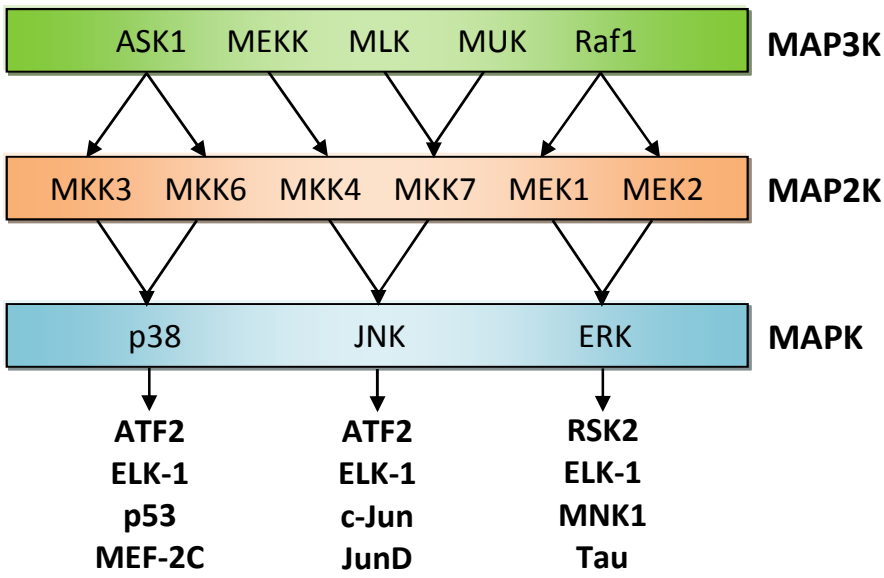

Figure 2. Mitogen- and stress-activated MAPK signalling pathways. The MAPKs are activated by dual phosphorylation on Thr and Tyr residues of the tripeptide motif (Thr-X-Tyr), induced by members of the MAP2K group of protein kinases. Upstream, a group of MAP3Ks mediate the activation of the MAP2Ks through phosphorylation. Signalling is thus activated through the sequential actions of a MAP3K, a MAP2K, and a MAPK (Adapted from [15]).

1.3. c-Jun N-terminal kinase

The JNK signalling cascade constitutes one class of MAP kinases that is activated mainly by exposure to cytokines (e.g., tumour necrosis factor and interleukin-1), growth factors, UV radiation, and other environmental stress stimuli (for a review see [16]). JNK is activated directly by the MAP2Ks of MKK4 and MKK7, dual specificity protein kinases that are each able to phosphorylate JNK at both of its activating Thr and Tyr residues (Figure 3) [17].

There are three JNK genes in mammals, namely *JNK1*, *JNK2*, and *JNK3* located on three different chromosomes [18]. JNK1 and JNK2 are ubiquitously expressed, whereas the expression of JNK3 is limited predominantly to the neurons of the central nervous system and to a lesser extent to cardiac muscle and the testes [13]. As they are MAPKs, the three JNK forms contain all 12 conserved protein kinase subdomains (section 1.3.1). However, structural complexity is added to the JNK forms through differential splicing of the three *JNK* genes. This results in the generation of ten distinct JNK isoforms ranging from 46-55 kDa, splicing products essentially with or without an N- and C-terminal extension (Figure 4) [14]. *JNK1* and *JNK2* undergo further alternative splicing, resulting from the selection for one of two specific exons encoding the amino acids located between subdomain IX and X (Figure 4) [14]. The Thr-Pro-Tyr motif situated within the activation lip of protein kinase subdomain VIII is the defining amino acid sequence for all ten JNK variants, the phosphorylation of which induces their activation [5].

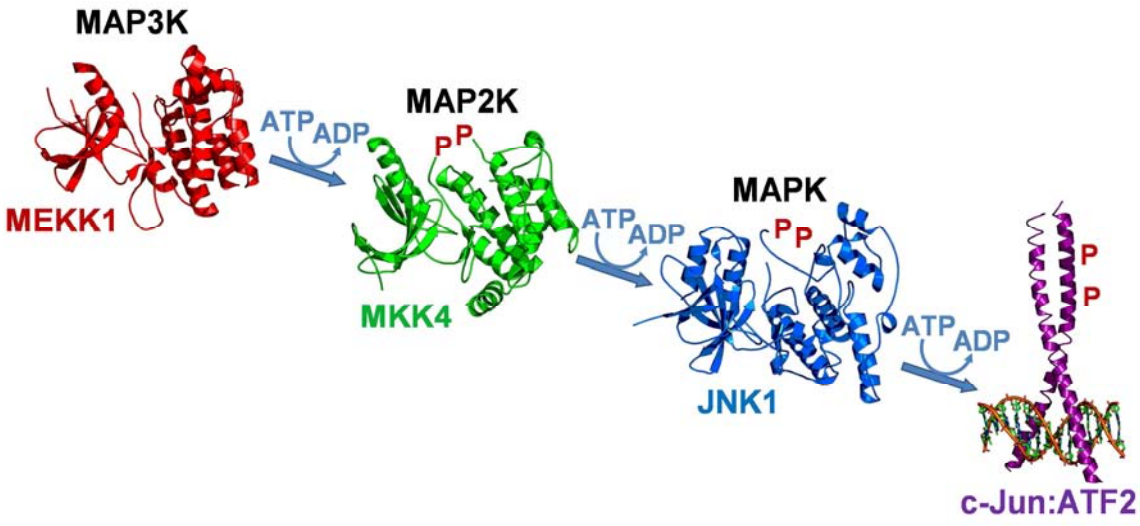

Figure 3. The JNK MAPK phosphorylative activation cascade. An example of the signalling cascade that leads to the phosphorylation and activation of JNK and its subsequent activation of downstream transcription factors. Here, the sequential actions of active MEKK1 (a MAP3K, in red) and MKK4 (a MAP2K, in green) activates JNK (blue).

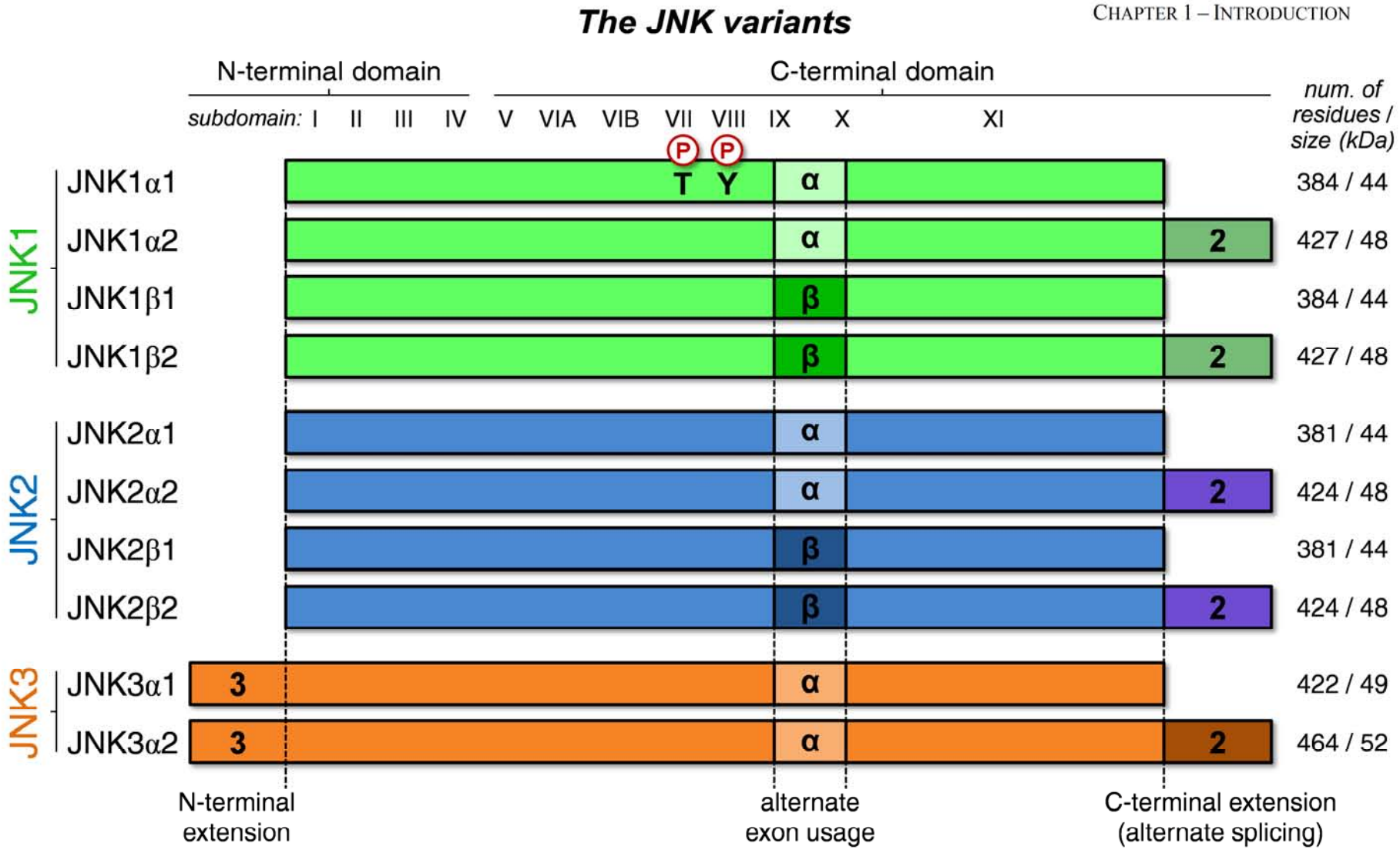

Figure 4. Comparison of the structural features of the JNK isoforms. The JNK group of MAPKs possess all 11 conserved protein kinase subdomains, the relative positions of which are indicated by I – XI. The activation lip is situated between domains VII and VIII, a region containing the threonine (T) and tyrosine (Y) residues that must be phosphorylated (P) for complete activation of the kinase. Alternative splicing of the three JNK genes (JNK1 – green, JNK2 – blue, JNK3 – orange) result in the production of ten different isoforms of JNK, whose differences are indicated by the relevant symbols and alternately coloured rectangles. The segment between subdomains IX and X constitutes one splicing site of the JNK1 and JNK2 genes, the resulting splice forms of which show altered substrate specificity, while another alternative splicing site occurs at the C-terminus of the protein. This site facilitates the production of protein isoforms differing in length by 42 or 43 amino acids (where the total number of amino acids in each isoform is indicated) so that each short isoform has a longer counterpart.

Although the significance of these distinct variants are yet to be fully understood, the ten alternative JNK isoforms can be differentially activated and possess varying affinities for Elk-1, ATF2, and c-Jun transcription factors [19], implying that the individual members may selectively and temporally target specific transcription factors within the cell. The various JNK isoforms therefore have specific and differential functions in the different cell types of multicellular organisms, which have been found to include gene expression, apoptosis, and metabolism (reviewed in [20]). JNK thus acts as a multifunctional kinase implicated in many critical physiological and pathological processes, playing its largest role in apoptosis and several cell death processes [13,16]. Consequently, the JNK pathway has been connected to the survival and/or death responses of cells to extra-cellular stimuli, as well as to many developmental processes and oncogenic transformation [21].

With respect to how it participates in these events, JNK was named as such because it was initially found to phosphorylate the Ser63 and Ser73 residues of the N-terminal domain of c-Jun, thereby enhancing its ability to activate the expression of its associated genes [22]. Nevertheless, JNK is also able to modify a number of substrates that include a variety of non-nuclear proteins and other transcription factors such as JunD, c-Fos, and ATF2 [23]. In association with c-Jun, these transcription factors form heterodimers to become activator protein-1 (AP-1) that mediates and controls the expression of numerous stress-receptive genes [19]. JNK however does not only mediate apoptosis through its influence on gene transcription, but additionally through transcriptional-independent mechanisms. It has been shown that JNK is able to modify both anti- and pro-apoptotic elements (e.g. Bcl-2 or Bcl-xL, and Bim or Bmf, respectively) and regulate their activity [13,15].

Therefore, due to the involvement of JNK in the many developmental activities and the survival/death responses of cells, as well as its corresponding implication in numerous related diseases upon its dysfunction, the JNK signalling cascade has recently become a significant focus of attention. These diseases include neurological disorders such as Parkinson's disease and amyotrophic lateral sclerosis, in addition to different tauopathies comprising Alzheimer's disease, Pick's disease and familial frontotemporal dementia [13,24-28]. The JNK signalling pathway also plays additional pathological roles in disorders such as type 2 diabetes, heart disease, cancer, and inflammatory diseases [19,29-31]. Knowledge about the biophysical basis of the activation of JNK is therefore highly desirable, and may facilitate the discovery of drugs that may interfere or enhance the functioning of the kinase.

1.3.1. Structure of JNK

Comparing the amino acid sequences and the X-ray crystallographic models of the more than 30 different protein kinases (including MAPKs) whose structures have been elucidated reveals that they display a common globular kinase fold comprising an N-terminal domain of ~85 amino acids that is mostly β-sheet in structure, and a larger C-terminal domain of ~170 amino acids that comprises mainly α-helices (as represented by the structure of JNK3 in Figure 5) (reviewed in [12]). The common globular fold, called the kinase domain, is also typically subdivided into 12 subdomains based on conserved motifs involved in ATP and peptide substrate binding, and are identified using the nomenclature I–XI [10]. The two terminal domains are connected by a small linker region that generates a binding pocket for ATP and the protein substrate (Figure 5). The adenine ring of ATP is deeply buried within the active site cleft that exists at the interface between the two domains, while the γ-phosphate group of the nucleotide is directed toward the periphery of the catalytic cleft where other protein substrates bind [10,12].

With respect to JNK specifically, the overall architecture of JNK1, 2 and 3 are highly equivalent to each other as a result of the high homology of their sequences, having 92% identity [32]. Their overall fold is typical of the monomeric protein kinases described, consisting of two domains with an active site cleft (Figure 5). The N-terminal domain of the JNKs (subdomains I-IV) contains seven β-strands and two α-helices, and assists in the binding and positioning of ATP [33]. Their C-terminal domain (subdomains VIA-XI) comprises a bundle of seven α-helices, five short 3_{10} helices and three β-strands (Figure 5), and is involved in recognition of the protein substrate and anchoring the phosphates of ATP [33]. The N-terminal domain is linked to the C-terminal domain by two loops; the first is located between β7 and β8 (a loop referred to as the hinge as it has been shown to act as the pivot point for interdomain movements), while the other is a long connector of α13 to α14 [33]. A deep cleft between the N- and C-terminal domains constitutes the nucleotide-binding site and active site, where the “glycine-rich phosphate anchor flap” (a consensus glycine-rich sequence found within all protein kinases) of the JNKs form a well-defined β-strand–turn–β-strand flap structure that covers the nucleotide almost completely (Figure 5) [32]. The phosphorylation or activation lip exists within the C-terminal, a region containing the JNK regulatory phosphorylation sites of Thr183 and Tyr185 (Figure 5) [32].

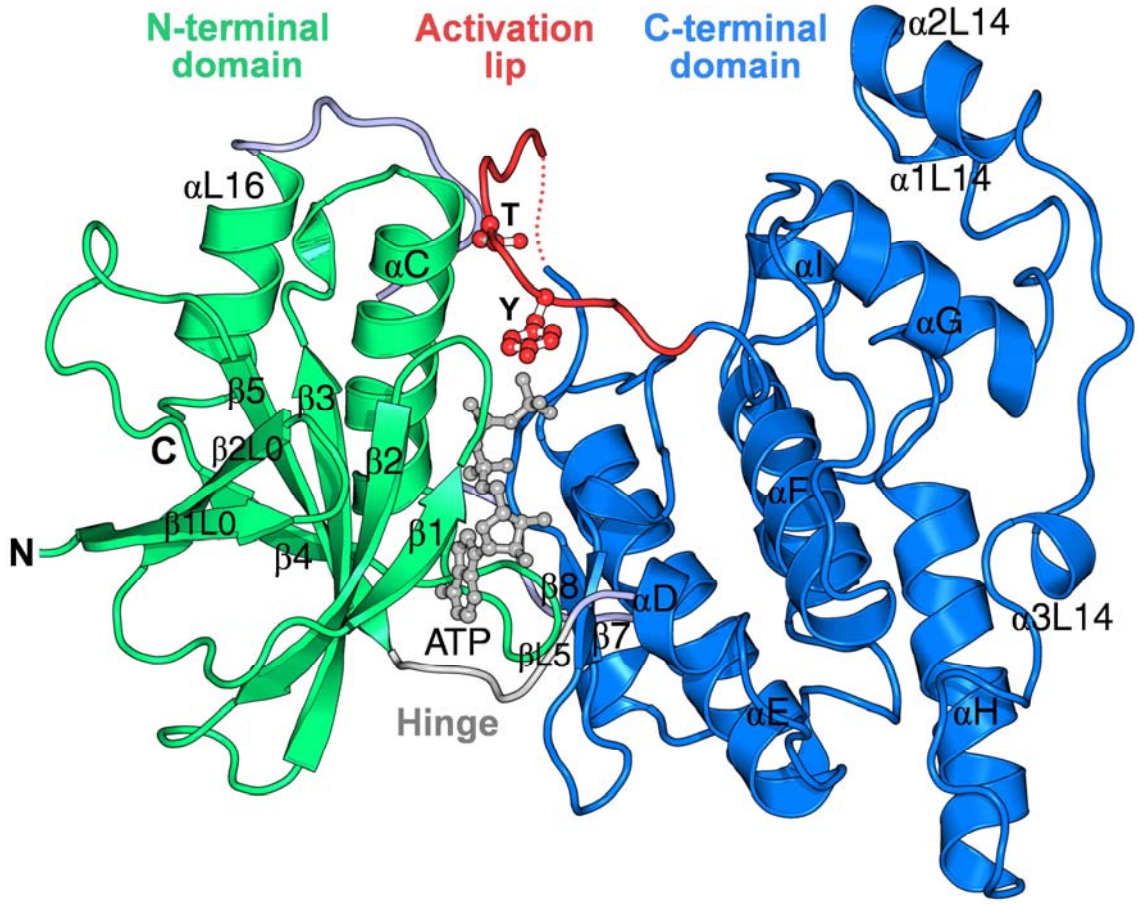

Figure 5. JNK3 crystal structure. A ribbon diagram demonstrates the three-dimensional crystal structure of the inactive (non-phosphorylated) form of JNK3, with the secondary-structure elements labelled as previously described by Zhang et al [34]. AMP-PNP (grey ball-and-stick model) is bound within the active site cleft created between the N-terminal (green) and C-terminal (blue) domains. The "hinge" domain linker is presented in grey. The two canonical phosphorylatable residues of JNK3, Thr221 and Tyr223 (Thr183 and Tyr185 in JNK1) are shown in the activation lip (red) as ball-and-stick models, while parts of the disordered regions (lacking electron density) are presented as a dotted line. The image was rendered using PyMOL™ v. 0.99 (DeLano Scientific, 2006) using the PDB code 1JNK [32].

1.3.2. The active site of JNK

Structural data for the nucleotide-bound form of the JNKs had been revealed first by the crystallisation of JNK3 with Mg^{2+} and the ATP analogue, adenosine 5′-(β,γ-imido)triphosphate (AMP-PNP) [32]. Since the amino acids involved in ATP binding are generally conserved among the different JNK isoforms, this data is likely to reflect that which may be present in the other variants.

Within the JNK3 structure, AMP-PNP is located deep within the active site cleft formed between the N- and C-terminal domains, while the Gly-rich flap of JNK3 extends almost completely over the nucleotide (Figure 6) [32]. The adenine base of the nucleotide binds toward the rear of the active site cleft, and interacts with both Met149 and Glu147 (Figure 6).

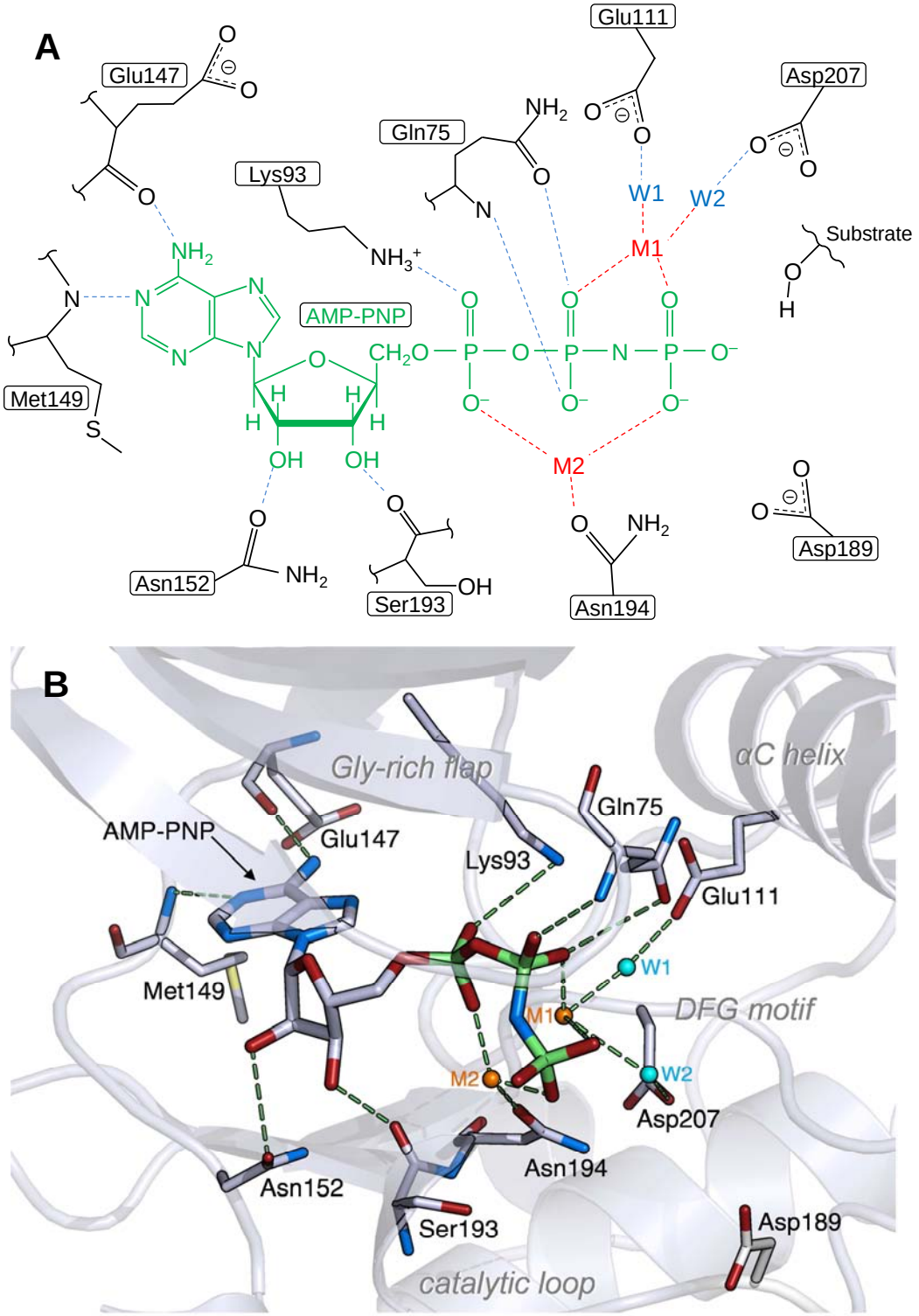

Figure 6. The active site of JNK3. The residues of JNK3 that interact via hydrogen bonds and electrostatic forces with the ATP analogue AMP-PNP within the active site of inactive (non-phosphorylated) JNK3 are illustrated. The two essential divalent metal ions, Mg^{2+}, required for the coordination of the phosphoryl oxygen atoms of AMP-PNP are labelled M1 and M2 (A & B) and represented by orange spheres (B). The water molecules involved in the indirect hydrogen bonds formed between selected residues and AMP-PNP are indicated by W1 and W2 (A & B), and shown as cyan spheres (B). **(A)** A schematic representation of the binary complex formed between AMP-PNP (green) and non-phosphorylated JNK3. Hydrogen bonds and electrostatic interactions are represented by blue and red dotted lines, respectively, yet are not drawn to scale. **(B)** A three-dimensional representation of the binary complex, in which the relevant interactions are indicated by green dashed lines. Oxygen, nitrogen, and phosphorus atoms are shown in red, blue, and green, respectively. The distal location of Asp189 in inactive JNK3 is indicated, a residue proposed to function in the correct positioning of the hydroxyl group of the substrate for catalysis in active JNK3 when the residue is positioned correctly upon JNK3 phosphorylation. The image was rendered using PyMOL™ v. 0.99 (DeLano Scientific, 2006) using the PDB code 1JNK [32].

Specific residues from the Gly-rich flap and from β7 form nonpolar interactions on both sides of the purine ring, while the side chain of Asn152 and the carbonyl group of Ser193 from a hydrogen-bonding network to the O2′ and O3′ hydroxyls of the ribose sugar [32]. Many hydrogen bonds, both direct and indirect, are formed between the triphosphate group and a number of the invariant amino acids of the protein kinases. The main chain amide and side chain carbonyl oxygen of Gln75, as well as the side chain amine of the conserved Lys93 interact with the β- and α-phosphate oxygen atoms, respectively (Figure 6) [32]. The JNK3–AMP-PNP complex also comprises two magnesium ions (M1 and M2). M2 contacts the side chain group of Asn194, allowing it to bridge the oxygens of the α- and γ-phosphoryl groups of AMP-PNP, while M1 interacts via water molecules with the carboxylate oxygens of Glu111 and Asp207 (a strictly conserved residue), allowing it to chelate the β- and γ-phosphoryl group oxygens (Figure 6) [32].

1.3.3. Catalytic mechanism of JNK

The JNK isoforms exhibit a random sequential reaction in that either protein substrate or ATP may bind to the active site of the kinase first, proceeded by the binding of the other substrate [35]. Kinases are then known to transfer the γ-phosphate of ATP to their protein substrates with inversion of its stereochemical configuration [36]. There is increasing evidence that this is a result of the hydroxyl group of the substrate directly displacing the phosphate in a single step, without the incorporation of any phospho-enzyme covalent intermediates (see [3] for a review). Although there is a possibility that other complex mechanisms entailing multiple covalent intermediates may be utilised to facilitate protein phosphorylation, the active site of kinases do not provide an adequate nucleophile in proximity to the terminal γ-phosphate of ATP for such a mechanism to be viable [36]. It has therefore been proposed that kinases facilitate a single direct displacement of the γ-phosphate by the hydroxyl group of their substrate without the creation of any intermediates.

In respect to how this is achieved, it is known based on primary and tertiary structural comparisons that most protein kinases place a conserved aspartate residue (Asp189 in JNK3) in hydrogen bonding distance to the substrate hydroxyl group (Figure 6) [5,37-40]. Mutational studies have also shown this residue to be critical for efficient catalysis, as the replacement of this aspartate with alanine in a variety of kinases decreases their k_{cat} by 2-3 orders of magnitude [41,42]. It has been illustrated through kinetic studies upon a number

of protein kinases that this residue does not have a role as a general-base catalyst [43-46], but it has rather been suggested that the carboxyl group may orient the substrate's hydroxyl group for efficient attack of the γ-phosphate of ATP. The hydrogen bond formed between these groups would immobilise a productive hydroxyl rotamer to allow an effective attack geometry to be attained [45], where upon phosphorylation of the hydroxyl group of the substrate, the negatively charged aspartate could facilitate dissociation by repelling the phospho-product [47]. The essential Mg^{2+} ion that protein kinases require for catalysis (M1) is seen to chelate the β- and γ-phosphates of ATP and Asp207 in JNK3, and has been proposed to orientate the terminal γ-phosphate group to facilitate its direct transfer to the hydroxyl acceptor (Figure 6). It is therefore likely that protein kinases utilise a mechanism that incorporates a positioning function for the two aspartate residues described, usually with the participation of a metal ion such as Mg^{2+} (M1) that helps to stabilise the negative charge that develops on the leaving group [44].

1.4. Mechanisms of kinase regulation and activation through phosphorylation

1.4.1. Autoinhibition

The control of protein kinases can be separated into two general yet distinct categories based on the mechanism through which regulation occurs. The first is regulation by autoinhibition, a mechanism in which a pseudosubstrate domain located within a polypeptide extension of the kinase catalytic core inhibits catalytic activity by interacting with the active site. Kinase activation occurs upon displacement of the autoinhibitory domain from the active site, indicating that this autoregulation relies on an inhibition mechanism commonly deemed competitive with regard to the interaction of protein substrates within the catalytic cleft [12]. An example includes the binding of cyclic adenosine monophosphate (cAMP) to the regulatory subunit of cAMP-dependent protein kinase (PKA) [48]. The regulatory subunit is an autoinhibitory domain formed from a discrete polypeptide subunit, whose binding to cAMP displaces it from the catalytic core of PKA to allow for binding of its substrate [26]. Protein phosphorylation is also known however to play an important role in autoinhibitory function, as observed within the displacement of the C-terminal tail from the active site of the Src tyrosine kinase upon its phosphorylation [49].

The phosphorylated and non-phosphorylated crystal structures of these and numerous other protein kinases have driven many to propose that the activation lip, the site at which kinases

are phosphorylated on select serine, threonine, and tyrosine residues, has an autoregulatory role [49]. These non-phosphorylated structures place the activation lip partly in the catalytic cleft, where phosphorylation causes extensive movements in the loop, supposedly enabling improved access of substrates to the active site [50,51]. The activation lip may thus function as “door” to the active site cleft and substrate binding pocket, thereby allowing the large enhancements to catalytic turnover observed upon phosphorylative activation. This corresponds to the model that the loop acts as a competitive inhibitor for the protein substrate when the kinase is inactive. Considering that the activation lip is positioned over the substrate binding site in non-phosphorylated inactive JNK3 (Figure 7), the autoinhibitory model described may also apply to this MAP kinase.

A few kinases however display an increase in activity independent of an increase in ATP and substrate binding affinity when phosphorylated. Within these kinases, the activation lip does not behave as a competitive inhibitor for either nucleotide or protein substrate, and must thus facilitate the phosphoryl transfer step via alternative mechanisms [3]. When comparing the phosphorylated and non-phosphorylated forms of a variety of other kinases, it is seen that while phosphorylation may modulate the dynamic motions of the activation lip, the character of the motions do not seem to be the conserved across the kinase superfamily. For example, the activation lip in the insulin receptor kinase (InRK) appears to obstruct the ATP and protein substrate binding pockets [51], while the loop in fibroblast growth factor receptor (FGFR) kinase exhibits localised changes in conformation upon phosphorylation that has been shown not to affect the binding of ATP [52]. Phosphorylation of the activation lip of some kinases may thus regulate kinase activity in a manner that is distinct from autoinhibitory mechanisms. Within this role, phosphorylation has been proposed to appropriately position the activation lip, which nucleates a network of interactions within the active site cleft essential for activity [12].

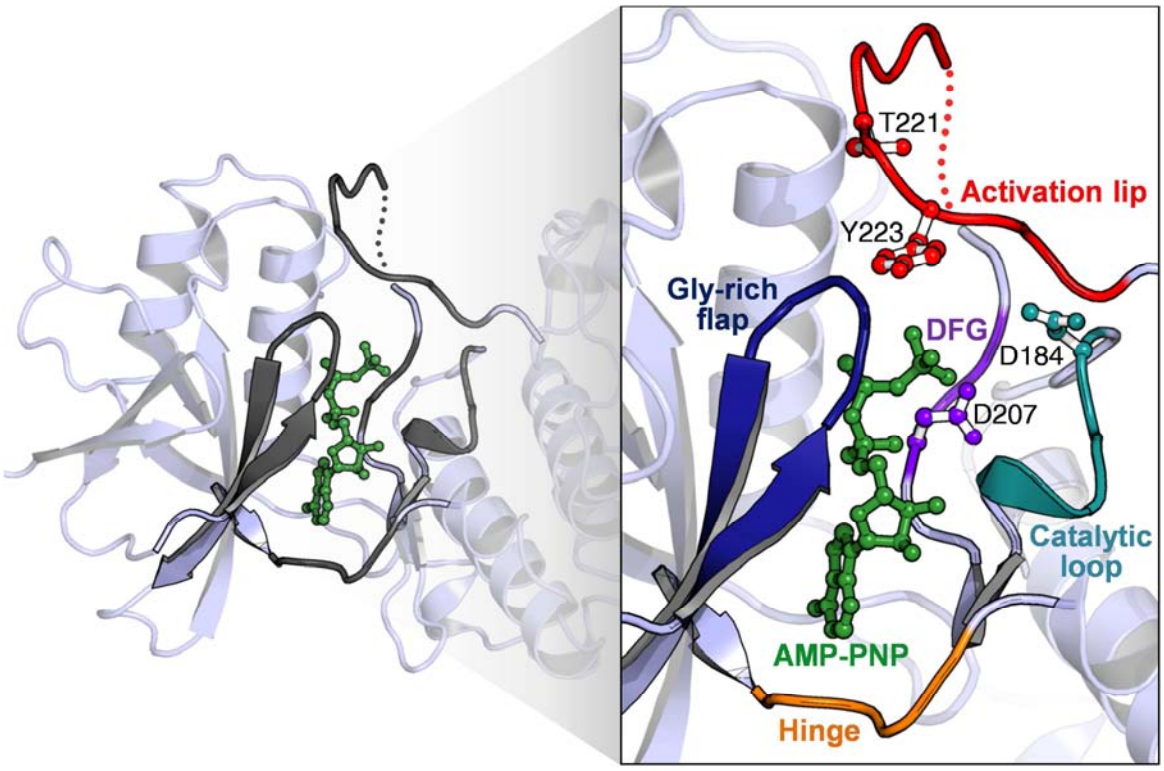

Figure 7. Structural features proposed to be involved in the activation of JNK3 upon phosphorylation. A ribbon representation of JNK3 illustrates the Gly-rich flap in blue, the hinge sequence in yellow, and the activation lip (including the regulatory phosphorylation sites of T221 and Y223) in red. The misalignment of the functionally important residues D184 and D207, situated in the catalytic loop (teal) and DFG motif (purple) respectively, are indicated in this inactive form of the kinase. The AMP-PNP molecule bound within the active site of JNK is shown as a green ball-and-stick representation. The disordered region of R212–T216 does not have visible electron density, and is represented as a dotted line. The image was rendered using PyMOL™ v. 0.99 (DeLano Scientific, 2006) using the PDB code 1JNK [32].

1.4.2. Remodelling of the active site

The optimisation of substrate binding and phosphoryl transfer through the remodelling of the active site represents the second type of kinase regulation. In illustration, phosphorylation is thought to activate ERK2 by inducing both local and global changes in conformation and conformational flexibility. The N-terminal and C-terminal domains of inactive ERK2 are situated ~17° further apart than the equivalent domains of active PKA [53], and phosphorylation has been shown to rotate the two domains to cause the closure of the catalytic cleft and the alignment of the functional residues [54,55]. Due to the highly conserved properties of the core kinase structure [38], an account of PKA, the first kinase structure to be elucidated using X-ray diffraction [56], is also useful here as it embodies the major characteristics of all the members of the superfamily. The phosphorylated amino acid in the activation lip of active PKA interacts with specific basic residues located within the

N-terminal domain to stabilise the closed domain form of the kinase [57]. The closed state of ERK2 may be stabilised by similar interactions, where domain rotation is brought about by homologous basic residues binding its phosphorylated Thr183 [53].

When comparing the structures of inactive JNK3 and active PKA, it is revealed that the N-terminal and C-terminal domains of JNK3 are also rotated further apart when compared to their relative positions in PKA [32,58]. This results in the misalignment of the two halves of the active site of JNK3, which comprise the catalytic loop (Arg188-Asn194) and the DFG motif (Asp207-Gly209) (Figure 7) [32]. As described above, the conserved residues of Asp189 and Asp207 and their correct orientation are thought to be essential for catalysing phosphoryl transfer, functioning to direct the hydroxyl group of the protein substrate for attack on the γ-phosphate of ATP [41]. Asp207 interacts via an H_2O molecule (W2) with M1, which in turn coordinates with the β- and γ-phosphoryl group oxygens (Figure 6) [32]. The equivalent residue in PKA (Asp184) however binds both M1 and M2 directly, an important difference that might contribute to the reduced catalytic activity of the non-phosphorylated form of JNK3 [53]. The direct interaction of the aspartic residue with the metal ion is significant because metal chelation has been proposed to be an important function for Asp184 in PKA [44]. Thus, as Asp207 is located within the misaligned DFG motif of non-phosphorylated JNK3, it is suggested that phosphorylation results in the reconfiguration of the activation lip and rotation of the two domains through the “hinge region”, bringing Asp207 closer to the nucleotide to allow its direct interaction with the metal ion (Figure 5 and 6) [32]. The critical importance of Asp189 and Asp207 therefore suggest that the open conformation of the two domains of JNK3 plays a role in the low activity of the non-phosphorylated form of the enzyme [3,32].

Ultimately, the data accumulated from structural and kinetic studies indicate that a common means of regulation through the activation lips of kinases does not exist. Phosphorylation induced changes of the activation lip may differ from kinase to kinase, while loop mediated regulation involves conformational changes in additional structural elements in the kinase core distant from the activation lip. The structures of JNK that have been determined are also only of the non-phosphorylated, inactive conformation of the kinase. Thus, due to the lack of a conserved means of phosphorylative kinase activation and of phosphorylated JNK structural data, the mechanisms through which JNK is activated upon its phosphorylation has not yet been fully elucidated. Although the misplacement of the catalytic residues associated with the open conformation of the N- and C-terminal domains, and the obstruction of the

catalytic cleft by the activation lip may be the causative factors of the low activity of non-phosphorylated JNKs, structural and biophysical data of phosphorylated JNK are required to confirm these proposals and uncover the exact nature of its mechanisms of activation.

1.5. Aim and objectives

The precise mechanisms by which phosphorylation facilitates the activation of JNK are not fully understood, as the crystal/solution structure of phosphorylated and active JNK has not yet been solved. The models proposed are thus based on the conformational changes (whether local or global) that occur within other protein kinases upon their activation, yet even separate kinases of the same family do not exhibit a conserved means of phosphorylative activation. The aim of this research was thus to elucidate the changes to the structure, stability, and dynamics of JNK1β1 (the most abundant JNK isoform [59]) that are induced by phosphorylation and to reveal how these changes facilitate its activation.

To this end, the specific objectives of this research were to:

1. Express and purify recombinant JNK1β1.
2. Develop a system for producing fully phosphorylated and active JNK1β1 by reconstituting the MAPK phosphorylation cascade *in vitro.*
3. Determine the effect that phosphorylation has on the specific activity of JNK1β1.
4. Characterise the nature of JNK1β1 phosphorylation by active MKK4 using mass spectrometry to identify the location of phospho-sites.
5. Compare the secondary and tertiary structural conformations of phosphorylated and non-phosphorylated JNK1β1 using spectroscopic techniques.
6. Assess the effect that nucleotide binding and phosphorylative activation has on the stability of JNK1β1 through thermal denaturation as well as equilibrium and kinetic unfolding studies.
7. Establish the changes to the dynamics of JNK1β1 that occur upon nucleotide binding and phosphorylation using amide hydrogen-deuterium exchange mass spectrometry.

CHAPTER 2

PUBLICATION 1

High yield purification of JNK1β1 and activation by *in vitro* reconstitution of the MEKK1 → MKK4 → JNK MAPK phosphorylation cascade

GAVIN R. OWEN, IKECHUKWU ACHILONU, AND HEINI W. DIRR

Protein Expression and Purification 87, 87-99 (2013)

This publication describes a unique system for expressing and purifying JNK1β1, as well as a novel means of phosphorylating the kinase by reconstituting the MAPK activation cascade *in vitro*. The impact of phosphorylative activation on the catalytic activity of JNK1β1 was also determined.

Author contributions: Gavin R. Owen performed all experimental work, analysed the data, and wrote the manuscript. Ikechukwu Achilonu and Heini W. Dirr supervised the project and assisted in data analysis and interpretation.

GRAPHICAL ABSTRACT

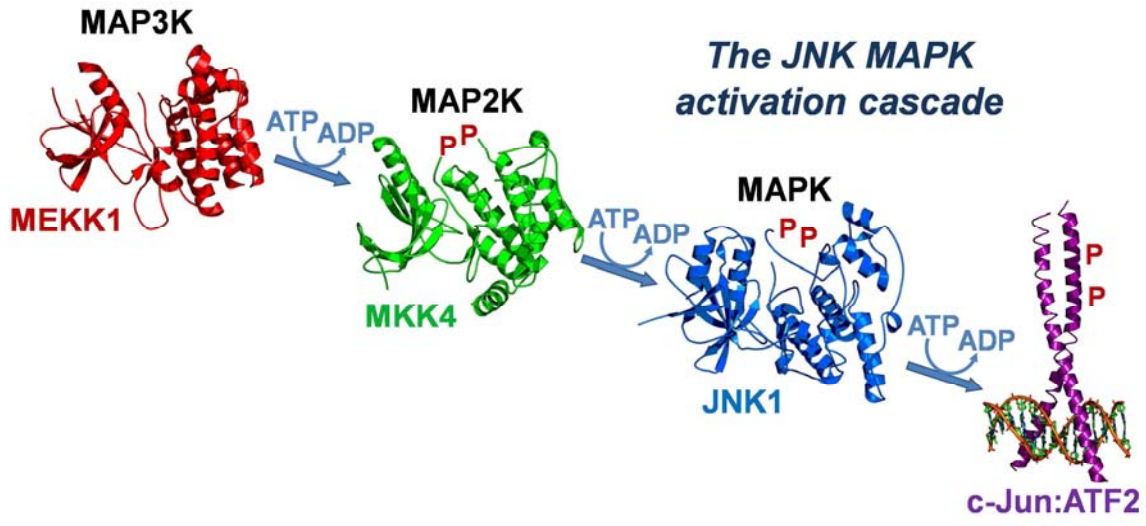

Protein Expression and Purification 87 (2013) 87–99

Contents lists available at SciVerse ScienceDirect

Protein Expression and Purification

journal homepage: www.elsevier.com/locate/yprep

High yield purification of JNK1β1 and activation by *in vitro* reconstitution of the MEKK1 → MKK4 → JNK MAPK phosphorylation cascade

Gavin R. Owen, Ikechukwu Achilonu, Heini W. Dirr *

Protein Structure–Function Research Unit, School of Molecular and Cell Biology, University of the Witwatersrand, Johannesburg 2050, South Africa

ARTICLE INFO

Article history:
Received 26 September 2012
and in revised form 29 October 2012
Available online 10 November 2012

Keywords:
c-Jun N-terminal kinase
MAP kinases
MAPK signaling cascade
Protein phosphorylation
Codon harmonization

ABSTRACT

The c-Jun N-terminal kinase (JNK) pathway forms part of the mitogen-activated protein kinase (MAPK) signaling pathways comprising a sequential three-tiered kinase cascade. Here, an upstream MAP3K (MEKK1) phosphorylates and activates a MAP2K (MKK4 and MKK7), which in turn phosphorylates and activates the MAPK, JNK. The C-terminal kinase domain of MEKK1 (MEKK-C) is constitutively active, while MKK4/7 and JNK are both activated by dual phosphorylation of S/Y, and T/Y residues within their activation loops, respectively. While improvements in the purification of large quantities of active JNKs have recently been made, inadequacies in their yield, purity, and the efficiency of their phosphorylation still exist. We describe a novel and robust method that further improves upon the purification of large yields of highly pure, phosphorylated JNK1β1, which is most suitable for biochemical and biophysical characterization. Codon harmonization of the JNK1β1 gene was used as a precautionary measure toward increasing the soluble overexpression of the kinase. While JNK1β1 and its substrate ATF2 were both purified to >99% purity as GST fusion proteins using GSH-agarose affinity chromatography and each cleaved from GST using thrombin, constitutively-active MEKK-C and inactive MKK4 were separately expressed in *E. coli* as thioredoxin-His_6-tagged proteins and purified using urea refolding and Ni^{2+}-IMAC, respectively. Activation of JNK1β1 was then achieved by successfully reconstituting the JNK MAPK activation cascade *in vitro*; MEKK-C was used to activate MKK4, which in turn was used to efficiently phosphorylate and activate large quantities of JNK1β1. Activated JNK1β1 was thereafter able to phosphorylate ATF2 with high catalytic efficiency.

Introduction

The c-Jun N-terminal kinases (JNKs)[1] are one sub-group of the Ser/Thr kinases that form the last tier of the eukaryotic mitogen-activated protein kinase (MAPK) signaling pathway, comprising a highly conserved, sequential three-tiered kinase cascade. Here, upon activation by extracellular and cellular stimuli, an upstream MAP3K (e.g. MEKKs, MLK, ASK1) phosphorylates and activates a MAP2K (e.g. MKKs), which in turn phosphorylates and activates the downstream MAPKs (such as the JNKs, ERKs, or p38 kinases) [1,2].

The JNK MAPK pathway is activated primarily by cytokines and exposure to environmental stresses such as UV irradiation [3], osmotic shock, and oxidative stress [4]. JNKs were originally identified by their ability to phosphorylate the N-terminal of the transcription factor c-Jun, thereby initiating a variety of transcription events [5]. They have since been found however to be multifunctional kinases involved in many physiological processes that include proliferation, apoptosis, motility, differentiation and DNA repair [6–8]. Consequently, dysfunction in JNK signaling has been shown to contribute to many pathological processes associated with neurodegeneration, diabetes, heart disease, and cancer [9]. This makes this family of protein kinases attractive drug targets for Parkinson's disease, Alzheimer's disease, obesity, arteriosclerosis and stroke [9]. Therefore, the production of active recombinant forms of these kinases remains vital for therapeutic development.

The JNKs are encoded by three separate and alternatively spliced genes (*JNK1*, *JNK2*, and *JNK3*), resulting in 10 distinct JNK isoforms [10]. The predominant isoforms JNK1 and JNK2 are expressed ubiquitously and have four isoforms each (α1, α2, β1, and β2), while JNK3, possessing an N-terminal amino acid extension and expressed primarily in the nervous system, has only 2 isoforms (α1 and α2) [6,10].

JNKs are activated by dual phosphorylation of the T183 and Y185 residues of the T-P-Y motif located in the activation loop, a modification catalyzed by the two upstream dual specificity MAP2Ks, MKK4 and MKK7 [11]. MKK4 and MKK7 are themselves

* Corresponding author. Fax: +27 11 7176351.
E-mail address: heinrich.dirr@wits.ac.za (H.W. Dirr).

[1] *Abbreviations used:* JNK, c-Jun N-terminal kinase; MAPK, mitogen-activated protein kinase; MEKK, mitogen-activated ERK-regulating kinase kinase; MKK, mitogen-activated protein kinase kinase; ATF2, activating transcription factor 2; GST, glutathione *S*-transferase; SEC, size-exclusive chromatography; TH-, thioredoxin-His_6; pm-, phosphomimetic; pp-, dual phosphorylated; IMAC, immobilized metal ion affinity chromatography.

1046-5928/$ - see front matter © 2012 Elsevier Inc. All rights reserved.
http://dx.doi.org/10.1016/j.pep.2012.10.010

activated by phosphorylation by a number of upstream MAP3Ks, including, to name just a few, MEKK1–4, ASK1, ASK2, MLK2, and MLK3 [2]. Once activated by phosphorylation, JNKs are in turn able to phosphorylate a variety of substrates that include a few cytoplasmic proteins and other nuclear transcription factors such as ATF2, Elk-1, JunD, c-Fos, and c-Myc [6,10]. Together with c-Jun, these proteins form heterodimers that constitute activator protein-1 (AP-1) transcription factors that regulate and control the expression of several stress-responsive genes [12].

The complete activation of JNKs requires phosphorylation on both the T183 and Y185 residues, modifications initially found to be catalyzed by the synergistic activity of both MKK4 and MKK7 [11,13,14]. This was due to the preference that MKK4 and MKK7 had shown for phosphorylating the threonine and tyrosine residues, respectively. Nevertheless, studies of *in vitro* phosphorylative activation of JNK has shown that high concentrations of active MKK4 is sufficient to phosphorylate both the T183 and Y185 residues of JNK, thereby activating it [6,15].

Many approaches have been attempted in the production of high yields of active JNKs. These can be described by three fundamentally similar methods; transient expression of JNKs within mammalian cells stressed to induce activation of the natural JNK MAPK pathway [16], co-expression of both JNKs and their upstream activating MAPKs in *E. coli* or other non-mammalian expression hosts [17,18], and recombinant purification of inactive JNKs followed by their later *in vitro* phosphorylation by commercially available (often only partially) active upstream kinases [19]. Unfortunately, expression using mammalian cell culture commonly results in very low yields of active kinases, while the latter methods often lead to large variations in the effectiveness of activation of the downstream target kinase. In part this is because the unpredictable and uncontrollable *in vivo*, cellular systems in which the target or their upstream kinases are phosphorylated (such as during the bacterial co-expression of MAPK cascade proteins) are only able to produce inconsistent degrees of partially phosphorylated kinases.

Within the current study, we describe an alternative method for the expression, purification and activation of the most abundant human JNK isoform, JNK1β1, which can be easily employed for the isolation and phosphorylation of any other JNK isoform. Aiming first to improve the yield of soluble MAP kinase during overexpression, the *JNK1β1* open reading frame was recoded by harmonizing the usage frequency of its codons with those observed in an *E. coli* expression host (full codon usage harmonization). We were thus able to recreate the natural rate at which JNK1β1 is translated in its native human host, hoping that it will lead to the production of soluble, correctly folded protein in *E. coli*. Removing the inconsistencies present in biological systems that rely on co-expression of active upstream kinases for *in vivo* phosphorylation of downstream kinase targets (as described in Refs. [17,18] and others), we obtained controlled and consistent levels of active, phosphorylated JNK1β1 by reconstituting the full JNK MAPK activation cascade *in vitro* by purifying both active MEKK1 and its downstream kinase MKK4. Offering full control over its *in vitro* activation, this robust yet flexible method is applicable for the acquisition of large quantities of any JNK isoform in a fully active or inactive state.

Material and methods

Codon usage harmonization of the JNK1β1 open reading frame

The codon usage frequencies of the human *JNK1β1* open reading frame (accession No. NM_139046.1), encoding full-length JNK1β1 (1–384) (EC 2.7.11.24) (accession No. AAI44064.1), when expressed naturally in its native human host and recombinantly in an *E. coli* K12 expression host, as well as the usage frequency of each of the known 64 codons in each of the described hosts, were computed using the Graphical Codon Usage Analyser (GCUA v 2.0) web-interface software (www.gcua.schoedl.de; [20]).

The *JNK1β1* codons that do not possess the same usage frequency when expressed in *E. coli* as compared to their expression in their native human host were manually adjusted by substitution with synonymous codons computed to be expressed within *E. coli* with a usage frequency identical or similar to their corresponding natural codons. For example, the triplet codon AGA of R3 possesses a natural codon usage frequency of 100% when expressed in *H. sapiens*, but has a codon usage frequency calculated to be 5% in *E. coli* (Supplementary Table S1). This AGA triplet codon was thus changed to CGC, a synonymous arginine encoding codon that has a calculated codon usage frequency of 100% in *E. coli*. The entire *JNK1β1* open reading frame was thus redesigned with synonymous *E. coli* codons having usage frequencies that match as closely as possible those that occur naturally in the human. This approach, termed "codon usage harmonization", is significant for heterologous protein expression in *E. coli* as it assists in the production of correctly folded, soluble and functional proteins [21]. See Supplementary Table S1 for a table illustrating the full procedure for codon usage harmonization of the *JNK1β1* open reading frame. Supplementary Fig. S1 presents the natural *H. sapiens* and codon-harmonized *JNK1β1* DNA sequences used, highlighting the nucleotide changes made in the codon harmonization process, while Fig. S2 shows the identical wild-type JNK1β1 protein product resulting upon translation of each DNA sequence.

Cloning, expression, and purification of JNK1β1 and its substrate ATF2

The methods for cloning synthetic codon-harmonized *JNK1β1* and human *ATF2* (residues 17–96) open reading frames into pGEX-4T-1 vector are described in the supplementary material.

Various conditions of cell type (*E. coli* BL21(DE3)pLysS and T7 Express I^q cells), culture media (LB, 2 × YT, and TB media), IPTG concentration (0–1 mM IPTG in 0.1 mM intervals), induction time (2, 4, 6, 8, and 16 h) and growth temperature (18, 20, 22, 25, 30, and 37 °C), and the numerous combinations thereof, were screened using SDS–PAGE and Western blot to obtain maximal yield of soluble GST-JNK1 and GST-ATF2. Greatest yields of GST-JNK1 were produced when 1 L of BL21(DE3)pLysS cell cultures in 2 × YT media were grown at 37 °C to an OD_{600nm} of 0.6, induced with 0.6 mM IPTG and grown at 22 °C for 6 h. The best production of soluble GST-ATF2 occurred when 1 L T7 Express I^q cell cultures in 2 × YT media were grown at 37 °C to an OD_{600nm} of 0.6, induced with 0.5 mM IPTG and grown at 37 °C for 2 h. Cells were harvested and resuspended in "Tris-Lysis Buffer" (10 mM Tris–HCl buffer, pH 8.0, comprising 150 mM NaCl, 1 mM EDTA, 1 mM DTT, 1 mM benzamidine, 2 mM phenylmethylsulfonyl fluoride (PMSF) and 0.02% (w/v) NaN_3), and stored at −20 °C. Cells were thawed, Triton X-100 added to a final concentration of 1% (v/v), and disrupted by sonication. The soluble fraction was clarified by centrifugation (27 000*g*, 30 min, 4 °C) and subjected to GSH-agarose (Sigma–Aldrich) affinity chromatography. After washing the column with Tris-Lysis Buffer containing 1% Triton X-100 and 1 M NaCl, the bound GST-fusion was eluted with "Glycine-Elution Buffer" (10 mM glycine, pH 10.0, 1 mM EDTA, 1 mM DTT and 0.02% (w/v) NaN_3). The eluted fraction was dialysed for 16 h at 4 °C against Tris-Lysis Buffer, concentrated by ultracentrifugation at 4 °C and the concentration of fusion protein was determined by Bradford assay and by measuring the absorbance at 280 nm. At this point, the GST-JNK1 fusion-protein form of JNK1β1 was used in its subsequent dephosphorylation and/or dual phosphorylation (the procedures of which are described below). This allows for the isolation of

modified GST-JNK1 from the modifying enzymes used by employing GSH-agarose affinity chromatography.

Using 0.4 U thrombin/mg fusion protein at 20 °C, the optimum time for cleavage of GST-JNK1 was established to be 15 min, whereas that of GST-ATF2 was determined to be 6 h (see Supplementary Information for the details of the thrombin cleavage trials). After cleavage, thrombin was immediately removed using 2 ml of heparin-agarose resin (GE Healthcare Bio-Sciences AB, Uppsala, Sweden) pre-equilibrated with Tris-Lysis Buffer, immediately followed by the removal of the GST tag by GSH-agarose as previously described. Recombinant JNK1β1 and ATF2 were concentrated and further purified using Sephacryl S-200 size-exclusive chromatography (SEC) (0.8 cm × 70 cm, 30 cm/h) (GE Healthcare Bio-Sciences AB) pre-equilibrated with Tris-Lysis Buffer.

Cloning, expression, and purification of MEKK-C

The methods for cloning the *MEKK-C* open reading frame (the constitutively active C-terminal kinase domain of MEKK1) into pET-32a vector are described in the supplementary material.

TH-MEKK-C was purified from inclusion bodies by urea refolding of the insoluble cell fraction in which it was expressed. Upon testing for the optimum conditions for its overexpression, the greatest yield of insoluble TH-MEKK-C was observed when 1 L of BL21(DE3)pLysS cell cultures in 2 × YT media were grown at 37 °C to an OD_{600nm} of 0.6, induced with 0.5 mM IPTG, and grown at 37 °C for a further 6 h. The cells were harvested, resuspended in Tris-Lysis Buffer, and stored at −20 °C. The cells were thawed and sonicated, and the insoluble cell fraction was collected by centrifugation (27 000*g*, 30 min, 4 °C). The pellet was washed once with 2% (w/v) deoxycholate solution, followed by two similar washes with distilled water. The insoluble constituents remaining were pelleted as before, and resuspended in 50 ml of "Refolding Buffer" (50 mM Tris–HCl, pH 8.0, 0.5 M NaCl, 10% (v/v) glycerol, 0.02% (w/v) NaN_3) containing 6.5 M urea. The pellet was allowed to solubilize for 1 h on a rotary mixer and the insoluble fraction removed by centrifugation. The supernatant was dialyzed against Refolding Buffer containing 4 M urea overnight at 4 °C. Insoluble precipitate was pelleted and the supernatant diluted 5× by drop-wise addition into Refolding Buffer containing 2 M urea and 5 mM DTT. The resulting solution was dialysed overnight at 4 °C against Refolding Buffer comprising 1 M urea and 2 mM DTT, and then against Kinase-Reaction Buffer at 4 °C (2× changes, 12 h/change). Any additional aggregated protein at this point was removed by centrifugation. The TH-MEKK-C was concentrated by ultracentrifugation and the concentration determined by measuring the absorbance at 280 nm.

Cloning, expression, and purification of wild-type and phosphomimetic MKK4 variants

The methods for cloning the wild-type *MKK4* open reading frame into pET-32a vector and the generation of a phosphomimetic MKK4 variant (S257E/T261D) are described in the supplementary material.

Screening various expression conditions as previously described, optimal yields of both TH-wtMKK4 and TH-pmMKK4, was obtained when 1 L T7 Express I^q cell cultures in 2× YT media were grown at 37 °C to an OD_{600nm} of 0.6, induced with 0.2 mM IPTG and grown at 20 °C overnight. TH-wtMKK4 and TH-pmMKK4 were then purified separately according to the following procedure; Cells were harvested, resuspended in "Phosphate-Lysis Buffer" (20 mM sodium phosphate buffer, pH 8.0, comprising 500 mM NaCl, 1 mM benzamidine, 2 mM PMSF and 0.02% (w/v) NaN_3), and stored at −20 °C. Cells were thawed and sonicated, where after the soluble cell fraction was clarified by centrifugation (27 000*g*, 30 min, 4 °C) and recombinant TH-wtMKK4 and TH-pmMKK4 were purified using a 5 ml HisTrap™ Ni^{2+}-immobilized metal ion affinity chromatography (IMAC) column (GE Healthcare) pre-equilibrated with Phosphate-Lysis Buffer. The matrix was first washed with Phosphate-Lysis Buffer followed by a 500 ml linear imidazole gradient consisting of Phosphate-Lysis Buffer and the same buffer containing 100 mM imidazole. The bound TH-fusion proteins were then eluted with a one-step gradient of Phosphate-Lysis Buffer comprising 250 mM imidazole. The eluted fractions were dialysed overnight at 4 °C against "Kinase-Reaction Buffer" (10 mM Tris–HCl, pH 8.0, comprising 150 mM NaCl, 1 mM DTT, 0.02% (v/v) Triton X-100, and 0.02% (w/v) NaN_3), concentrated by ultracentrifugation at 4 °C and the concentration of protein determined by measuring the absorbance at 280 nm.

In vitro dephosphorylation of partially phosphorylated GST-JNK1 purified from E. coli and purification of inactive JNK1β1

Complete inactivation of partially phosphorylated JNK1β1 by dephosphorylation was achieved by incubating GST-JNK1 with shrimp alkaline phosphatase (SAP, Thermo Scientific) at 5 U SAP/mg phosphoprotein in Kinase-Reaction Buffer supplemented with 10 $MgCl_2$ and 0.2 mg/ml bovine serum albumin (BSA). The mixture was incubated at 25 °C for 5 h during which time samples were removed at regular intervals and immediately treated for reducing SDS–PAGE. Upon complete dephosphorylation of GST-JNK1, SAP was removed by passing the reaction mixture through a column of GSH-agarose affinity chromatography resin pre-equilibrated with Kinase-Reaction Buffer. After washing the matrix with Kinase-Reaction Buffer, the bound dephosphorylated GST-JNK1 fusion protein was eluted with Glycine-elution buffer. SAP-dephosphorylated JNK1β1 was then purified as previously described.

In vitro phosphorylation of TH-wtMKK4 and GST-JNK1, and purification of active JNK1β1

To obtain active MKK4 for later use in the phosphorylation of JNK1β1, TH-wtMKK4 was incubated with constitutively-active TH-MEKK-C in a 10:1 molar ratio (typically 10:1 μM, respectively) in Kinase-Reaction Buffer containing 10 $MgCl_2$, 1 mM ATP and 0.2 mg/ml BSA. The reaction mixture was incubated overnight at 25 °C to allow for the complete phosphorylative activation of TH-wtMKK4 (producing TH-ppMKK4). The TH-ppMKK4/TH-MEKK-C mixture was then used directly for the phosphorylation of JNK1β1 by mixing GST-JNK1 with the active upstream-kinase reaction mixture to produce a 10:1:0.1 molar ratio of GST-JNK1, TH-ppMKK4 and TH-MEKK-C, respectively, in Kinase-Reaction Buffer containing 10 mM $MgCl_2$, 1 mM ATP and 0.2 mg/ml BSA. The mixture was incubated at 25 °C, during which time samples were removed at regular intervals for analysis by SDS–PAGE and Western blot.

As a control for the possibility of autophosphorylation under these conditions, GST-JNK1 in Kinase-Reaction Buffer was incubated at similar concentrations with 10 mM $MgCl_2$, 1 mM ATP and 0.2 mg/ml BSA without the addition of its upstream kinases, and the reaction monitored.

The pmMKK4 variant was then tested to ascertain whether it could be used to phosphorylate and activate JNK1β1. This was performed by incubating GST-JNK1 with TH-pmMKK4 in a 10:1 molar ratio in Kinase-Reaction Buffer containing 10 mM $MgCl_2$, 1 mM ATP and 0.2 mg/ml BSA, and monitoring the reaction as described.

Upon complete dual phosphorylation of GST-JNK1 (producing GST-ppJNK1), the TH-ppMKK4 and TH-MEKK-C proteins were removed by passing the reaction mixture through GSH-agarose affinity chromatography resin pre-equilibrated with Kinase-Reaction

Buffer. After washing the matrix with Kinase-Reaction Buffer, the bound phosphorylated GST-ppJNK1 fusion protein was eluted with Glycine-elution buffer. Active, dual phosphorylated JNK1β1 (ppJNK1β1) was then purified as described.

Enzymatic assays of JNK1β1 and determination of its specific activity

To determine the specific activity of phosphorylated, active JNK1β1, an ATP Bioluminescent Assay Kit (Sigma) was used to monitor the depletion of ATP during the dual phosphorylation of ATF2. When ATP is the limiting reagent, this kit allows for the quantitative bioluminescent determination of the amount of ATP in a sample, as the firefly luciferase included in the kit catalyses the ATP-dependent oxidation of D-luciferin, emitting light that is proportional to the ATP present [22]. An ATP standard curve was first generated by mixing increasing concentrations of ATP in Kinase-Reaction Buffer (90–120 μM ATP in a final volume of 250 μl) with 250 μl "ATP Assay Mix" (diluted 5× with "ATP Assay Mix Dilution Buffer") in a 1 ml quartz cuvette with a 1 cm pathlength, and immediately determining the amount of light emitted for each ATP concentration. Emitted light intensity measurements were performed using a Jasco FP-6300 spectrofluorometer without using the excitation bulb, and measuring the amount of light of 550 nm produced over a 6 s interval. The amount of light generated within this period was integrated, the experiment repeated independently, and the average data plotted against the concentration of ATP present. A linear function was fit to the data and the slope of this standard curve, in bioluminescence intensity (arbitrary units)/μM of ATP, was used to calculate the amount of ATP hydrolysed at each JNK1β1 concentration in the subsequent kinase assay.

The JNK1β1 kinase assay reactions were conducted by incubating 25 μM ATF2, 120 μM ATP, 5 mM $MgCl_2$, and 0.2 mg/ml BSA in Kinase-Reaction Buffer with increasing concentrations of dephosphorylated or phosphorylated JNK1β1 (0–100 nM) for 1 min at 25 °C. Two hundred and fifty microliters of each reaction was then immediately mixed with 250 μl diluted ATP Assay Mix, and the amount of light produced over a 6 s period was measured as described for the ATP standard curve. The light generated within this time was integrated and converted to the concentration of ATP hydrolyzed by subtracting the concentration of ATP remaining (determined using the slope of the ATP standard curve) from the initial concentration of ATP (120 μM). The data was fit to a linear function and the slope of this curve, in μM of ATP hydrolyzed/nM of JNK1β1, was used to calculate the specific activity of phosphorylated JNK1β1, in μmol of phosphorylated ATF2/min/mg of kinase, assuming the stoichiometry that 2 ATP molecules are hydrolyzed per ATF2 protein that is dually phosphorylated. The phosphorylated JNK1β1 kinase assay was performed twice in two independent experiments, while the dephosphorylated JNK1β1 kinase assay was performed once merely for comparison and ensure that it was indeed dephosphorylated.

SDS–PAGE and Western blot analysis

Samples comprising JNK1β1, MKK4, or MEKK-C (those samples whose primary analysis did not concern ATF2) were resolved by Laemmli SDS–PAGE on a 12.5% Tris–glycine gel [23], while samples containing ATF2 were resolved by Tricine–SDS–PAGE on a 16% Tris-Tricine gel [24]. Gels were stained with Coomassie Blue R-250 solution. Protein resolved by SDS–PAGE were transferred to BioTrace™ NT nitrocellulose membrane (Pall) using "Blotting Buffer" (50 mM Tris–HCl, 200 mM glycine, pH 8.3, containing 0.1% (w/v) SDS and 20% (v/v) methanol) at 350 mA for 1 h on ice. Membranes were blocked with 5% (w/v) fat-free milk powder (Elite®) in Tris-buffered saline (TBS; 0.2 M NaCl and 20 mM Tris–HCl, pH 7.4) for 1 h at room temperature. Membranes were then washed 3× with TBS (5 min/wash).

To detect total JNK1β1, polyclonal rabbit antibodies raised against the C-terminus of human JNK1 (anti-JNK1; BioLegend) were utilized. To test for dual phosphorylation of JNK1β1, monoclonal rabbit antibodies specific to JNK1 phosphorylated at both T183 and Y185 residues (anti-pT183/pY185 JNK1; Cell Signaling Technology) were employed. Polyclonal rabbit anti-*Schistosoma japonicum* GST antibodies (anti-GST; USBiological) were used to detect GST-ATF2 fusion. To test for the dual phosphorylation of ATF2, monoclonal rabbit antibodies against ATF2 phosphorylated at both T69 and T71 (anti-pT69/pT71 ATF2; Cell Signaling Technology) were used. Anti-GST primary antibody was diluted 1:10 000 in TBS containing 0.5% (w/v) BSA (TBS-BSA), while all other primary antibodies were diluted 1:1000 in TBS-BSA. Membranes were incubated with their relevant primary antibodies for 3 h at room temperature, washed with TBS (3×, 5 min/wash) and incubated with donkey anti-rabbit IgG secondary antibody (1:1000 dilution in TBS-BSA) conjugated to horseradish peroxidase (BioLegend) for 1 h at room temperature. After washing with TBS (4×, 5 min/wash), membranes were incubated in substrate reagent (0.06% (w/v) 4-chloro-1-naphthol, 0.0015% (v/v) H_2O_2, and 20% (v/v) methanol in TBS) and the image captured with the GelDoc™ XR imaging system (Bio-Rad®).

Results and discussion

Recent work by Thevenin et al. [18] describes an efficient method for the purification and activation of various JNK α isoforms (including JNK1α1, JNK1α2, and JNK2α2). While it can be appreciated as an advancement in the pursuit to acquire large amounts of pure and active JNKs, minor inadequacies in their purification still exist. Within this current work, we sought to further improve upon the purification of large yields of highly pure, phosphorylated JNK by using the most abundant yet less studied JNK isoform, JNK1β1.

To achieve this, we first hoped to improve the soluble expression of JNK1β1 by harmonizing the codon usage frequencies of its open reading frame to those of an *E. coli* expression host (Fig. 1), as well as by employing the GST protein solubility tag (Fig. 2C). We then sought to obtain active, phosphorylated JNK1β1 by reconstituting the JNK MAPK activation cascade *in vitro*. This was accomplished by purifying both the constitutively-active C-terminal domain of MEKK1 and its downstream kinase MKK4 to use in phosphorylation experiments of inactive JNK1β1 (Fig. 2 and Fig. 3). Providing full control over its *in vitro* activation, this method allowed for the purification of large yields of active JNK1β1 that was able to phosphorylate its substrate, ATF2, with high catalytic efficiency.

Harmonization of JNK1β1 codon usage frequencies and overexpression of GST-JNK1

The *Escherichia coli* expression system is the foremost choice for recombinant protein expression in a heterologous system due to the robustness of the bacteria, cost, high-level protein yield and simplicity of the system, compared to other expression systems such as the baculovirus, mammalian and the yeast expression systems [25,26]. However, the *E. coli* expression system has several shortcomings, including production of incorrectly folded insoluble protein, truncated protein products, and in the worst case, no protein production. Several factors are believed to result in the misfolding of recombinant proteins, one of which has shown to be the disparity in codon usage frequency between prokaryotes and eukaryotes [27]. There is accumulating evidence indicating that co-translational protein folding is modulated by subtle variations

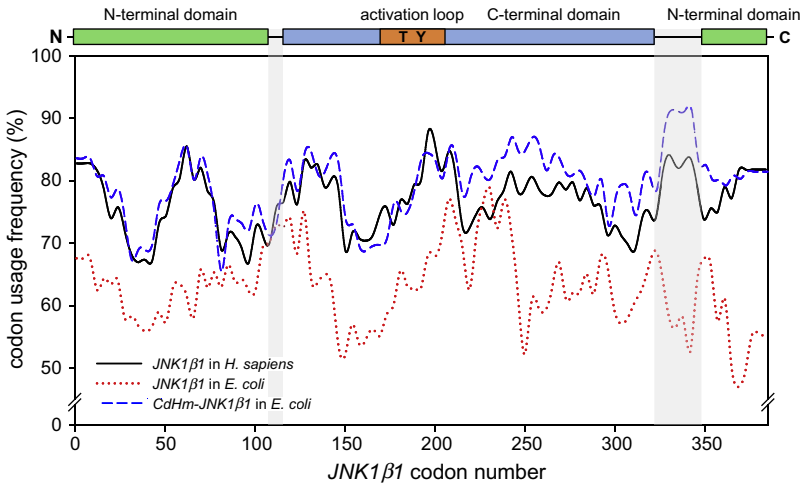

Fig. 1. Codon usage frequency profiles of the natural *JNK1β1* and codon-harmonized *JNK1β1* (*CdHm-JNK1β1*) open reading frame illustrate that a drastic shift in the natural usage frequencies (solid black line) occurs when the native *H. sapiens JNK1β1* gene sequence is introduced into *E. coli* for expression (dotted red line). Upon full codon harmonization of the *JNK1β1* open reading frame for expression in *E. coli* (dashed blue line), usage patterns show good agreement with those of the gene in its native host, including the codons encoding its interdomain connecting segments (major link/end regions, residues 110–112 and 330–345) (highlighted). Codon usage frequency profiles were generated using a running average smoothing procedure of the codon usage frequency data (0.05 sampling proportion, nearest neighbors, Sigmaplot v. 11.0).

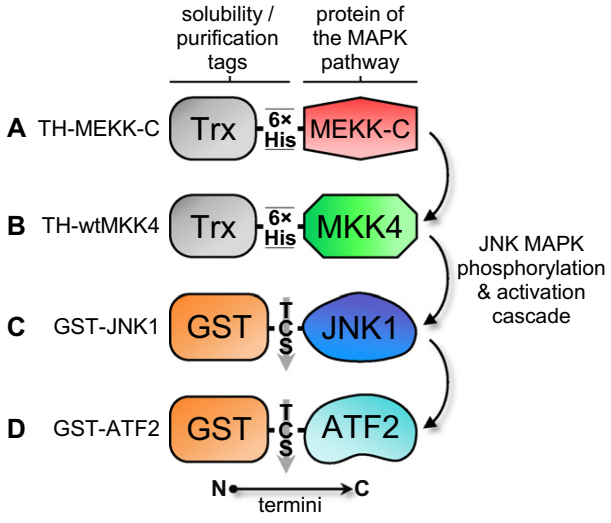

Fig. 2. Protein constructs of each MAPK cascade protein purified, detailing the fusion tags that facilitated their purification and possibly their soluble overexpression. MEKK-C (A) and wtMKK4 (B) were each expressed as thioredoxin(Trx)-His_6 fusion proteins (TH-MEKK-C and TH-wtMKK4, respectively). The 6× His residues present allow protein purification by Ni^{2+}-IMAC. JNK1β1 (C) and ATF2 (D) were both expressed as glutathione *S*-transferase(GST) fusion proteins (GST-JNK1 and GST-ATF2, respectively), permitting their purification by GSH-agarose affinity chromatography. A thrombin cleavage sequence (TCS) exists between the GST tag and each target protein, which allows cleavage of the fusion protein by thrombin. The hierarchical cascade of phosphorylative activation of the MAPK proteins is represented, a pathway that was recreated *in vitro* for the activation of JNK1β1.

in the rate of mRNA translation, and that this plays a key role in developing secondary structure in nascent proteins [28,21]. Failures in recombinant protein expression by heterologous expression hosts may thus be attributable to differences in synonymous codon usage frequencies between expression and natural hosts [21].

Adjusting target gene sequences for heterologous expression in *E. coli* by substituting the native codons with synonymous ones possessing the same or similar usage frequencies in the expression host (termed "codon harmonization") may provide the optimal translational kinetics for its soluble overexpression [21]. Studies have shown that improving synonymous codon usage frequencies in heterologous genes by codon harmonization can result in a more than 40-fold increase in the yield of soluble, recombinant protein [21,29]. Because the expression and purification of JNK is notoriously difficult, we used codon harmonization within this study to recode the entire open reading frame of the JNK1β1 gene as a precautionary measure to possibly enhance the production of soluble, correctly folded protein during expression in *E. coli*. This was based on the method described by Angov et al. [21]. However, a full codon harmonization approach was employed in this study, selecting synonymous codons from the *E. coli* expression host having usage frequencies that best reflect the usage frequencies of the native JNK1β1 gene in its human host (potential link/end segments were not specifically considered). Although Angov et al. [21] concluded that their algorithm enhances heterologous protein expression of particular codon-harmonized *Plasmodium falciparum* proteins, attempting to fully replicate the native translation kinetics of human JNK1β1 within *E. coli* was an attractive means of potentially facilitating soluble overexpression.

When the native *H. sapiens* JNK1β1 gene sequence is introduced for expression into *E. coli*, a significant shift in its natural codon usage frequencies occurs (Fig. 1). This shift is well illustrated by the codons encoding the first 20 N-terminus amino acids (M1-F20) as there is a particularly large discordance in the codon usage patterns of this region when comparing its expression in each host (Supplementary Fig. S9A). Several codons within this region, namely R3, K5, D7, E14, G16, S18, and T19 are used at high frequency in the native host but are used at a dramatically lower frequency in *E. coli*. The usage frequency for the residue R3 (AGA), for example, dropped from 100% in *H. sapiens* to 5% in *E. coli* (Supplementary Fig. S9A).

Following full codon harmonization, the codon usage patterns were in good agreement with those of the JNK1β1 gene in its native host (Fig. 1. and Supplementary Fig. S9B) highlighting the potential of the harmonization process to assist in its increased soluble overexpression. For example, the usage rate for R3 increased from 5% to 100%, identical to the natural 100% codon usage frequency in *H. sapiens*. The interdomain connecting segments (residues 110–112 and 330–345) representing the major link/end segments of JNK1β1 also show good accordance between native and codon-harmonized frequencies (Fig. 1). Fath et al. [29] recently reported that "multi-parameter DNA sequence optimization" of JNK1 (isoform not specified), although a method that uses a different algorithm to that

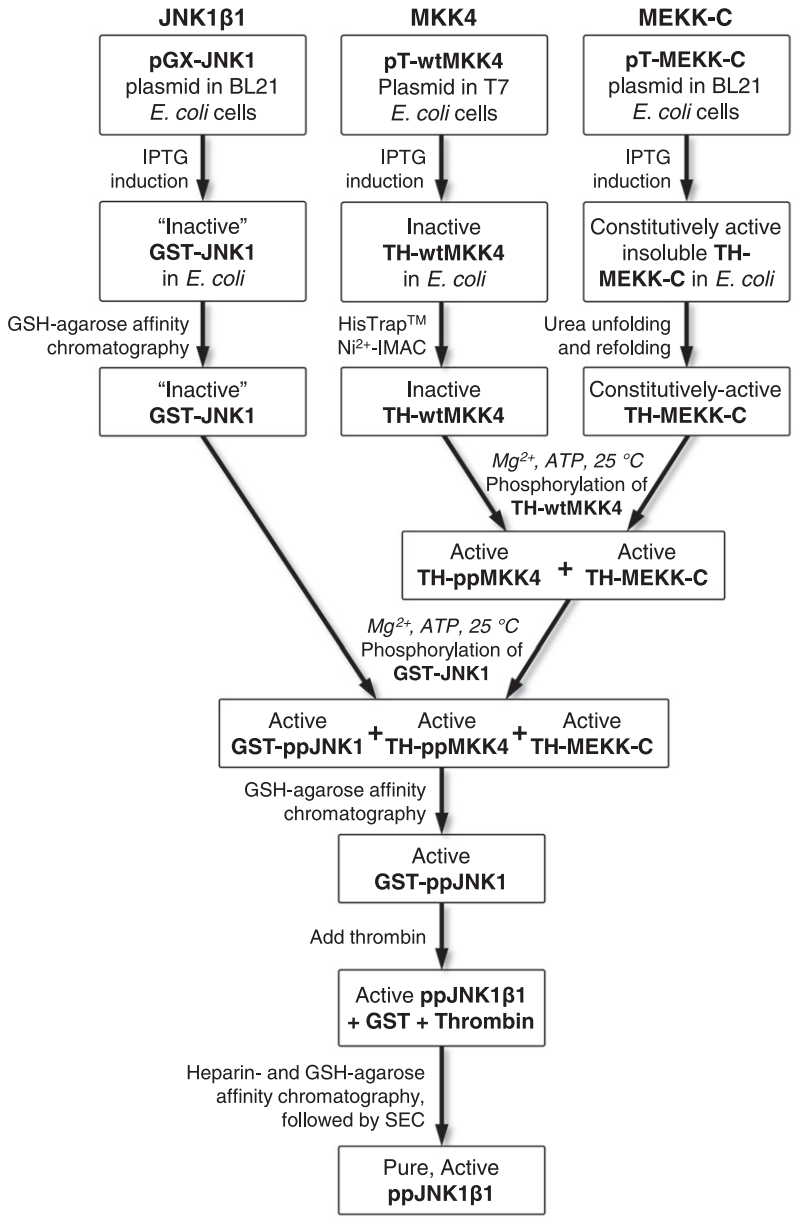

Fig. 3. Outline of the expression, purification and phosphorylation of the MAPK cascade proteins used to produce pure and active JNK1β1. A pGEX-4T-1 plasmid containing JNK1β1 (pGX-JNK1) in *E. coli* BL21(DE3)pLysS cells was induced with IPTG to express soluble, "inactive" GST-JNK1, which was purified using GSH-agarose affinity chromatography ("inactive" indicates that partial phosphorylation of GST-JNK1 occurred during expression). Concurrently, pET-32a plasmids containing wild-type MKK4 (pT-wtMKK4) in *E. coli* T7 Express I^q cells, and constitutively-active MEKK1 (MEKK-C) (pT-MEKK-C) in *E. coli* BL21(DE3)pLysS cells, were induced to express inactive TH-wtMKK4 and active TH-MEKK-C, respectively. Inactive TH-wtMKK4 was purified using HisTrap™ Ni^{2+}-IMAC, while the insoluble yet constitutively-active TH-MEKK-C was purified by urea unfolding and refolding. Inactive TH-wtMKK4 was then mixed with active TH-MEKK-C as well as $MgCl_2$ and ATP, and incubated overnight at 25 °C to phosphorylate and activate TH-wtMKK4. The activated upstream-kinase mixture was mixed with inactive GST-JNK1, along with $MgCl_2$ and ATP, and incubated at 25 °C until the JNK1β1 was fully phosphorylated. The active MAP kinase mixture was then subjected to GSH-agarose affinity chromatography to isolate active GST-ppJNK1. Thrombin was added to GST-ppJNK1 to cleave the GST-tag, and the thrombin and GST removed by heparin- and GSH-agarose affinity chromatography, respectively. SEC was then performed to obtain pure and active ppJNK1β1.

employed here, increased the production of soluble kinase by 2.6-fold compared to the wild-type gene.

Unfortunately, due to the lack of a non-codon harmonized JNK1β1 gene fragment control to compare with, the soluble protein expression observed within the system employed cannot be ascribed to the codon harmonization process alone. Nonetheless, there was at least a 2-fold improvement in the soluble overexpression of JNK1β1 over that produced from previous attempts reported in the literature [16–19].

To further improve the production of soluble JNK1β1, the degree of expression of soluble GST-JNK1 was examined under many different combinations of experimental conditions (see Materials and methods). It was established that induction with a final IPTG concentration of 0.6 mM for a period of 6 h at 22 °C, expressed in BL21(DE3)pLysS cell cultures in 2 × YT media would result in the highest yield of soluble GST-JNK1, although substantial amounts of the insoluble form was also expressed under these conditions (Fig. 4 and Supplementary Fig. S10). That there is a degree of insoluble overexpression and that different degrees of soluble JNK1β1 production occur when expressed under different bacterial culture conditions (e.g. complete and considerable insoluble overexpression occurred at 37 °C; see Supplementary Fig. S10) indicates that

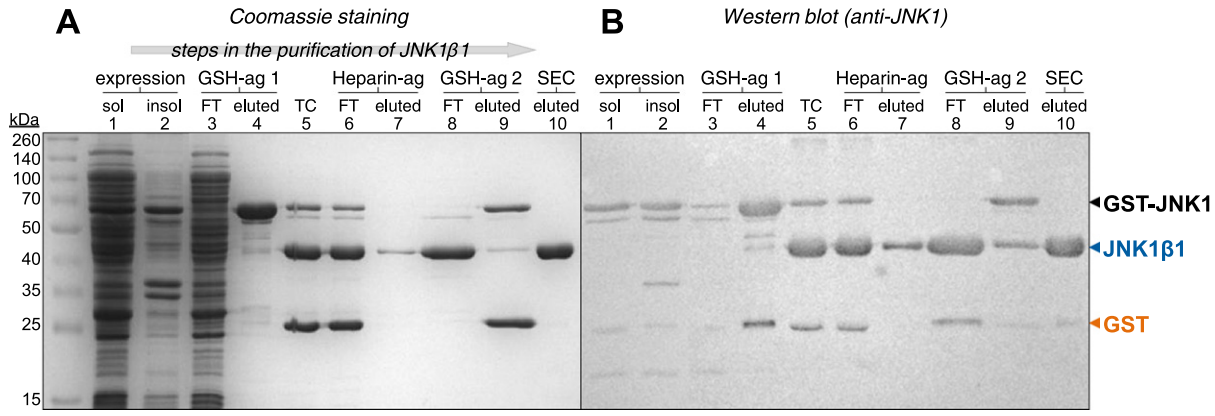

Fig. 4. Expression and purification of JNK1β1. (A) 12.5% acrylamide SDS–PAGE and (B) Western blot analyses of the purification procedure (employing anti-JNK1 antibodies for detection of GST-JNK1 fusion and JNK1β1) illustrated that upon efficient soluble overexpression and purification of GST-JNK1 by GSH-agarose (GSH-ag) affinity chromatography (lanes 1 and 4, respectively), cleavage of the 65 kDa fusion by thrombin (TC) was successful (lane 5). The contaminating thrombin (undetectable) and GST tag (27 kDa) proteins remaining were then separated from JNK1β1 (44 kDa) using heparin-agarose (Heparin-ag) affinity chromatography (lane 6), followed by a second GSH-agarose affinity chromatography step (lane 8) for the removal of thrombin and GST, respectively. Only small quantities of JNK1β1 bound to either column (lanes 7 and 9) and the contaminants that still remained were effectively removed by size-exclusion chromatography (SEC), resulting in large yields of highly pure JNK1β1 (lane 10). Densitometric analysis revealed that the resulting protein solution comprised >99% JNK1β1.

mechanisms other than rates of translation are affecting the co-translational folding [21]. For example, the expression of JNK1β1 at the lower temperature of 22 °C may have reduced the kinetics of off-pathway protein aggregation (which occurs increasingly at 37 °C) relative to its folding reaction, resulting in higher yields of properly folded JNK1β1 [30].

Protein solubility may have also been enhanced by expressing the recombinant protein as a fusion with the highly soluble polypeptide GST. Not only does it allow for its simple purification, the high solubility of GST has been shown to impart to the hybrid a lower propensity to aggregate [31].

The combination of regulation of JNK1β1 translation kinetics through codon harmonization and the alteration in the kinetics of its folding by a reduced cultivation temperature of 22 °C, as well as its concurrent expression with the highly soluble GST, may thus be major complementary factors that possibly facilitated the redirection of the previously insoluble to soluble overexpression of JNK1β1.

Purification of human JNK1β1 and ATF2

Upon optimizing the soluble overexpression of both GST-JNK1 and GST-ATF2, each fusion and their respective target proteins (JNK1β1 and ATF2) were purified according the same protocol; a simple method that can be easily employed when using the GST-fusion system to purify target proteins (Fig. 3). The large quantities of each GST-fusion protein present within the soluble *E. coli* cell fractions after expression were isolated using GSH-agarose affinity chromatography, with only small amounts unable to bind and lost in the flow-through (Figs. 4 and 5). After eluting each fusion, the optimal time that GST-JNK and GST-ATF2 needed to be incubated with thrombin for the complete cleavage of each target from the GST tag (while also preventing their degradation) was determined in a thrombin cleavage time trial (see Supplementary Information and Figs. S11–S13 for the results and discussion of these trials). Upon efficient cleavage of each fusion, the contaminating thrombin and GST tag proteins remaining were effectively separated from the JNK1β1 and ATF2 targets (Figs. 4 and 5). The small, undetectable quantity of thrombin was assumed confidently to have been removed by efficient binding to the heparin column, as no further undesirable proteolytic degradation of JNK1β1 (see Supplementary Information) took place after purification and within the weeks thereafter. Although a small proportion of the JNK1β1 bound to the heparin- and GSH-agarose columns, the majority of JNK1β1 was present within the eventual flow-through (Fig. 4). Any additional contaminants remaining were then effectively removed by Sephacryl S-200 SEC. Densitometric analysis of the SDS–PAGE purification profiles revealed that the final purity of both JNK1β1 and ATF2 after SEC was >99% pure, with final yields of ±60 mg and ±8 mg of protein/liter of *E. coli* culture, respectively (Table 1). This is significant when considering that recent studies were able to purify JNK1 (of various isoforms) in the lower range of 20–50 mg protein/liter culture, and with slightly less purity [18]. The expression and purification system described within this study is thus an effective means of acquiring high levels of JNK1β1.

Expression and purification of MEKK-C and MKK4 variants

In an effort to obtain large quantities of dually phosphorylated JNK1β1, two alternate methods were employed. Within the first approach, we attempted to generate a constitutively-active MKK4 that does not require phosphorylation by upstream kinases to become active, as reported by [32]. To this end, a phosphomimetic form of MKK4 (S257E/T261D) was produced through site-directed mutagenesis by substituting its phosphorylatable residues (S257 and T261) with negatively charged residues (glutamate and aspartate, respectively) that mimic the geometry and charge of the phosphoserine and phosphotheronine (Supplementary Fig. S5). The alternate approach entailed the purification and use of the constitutively-active C-terminal kinase fragment of MEKK1, termed MEKK-C, to first phosphorylate and activate MKK4. Active ppMKK4 would then be used to dually phosphorylate JNK1β1.

In order to purify the wild-type and phosphomimetic variants of MKK4, each were expressed with a thioredoxin-His_6 fusion-tag on their N-terminus (Fig. 2), allowing their purification by HisTrap™ Ni^{2+}-IMAC (Fig. 6). Significant soluble overexpression of each was achieved after testing many expression conditions, assisted possibly by the presence of the thioredoxin tag, with only slightly higher quantities of insoluble MKK4 being produced (Fig. 6). Almost all of each MKK4 variant bound to the HisTrap™ column with little found in each flow-through, yet a small degree of both proteins were washed off during the necessary low concentration imidazole wash. Nevertheless, upon elution, both TH-wtMKK4 and TH-pmMKK4 were purified to sufficiently high purity (Fig. 6) with total yields of ±13 mg protein/L culture (Table 1).

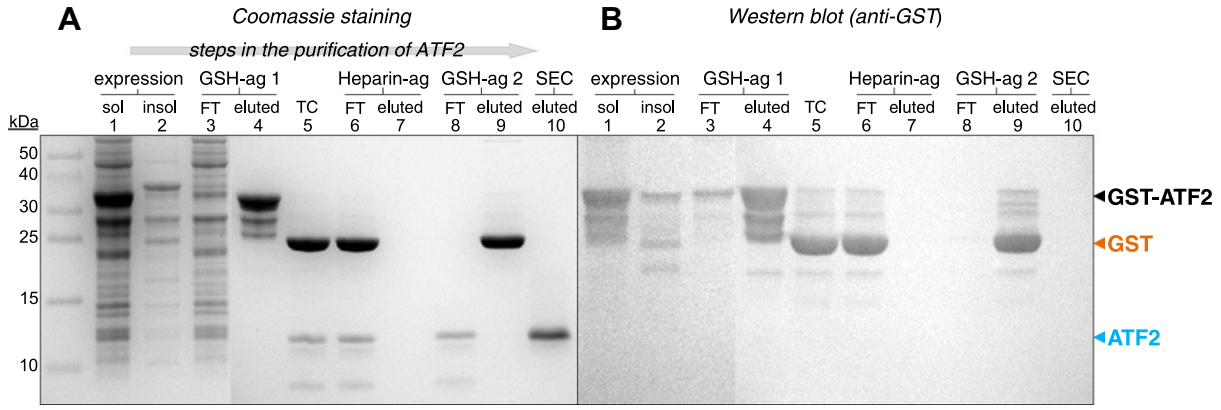

Fig. 5. Expression and purification of ATF2. Samples taken at each step of the purification of ATF2 (17–96) were analyzed by (A) 16% acrylamide Tricine–SDS–PAGE and (B) Western blot (employing anti-GST antibodies for detection of GST-ATF2 fusion) and illustrated that the success of each step was comparable to that of the identical protocol used for JNK1β1 (see Fig. 3 legend). In brief; Lane 1 and 2 – soluble and insoluble cell fraction, respectively, showing the extensive soluble overexpression of GST-ATF2 (35 kDa); Lanes 3 and 4 – flow-through (FT) and eluted samples from the first GSH-agarose (GSH-ag) affinity chromatography step for purification of GST-ATF2; Lane 5 – after 6 h thrombin cleavage (TC) of purified GST-ATF2, demonstrating its successful cleavage; Lanes 6 and 7 – FT and eluted samples from Heparin-agarose (Heparin-ag) affinity chromatography for removal of thrombin (undetectable); Lane 8 and 9 – FT and eluted samples from the second GSH-ag affinity chromatography step, showing the successful removal of the GST tag (27 kDa); Lane 10 – ATF2 after the final size-exclusion chromatography (SEC) step, illustrating the resulting high purity of ATF2.

Table 1
Final yields of the JNK MAPK cascade proteins after purification.

Purified protein	Yield (mg protein/L of culture)
MEKK-C	3
MKK4 (both wt and pm variants)	13
JNK1β1	60
ATF2	8

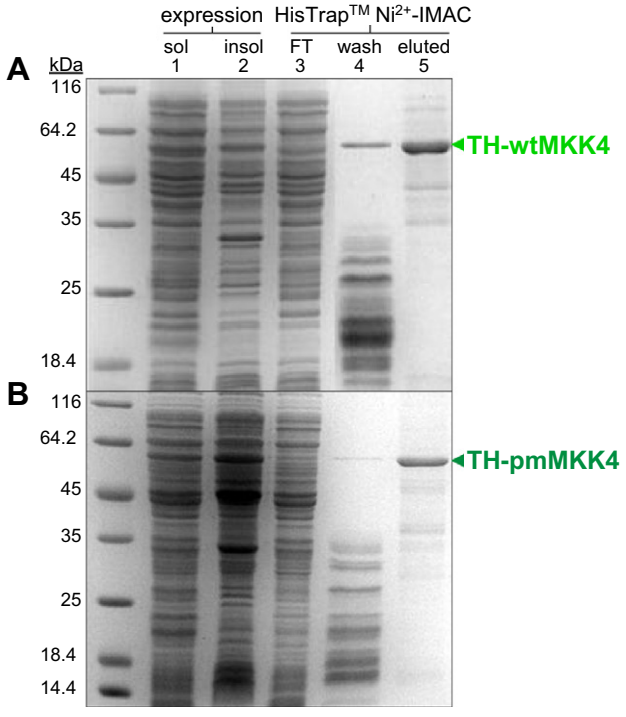

Fig. 6. Expression and purification of the MKK4 variants. 12.5% acrylamide SDS–PAGE analyses of the purification procedures of the (A) TH-wtMKK4 and (B) TH-pmMKK4 variants (62 kDa each) illustrate that although both MKK4s are expressed largely in an insoluble form (lane 2), large quantities of the solubly expressed protein (lane 1) were isolated using HisTrap™ Ni^{2+}-IMAC (lane 5) employing their His_6-tag. The flow-throughs (FT) of both variants (lane 3) indicates that while the majority of each bound to the HisTrap™ column, a small degree of each was removed during the necessary low concentration imidazole wash (lane 4).

During the optimization of MEKK-C overexpression, unfortunately only insignificant quantities of soluble TH-MEKK-C were produced under the expression conditions screened (Fig. 7). The thioredoxin tag did not therefore assist in promoting the soluble overexpression of MEKK-C. However, due to the extensive quantities of insoluble TH-MEKK-C fusion consistently expressed by this plasmid, purification by urea refolding was reasoned to be an achievable means of obtaining functional MEKK-C for the phosphorylative activation of MKK4. Upon overexpression of insoluble TH-MEKK-C and washing the resulting pelleted insoluble cell fraction with 2% deoxycholate, the insoluble cell fraction was well solubilized in 6.5 M urea. This fraction contained large amounts of unfolded and solubilized TH-MEKK-C (Fig. 7). During its subsequent refolding by dialysis and dilution into lower concentration of urea, notable quantities of TH-MEKK-C were lost through aggregation when the urea concentration was dropped to 1 and 0 M urea (Fig. 7). Nevertheless, since only small concentrations of the upstream kinase are required for the activation of MKK4, sufficient quantities of refolded, soluble and adequately pure TH-MEKK-C (at a yield of ±3 mg/L culture; Table 1) was remaining for this purpose (Fig. 7).

Preparation of inactive (dephosphorylated) and active (phosphorylated) JNK1β1

Within our first attempts to phosphorylate GST-JNK1 using active MKK4, it was revealed that even before the purified GST-JNK1 fusion had encountered the components thought necessary for activation (i.e. before the addition of active MKK4, ATP, or $MgCl_2$), JNK1β1 already exhibited a significant degree of dual phosphorylation (initial trial data not shown, but see Fig. 8). In order to elucidate the means by which this JNK1 isoform is already partially phosphorylated without additional *in vitro* modifications or treatment after purification from *E. coli*, a few further experiments were conducted;

To determine whether JNK1β1 was undergoing phosphorylation within the *E. coli* BL21(DE3)pLysS cells during overexpression, samples of the soluble and insoluble cell lysates were tested for dually phosphorylated GST-JNK1 (Fig. 8). Phosphorylated JNK1β1 was indeed detected in large quantities in the soluble cell fraction, comprising almost all of the soluble JNK1β1 expressed, while only

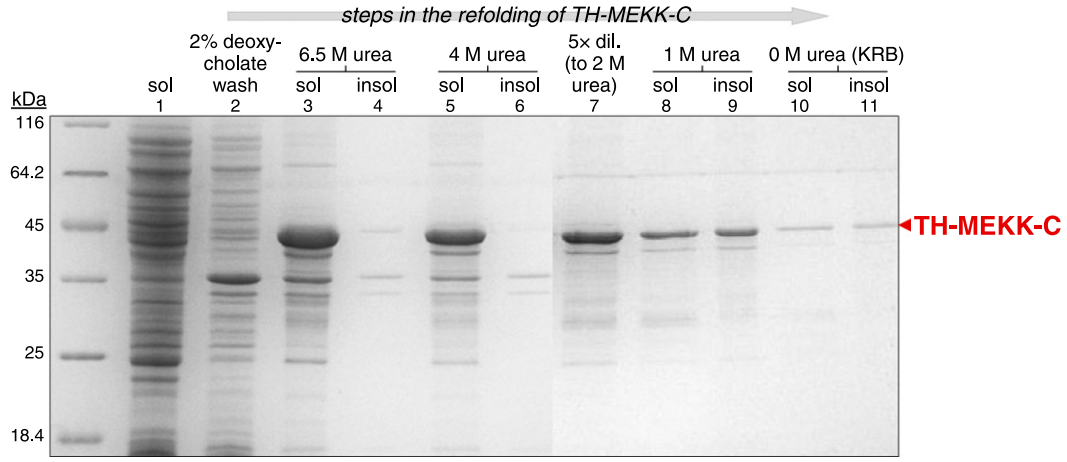

Fig. 7. Expression and purification of MEKK-C. Since little TH-MEKK-C (43 kDa) was expressed in a soluble form (lane 1), urea refolding of the large quantities of insolubly expressed TH-MEKK-C was performed for its purification. After expression of insoluble TH-MEKK-C and washing the resulting insoluble cell lysate with 2% deoxycholate (lane 2), the remaining insoluble protein comprising large amounts of TH-MEKK-C was well solubilized in 6.5 M urea (lane 3 and 4). In the course of refolding the denatured TH-MEKK-C (lanes 5 through to 11), steadily less soluble kinase was available as protein was lost by aggregation, particularly when the urea concentration was dropped to 1 M and 0 M urea (Kinase-Reaction Buffer; KRB) (lanes 10 and 11). Nonetheless, adequate quantities of soluble TH-MEKK-C were available once refolding was complete (lane 10). Efforts were made to analyse the relative amounts of protein that was available after each step of the refolding.

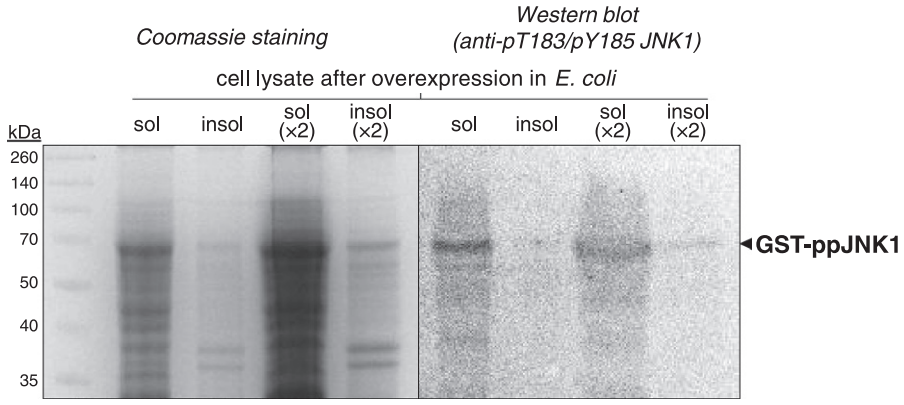

Fig. 8. JNK1β1 is phosphorylated in *E. coli* BL21(DE3)pLysS during expression. Western blot analyses of the soluble and insoluble bacterial cell lysates after overexpression of GST-JNK1 employing anti-pT183/pY185 JNK1 antibodies illustrates that a large quantity of dually phosphorylated JNK1β1 is present in the soluble cell fraction, with little occurring in the insoluble fraction. This indicates that JNK1β1 is phosphorylated during production in *E. coli* BL21(DE3)pLysS cells.

a small degree of the population of insoluble JNK1β1 exhibited phosphorylation (Fig. 8).

To confirm that the untreated JNK1β1 was in fact already phosphorylated, and to test that the monoclonal anti-pT183/pY185 JNK1 antibodies that we employed indeed bind their specified residues only when they are phosphorylated, we dephosphorylated GST-JNK1 using the non-specific phosphatase Shrimp Alkaline Phosphatase (SAP), and monitored the reaction overtime by Western blotting analysis using the anti-pT183/pY185 JNK1 antibodies. This would also ensure that we could generate completely non-phosphorylated JNK1β1 for future comparative studies of its active and inactive forms. We found that SAP is able to dephosphorylate the untreated GST-JNK1 within 5 h (Fig. 9B), with the intensity of the anti-ppJNK1 bands before and after treatment with SAP indicating a drastic decrease in the population of active JNK1β1 (Figs. 9B and 10). This verified that the antibody binds only the phosphorylated form of T183/Y185 of JNK1β1 (and not non-specifically to their unmodified form), and proved that the kinase had been phosphorylated by some means within *E. coli*. Following this, the GST-JNK1 was isolated from SAP by GSH-agarose affinity chromatography (confirmed by the ability to later phosphorylate the newly dephosphorylated kinase), and the dephosphorylated JNK1β1 purified as described.

There are a few possibilities why JNK1β1 may become phosphorylated during expression in *E. coli*. It is a well-known observation that many kinases undergo autophosphorylation during heterologous protein expression. It has been suggested that as the expression host is inundated with recombinant protein during overexpression from strong promoters, the high concentrations of inactive kinase are able to phosphorylate the newly-produced kinase polypeptides during co-translational or post-translational, cytoplasmic folding [33]. In this way, phosphate groups may be introduced at both the natural canonical sites of phosphorylation (at the known T/S/Y residues of the activation loop whose phosphorylation enables kinase activation), and/or at non-standard yet sites that may or may not be surface exposed at all. Due to the inaccessibility of some of the phospho-residues upon final folding of the protein, these phosphate groups may not be able to be removed by subsequent treatment with phosphatases, or cannot be achieved during *in vitro* autophosphorylation experiments (i.e. the fully folded protein cannot catalyse these phosphorylations on themselves *in vitro*) [34,35].

Shrestha et al. [33] analyzed the conditions under which specific human kinases (including a brief analysis of JNK1α1) exhibited autophosphorylation during bacterial overexpression. They showed that reducing the rate of protein production by either low-

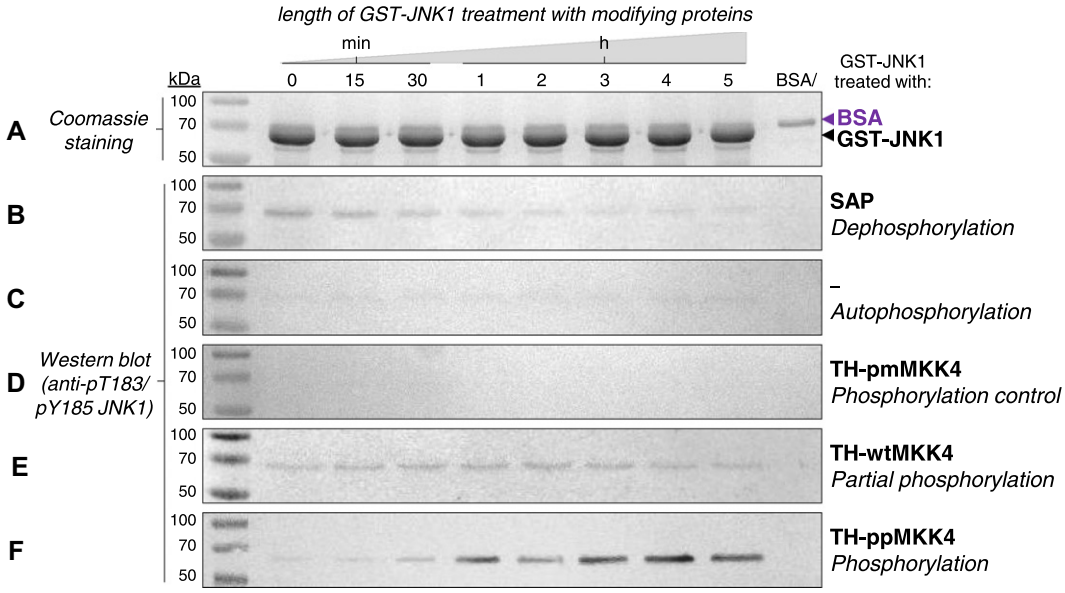

Fig. 9. Preparation of dephosphorylated and phosphorylated GST-JNK1 using SAP and MKK4 variants respectively; (A) Coomassie blue staining to indicate the total, consistent amounts of GST-JNK1 (10 μM), BSA (0.2 mg/ml) and modifying enzyme (SAP or MKK4 variant) in each reaction over time. (B-F) Western blot analysis of each reaction profile employing anti-pT183/pY185 JNK1 antibodies to detect dually phosphorylated JNK1β1; (B) Dephosphorylation of unmodified GST-JNK1 (purified from *E. coli*) by SAP, illustrating that at 25 °C, partially-phosphorylated GST-JNK1 is dephosphorylated within 5 h. (C) Reaction control for potential autophosphorylation, indicating that 10 μM GST-JNK1 does not phosphorylate itself over time at 25 °C. (D) Inactive, phosphomimetic TH-pmMKK4 negative phosphorylation control, demonstrating that phosphomimetic MKK4 is unable to phosphorylate GST-JNK1, and is thus not constitutively-active *in vitro*. (E) Partial phosphorylation of GST-JNK1 by unmodified TH-wtMKK4, indicating that TH-wtMKK4 may become partially active by phosphorylation during expression in *E. coli*. (F) Dual phosphorylation of GST-JNK1 by active, TH-ppMKK4 (previously activated by MEKK-C). JNK1β1 is completely phosphorylated within 3 h of incubation with 1 μM TH-ppMKK4 at 25 °C.

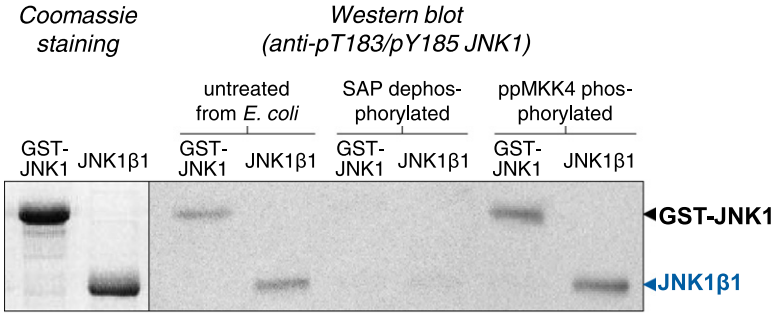

Fig. 10. Summary of JNK1β1 phosphorylation states. To demonstrate the relative degree of phosphorylation before and after treatment of unmodified, partially-phosphorylated GST-JNK1 with the modifying enzymes SAP and ppMKK4, and to illustrate the success of the dephosphorylation and re-phosphorylation respectively, Western blotting was used to analyze samples of these GST-JNK1 modifications. The JNK1β1 resulting from the subsequent processing of their corresponding modified GST-JNK1 is included to illustrate that the phosphorylation state of JNK1β1 is unaltered during the subsequent processing.

ering the induction temperature and/or inducer concentration leads to a reduction in the level of phosphorylation during expression, and suggested that proteins that fold "faster" may be less susceptible to autophosphorylation at internal sites [33].

The phosphorylation of JNK1β1 observed during overexpression within this current study may thus be the product of this "co-folding autophosphorylation" phenomenon. Since this has not been observed or reported to a large extent during the overexpression of JNK1 elsewhere, we believe that the unique translation and folding kinetics of our JNK1β1 provided by the codon harmonization of its open reading frame performed here, may have allowed for the observed phosphorylation to occur during co-translational folding.

Nevertheless, as we were able to efficiently dephosphorylate JNK1β1 after purification (Fig. 9B), optimizing the expression conditions to minimize this phosphorylation was unnecessary, especially when maximizing the overall production of soluble protein was of most importance. As illustrated by Shrestha et al. [33], expression of JNK1β1 at the lower temperatures used (22 °C) may be best in minimizing the cellular phosphorylation anyway.

We can also now not discount the fact that other endogenous bacterial *E. coli* S/T/Y protein kinases may be catalyzing the observed JNK1β1 phosphorylation while within the expression host. A recent growing body of evidence indicates that, while relatively few kinases capable of phosphorylating proteins at S/T/Y residues have been directly identified in *E. coli*, more than 80 bacterial proteins are naturally phosphorylated on S/T/Y residues [36]. Given the recently realized potential for eukaryotic-like kinases in *E. coli* to phosphorylate proteins at these residues, we now cannot assume that eukaryotic proteins expressed in bacterial cells will purify in a homogenous nonphosphorylated form [36]. Therefore, it may be possible that *E. coli* protein kinases are recognizing JNK1β1 in a manner that is comparable to the recognition by its natural activator, MKK4, thereby enabling the dual phosphorylation displayed. As this has not been observed or reported before, this possible means of phosphorylation would also occur during co-translational folding, since the novel yet natural translation kinetics of JNK1β1 provided here through codon harmonization may now allow the *E. coli* kinases to recognize phos-

phorylatable motifs during their translation and subsequent folding.

To determine whether the potential autophosphorylation we observed during JNK1β1 overexpression was occurring during folding of newly synthesized JNK1β1 polypeptides (co-translationally), or between fully-folded native JNK1β1 proteins (post-translationally), *in vitro* autophosphorylation experiments were performed. Here we incubated dephosphorylated GST-JNK1 at both low (10 μM; Fig. 9C) and high concentration (60 μM; data not shown) to mimic the high concentrations of protein that may exist in the cell during overexpression, with only BSA, $MgCl_2$, and ATP, at 25 °C, and monitored the potential phosphorylation over time. Notably, the temperature at which the autophosphorylation was performed was similar to that at which the GST-JNK1 was expressed (25 vs. 22 °C), eliminating temperature-dependant factors affecting the autophosphorylation analysis. Western blot analysis demonstrates that native JNK1β1 does not phosphorylate itself (autophosphorylate) *in vitro* in the absence of its activating upstream kinases under the conditions tested, at neither low (Fig. 9C) nor high concentrations. Concentrations higher than 60 μM JNK1β1 could not be achieved for extended periods due to the instability of the kinase and its tendency to aggregate.

Investigating the autophosphorylation activity of all 10 JNK isoforms, Tsuiki et al. [37] discovered that only 5 isoforms exhibit autophosphorylation in the absence of upstream kinase, the strongest activity of which was presented by the four JNK2 isoforms (in order of autophosphorylation activity strength; JNK2α2 > JNK2β2 > JNK2α1 > JNK2β1, with JNK3α2 showing very little activity). Importantly though, not a single isoform of JNK1 demonstrated even the slightest autophosphorylation activity [37]. Cui [38] proceeded to illustrate that the ability of JNKs to autophosphorylate depends on the amino acids at position 218–226 between subdomain IX and X. Specifically, they found that the amino acid sequence LVKGCVIFQ at that position in JNK2α2 is crucial for its autophosphorylation, and the C-terminal extension present the in α2/β2 isoforms (residues 383–424) drastically enhance autophosphorylation [38]. It is therefore to be expected that JNK1β1, a JNK1 isoform that do not possess neither the C-terminal extension nor the required amino acids at position 218–226 (having MIKGGVLFP), does not display autophosphorylation *in vitro* in this study. These results then affirm that if the JNK1β1 phosphorylation that we observe during expression is due to autophosphorylation, this process occurs during the now naturalized co-translational folding of the kinase, and not post-translationally between native JNK1β1 molecules. Moreover, since phosphorylated JNK1β1 was only detected in the soluble cell fraction, is it possible that either the co-translational phosphorylation of JNK1β1 promotes it to fold into a soluble state by shifting it onto its native folding pathway, or perhaps only those JNK1β1 polypeptides presently following the native folding pathway are able to be phosphorylated during translational.

Upon generating non-phosphorylated JNK1β1 and eliminating the possibility of *in vitro* autophosphorylation, we sought to generate dual phosphorylated, fully active JNK1β1. The first means by which we attempted to achieve this was by using a phosphomimetic variant of MKK4 (S257E/T261D) (TM-pmMKK4) that has been reported previously to be a constitutively-active in transfected cells (*in vivo*) [32]. Upon incubating dephosphorylated GST-JNK1 with TH-pmMKK4 *in vitro* however, no JNK1β1 phosphorylation (using several experimental conditions) was detectable over time (Fig. 9D). The phosphomimetic S257E/T261D MKK4 variant is thus unable to catalyse the *in vitro* dual phosphorylation of JNK1β1, implying that the phosphomimetic, now non-phosphorylatable (glutamate and aspartate) residues in fact eradicate all *in vitro* kinase activity so that it becomes constitutively-inactive. Nevertheless, the pmMKK4 variant thereafter acted as a useful negative control for JNK1β1 phosphorylation by MKK4, re-highlighting the incidence of phosphorylation of kinases during heterologous expression when we later analyzed wild-type MKK4 (see below). Therefore, although pmMKK4 may be active *in vivo*, phosphomimetics cannot be employed to effectively generate perpetually active MKK4 for use in downstream *in vitro* protein phosphorylation applications.

The next approach by which we generated active, dual phosphorylated JNK1β1 entailed the reconstitution of the full JNK MAPK cascade *in vitro*, in which we used constitutively-active MEKK-C to activate MKK4, which in turn was used to phosphorylate JNK1β1 (Fig. 2 and Fig. 3). To assess the success of the subsequent phosphorylative activation of MKK4 by MEKK-C, and to control for the effect that unmodified wild-type MKK4 has on JNK1β1, we first incubated untreated TH-wtMKK4 with dephosphorylated GST-JNK1, and monitored the change in the state of JNK1β1 phosphorylation over time. Interestingly, we detected a slight degree of JNK1β1 phosphorylation by the wild-type MKK4 that had not been treated with MEKK-C (Fig. 9E). This indicates that when recombinantly expressed in *E. coli*, wild-type MKK4 also becomes phosphorylated to a small degree (by any of the means discussed) as observed for JNK1β1. The level of cellular phosphorylative activation of TH-wtMKK4 was consistently low however, as the effectiveness of JNK1β1 phosphorylation was poor (Fig. 9E). Nevertheless, this fact reiterated the importance of evaluating the homogeneity and phosphorylation state of heterologously expressed proteins before performing downstream analyses that may be influenced by these undesired modifications.

Efficient activation of JNK1β1 was then achieved by incubating TH-ppMKK4 that had been previously activated by overnight incubation with TH-MEKK-C, with dephosphorylated GST-JNK1 (Fig. 3). Monitoring its activation with anti-ppJNK1 antibodies, it was demonstrated that full phosphorylation of JNK1β1 was reached within 3 h (Fig. 9F). As Thevenin et al. [18] confirmed confidently that active MKK4 alone is able to phosphorylate both T183 and Y185 in the activation loop of JNK1 as reported originally by Lawler et al. [11], we felt it adequate to assume that both residues were phosphorylated in our activation of JNK1β1. Furthermore, it is also significant that previously SAP-dephosphorylated GST-JNK1 is able to be re-phosphorylated by TH-ppMKK4, confirming the initial successful removal of SAP and its innocuous effect on JNK1β1.

Upon dual phosphorylation of GST-JNK1, active TH-ppMKK4 and TH-MEKK-C were efficiently removed by passing the mixture through GSH-agarose affinity chromatography, where after the active, phosphorylated JNK1β1 was purified as described (Fig. 3). Western blot analysis was thereafter used to confirm that the final phosphorylation state of each JNK1β1 resulting from the subsequent cleavage and processing of their corresponding modified GST-JNK1 fusion (dephosphorylated or phosphorylated) remained unaltered during the final steps of its purification (Fig. 10). We also intend however to use mass spectrometry to identify and confirm the phosphorylation states of the JNK1β1 species described above.

Determination of JNK1β1 specific activity

To determine the specific activity of phosphorylated JNK1β1 we measured the depletion of ATP during the dual phosphorylation of it substrate, ATF2, using an ATP Bioluminescent Assay Kit (Sigma). To calculate the rate at which JNK1β1 uses ATP to phosphorylate ATF2 as a specific activity (in μmol of ATF2/min/mg of JNK1β1), we first generated an ATP standard curve of the relative bioluminescence intensity of light produced by known concentrations of ATP (Fig. 11A). After fitting a linear function to the data, the slope (3.38 ± 0.52 bioluminescence intensity (arbitrary units)/μM of ATP, $R^2 = 0.96$) was used in calculations to determine the specific activity of phosphorylated JNK1β1.

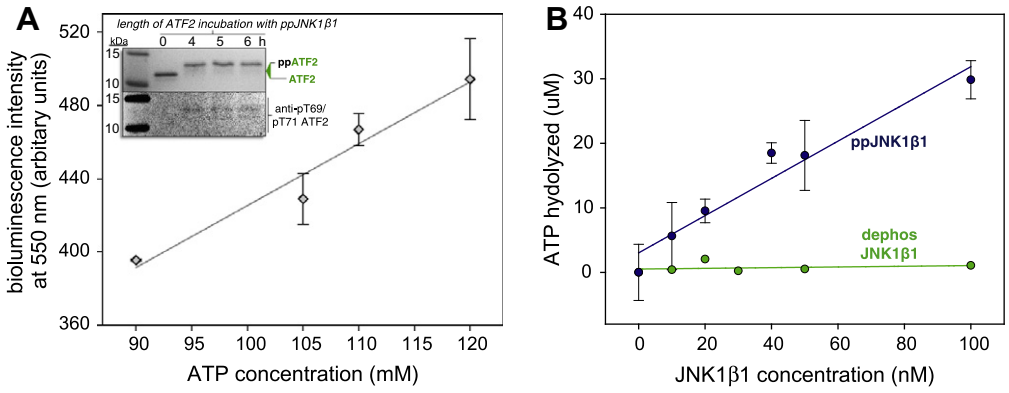

Fig. 11. Determination of the specific activity of JNK1β1. An ATP Bioluminescent Assay Kit was used to determine the specific activity of JNK1β1 by measuring the decrease in bioluminescence intensity as ATP is depleted during the dual phosphorylation of it substrate, ATF2. (A) ATP calibration curve, produced by measuring the relative bioluminescence intensity of 550 nm light generated by 90–120 μM of ATP. The slope of the linear function fit to the data (in bioluminescence intensity/μM of ATP) was used to calculate the amount of ATP hydrolysed at each JNK1β1 concentration in the subsequent kinase assay. The data is the mean of two independent experiments. (B) Level of ATP hydrolysis by different concentrations of JNK1β1 during the phosphorylation of ATF2. The amount of bioluminescence produced was converted to the concentration of ATP hydrolyzed using the slope determined in (A) and the initial concentration of ATP. The data was fit to a linear function and the slope of the ppJNK1β1 curve (in μM of ATP hydrolyzed/nM of JNK1β1), was used to calculate the specific activity of phosphorylated JNK1β1. The ppJNK1β1 kinase assay data is the mean of two independent experiments. The dephosphorylated JNK1β1 kinase assay was performed once merely for comparison, the shallow slope of which indicates that the dephosphorylation efficiently deactivated JNK1β1 and highlights the high activity of phosphorylated JNK1β1. Insert – Phosphorylation of ATF2 by ppJNK1β1 was confirmed by Western blot (using monoclonal anti-pT69/pT71 ATF2 antibodies), and the electrophoretic shift of the phosphorylated form of ATF2 observed during 16% Tricine–SDS–PAGE. 30 μM ATF2 was incubated with 1 μM ppJNK1β1 for ⩾4 h at 25 °C.

The specific activity of phosphorylated JNK1β1 was determined to be 3.3 ± 0.4 μmol of ATF2/min/mg of kinase (Fig. 11B), with a k_{cat} value of 2.4 ± 0.3 s^{-1} (calculated by converting the specific activity value from μmol of ATF2/min/mg of kinase to μmol of ATF2/min/μmol of kinase, and dividing by 60 s). The errors reported represent the mean ± standard error. Repeating the activity assay for dephosphorylated JNK1β1 (performing only a single experiment) revealed that this form of the kinase had no significant activity (shallow slope of dephosphorylated JNK1β1, Fig. 11B), and thus that the initial dephosphorylation and inactivation of partially phosphorylated GST-JNK1 by SAP was effective. This also reaffirms that the ability of JNK1β1 to phosphorylate ATF2 is fully re-established when SAP-dephosphorylated JNK1β1 is re-activated by MKK4 phosphorylation. The enzymatic characterization of the JNK1β1 isoform has been performed only once elsewhere, with a reported k_{cat} value of 2.2 ± 0.7 min^{-1} for ATF2 [39]. This value equates to a k_{cat} of approximately 0.04 s^{-1} (converted by dividing by 60), which is more than 60-fold lower than the k_{cat} value for phosphorylated JNK1β1 determined in this study. A possible reason why our JNK1β1 is more active may be due to the efficiency of our *in vitro* kinase phosphorylation reactions. The previous authors employed commercially available active MKK4 and MKK7 for the activation of JNK1β1 [39]. As we prepared dual phosphorylated, active MKK4 ourselves using constitutively (and thus completely and homogenously) -active MEKK-C overnight at 25 °C, we suspect that we generated an almost completely active population of fully phosphorylated MKK4. Employing our active MKK4 in the subsequent *in vitro* activation of JNK1β1 likely allowed for more efficient dual phosphorylation of the downstream kinase, generating a higher population of completely active JNK1β1 than can be achieved by the commercially available MKK4/MKK7. Another possibility for the discrepancy in the k_{cat} values may be the fact that Figuera-Losada and LoGrasso [39] also used a biotinylated Bioease-FLAG tag ATF2 (residues 2–115) construct within their enzymatic assays, where we used untagged ATF2 of a different length (residues 17–96). As the authors did not control for the effect that the large 80 amino acid Bioease(72 residues)-FLAG(8 residues) tag, or the effect that the biotinylation may have on the ability of ATF2 to be phosphorylated, their presence may have influenced the measured activity.

Conclusions

We describe here a purification and activation protocol for JNK1β1 that can be easily applied to any JNK isoform. Precautionary codon harmonization of its open reading frame may have contributed to the significant quantities of soluble JNK1β1 that was overexpressed, yet the lack of a non-harmonized JNK1β1 gene control prevents the increase from being attributed to the codon harmonization process alone. Nonetheless, this study exhibits improvements in the soluble overexpression of JNK1β1 when compared to that produced elsewhere. High yields of >99% pure JNK1β1 was purified and proficiently activated by successfully reconstituting the MEKK1 → MKK4 → JNK MAPK phosphorylation cascade *in vitro*. The methods described therefore provide a potential means for the acquisition of large quantities of the JNK isoforms in their most pure and active form, allowing for many additional biochemical and biophysical studies of the kinases to be performed in the future.

We hope too that these methods will enable the attainment of the elusive crystal structure of phosphorylated, active JNK. Although it is known that JNK is activated by dual phosphorylation of T183 and Y185, the changes in its structure and stability that occur upon phosphorylative activation is not fully understood. The knowledge provided by the crystal structure about the structural basis of its activation would thus be invaluable, and may facilitate the development of therapeutics that may combat the pathological effects of its associated diseases.

Acknowledgments

This work was supported by the University of the Witwatersrand, South African National Research Foundation (Grants: 60810, 65510 and 68898 to H.W.D) and South African Research Chairs Initiative of the Department of Science and Technology and National Research Foundation (Grant 64788 to H.W.D). The authors thank Dr. Melanie Cobb (Texas Southwestern Medical Center) for her gift of the pCMV5myc-MEKKXuA and pGX-KG-MKK4 plasmids.

Appendix A. Supplementary data

Supplementary data associated with this article can be found, in the online version, at http://dx.doi.org/10.1016/j.pep.2012.10.010.

References

[1] L. Chang, Mammalian MAP kinase signaling cascades, Nature 410 (2001) 37–40.
[2] Z. Chen, T.B. Gibson, F. Robinson, L. Silvestro, G. Pearson, B. Xu, A. Wright, C. Vanderbilt, M.H. Cobb, MAP kinases, Chem. Rev. 101 (2001) 2449–2476.
[3] B. Dérijard, M. Hibi, I.H. Wu, T. Barrett, B. Su, T. Deng, M. Karin, R.J. Davis, JNK1, a protein kinase stimulated by UV light and Ha-Ras that binds and phosphorylates the c-Jun activation domain, Cell 76 (1994) 1025–1037.
[4] J.M. Kyriakis, J. Avruch, Protein kinase cascades activated by stress and inflammatory cytokines, BioEssays 18 (1996) 567–577.
[5] B.J. Pulverer, J.M. Kyriakis, J. Avruch, E. Nikolakaki, J.R. Wood-gett, Phosphorylation of c-jun mediated by MAP kinases, Nature 353 (1991) 670–674.
[6] R.J. Davis, Signal transduction by the JNK group of MAP kinases, Cell 103 (2000).
[7] Y.T. Ip, R.J. Davis, Signal transduction by the c-Jun N-terminal kinase transduction by the c-Jun N-terminal kinase (JNK)–from inflammation to development, Curr. Opin. Cell Biol. 10 (1998) 205–219.
[8] A. Minden, M. Karin, Regulation and function of the JNK subgroup of MAP kinases, Biochim. Biophys. Acta 1333 (1997) F85–F104.
[9] J. Cui, M. Zhang, Y. Zhang, Z. Xu, JNK pathway: diseases and therapeutic potential, Acta Pharmacol. Sin. 28 (2007) 601–608.
[10] S. Gupta, T. Barrett, A.J. Whitmarsh, J. Cavanagh, H.K. Sluss, B. Derijard, R.J. Davis, Selective interaction of JNK protein kinase isoforms with transcription factors, EMBO J. 15 (1996) 2760–2770.
[11] S. Lawler, Y. Fleming, M. Goedert, P. Cohen, Synergistic activation of SAPK1/JNK1 by two MAP kinase kinases *in vitro*, Curr. Biol. 8 (1998) 1387–1390.
[12] G.J. Johnson, The c-Jun kinase/stress-activated pathway: regulation, function and role in human disease, Biochim. Biophys. Acta 1773 (2007) 1341–1348.
[13] J. Lisnock, P. Griffin, J. Calaycay, B. Frantz, J. Parsons, S.J. O'Keefe, P. LoGrasso, Activation of JNK3 alpha 1 requires both MKK4 and MKK7: kinetic characterization of *in vitro* phosphorylated JNK3 alpha 1, Biochemistry 39 (2000) 3141–3148.
[14] H. Kishimoto, K. Nakagawa, T. Watanabe, D. Kitagawa, H. Momose, J. Seo, G. Nishitai, N. Shimizu, S. Ohata, S. Tanemura, S. Asaka, T. Goto, H. Fukushi, H. Yoshida, A. Suzuki, T. Sasaki, T. Wada, J.M. Penninger, H. Nishina, T. Katada, Different properties of SEK1 and MKK7 in dual phosphorylation of stress-induced activated protein kinase SAPK/JNK in embryonic stem cells, J. Biol. Chem. 278 (2003) 16595–16601.
[15] Y. Fleming, C.G. Armstrong, N. Morrice, A. Paterson, M. Goedert, P. Cohen, Synergistic activation of stress-activated protein kinase 1/c-Jun N-terminal kinase (SAPK1/JNK) isoforms by mitogen-activated protein kinase kinase 4 (MKK4) and MKK7, Biochem. J. 352 (2000) 145–154.
[16] Q. Zhao, P. Chen, M.E. Manson, Y. Liu, Production of active recombinant mitogen-activated protein kinases through transient transfection of 293T cells, Protein Expr. Purif. 46 (2006) 468–474.
[17] A. Khokhlatchev, S. Xu, J. English, P. Wu, E. Schaefer, M.H. Cobb, Reconstitution of mitogen-activated protein kinase phosphorylation cascades in bacteria. Efficient synthesis of active protein kinases, J. Biol. Chem. 272 (1997) 11057–11062.
[18] A.F. Thévenin, C.L. Zony, B.J. Bahnson, R.F. Colman, Activation by phosphorylation and purification of human c-Jun N-terminal kinase (JNK) isoforms in milligram amounts, Protein Expr. Purif. 75 (2011) 138–146.
[19] J.W. Savopoulos, S. Dowd, C. Armour, P.S. Carter, C.J. Greenwood, D. Mills, D. Powell, G.R. Pettman, O. Jenkins, F.S. Walsh, K.L. Philpott, Expression and purification of functional JNK2beta2: perspectives on high-level production of recombinant MAP kinases, Protein Expr. Purif. 24 (2002) 25–32.
[20] M. Fuhrmann, A. Hausherr, L. Ferbitz, T. Schödl, M. Heitzer, P. Hegemann, Monitoring dynamic expression of nuclear genes in *Chlamydomonas reinhardtii* by using a synthetic luciferase reporter gene, Plant Mol. Biol. 55 (2004) 869–881.
[21] E. Angov, C.J. Hillier, R.L. Kincaid, J.A. Lyon, Heterologous protein expression is enhanced by harmonizing the codon usage frequencies of the target gene with those of the expression host, PLoS Biol. 3 (2008) 1–10.
[22] F.R. Leach, J.J. Webster, Commercially available firefly luciferase reagents, Methods Enzymol. 133 (1986) 51–70.
[23] U.K. Laemmli, Cleavage of structural proteins during the assembly of the head of bacteriophage T4, Nature 227 (1970) 680–685.
[24] H. Schägger, G. von Jagow, Tricine-sodium dodecyl sulfate-polyacrylamide gel electrophoresis for the separation of proteins in the range from 1 to 100 kDa, Anal. Biochem. 166 (1987) 368–379.
[25] H.P. Sørensen, K.K. Mortensen, Soluble expression of recombinant proteins in the cytoplasm of *Escherichia coli*, Microb. Cell Fact. 4 (2005) 1.
[26] H.P. Sørensen, K.K. Mortensen, Advanced genetic strategies for recombinant protein expression in *Escherichia coli*, J. Biotechnol. 115 (2005) 113–128.
[27] C. Kurland, J. Gallant, Errors of heterologous protein expression, Curr. Opin. Biotechnol. 7 (1996) 489–493.
[28] T.A. Thanaraj, P. Argos, Ribosome-mediated translational pause and protein domain organization, Protein Sci. 5 (1996) 1594–1612.
[29] S. Fath, A.P. Bauer, M. Liss, A. Spriestersbach, B. Maertens, P. Hahn, C. Ludwig, F. Schäfer, M. Graf, R. Wagner, Multiparameter RNA and codon optimization: A standardized tool to assess and enhance autologous mammalian gene expression, PLoS ONE 6 (2011) e17596.
[30] G. Georgiou, P. Valax, Expression of correctly folded proteins in *Escherichia coli*, Curr. Opin. Biotechnol. 7 (1996) 190–197.
[31] M. Piatak, J.A. Lane, W. Laird, M.J. Bjorn, A. Wang, M. Williams, Expression of soluble and fully functional ricin A chain in *Escherichia coli* is temperature-sensitive, J. Biol. Chem. 263 (1988) 4837–4843.
[32] Z. Guan, S.Y. Buckman, A.P. Pentland, D.J. Templeton, A.R. Morrison, Induction of cyclooxygenase-2 by the activated MEKK1 → SEK1/MKK4 → p38 mitogen-activated protein kinase pathway, J. Biol. Chem. 273 (1998) 12901–12908.
[33] A. Shrestha, G. Hamilton, E. O'Neill, S. Knapp, J.M. Elkins, Analysis of conditions affecting auto-phosphorylation of human kinases during expression in bacteria, Protein Expr. Purif. 81 (2012) 136–143.
[34] M.A. Seeliger, M. Young, M.N. Henderson, P. Pellicena, D.S. King, A.M. Falick, J. Kuriyan, High yield bacterial expression of active c-Abl and c-Src tyrosine kinases, Protein Sci. 14 (2005) 3135–3139.
[35] R. Kinstrie, N. Luebbering, M.-S. Diego, G. Sibbet, J. Han, P.A. Lochhead, V. Cleghon, Characterization of a domain that transiently converts class 2 DYRKs into intramolecular tyrosine kinases, Sci. Signal. 3 (2009) ra16.
[36] B. Macek, F. Gnad, B. Soufi, C. Kumar, J.V. Olsen, I. Mijakovic, M. Mann, Phosphoproteome analysis of *E. coli* reveals evolutionary conservation of bacterial Ser/Thr/Tyr phosphorylation, Mol. Cell. Proteomics 2 (2008) 299–307.
[37] H. Tsuiki, M. Tnani, I. Okamoto, L.C. Kenyon, D.R. Emlet, M. Holgado-Madruga, I.S. Lanham, C.J. Joynes, K.T. Vo, A.J. Wong, Constitutively active forms of c-Jun NH_2-terminal kinase are expressed in primary glial tumors, Cancer Res. 63 (2003) 250–255.
[38] J. Cui, M. Holgado-Madruga, W. Su, H. Tsuiki, P. Wedegaertner, A.J. Wong, Identification of a specific domain responsible for JNK2α2 autophosphorylation, J. Biol. Chem. 280 (2005) 9913–9920.
[39] M. Figuera-Losada, P.V. LoGrasso, Enzyme kinetics and interaction studies for human JNK1β1 and substrates activating transcription factor 2 (ATF2) and c-Jun N-terminal kinase (c-Jun), J. Biol. Chem. 287 (2012) 13291–13302.

High yield purification of JNK1β1 and activation by *in vitro* reconstitution of the MEKK1 → MKK4 → JNK MAPK phosphorylation cascade

GAVIN R. OWEN, IKECHUKWU ACHILONU, AND HEINI W. DIRR

Protein Structure-Function Research Unit, School of Molecular and Cell Biology,
University of the Witwatersrand, Johannesburg 2050, South Africa.

APPENDIX A.

SUPPLEMENTARY MATERIAL

- Table of Contents -

Table S1. Illustration of the *JNK1β1* codon harmonization process. The procedure for recoding the *JNK1β1* open reading frame to fully harmonize its codon usage frequencies for expression in *E. coli* is illustrated using the codons encoding its first twenty amino acids (M1-F20).

Native host data					**Method of recoding *JNK1β1* for expression in *E. coli***								**Recoded *JNK1β1* DNA**	
***H. sapiens JNK1β1* open reading frame**					**Nearest lower frequency codon**		**Nearest higher frequency codon**		**Nearest matching frequency codon**		**Harmonized codon**		**Full harmonization**	
Residue number	Amino acid	Codon	Usage frequency in *H. sapiens* (%)	Usage frequency in *E. coli* (%)	Codon	Usage frequency (%)	Codon	Usage frequency (%)	Codon	Usage frequency (%)	Codon	Usage frequency (%)	Synonymous codon changes (X)	Usage frequency in *E. coli* (%)
1	Met	ATG	100	100	ATG	100	ATG	100	ATG	100	ATG	100	—	100
2	Ser	AGC	100	100	TCC	92	AGC	100	AGC	100	AGC	100	—	100
3	Arg	AGA	100	5	CGC	100	CGC	100	CGC	100	CGC	100	CGC	100
4	Ser	AGC	100	100	AGC	100	AGC	100	AGC	100	AGC	100	—	100
5	Lys	AAG	100	37	AAA	100	AAA	100	AAA	100	AAA	100	AAA	100
6	Arg	CGT	38	82	CGA	16	CGT	82	CGA	16	CGA	16	CGA	16
7	Asp	GAC	100	54	GAT	100	GAT	100	GAT	100	GAT	100	GAT	100
8	Asn	AAC	100	100	AAC	100	AAC	100	AAC	100	AAC	100	—	100
9	Asn	AAT	89	89	AAT	89	AAT	89	AAT	89	AAT	89	—	89
10	Phe	TTT	85	100	TTC	75	TTT	100	TTC	75	TTC	75	TTC	75
11	Trp	TAT	79	100	—		TAT	100	TAT	100	TAT	100	—	100
12	Ser	AGT	63	42	TCG	48	AGC	100	TCG	48	TCG	48	TCG	48
13	Val	GTA	26	43	—		GTA	43	GTA	43	GTA	43	—	43
14	Glu	GAG	100	43	GAA	100	GAA	100	GAA	100	GAA	100	GAA	100
15	Ileu	ATT	77	100	ATC	60	ATT	100	ATC	60	ATC	60	ATC	60
16	Gly	GGA	74	28	GGT	63	GGC	100	GGT	63	GGT	63	GGT	63
17	Asp	GAT	85	100	GAC	54	GAT	100	GAT	100	GAT	100	—	100
18	Ser	TCT	79	33	TCG	48	AGC	100	AGC	100	AGC	100	AGC	100
19	Thr	ACA	78	28	ACG	51	ACC	100	ACC	100	ACC	100	ACC	100
20	Phe	TTC	100	75	TTT	100	TTT	100	TTT	100	TTT	100	TTT	100

- JNK1β1 sequence data -

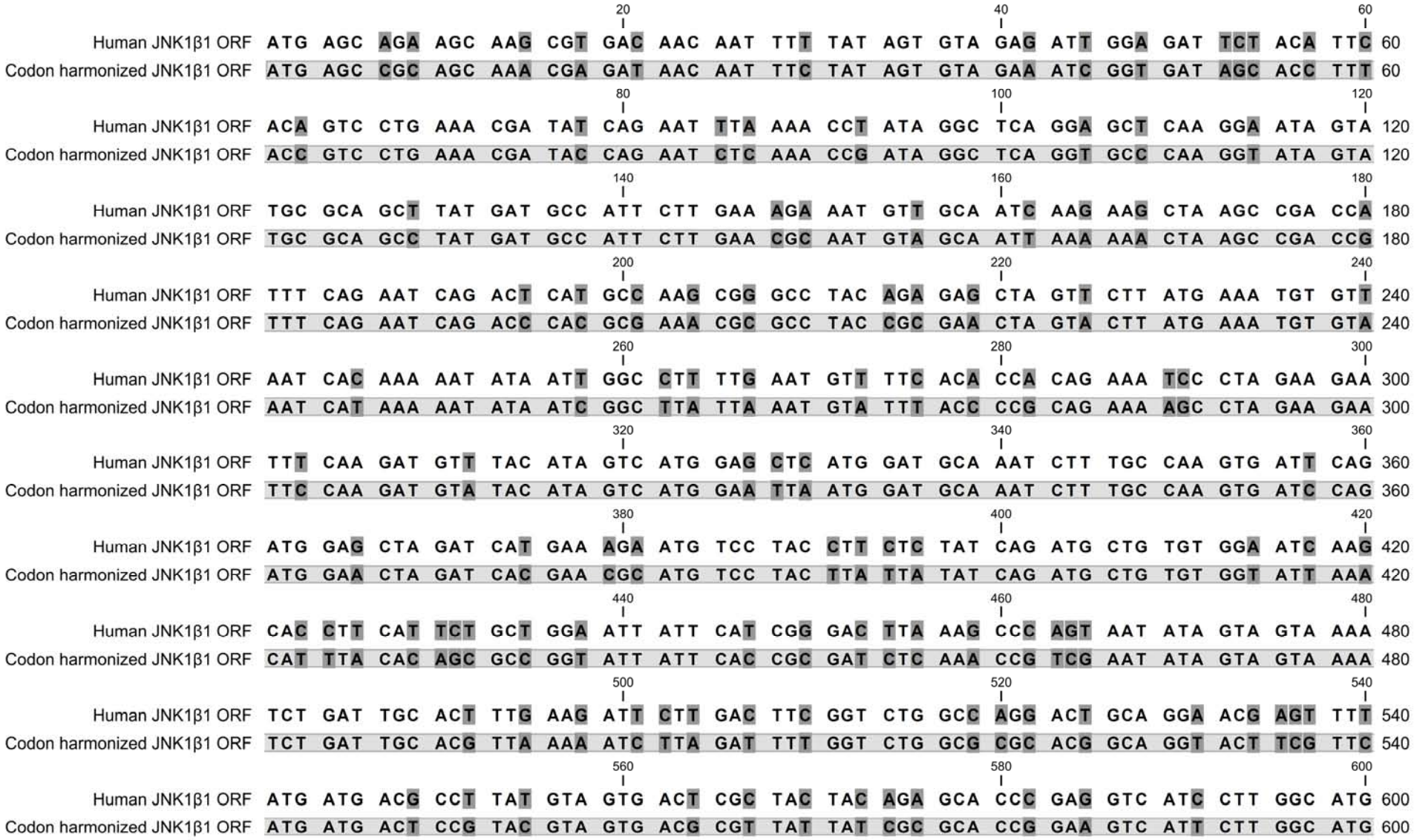

(*See the remaining sequence data of Fig. S1 continued onto the next page, as well as its figure legend*)

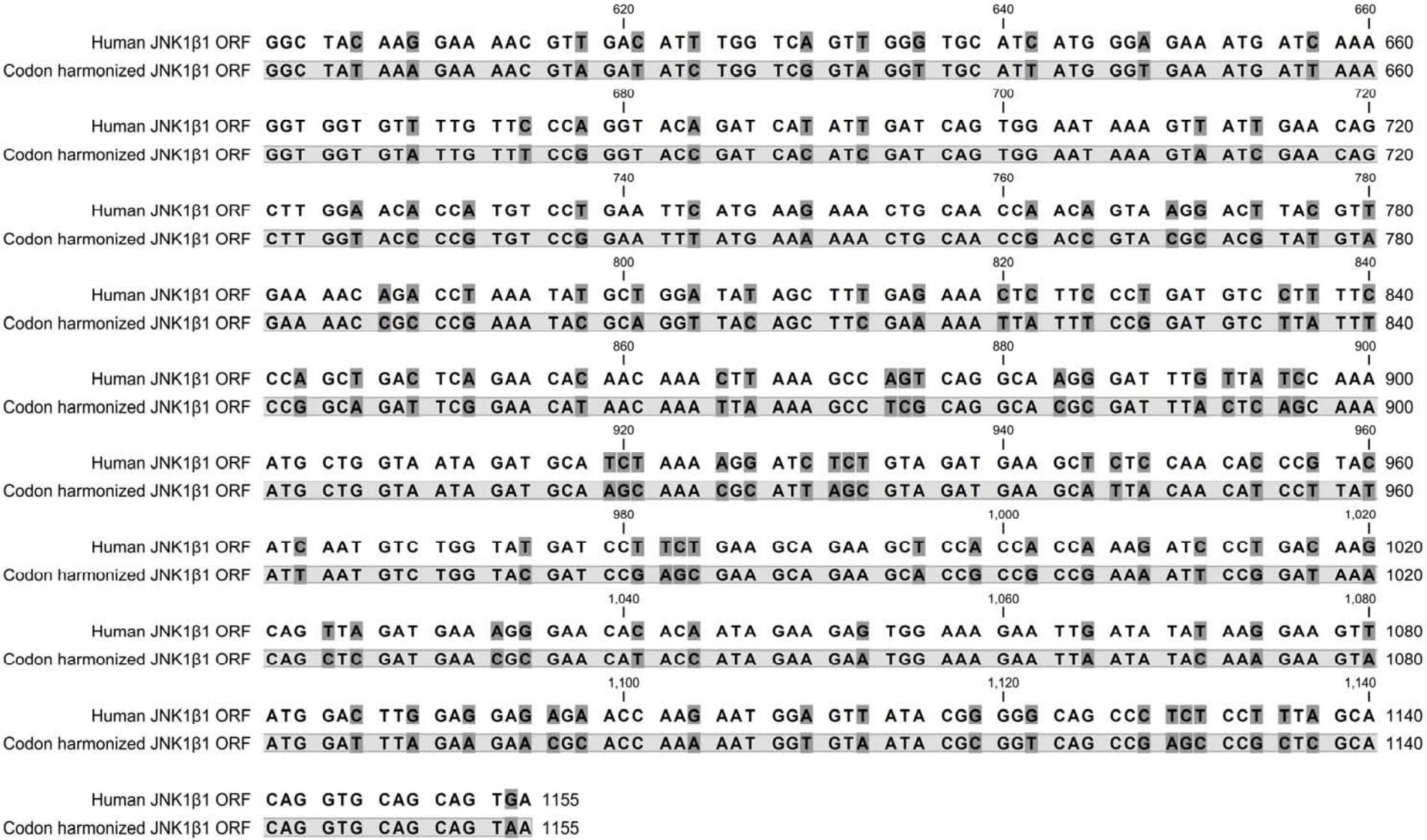

Fig. S1. Codon harmonization of the open reading frame (ORF) of the *H. sapiens JNK1β1* gene to replicate as closely as possible its native rates of translation when expressed in *E. coli.* The upper DNA strand shows the natural *H. sapiens JNK1β1* open reading frame sequence, while the lower highlighted strand shows the redesigned, fully codon-harmonized sequence. Nucleotides changed for synonymous codons are indicated in shaded letters.

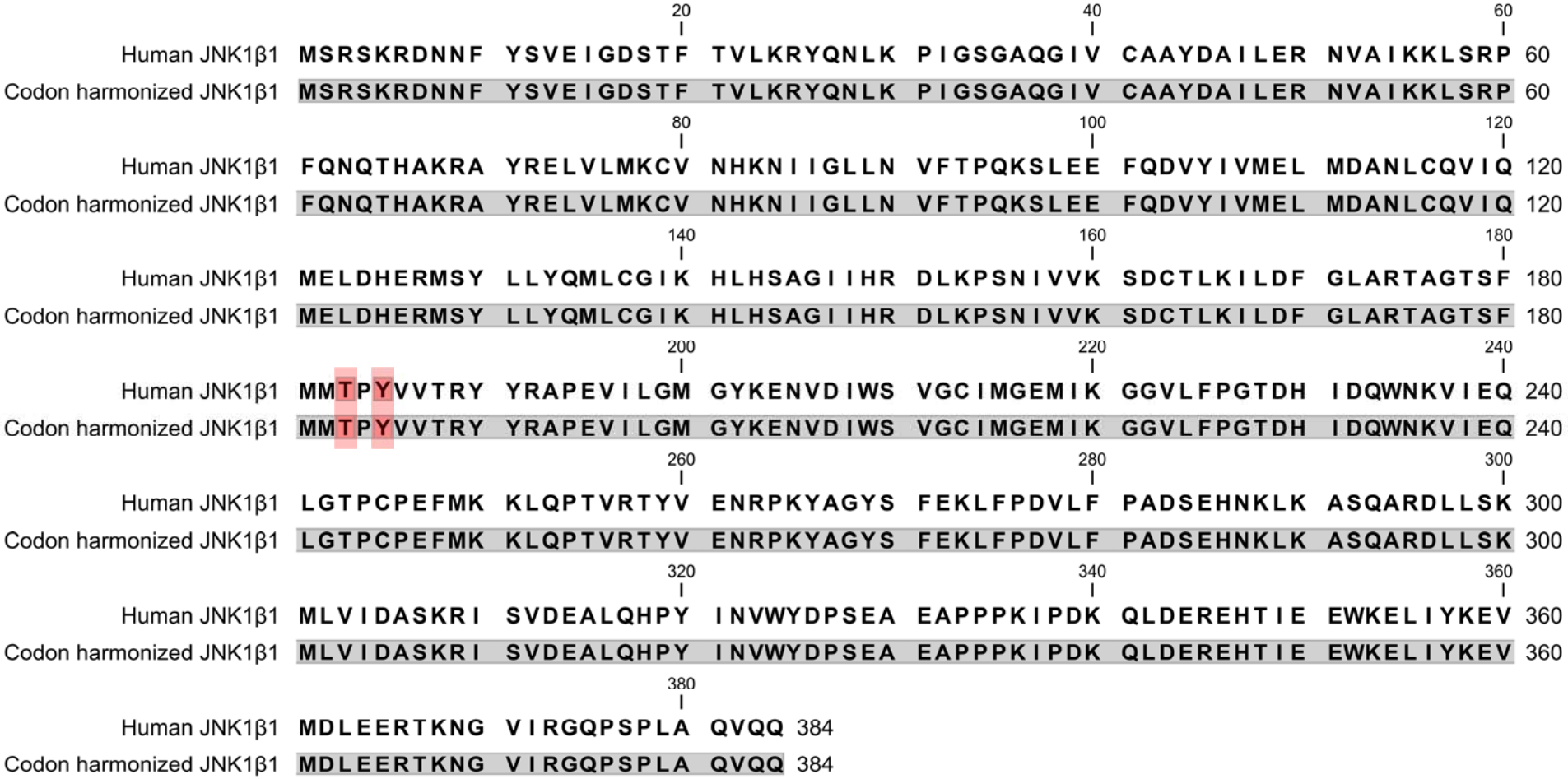

Fig. S2. Recoding the *JNK1β1* open reading frame through codon harmonization does not alter the native amino acid sequence of JNK1β1 as a result of the synonymous codons used. The upper amino acid strand shows the natural *H. sapiens* JNK1β1 sequence, while the lower highlighted strand shows the identical amino acid sequence resulting upon translation of the synthetic, codon-harmonized DNA sequence. The phosphorylatable T183 and Y185 residues of JNK1β1 are highlighted in red.

SUPPLEMENTARY INFORMATION

Cloning of synthetic codon-harmonized *JNK1β1* and human *ATF2* genes into pGEX-4T-1 vector

Additional nucleotide sequences containing BamHI and NotI restriction sites were incorporated at the 5′ and 3′ ends, respectively, of both the codon-harmonized JNK1β1 and human ATF2 (residues 17-96) (accession number: **NM_001256094.1**) nucleotide sequences to enable subcloning into pGEX-4T-1 plasmids (Fig. S3). The redesigned sequences were synthesized and individually cloned into pUC57 plasmids (GenScript^{TM} USA Inc., NJ, USA), and each plasmid used to transform *E. coli* JM109 for propagation. The JNK1β1 and ATF2 gene fragments were excised from pUC57 using BamHI and NotI restriction endonucleases and each ligated into pGEX-4T-1 to form pGX-JNK1 and pGX-ATF2 recombinant plasmids. pGX-JNK1 and pGX-ATF2 were propagated in *E. coli* JM109, and finally each used to transform both *E. coli* BL21(DE3)pLysS (Stratagene) and T7 Express I^q (New England Biolabs) expression cells for the overexpression of recombinant GST-JNK1 and GST-ATF2 fusion proteins (Fig. S3).

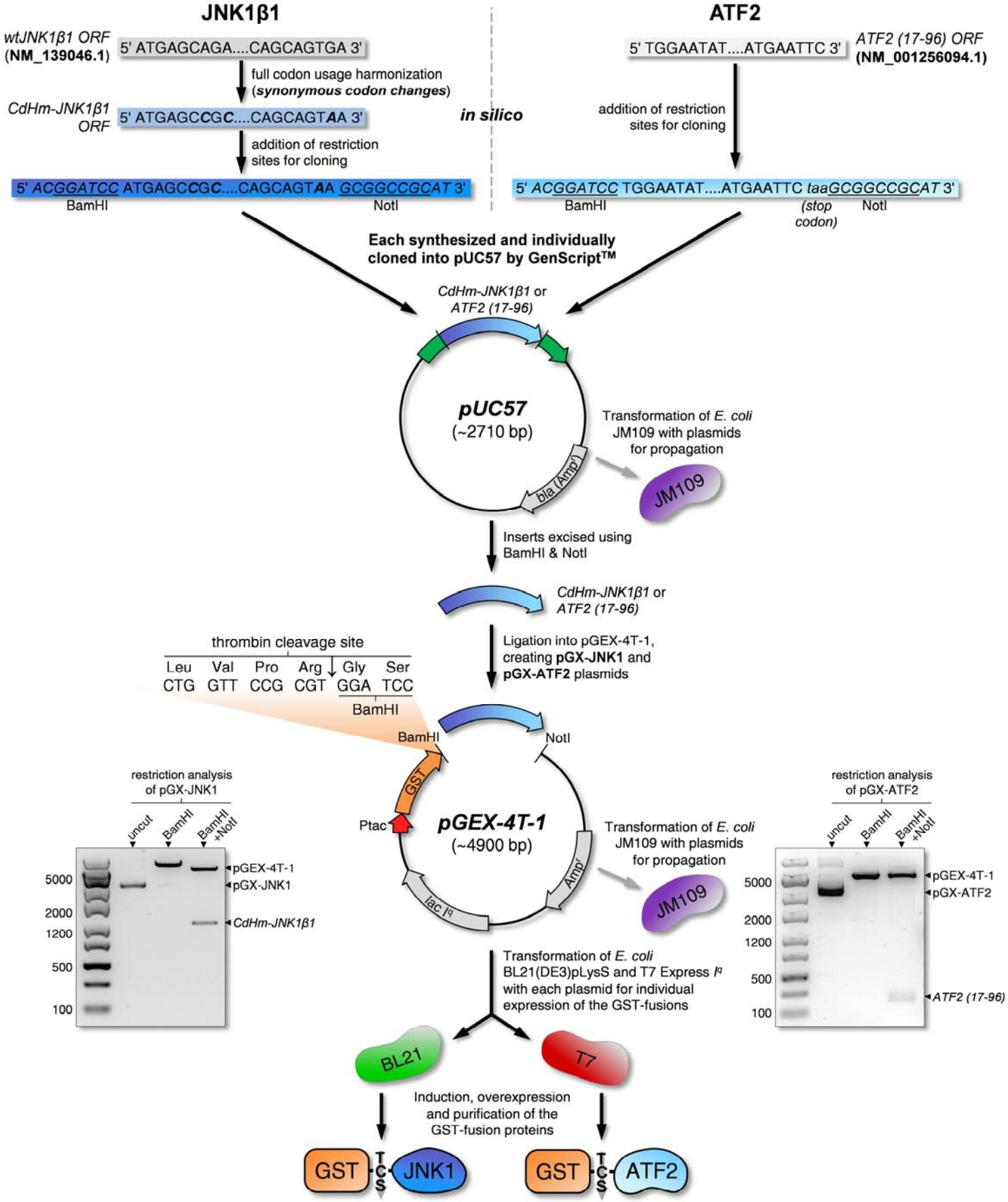

Fig. S3. Cloning strategy of the synthetic codon-harmonized *JNK1β1* (*CdHm-JNK1β1*) and human *ATF2* (residues 17-96) open reading frames.

Cloning of *MEKK-C* and wild-type *MKK4* into pET-32a vector and generation of phosphomimetic MKK4 variant (S257E/T261D)

Plasmids encoding full-length rat *MEKK1* (pCMV5myc-MEKKXuA) and human *MKK4* (pGX-KG-MKK4) were generous gifts from Dr. Melanie Cobb (University of Texas, Southwestern Medical Center). MEKK-C, the constitutively-active C-terminal kinase domain fragment of MEKK1 (EC 2.7.11.25) [1], was used to phosphorylate and activate full-length MKK4 (1-399) (EC 2.7.12.2), which in turn was used to phosphorylate and activate JNK1β1. To obtain the MEKK-C fragment of the MEKK1 gene, high-fidelity PCR was used to amplify the DNA sequence of pCMV5myc-MEKKXuA encoding the C-terminal 281 amino acids of rat MEKK1 (residues 1212-1493) (Fig. S4). The primer sequences were:

Forward - 5′ CATGGATCCAAAGCGAACG 3′
Reverse - 5′ ATTGCGGCCGCTTACCATG 3′

encoding BamHI and NotI recognition sites (underlined), respectively.

The *MEKK-C* PCR fragment was ligated into pJET1.2/blunt vector (Fermentas), propagated in *E. coli* DH5α cells, and thereafter subcloned into pET-32a plasmid via the BamHI and NotI restriction sites to create pT-MEKK-C recombinant plasmid (Fig. S4). pT-MEKK-C was propagated in *E. coli* DH5α cells and used to transform both *E. coli* BL21(DE3)pLysS and T7 Express I^q expression cells for the overexpression of recombinant thioredoxin-His_6-MEKK-C (TH-MEKK-C) fusion protein (Fig. S4).

The pGX-KG-MKK4 plasmid was propagated in *E. coli* DH5α cells, after which the NcoI and HindIII fragment was cleaved from the plasmid and subcloned into pET-32a, forming pT-wtMKK4 recombinant plasmid (Fig. S4). pT-wtMKK4 was propagated in *E. coli* JM109 cells and used to transform both *E. coli* BL21(DE3)pLysS and T7 Express I^q expression cells for the overexpression of recombinant, wild-type thioredoxin-His_6-MKK4 (TH-wtMKK4) fusion protein.

In an attempt to produce constitutively-active MKK4 that does not require phosphorylation by an active upstream kinase (such as MEKK1) to function, a phosphomimetic form of MKK4 was generated. This was achieved by replacing its phosphorylatable residues (S257 and T261) with negatively charged residues (glutamate and aspartate, respectively) that mimic the geometry and charge of the phosphoserine and phosphotheronine (Fig. S5). This S257E/T261D

phosphomimetic MKK4 variant (pmMKK4) has been reported previously to be constitutively-active in transfected cells (*in vivo*), but has not yet been analysed *in vitro* [2].

This was achieved through PCR-mediated site-directed mutagenesis employing complementary primers encoding for both amino acid mutations simultaneously, and using the pT-wtMKK4 plasmid as a template. The sequence of the forward primer was:

5′ GTGGACAGCTTGTGGACGAAATTGCCAAGGATAGAGATGCTGGCTGTAGG 3′

while its reverse complement corresponded to the reverse primer (the mutant codons encoding the phosphomimetic residues are underlined). The PCR reaction, employing the QuikChange® Lightning Site-directed Mutagenesis kit (Agilent Technologies), was conducted according to the manufacturer's instructions. The mutated plasmid (pT-pmMKK4 encoding the pmMKK4 variant), was propagated in *E. coli* JM109 and used to transform both *E. coli* BL21(DE3)pLysS and T7 Express I^q expression cells for the overexpression of recombinant thioredoxin-His_6-phosphomietic MKK4 (TH-pmMKK4) fusion protein.

The insert of each plasmid described was sequenced by Inqaba Biotech (Pretoria, South Africa) to ensure that the DNA sequences encoding for their respective proteins were correct. See Supplementary Figures S1-S2 (JNK1β1 sequence data), and Figures S6-S8 (MEKK-C, ATF2, and MKK4 sequence data) for the DNA and protein sequences of each protein employed in this study.

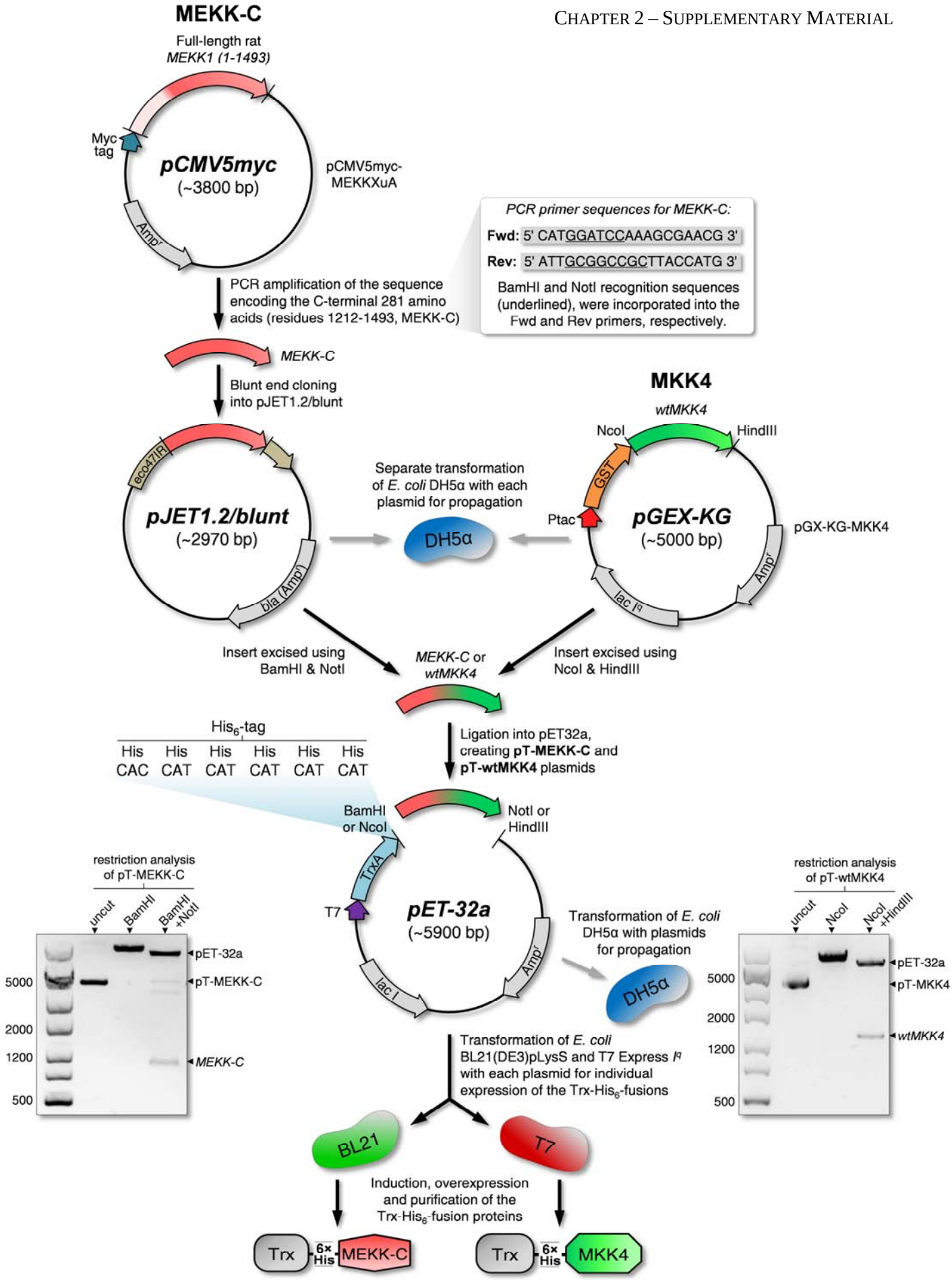

Fig. S4. Cloning strategy of the *MEKK-C* and *MKK4* open reading frames.

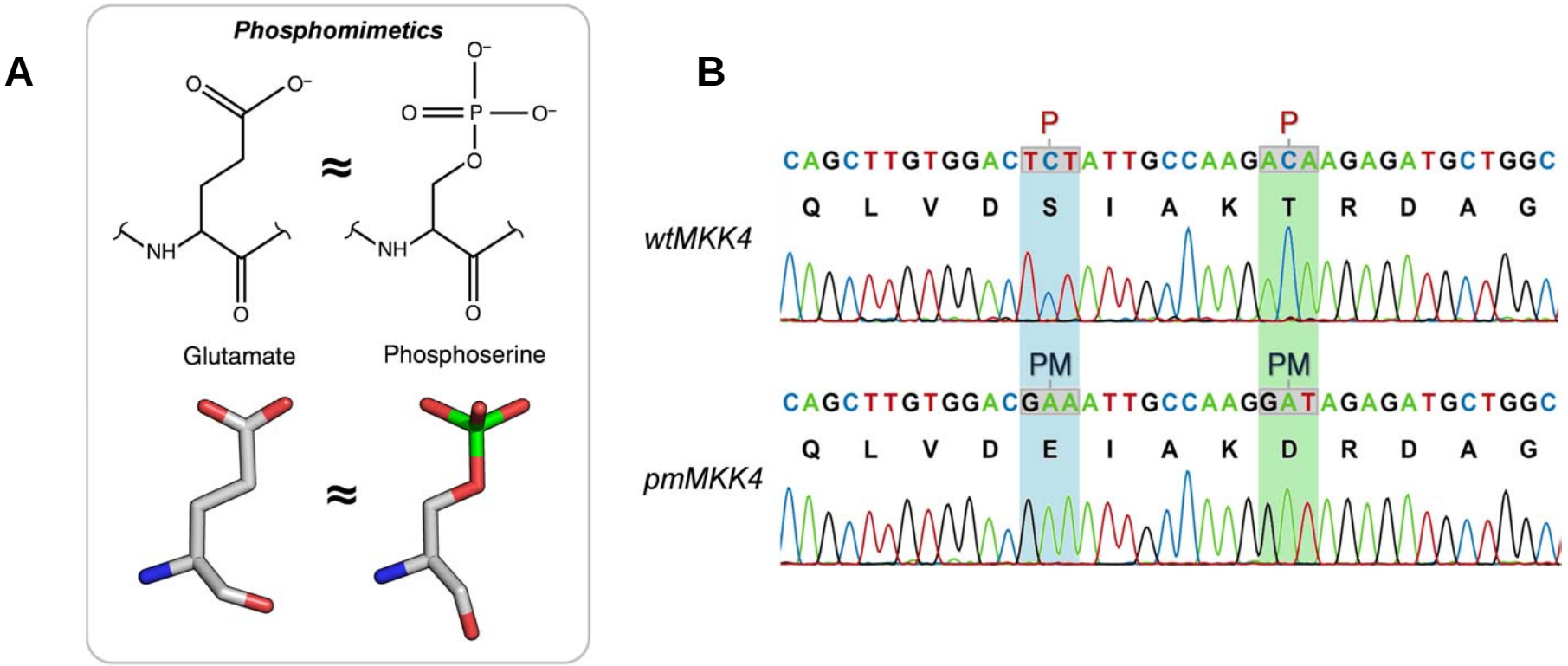

Fig. S5. The phosphomimetic amino acids, glutamate and aspartate, mimic phosphorylated serine or threonine residues. (A) By substituting phosphorylatable serine or threonine residues (whose phosphorylation is known to induce the activation or deactivation of the protein in which they are situated) with negatively charged residues such as glutamate and aspartate, one is able to mimic the geometry and charge of their phosphoserine and phosphotheronine forms. Recreating the electrostatic and geometric properties of phosphorylated residues through these phosphomimetic mutations have been shown, in many instances, to induce structural changes in the protein that is comparable to the changes induced upon natural phosphorylation, generating constitutively-active or -inactive enzymes that does not require phosphorylation by upstream kinases for their associated regulation. Within this study, a phosphomimetic form of MKK4 (S257E/T261D) was generated through site-directed mutagenesis by substituting its phosphorylatable S257 and T261 residues with glutamate and aspartate, respectively. The S257E/T261D MKK4 variant has been reported previously to be a constitutively-active *in vivo* [2]. (B) DNA chromatograms of the *wtMKK4* and *pmMKK4* open reading frames, indicating that the nucleotides encoding the two phosphorylatable (P) residues of wtMKK4 (S257 and T261) were successfully mutated to nucleotides encoding the phosphomimetic (PM) residues, E and D.

- MEKK-C sequence data -

Page 1 of 2

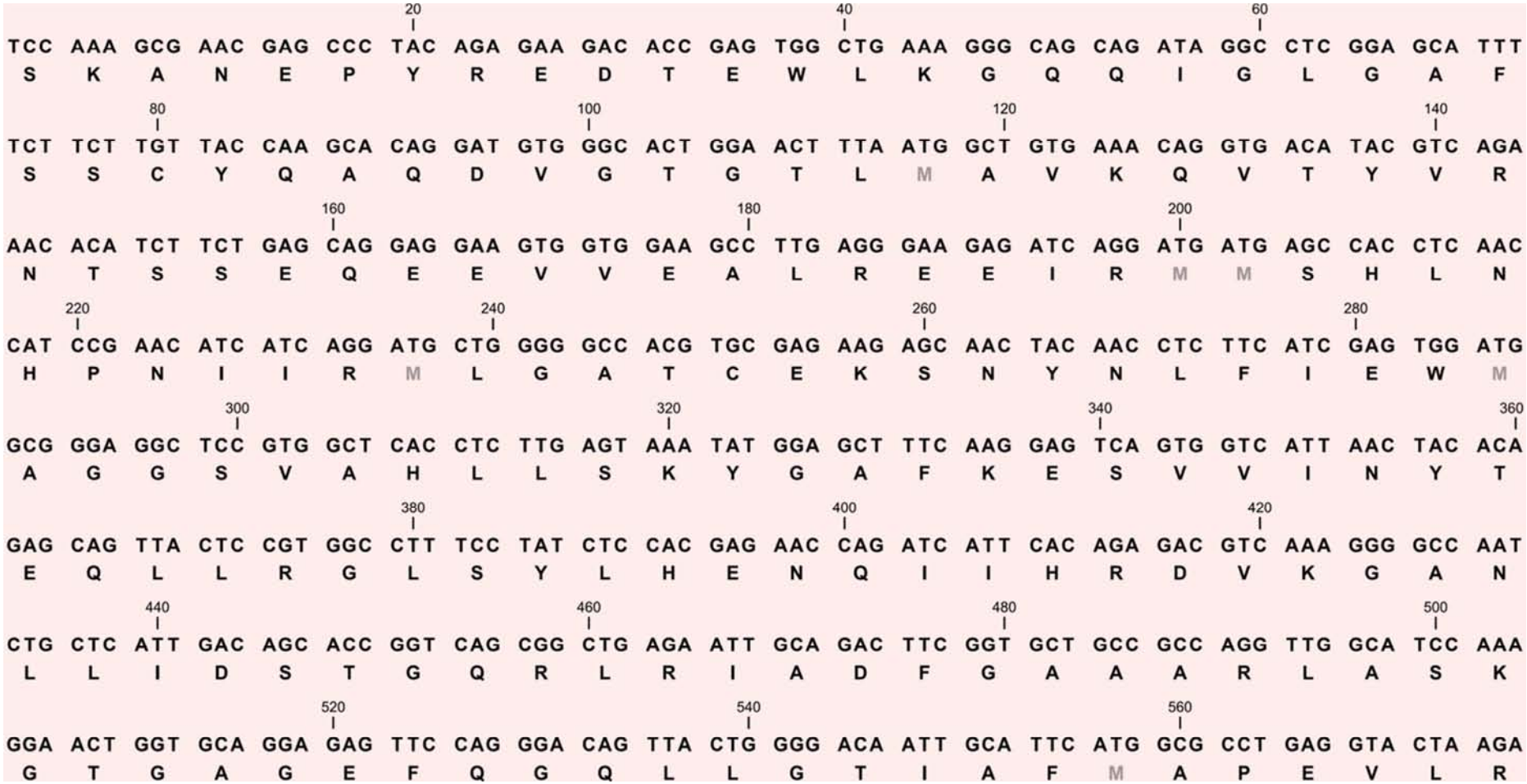

(*See the remaining sequence data of Fig. S6 continued onto the next page, as well as its figure legend*)

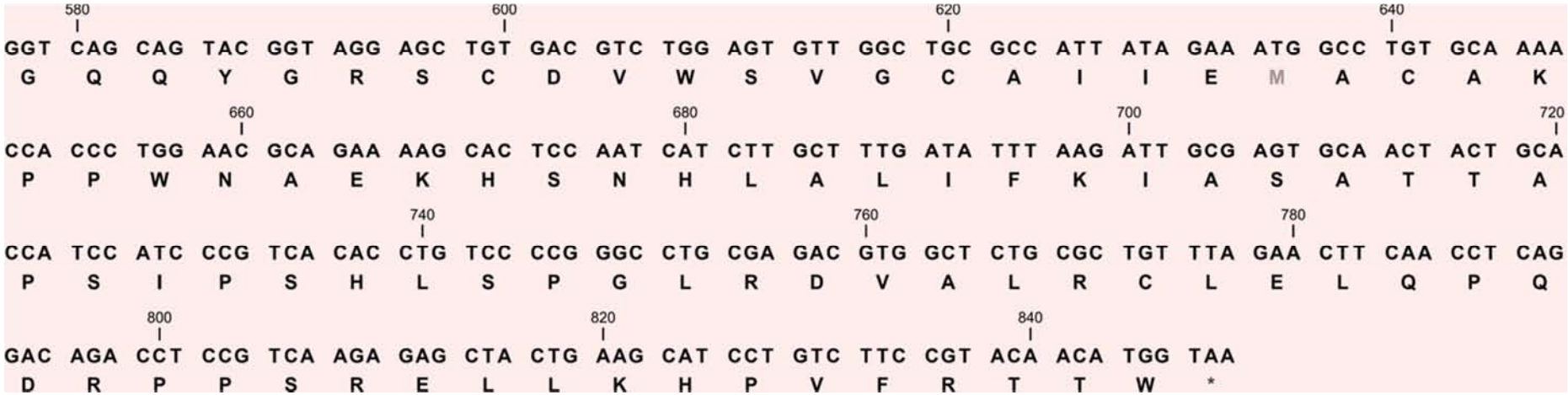

Fig. S6 (Page 2 of 2). MEKK-C sequence data. The coding DNA sequence (top) and the protein product resulting upon its translation (bottom) of the constitutively-active C-terminal kinase domain (residues 1212-1493) of rat MEKK1.

- ATF2 sequence data -

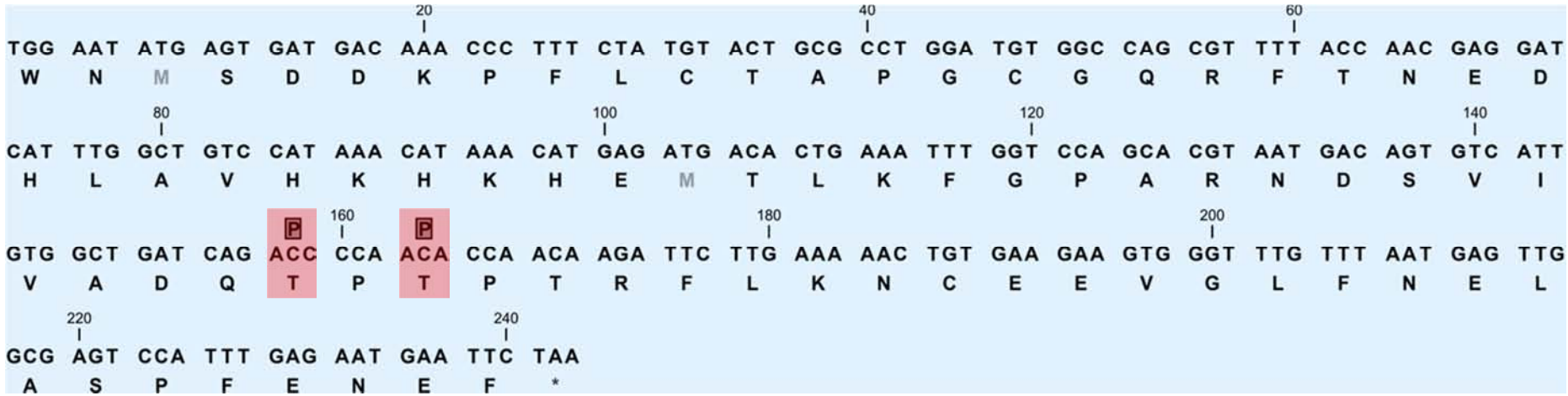

Fig. S7. ATF2 sequence data. The coding DNA sequence (top) and the protein product resulting upon its translation (bottom) of residues 17-96 of human ATF2. The phosphorylatable T69 and Y71 residues of ATF2 are highlighted and indicated by red P "flags".

- MKK4 sequence data -

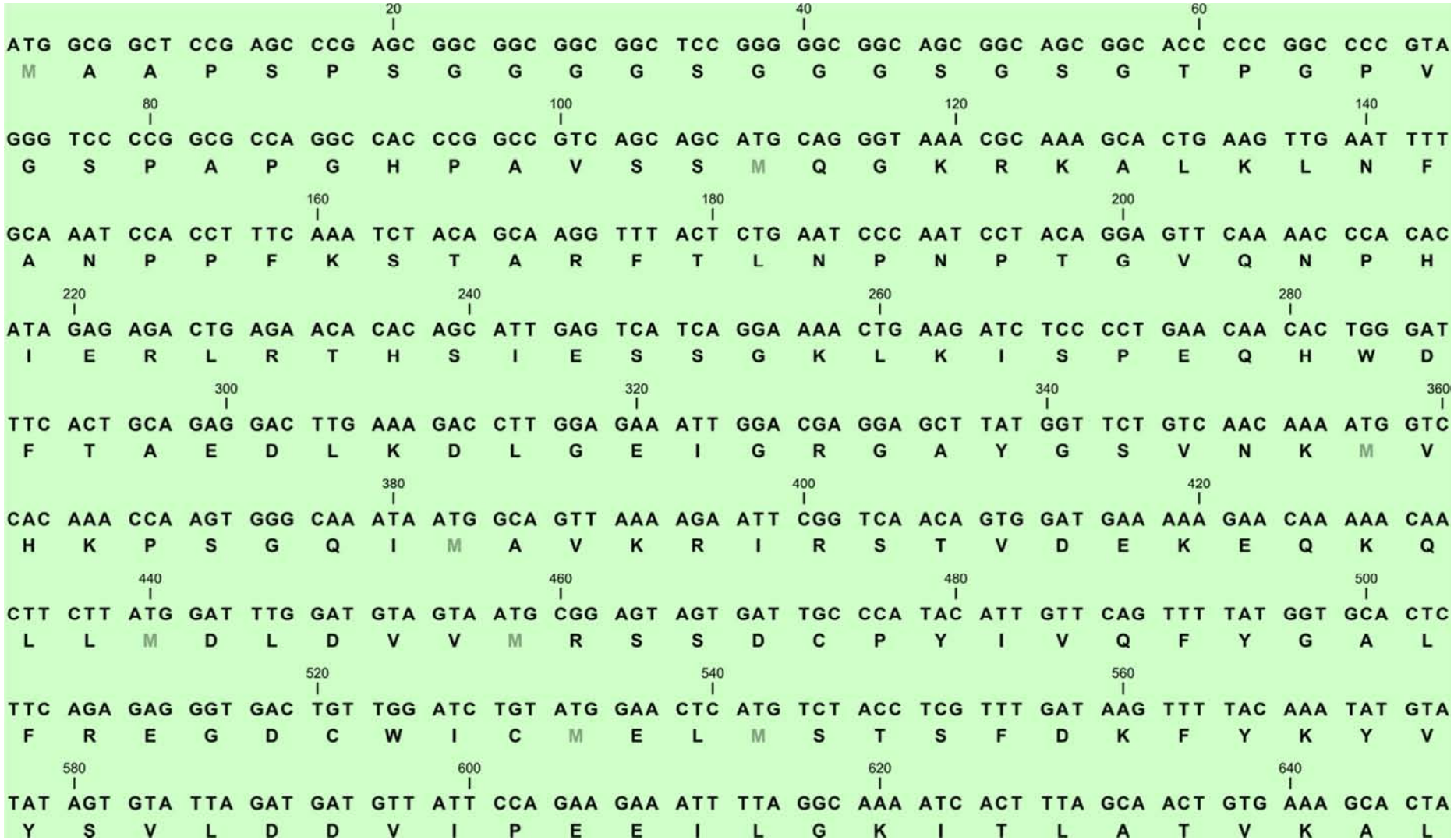

(*See the remaining sequence data of Fig. S8 continued onto the next page, as well as its figure legend*)

Fig. S8 (Page 2 of 2). MKK4 sequence data. The coding DNA sequence (top) and the protein product resulting upon its translation (bottom) of full-length, wild-type, human MKK4. The phosphorylatable S257 and T261 residues of MKK4 are highlighted and indicated by red P "flags".

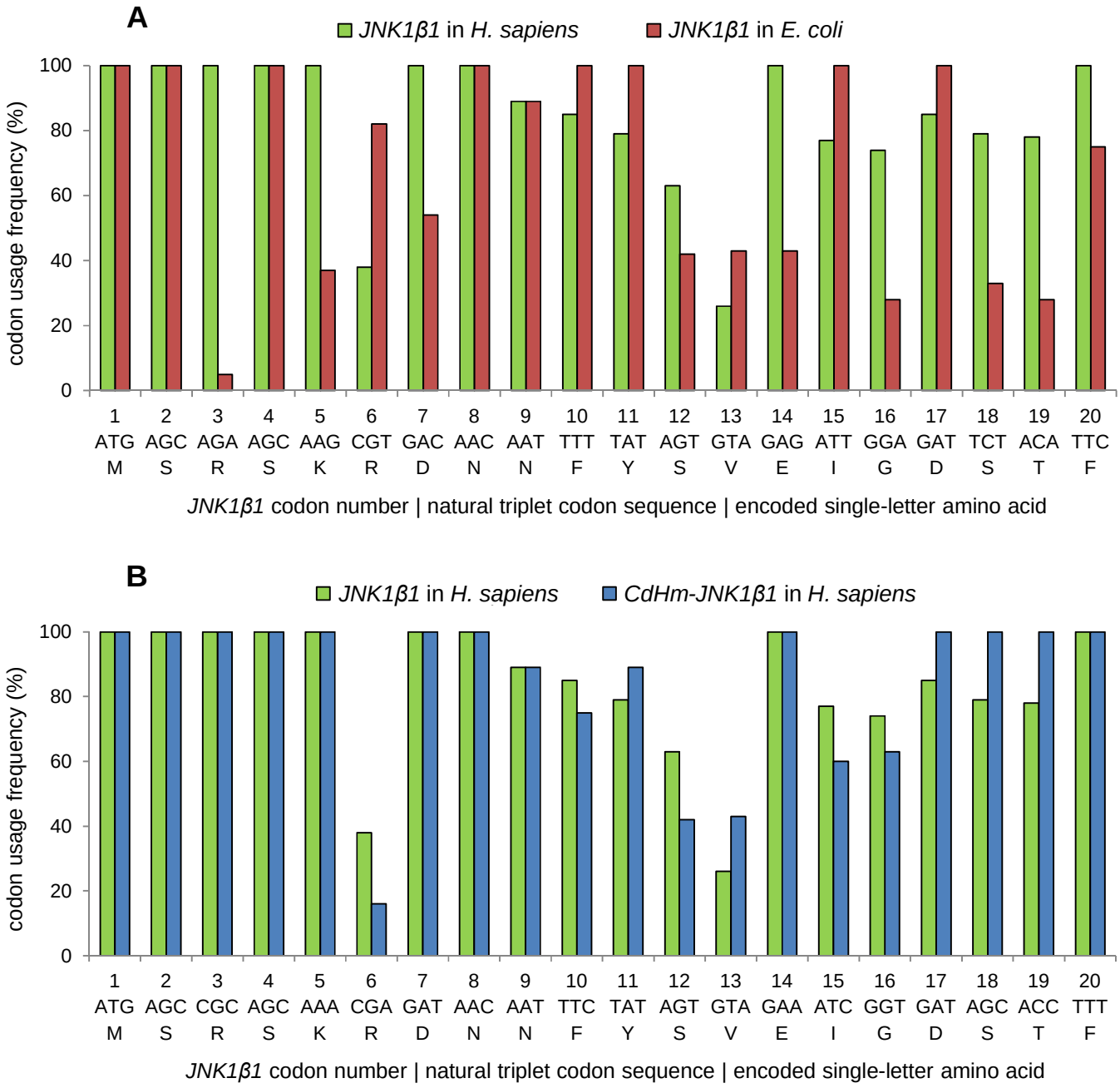

Fig. S9. (A) The codon usage frequencies of the native codons (non-codon harmonized) encoding the first 20 N-terminus amino acids of JNK1β1 (M1-F20) when expressed in *H. sapiens* (green bars) and *E. coli* (red bars) illustrates the great discordance in the codon usage patterns. (B) The codon usage frequencies of the same codons presented in (A) following full codon harmonization and when expressed again in both *H. sapiens* (green bars) and *E. coli* (blue bars) illustrates the now good agreement in the codon usage patterns.

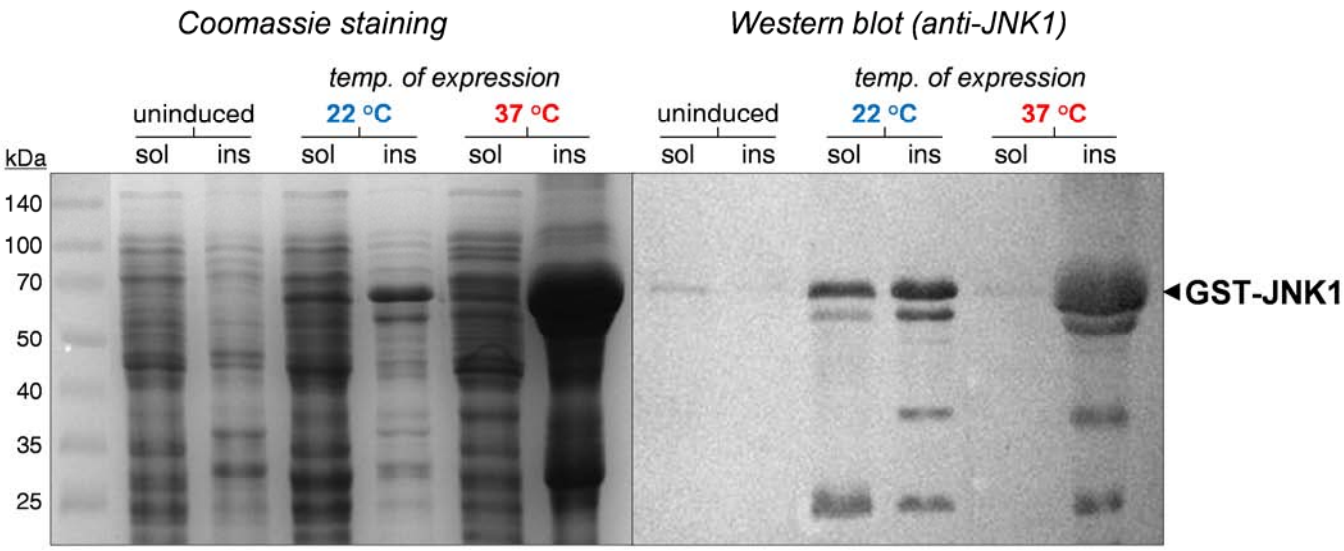

Fig. S10. Expression patterns of GST-JNK1 at low and high induction temperatures. Representative samples of the soluble and insoluble cell fractions resulting after overexpression of GST-JNK1 at 22 °C and 37 °C were compared using 12.5% SDS-PAGE and Western blot (employing anti-JNK1 antibodies). The expression conditions that yielded the greatest quantity of soluble GST-JNK1 (1 L of BL21(DE3)pLysS cell cultures in 2×YT media, induced with 0.6 mM IPTG for 6 h) was used in the analysis to isolate the effect that temperature has on optimal soluble overexpression. Expression at 22 °C results in the production of large yields of soluble GST-JNK1, although significant amounts of its insoluble form were also expressed at this temperature. Contrastingly, expression at 37 °C results in extensive quantities of insoluble GST-JNK1 being produced, with no concurrent production of its soluble form. Expression at 22 °C was therefore adopted for large scale expression of soluble GST-JNK1. Samples of the insoluble and soluble fraction of cells grown in the absence of IPTG (uninduced) were included as a control for overexpression.

SUPPLEMENTARY INFORMATION

GST-JNK1 and GST-ATF2 thrombin cleavage trials

Off-column thrombin cleavage time-trials were performed to determine the optimal time that the GST-JNK and GST-ATF2 fusion proteins should be incubated with thrombin for the complete cleavage of each target from the GST-tag, while also avoiding the undesirable degradation of JNK1β1 and ATF2. Here, 2 mg of each GST-JNK1 and GST-ATF2 in Tris-Lysis Buffer was incubated at 20 °C with 0.8 U of human plasma thrombin possessing an activity of 3152.0 U/mg (Merck), each in a 1 ml total reaction volume. Samples were removed periodically and immediately treated for reducing SDS-PAGE.

It should be noted at this point that on-column cleavage of each fusion (cleaving GST-JNK1 or GST-ATF2 while still bound to GSH-agarose) resulted in an extensive degree of protein aggregation, and thus only off-column thrombin cleavage trials were performed for both. Although it is recommended by the suppliers of the protease (Sigma^{TM}) that 1 U of human plasma thrombin should be added to 100 μg of test fusion protein for 16 h at 22 °C to allow >90% to be digested, within these trials 25× less thrombin than suggested (0.8 U as opposed to 20 U) was added to 2 mg of GST-JNK1 or GST-ATF2 fusion in a 1 ml reaction volume.

With respect to GST-JNK1, the SDS-PAGE gel and corresponding Western blot of Fig. S11 nevertheless indicates that >95% of the 2 mg GST-JNK1 fusion (observed before the addition of thrombin at 0 min) was cleaved into its component JNK1β1 (±48 kDa band) and GST (±28 kDa bands) proteins within the first 15 min of incubation with 0.8 U of thrombin (Fig. S11). Furthermore, while the quantity of the resulting GST remains consistent throughout the entire duration of the GST-JNK1 time trial, JNK1β1 progressively and rapidly degrades as the time course of the cleavage trial lengthens until very little of the protein is present at 16 h. This was not expected considering the recommendation that the fusion protein be incubated with much higher concentrations of thrombin for at least 16 h to allow efficient cleavage (Amersham Biosciences, 2002). These observations first illustrate the extreme ease at which thrombin cleaves the GST-JNK1 fusion into its component proteins, yet more importantly, illustrates the exceptionally high susceptibility of JNK1β1 to proteolytic degradation by thrombin.

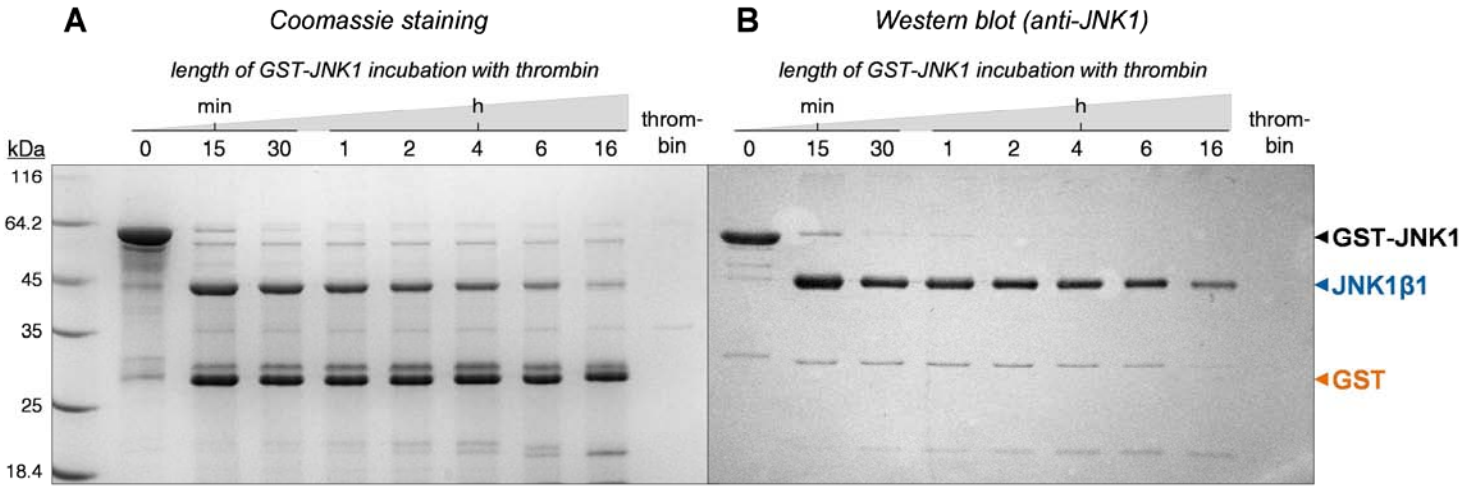

Fig. S11. Thrombin cleavage time trials of GST-JNK1. The relative degree of cleavage of 2 mg GST-JNK1 into its component JNK1β1 and GST proteins by 0.8 U human plasma thrombin over-time at 20 °C was analysed by (A) SDS-PAGE and (B) Western blotting employing anti-JNK1 antibodies. The data indicates that almost complete cleavage of the fusion occurs within 15 min of incubation and illustrates the high susceptibility of JNK1β1 to proteolytic degradation by thrombin, observed by the steady decrease in the intensity of the JNK1β1 band. As on-column cleavage (data not shown) resulted in protein aggregation, a 15 min off-column cleavage was determined to be optimal for separation of JNK1β1 from GST. A thrombin control comprising only 0.8 U thrombin in buffer was included to indicate the electrophoretic location and size of the protease.

Contrastingly, the GST-ATF2 fusion required 6 h for efficient cleavage into its component proteins with the same amount of thrombin (Fig. S12). There is additionally no discernible proteolytic degradation of ATF2 within the course of the trial, with the amount of the resulting ATF2 only steadily increasing over time (Fig. S12). This too highlights the sensitivity of JNK1β1 to unspecific cleavage by thrombin.

Therefore, a controlled 15 min off-column GST-JNK1 thrombin cleavage is optimal for the separation of JNK1β1 from GST and the simultaneous prevention of its proteolytic degradation by thrombin. Thrombin is thus an extremely efficient and cost effective protease to employ in separating JNK1β1 from an invaluable purification and/or solubility tag such as GST. However, to prevent avoidable proteolytic degradation, we recommend the use of thrombin only in combination with a highly efficient means of removing the protease from JNK1β1, such as (the simple and inexpensive) heparin-agarose affinity chromatography as employed in this study.

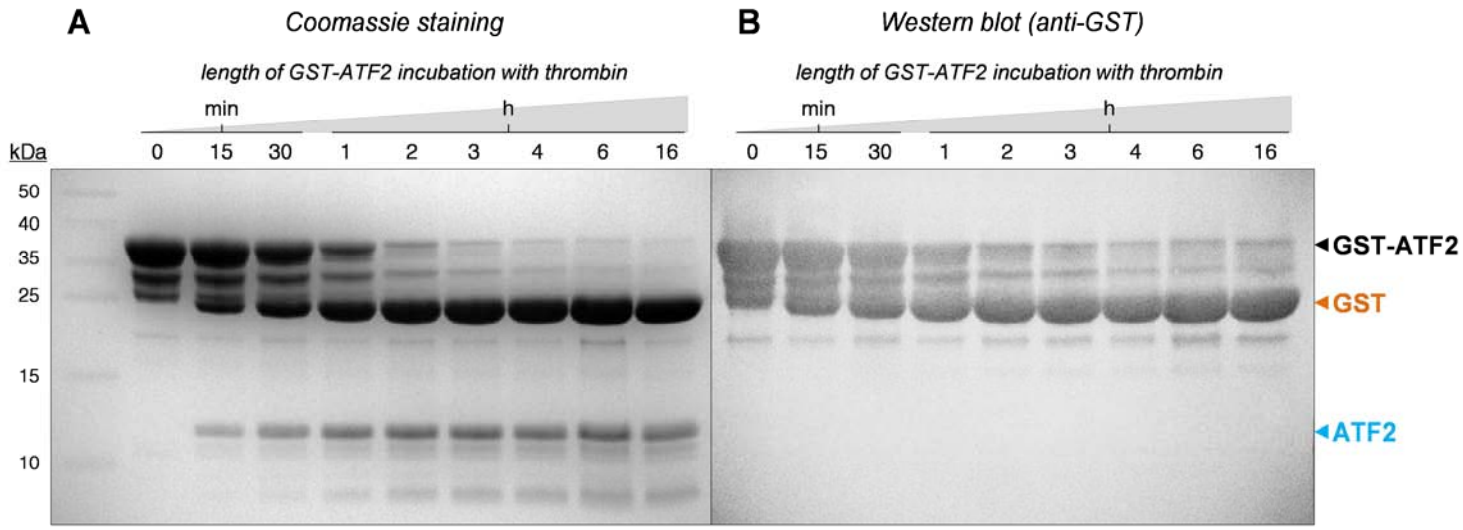

Fig. S12. Thrombin cleavage time trials of GST-ATF. Time dependence study of off-column thrombin cleavage of GST-ATF2 fusion was analysed by (A) Tricine–SDS-PAGE and (B) Western blotting employing anti-GST antibodies. The relative degree of cleavage of 2 mg GST-ATF2 at specific times after incubation with 0.8 U of thrombin at 20 °C indicates that the optimal cleavage time for the separation of ATF2 from GST is 6 h. No proteolytic degradation of ATF2 is detectable within the course of the trial, re-highlighting the high susceptibility of JNK1β1 to unspecific cleavage by thrombin.

The high susceptibility of JNK1β1 to proteolytic degradation by thrombin

Thrombin is one of the most commonly used restriction proteases for the cleavage of GST-fusion proteins due to its relatively low cost and optimum cleavage activity at pH 6-8, as well as its apparently high specificity [3]. Nevertheless, despite the extensive use of thrombin and the fact that it preferentially cleaves polypeptide substrates at R/K-Xaa bonds, thrombin has been reported to cleave non-specifically at secondary sites located in some over-expressed recombinant proteins [4,5]. Thrombin mediated non-specific cleavage is thus quite common, corresponding to the observed high susceptibility of JNK1β1 to its proteolytic degradation by thrombin.

The optimum cleavage site for thrombin comprises either: (a) *P4*-*P3*-P-R↓-*P1′*-*P2′*, where *P3* and *P4* are hydrophobic amino acids and *P1′*, *P2′* are apolar, non-acidic amino acids, or (b) *P2*-R↓-*P1′*, where *P2* or *P1′* are G (arrows indicate the sites at which the R/K-Xaa bonds are cleaved) [4]. To help understand the basis of the susceptibility of JNK1β1 to degradation by thrombin, its R/K-Xaa bonds were examined to assess if they possess the properties of the optimum thrombin cleavage site described, and were compared with the sequences of the

polypeptides known to be susceptible to thrombin cleavage. Of the 54 R/K-Xaa bonds in JNK1β1, 5 were revealed to have characteristics for potential candidacy for thrombin recognition and cleavage (see Fig. S13). These sites are also seen to be highly exposed to the surrounding environment, making them easily accessible to contact recognition by thrombin.

Ultimately, the non-specific cleavage sequences described resemble that of the primary thrombin cleavage sequence, and hence represent possible non-specific secondary sites within JNK1β1 that are recognised for cleavage by thrombin. GST-JNK1 fusion proteins that can be cleaved using, for example, the expensive protease enterokinase may be beneficial for its purification by reducing the risk of proteolytic degradation, but this will unnecessarily and extensively increase the cost of purifying JNK1β1. The use of a purification tag that may not require removal (e.g. His-tags) may eliminate the danger of exposing JNK1β1 to cleavage agents, yet as has been demonstrated numerous times before, the absence of a highly soluble fusion protein partner may result in a decrease in its soluble overexpression and ultimately reduce the resulting yield of purified protein.

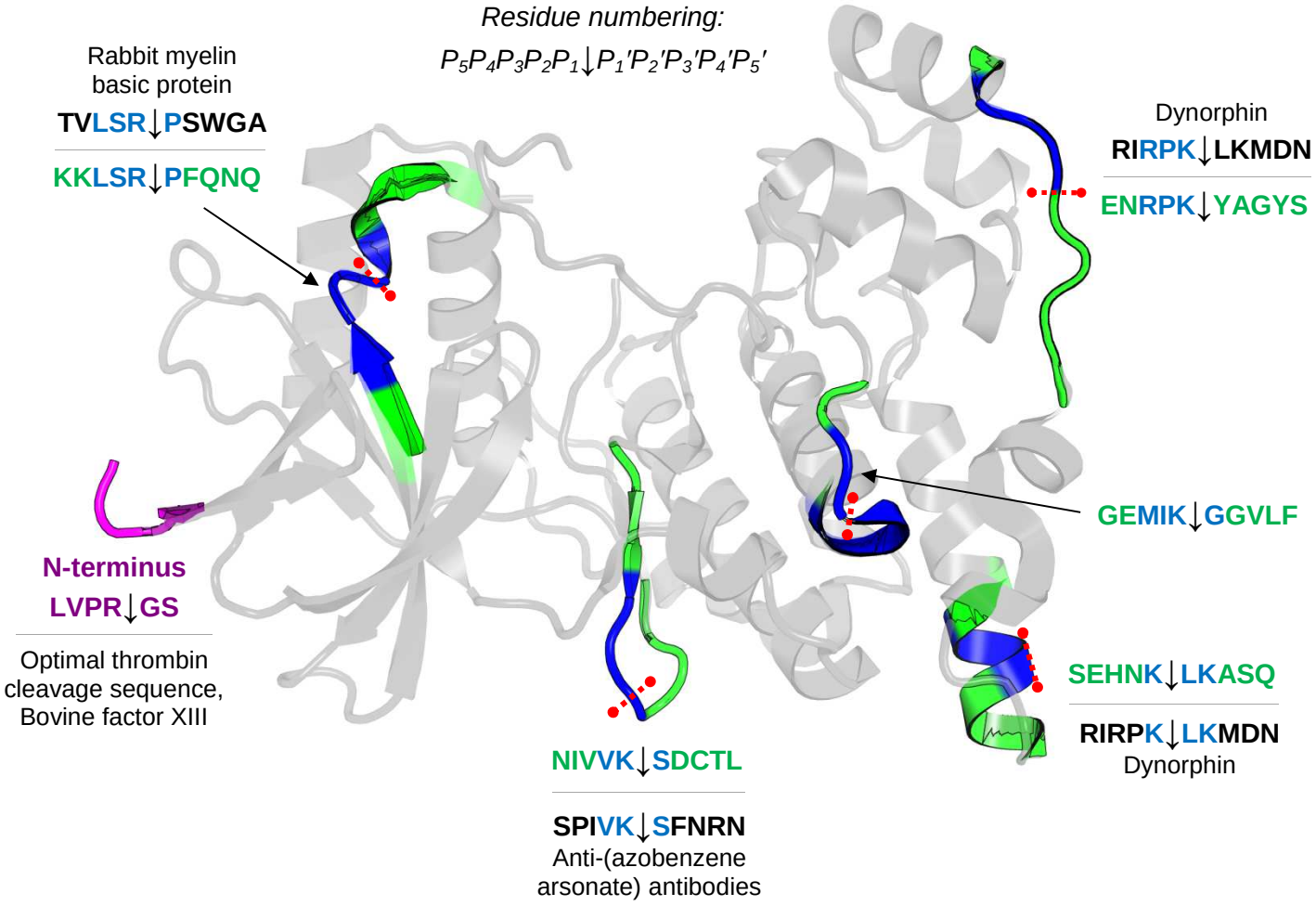

Fig. S13. Possible thrombin susceptible cleavage sites in JNK1β1. The potential thrombin-cleavage susceptible amino acid sequences and their location within JNK1β1 are indicated in green and blue. Possible sequences were identified through sequence comparison with known thrombin susceptible R/K -Xaa bonds, and by identifying sequences with properties known to promote sensitivity to thrombin cleavage. The known thrombin susceptible sequences and the proteins from which they are derived are shown adjacent to their corresponding sequences in JNK1β1. Amino acids sequences and protein secondary structure in blue represent those with complete sequence identity to their related thrombin susceptible R/K-Xaa sequences, and/or those that possess the properties ideal for thrombin cleavage. Sequence and structure in green indicate the typical length of the amino acid sequence (a heptapeptide) that may contribute to recognition and subsequent cleavage by thrombin. The sites at which the peptide backbone would be cleaved by thrombin are indicated by arrows and dashed red lines. Shown in purple is the N-terminus at which the optimal thrombin cleavage sequence (LVPR↓GS) was initially located, a sequence that linked the GST and JNK1β1 within the GST-JNK1 fusion allowing their later separation by thrombin. The image was rendered using PyMOL™ v. 0.99 (DeLano Scientific, San Carlos, CA) using the PDB code 3ELJ [6].

SUPPLEMENTARY REFERENCES

[1] S. Xu, D. Robbins, J. Frost, A. Dang, C. Lange-Carter, M.H. Cobb, MEKK1 phosphorylates MEK1 and MEK2 but does not cause activation of mitogen-activated protein kinase. Proc Natl Acad Sci USA 92 (1995) 6808–6812.

[2] Z. Guan, S.Y. Buckman, A.P. Pentland, D.J. Templeton, A.R. Morrison, Induction of cyclooxygenase-2 by the activated MEKK1 → SEK1/MKK4 → p38 mitogen-activated protein kinase pathway. J Biol Chem 273 (1998) 12901-12908.

[3] R.J. Jenny, K.G. Mann, L. R.L., A critical review of the methods for cleavage of fusion proteins with thrombin and factor Xa. Protein Expres Purif 31 (2003) 1-11.

[4] J.-Y. Chang, Thrombin specificity - requirement for apolar amino acids adjacent to the thrombin cleavage site of polypeptide substrate. Eur J Biochem 151 (1985) 217-224.

[5] D. Rajalingam, K.M. Kathir, K. Ananthamurthy, P.D. Adams, T.K.S. Kumar, A method for the prevention of thrombin-induced degradation of recombinant proteins. Anal Biochem 375 (2008) 361-363.

[6] S.D. Chamberlain, A.M. Redman, J.W. Wilson, F. Deanda, J.B. Shotwell, R. Gerding, H. Lei, B. Yang, K.L. Stevens, A.M. Hassell, L.M. Shewchuk, M.A. Leesnitzer, J.L. Smith, P. Sabbatini, C. Atkins, A. Groy, J.L. Rowand, R. Kumar, R.A.J. Mook, G. Moorthy, S. Patnaik, Optimization of 4,6-bis-anilino-1*H*-pyrrolo[2,3-*d*]pyrimidine IGF-1R tyrosine kinase inhibitors towards JNK selectivity. Bioorg Med Chem Lett 19 (2009) 360-364.

CHAPTER 3

PUBLICATION 2

JNK1β1 is phosphorylated during expression in *E. coli* and *in vitro* by MKK4 at three identical novel sites

GAVIN R. OWEN, STOYAN STOYCHEV, IKECHUKWU ACHILONU, AND HEINI W. DIRR

Biochemical and Biophysical Research Communications 432, 683-688 (2013)

In this publication, the exact sites at which JNK1β1 is phosphorylated during expression in *E. coli* and *in vitro* by its activator, MKK4, were characterised.

Author contributions: Gavin R. Owen performed all experimental work, analysed the data, and wrote the manuscript. Stoyan Stoychev assisted with the MS experiments. Ikechukwu Achilonu and Heini W. Dirr supervised the project and assisted in data analysis and interpretation.

GRAPHICAL ABSTRACT

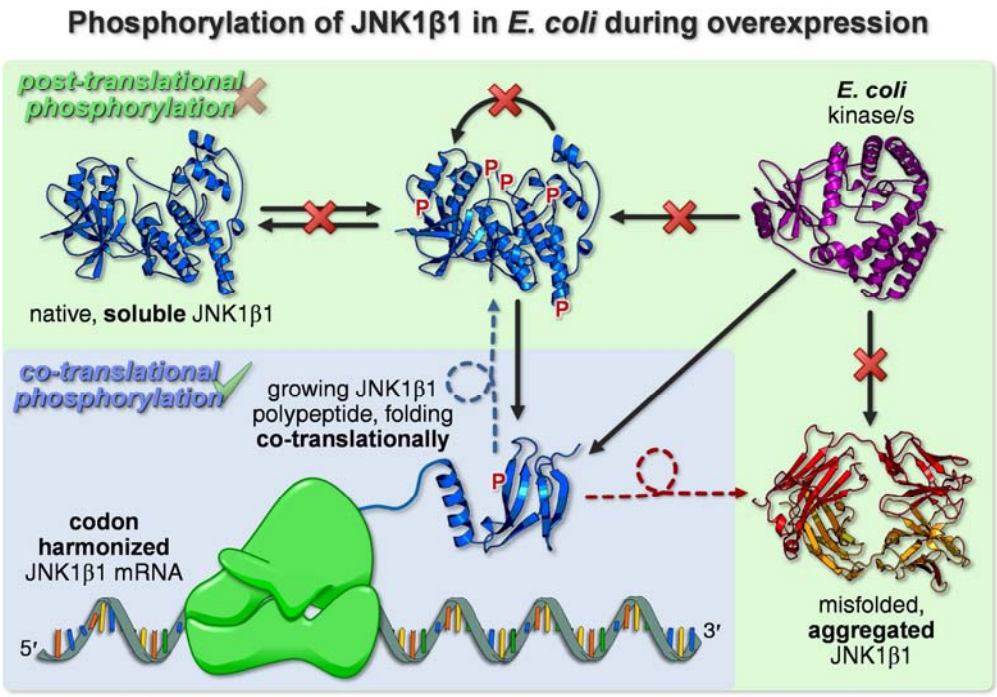

Biochemical and Biophysical Research Communications 432 (2013) 683–688

Contents lists available at SciVerse ScienceDirect

Biochemical and Biophysical Research Communications

journal homepage: www.elsevier.com/locate/ybbrc

JNK1β1 is phosphorylated during expression in *E. coli* and *in vitro* by MKK4 at three identical novel sites

Gavin R. Owen [a], Stoyan Stoychev [b], Ikechukwu Achilonu [a], Heini W. Dirr [a,*]

[a] Protein Structure–Function Research Unit, School of Molecular and Cell Biology, University of the Witwatersrand, Johannesburg 2050, South Africa
[b] Council for Scientific and Industrial Research, Biosciences, Pretoria 0001, South Africa

ARTICLE INFO

Article history:
Received 23 January 2013
Available online 12 February 2013

Keywords:
MAP kinases
c-Jun N-terminal kinase
MKK4
Recombinant protein expression
Protein phosphorylation
Mass spectrometry

ABSTRACT

JNK1 is activated by phosphorylation of the canonical T183 and Y185 residues, modifications that are catalysed typically by the upstream eukaryotic kinases MKK4 and MKK7. Nonetheless, the exact sites at which the most abundant JNK variant, JNK1β1, is further modified by MKK4 for phospho-regulation has not been previously investigated. Aiming to characterise the nature of JNK1β1 phosphorylation by active MKK4 using mass spectrometry, a recognised yet uncharacterised phospho-site (S377) as well as two novel phospho-residues (T228 and S284) were identified. Interestingly, the identical sites were phosphorylated during overexpression of JNK1β1 in *Escherichia coli*, raising important questions that have significant implications for heterologous protein expression.

1. Introduction

The c-Jun N-terminal kinases (JNKs) constitute one sub-group of the eukaryotic mitogen activated protein kinases (MAPKs) that mediate the cellular response to an array of extracellular stimuli, including cytokines and stresses such as UV irradiation [1]. Upon activation by these stimuli, the multifunctional JNK pathway initiates a variety of transcription events implicated in many physiological processes that include differentiation, apoptosis, and DNA repair [1].

Three JNK isoforms have been identified; JNK1, JNK2 (both with broad tissue distribution), and JNK3 (localised predominantly in the CNS) [1,2]. These kinases are encoded by three alternatively spliced genes, (*JNK1*, *JNK2*, and *JNK3)*, resulting in 10 distinct JNK splice variants that differ in the length of their N- and C-termini, as well as in amino acids within and around their substrate binding sites [2].

JNKs are typically activated by a cascade of MAPK-mediated phosphorylation events. Within this highly conserved three-tiered kinase cascade, an upstream MAP3K (e.g. MEKK1) phosphorylates a MAP2K (e.g. MKK4 and MKK7), which in turn phosphorylates and activates the downstream MAPKs (e.g. JNK, ERK, and p38) [3]. Phosphorylation of the canonical T183/Y185 residues in the activation loop of JNK1 primes the enzyme for activities that include the phosphorylation of the transcription factors c-Jun and ATF2 [1,2], as well as interaction with several non-substrate, regulatory proteins [4]. T183/Y185 phosphorylation is typically catalysed by the dual-specificity MAP2Ks, MKK4 and MKK7, respectively [5] yet it has been shown that high concentrations of either kinase, once activated by upstream MAP3Ks, is sufficient to phosphorylate both residues [1,5].

In addition to the phosphorylation of its activation residues, which are topologically conserved across the JNK family (Supplementary Fig. S1), the kinase has been found to be phosphorylated at a variety of additional S/T/Y residues distributed throughout its structure (Supplementary Table S1 reports all JNK phospho-residues identified up to date). Unfortunately, the majority of these possible phosphorylation sites have been assigned using only proteomic-based discovery-mode mass spectrometry (MS), leaving their functional relevance and the upstream kinases that catalyse their phosphorylation uncharacterised. Few additional JNK phospho-sites have been determined unequivocally using site-specific methods such as specific MS strategies, amino acid sequencing, phosphorylated site-specific antibodies, and site-directed mutagenesis (Table S1). Many of these additional sites are also not conserved across the JNK family, suggesting that they may represent a means of differential phospho-regulation of the JNK variants, and may be responsible for the diversity in the function of the individual JNKs. Although the mechanism by which the JNKs are regulated

Abbreviations: JNK, c-Jun N-terminal kinase; MAPK, mitogen-activated protein kinase; MEKK, mitogen-activated ERK-regulating kinase kinase; MKK, mitogen-activated protein kinase kinase; ATF2, activating transcription factor 2; LC–MS, liquid chromatography mass spectrometry; wt-, wild-type; pp-, dual phosphorylated.

* Corresponding author. Fax: +27 11 7176351.
E-mail address: heinrich.dirr@wits.ac.za (H.W. Dirr).

0006-291X/$ - see front matter © 2013 Elsevier Inc. All rights reserved.
http://dx.doi.org/10.1016/j.bbrc.2013.02.018

in the cell by phosphorylation before and immediately after stress in still not fully understood, the involvement of JNKs in various neurodegenerative and other pathological disorders makes these kinases attractive therapeutic targets [6], and stress the need to fully characterise the significance of the non-canonical phosphosites.

In this study, we explored the phosphorylation events of the most abundant yet least studied JNK variant, JNK1β1 [7], that take place during its heterologous expression in *Escherichia coli* and that are catalysed by active MKK4 *in vitro*. We thus aimed to characterise the nature of phospho-regulation of JNK1β1 by MKK4, since the exact effect that MKK4 has on this JNK variant has not been specifically investigated. Intact protein LC–MS analysis and peptide sequencing was performed to track the phosphorylation sites and patterns of the various forms of JNK1β1 obtained, resulting in the unambiguous identification of novel sites at which MKK4 phosphorylates JNK1β1. ATF2 phosphorylation was used as an index of the catalytic activity of the JNK1β1 phospho-forms. The surprising patterns of JNK1β1 phosphorylation observed here upon its purification from *E. coli* raise important questions that have significant implications for heterologous protein expression.

2. Materials and methods

2.1. Purification and modification of the JNK MAPK phosphorylation cascade proteins

Overexpression and purification of JNK1β1 from *E. coli*, dephosphorylation and deactivation of *E. coli* phosphorylated JNK1β1 by shrimp alkaline phosphatase (SAP), activation of JNK1β1 by reconstituting the MEKK1 → MKK4 → JNK MAPK phosphorylation cascade *in vitro*, as well as the purification of ATF2 (residues 17–96), were performed as previously described [8].

2.2. Additional methods

Methods for the mass spectrometric analysis and sequencing of the JNK1β1 phospho-forms, as well as for determining their relative catalytic activities, are described in Supplementary Methods.

3. Results and discussion

Recently, we have described an improved method to obtain large quantities of active, phosphorylated JNK1β1 [8]. This method aimed first to improve the soluble overexpression of JNK1β1 by harmonising the codon usage frequencies of its open reading frame to those of an *E. coli* expression host (full "codon usage harmonisation" [9]). We were thus able to recreate the natural rate at which JNK1β1 is translated in its native human host as a precautionary measure toward increasing the production of soluble, correctly folded protein in *E. coli*. Purified JNK1β1 was activated by reconstituting the MEKK1 → MKK4 → JNK MAPK phosphorylation cascade *in vitro*; MEKK-C (the constitutively active kinase domain of MEKK1) was used to activate MKK4, which in turn was used to phosphorylate and activate JNK1β1. MKK4 activated JNK1β1 phosphorylated its substrate, ATF2, with high catalytic efficiency [8].

To expand upon the successes of our previous study, we sought to characterise the nature of JNK1β1 phosphorylation by active MKK4, particularly since the efficiency and the precise sites at which the β1 variant of JNK1 is modified for regulation by MKK4 has not been investigated.

MKK4 binds to each JNK isoform selectively, interactions that are mediated by the docking-domains and common docking-domain of MKK4 and JNK, respectively [10]. The affinity of these interactions exhibit isoform-specificity, with JNK1 displaying the greatest specificity for its cognate docking-domain in MKK4 [10]. It has therefore been suggested that MKK4 may have distinct affinities and activities toward the different JNK1 splice variants. Since it has been realised that the effects of MKK4 are splice-variant specific, it becomes significant to characterise the nature of its phosphorylative regulation of each individual JNK variant. Additionally, although they have been shown to display distinct biochemical properties, little is known about the functional relevance of the different JNK slice variants. Studying the individual JNK variants thus expands our understanding of their differences, and will hopefully lead to elucidating their functional diversity. This was achieved in this study using mass spectrometric techniques and enzymatic analysis to identify the states and sites of phosphorylation of the resulting JNK1β1 phospho-forms described in [8].

Intriguingly, our pursuit to acquire and phosphorylate JNK1β1 revealed that the kinase undergoes a significant degree of phosphorylation during overexpression in *E. coli* (even before JNK1β1 had encountered the components thought necessary for its activation) (Supplementary Fig. S2) [8]. We thus used similar tools to provide insight into the means by which JNK1β1 is already partially phosphorylated in *E. coli* without additional *in vitro* treatment, stressing important implications for recombinant expression of kinases in *E. coli*. Therefore, using intact LC–MS protein analysis, we determined the relative populations of the JNK1β1 phospho-forms to provide an indication of the efficiency at which it is phosphorylated. Peptide sequencing was then performed to identify the amino acid locations that are phosphorylated during JNK1β1 overexpression and *in vitro* by MKK4.

3.1. JNK1β1 phosphorylation during expression in E. coli

Intact LC–MS analysis of the untreated JNK1β1 purified from *E. coli* (p*JNK1β1) confirmed that the kinase had indeed been phosphorylated during overexpression in the bacterium (profile 1, Fig. 1). Although the majority of p*JNK1β1 had not been phosphorylated (74%), its mass profile revealed unexpectedly that a small percentage of JNK1β1 (8%) had been phosphorylated in *E. coli* at no less than 4 sites, with concurrently slightly larger populations of singularly (11%) and doubly (7%) phosphorylated kinase existing after expression (Fig. 1).

Peptide sequencing following trypsin digestion of p*JNK1β1 revealed that it was in fact phosphorylated at five discrete sites (Fig. 2; see Supplementary Figs. S4 and S5 for the theoretical trypsin cleavage pattern of JNK1β1 and the high-confidence MS/MS product ion spectra of the resulting phospho-peptides, respectively). Despite being detected in relatively low abundance, corresponding to the small population of each p*JNK1β1 phospho-species (profile 1, Fig. 1), four unambiguous phospho-peptides were detected with >99% confidence (Fig. 2). The canonical JNK T183/Y185 residues were located on the same peptide due to their proximity and properties preventing the generation of peptides that contained each residue separately. Nevertheless, the T183/Y185 phospho-peptides detected were unambiguously and consistently phosphorylated at both residues (Supplementary Fig. S5). The other phospho-peptides identified each contained a single phosphorylated residue, revealing that JNK1β1 is also phosphorylated by some means at T228, S284, and S377 during expression in *E coli* (Fig. 2). While these phospho-sites may initially be considered nothing more than artefacts common to the recombinant overexpression of kinases, the significance of these residues became strikingly evident when determining the sites at which active MKK4 phosphorylates JNK1β1 (discussed below).

To determine if the phosphate groups added to the activation (T183/Y185) and additional residues (T228/S284/S377) during expression induce activation of JNK1β1, and to approximate the

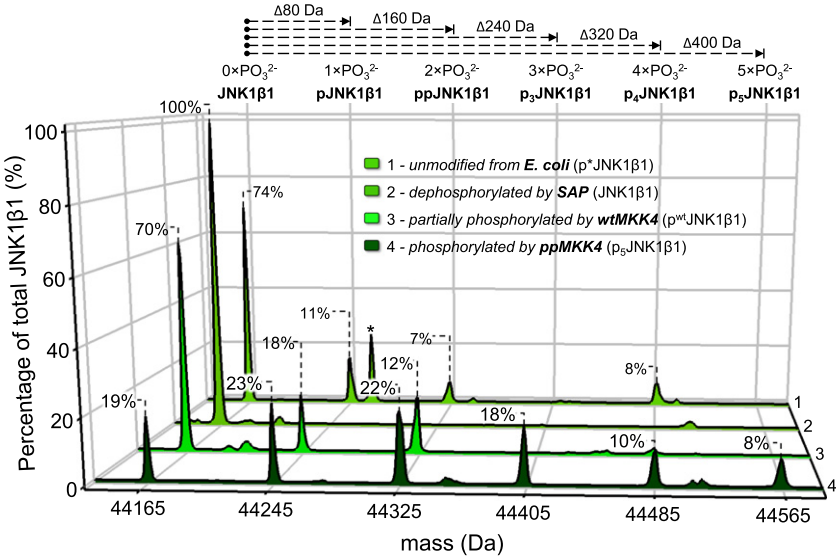

Fig. 1. The extent of phosphorylation of each JNK1β1 phospho-form, determined by intact protein LC–MS analysis. Intact protein mass profiles were generated by transforming the deconvoluted mass spectra of each phospho-form (Supplementary Fig. S3) so that the intensities of each JNK1β1 mass peak are expressed as a percentage of the total JNK1β1 present. This was calculated using the area under a particular peak relative to the total area under all JNK1β1 mass peaks. Non-phosphorylated JNK1β1 has a modal mass of 44 165 Da. The additional mass species increasing by multiples of 80 Da correspond to the addition of up to 5 phosphate groups. Profiles are representative of at least two independent experiments. "*" denotes likely contaminants.

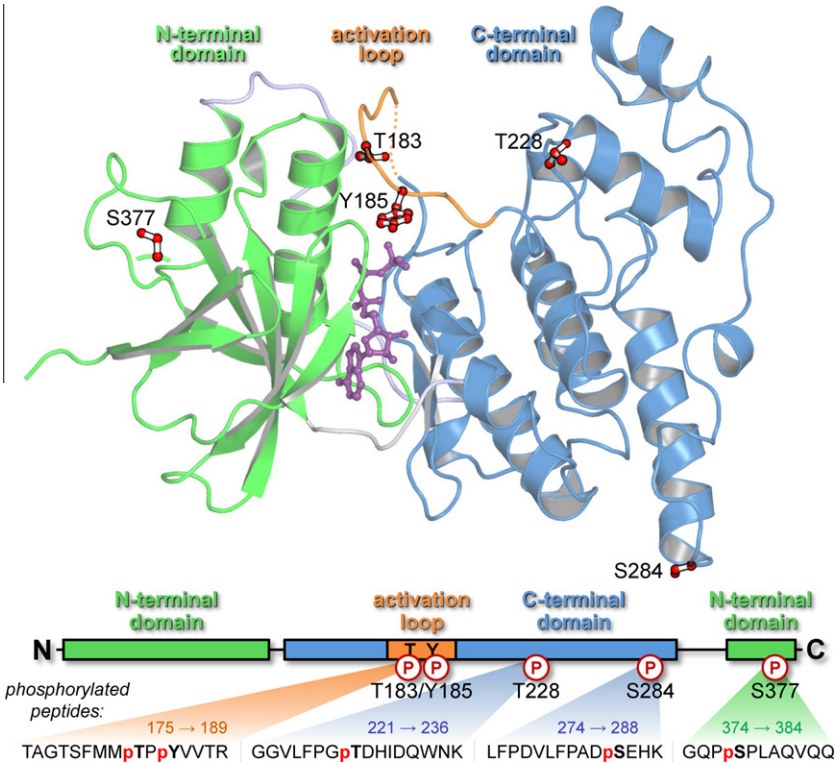

Fig. 2. Mapping JNK1β1 residues that are phosphorylated both during expression in *E. coli* and *in vitro* by active MKK4. The tryptic phospho-peptides identified and the location of the canonical (T183/Y185) and novel (T228/S184/S377) phosphorylated residues are shown. As the C-terminal residues L364-Q384 were not resolved in the crystal structure, an additional serine has been used to indicate the position of S377. The protein structure was rendered using PyMOL™ v. 0.99 (DeLano Scientific, San Carlos, CA) using the PDB code 3ELJ [18].

relative activity of the kinase if they do, we monitored the rate at which p*JNK1β1 produces an electrophoretic shift in ATF2 observed on a Tricine–SDS-PAGE gel when it is singularly and doubly phosphorylated (the first report of its kind) (Fig. 3). This novel approach to an electrophoretic mobility shift assay revealed that p*JNK1β1 was in fact active and able to phosphorylate ATF2, but at a relatively slow rate (panel A, Fig. 3). JNK1β1 is thus activated in *E. coli* by, not unexpectedly, phosphorylation of its T183/Y185 (and possibly the other) residues, yet the small degree at which it had become modified in the bacterium (Fig. 1) can account for the low activity displayed.

Considering recent findings, only a few possibilities exist why JNK1β1 may become phosphorylated during bacterial overexpression (Supplementary Fig. S6, and discussed briefly in [8]). It is

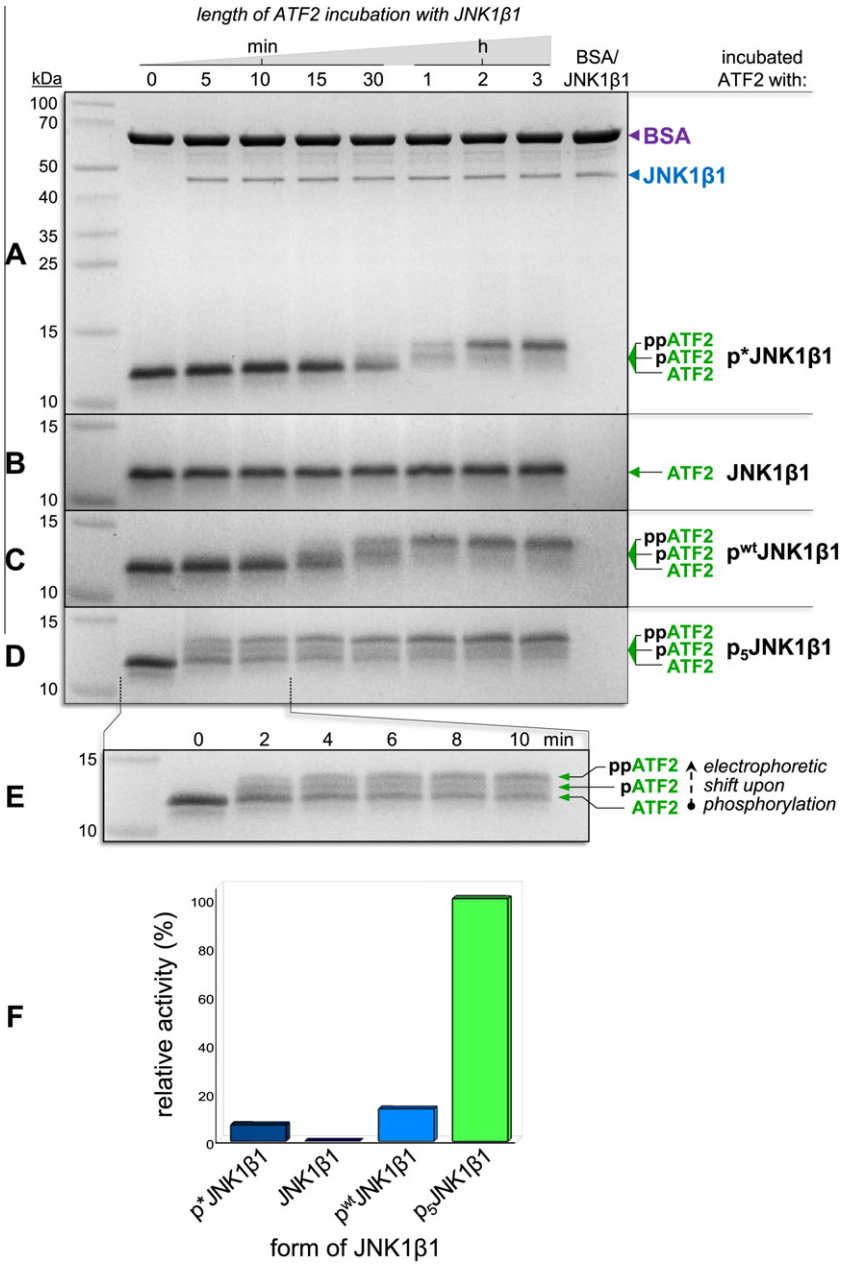

Fig. 3. Relative catalytic activities of the JNK1β1 phospho-forms. (A–E) The rate at which each JNK1β1 phospho-form induces an electrophoretic shift in ATF2(17–96), observed on a 16% Tris–Tricine gel, when it is singularly and doubly phosphorylated at T69/T71 (as confirmed in [8]) was used as an indication of their catalytic activities. (A) The slow phosphorylation of ATF2 by *E. coli* purified p*JNK1β1, and the lack thereof by (B) dephosphorylated, inactive JNK1β1. (C) The slow rate of ATF2 phosphorylation by p^{wt}JNK1β1 partially phosphorylated by untreated MKK4. (D and E) Efficient ATF2 phosphorylation by p_5JNK1β1 phosphorylated by ppMKK4. 1 μM of each JNK1β1 was incubated with 30 μM ATF2, 0.2 mg/ml BSA, 10 mM $MgCl_2$, and 1 mM ATP for 3 h at 25 °C. (F) Graphical comparison of the relative activities determined in A–E, each expressed as a percentage of the activity of p_5JNK1β1.

recognised that kinases may undergo phosphorylation/autophosphorylation during heterologous protein expression. Shrestha et al. [11] has suggested that as the cell is flooded with recombinant protein during overexpression, native kinases are capable of phosphorylating the newly-produced kinase polypeptides during co- or post-translational folding. This would allow phosphate groups to be introduced at both canonical and/or non-standard sites that may or may not be surface exposed. Their study analysed the conditions under which human kinases exhibit autophosphorylation during overexpression, and demonstrated indirectly that altering the kinetics of protein production and folding by adjusting the induction temperature and/or inducer concentration, influences the degree of phosphorylation.

Since native, fully folded JNK1 is unable to undergo post-translational autophosphorylation both *in vivo* and *in vitro* [8,12], the *E. coli* phosphorylation of JNK1β1 described here may be due to this "co-folding autophosphorylation" phenomenon (Fig. S6). As the phosphorylation of non-codon harmonised JNK1 during its overexpression has not been observed elsewhere or reported before, it is possible that the unique yet natural kinetics of translation and folding of our JNK1β1 provided by codon usage harmonisation [8], may allow phosphorylation to occur during co-translational folding. Since codon harmonisation is the only noteworthy difference in our expression system when compared to those used elsewhere for JNK1, these other systems act as numerous controls that highlight the absence of phosphorylation of non-codon

harmonised JNK1 when expressed in *E. coli*. It is therefore fair to propose that the translation kinetics of JNK1β1 influence its ability to be phosphorylated during its overexpression, as implied by Shrestha et al. [11].

We also cannot exclude the idea that unidentified endogenous *E. coli* S/T/Y kinases may be responsible for the phosphorylation of JNK1β1 during expression, as initially suggested by Yang and Lui [13]. It has been found recently that, while few S/T/Y kinases have been directly identified in prokaryotes, at least 80 bacterial proteins are naturally phosphorylated at S/T/Y residues [14]. Considering the recently realised existence of these eukaryotic-like bacterial kinases, it is becoming increasingly unwise to assume that recombinant eukaryotic proteins will purify in a homogenous, non-phosphorylated form [14,15]. It is therefore a possibility that *E. coli* kinases may recognise JNK1β1 in a manner similar to that of its natural activator, MKK4, thereby catalysing its phosphorylation (Fig. S6). As this has not been previously observed for JNK, it is likely that this too occurs during co-translational folding, since the natural kinetics of translation of JNK1β1 imparted by our codon harmonisation may now permit bacterial kinases to interact with phosphorylatable motifs during the translational folding of JNK1β1 (Fig. S6).

Interestingly, only the soluble cell fraction contained phosphorylated JNK1β1 (Fig. S2). It is therefore conceivable too that either co-translational phosphorylation of JNK1β1 promotes its proper native folding, or perhaps only the partially folded JNK1β1 polypeptides following the native folding pathway are able to be phosphorylated during translation.

3.2. Dephosphorylation and deactivation of E. coli purified JNK1β1

We initially dephosphorylated p*JNK1β1 using shrimp alkaline phosphatase (SAP) and monitored the reaction by Western blotting [8], yet to verify that the phosphate groups that had been added during expression had all been removed, we also performed intact LC–MS on the dephosphorylated JNK1β1. It was important to establish that this could be achieved because, due to the inaccessibility of some of the phospho-residues upon final folding of the protein, the incorporated phosphate groups may not be able to be removed by subsequent treatment with phosphatases [16]. The LC–MS analysis revealed that after incubation of p*JNK1β1 with SAP for 5 h, the kinase becomes completely dephosphorylated as the additional peaks situated at multiples of 80 Da above the mass of non-phosphorylated JNK1β1 seen in untreated kinase were no longer detected (profile 2, Fig. 1). Testing the catalytic activity of the kinase also revealed that dephosphorylation completely deactivates the kinase, as all of it activity toward ATF2 was eliminated (panel B, Fig. 3). The phosphate groups introduced during expression were thus all available and susceptible to SAP dephosphorylation, consistent with the observed external accessibility of the phospho-residues (Fig. 2).

3.3. JNK1β1 phosphorylation by MKK4 in vitro

Upon acquiring non-phosphorylated JNK1β1, we sought to generate phosphorylated, fully active JNK1β1 by reconstituting the JNK MAPK cascade *in vitro*.

To first control for the effect of unmodified, wild-type MKK4 (that has not encountered MEKK-C), we first incubated untreated MKK4 with dephosphorylated JNK1β1, and evaluated the change in its state of phosphorylation by intact LC–MS. Interestingly, JNK1β1 is able to be re-phosphorylated to a small degree by untreated MKK4, producing small populations of singly (18%) and doubly (12%) phosphorylated JNK1β1 (p^{wt}JNK1β1, profile 3, Fig. 1). This suggests that MKK4, when recombinantly expressed in *E. coli*, also becomes partially phosphorylated. This finding reiterates the value of determining if heterologously expressed proteins have already undergone co- or post-translational modifications before performing downstream analyses that may be affected by their presence. p^{wt}JNK1β1 is also partially active and can phosphorylate ATF2 (panel C, Fig. 3), yet also at a slow rate due to its ineffective activation and the consequential low population of phosphorylated kinase (profile 3, Fig. 1).

Efficient phospho-activation of JNK1β1 was then achieved by incubating active MKK4 (ppMKK4; previously phosphorylated by MEKK-C), with dephosphorylated JNK1β1 for $\geqslant$3 h at a 10:1 JNK1β1:ppMKK4 molar ratio. Intact LC–MS indicated that JNK1β1 is phosphorylated *in vitro* at five sites by ppMKK4, and to a sufficient efficiency that only a small population of JNK1β1 was not modified at all (p_5JNK1β1, profile 4, Fig. 1). Significant levels of the other phospho-forms existed, with the largest populations comprising singularly and doubly phosphorylated JNK1β1 (profile 4, Fig. 1).

Peptide sequencing of a tryptic digest of p_5JNK1β1 illustrated that ppMKK4 not only phosphorylates JNK1β1 efficiently and expectedly at its canonical T183/Y185 residues *in vitro*, but also unequivocally at T228, S284, and S377 (Fig. 2, and see Fig. S5 for the MS/MS product ion spectra of the resulting phospho-peptides). Curiously, these are the identical sites at which JNK1β1 became phosphorylated during expression in *E. coli*, albeit to a significantly higher degree (Figs. 1 and 2). The initial complete dephosphorylation of the residues phosphorylated during expression followed by their subsequent *in vitro* re-phosphorylation by ppMKK4, suggests that the *E. coli* phospho-activation of JNK1β1 is more a systematic than random event. In other words, the phosphorylation of JNK1β1 in *E. coli* appears to mimic the events that occur in its natural host environment, since the canonical and additional sites were phosphorylated both endogenously in *E. coli* and exogenously by reconstituting the JNK MAPK pathway.

While S377 has been identified previously as a JNK1β1 phospho-site in MS-based proteomics analysis of the human kinome (Table S1), its physiological relevance or the regulatory kinase/s that catalyse its phosphorylation has not been characterised. T228 and S284 are newly identified JNK1β1 phospho-sites, and novel residues known to be phosphorylated by MKK4. S377 and S284 are fully conserved across the JNK splice variants, while T228 is conserved within the β variants of JNK1 and the α variants of JNK2 (Fig. S1). Phosphorylation of S377 and S284 may therefore represent a general mechanism for JNK regulation, whereas T228 phosphorylation may allow differential regulation of the relevant JNK variants to induce their divergent and partially contradictory cellular actions.

A possible explanation for the phosphorylation of these residues is that, once activated by the ppMKK4-dependent phosphorylation of T183/Y185, JNK1β1 then phosphorylates itself at T228/S284/S377. While this may be possible for S377, neither T228 nor S284 is followed by a proline, a requirement for JNK to phosphorylate other proteins [4]. This strongly suggests that at least T228 and S284 are phosphorylated by ppMKK4.

To begin to understand the biological role of the three additional JNK1β1 phospho-sites, we intend to determine the conditions under which pT228, pS284 and pS377 naturally occur in human cells (e.g. 293T cells), and how they affect normal cellular functioning. We also intend to fully elucidate the structural and thus functional relevance of T228/S284/S377 phosphorylation, yet examining the relative activity of p_5JNK1β1 indicates that these modifications, in combination, do not have an overall or net inhibitory effect on the kinase. It is clear that p_5JNK1β1 is highly active and phosphorylates ATF2 efficiently (Fig. 3), emphasising the effectiveness at which ppMKK4 generates large quantities of phosphorylated, active JNK1β1 (profile 4, Fig. 1). We have also previously determined the specific activity of p_5JNK1β1, which was measured

at a high 3.3 ± 0.4 μmol of ATF2/min/mg of kinase [8]. Although the relevance of the three additional phospho-sites may not be known at present, it is possible that in addition to the effect that they may have on the activity of JNK1β1, they may play other roles that could include the regulation of; the interaction of JNK1β1 with its >50 binding partners [4], its translocation between different cellular compartments, the rate at which T183/Y185 are dephosphorylated, or the stability of the kinase.

Furthermore, T228 and S284 neighbour the N-capping motifs of the α-helices comprising N229-L241 and E285-M301, respectively (Fig. 2). Helix-capping motifs contribute to the conformational stability of both the α-helix and the overall protein in which they are situated, and as such the capacity for phosphorylation to regulate the function of proteins by modulating the stability of their α-helices is well known (e.g. see [17]). The locations of T228 and S284 therefore allow this mechanism to be a promising means by which their phosphorylation may affect JNK1β1 functioning.

Evaluating the propensity that each JNK1β1 phospho-site has to be phosphorylated *in vitro* by ppMKK4 by comparing the relative abundance of the phosphorylated and non-phosphorylated populations of each precursor p_5JNK1β1 phospho-peptide (see Supplementary material), the order of their phosphorylation propensity was determined to be: T183/Y185 > S377 > T228 ⩾ S284. As T183 and Y185 have, unsurprisingly, the greatest predisposition to be phosphorylated, p_5JNK1β1 likely comprises approximately 60% kinase phosphorylated on at least T183 and Y185.

The relatively low percentage of JNK1β1 phosphorylated at either pT228 and/or pS284 (each comprising ±10% of the total phosphorylated kinase population; Table S2) may account for their previous non-detection in mammalian cells, yet the power and sensitivity of single-protein mass spectrometry (as performed here) confirm that these phospho-sites are not false positives.

Our studies provide important insights into the fate of JNK1β1 overexpressed in *E. coli*, raising interesting new questions of the possibility that endogenous *E. coli* kinases may be involved in the activation of heterologously expressed MAPKs. This points at the prospect that prokaryotic kinases may recognise eukaryotic phosphorylation motifs, or that there may be degree of evolutionary relatedness between prokaryotes and eukaryotes. We are however not able to affirmatively conclude that JNK1β1 is subject to phosphorylative activation by endogenous bacterial kinases because this study was not designed to prove this hypothesis. Nevertheless, future research could be aimed at exploring and identifying bacterial kinases possibly capable of phosphorylating JNK1β1 and other eukaryotic proteins that undergo post-translational modification. The concept of using a codon-harmonised JNK1β1 gene to improve or naturalise its transitional kinetics to prime the protein for co- or post-translational modification, catalysed either by itself or endogenous host proteins, also has significant implications for all heterologous protein expression, highlighting the value of its further investigation. Furthermore, the functional and biochemical relevance of the novel JNK1β1 phosphorylation sites we have identified could also give important insights into the molecular mechanisms by which JNK1β1 is regulated, as well as shed light on the differential regulation and hence functional relevance of the different JNK splice variants.

Acknowledgments

This work was supported by the University of the Witwatersrand, South African National Research Foundation (Grants: 60810, 65510 and 68898 to H.W.D) and South African Research Chairs Initiative of the Department of Science and Technology and National Research Foundation (Grant: 64788 to H.W.D).

Appendix A. Supplementary data

Supplementary data associated with this article can be found, in the online version, at http://dx.doi.org/10.1016/j.bbrc.2013.02.018.

References

[1] R.J. Davis, Signal transduction by the JNK group of MAP kinases, Cell 103 (2000).
[2] S. Gupta, T. Barrett, A.J. Whitmarsh, J. Cavanagh, H.K. Sluss, B. Derijard, R.J. Davis, Selective interaction of JNK protein kinase isoforms with transcription factors, EMBO J. 15 (1996) 2760–2770.
[3] L. Chang, Mammalian MAP kinase signaling cascades, Nature 410 (2001) 37–40.
[4] M.A. Bogoyevitch, B. Kobe, Uses for JNK: the many and varied substrates of the c-Jun N-terminal kinases, Microbiol. Mol. Biol. R. 70 (2006) 1061–1095.
[5] Y. Fleming, C.G. Armstrong, N. Morrice, A. Paterson, M. Goedert, P. Cohen, Synergistic activation of stress-activated protein kinase 1/c-Jun N-terminal kinase (SAPK1/JNK) isoforms by mitogen-activated protein kinase kinase 4 (MKK4) and MKK7, Biochem. J. 352 (2000) 145–154.
[6] J. Cui, M. Zhang, Y. Zhang, Z. Xu, JNK pathway: diseases and therapeutic potential, Acta. Pharmacol. Sin. 28 (2007) 601–608.
[7] S.C. Dreskin, G.W. Thomas, S.N. Dale, L.E. Heasley, Isoforms of Jun kinase are differentially expressed and activated in human monocyte/macrophage (THP-1) cells, J. Immunol. 166 (2001) 5646–5653.
[8] G.R. Owen, I. Achilonu, H.W. Dirr, High yield purification of JNK1β1 and activation by *in vitro* reconstitution of the MEKK1 → MKK4 → JNK MAPK phosphorylation cascade, Protein Expr. Purif. 87 (2013) 87–99.
[9] E. Angov, C.J. Hillier, R.L. Kincaid, J.A. Lyon, Heterologous protein expression is enhanced by harmonizing the codon usage frequencies of the target gene with those of the expression host, PLoS Biol. 3 (2008) 1–10.
[10] D.T. Ho, A.J. Bardwell, M. Abdollahi, L. Bardwell, A docking site in MKK4 mediates high affinity binding to JNK MAPKs and competes with similar docking sites in JNK substrates, J. Biol. Chem. 278 (2003) 32662–32672.
[11] A. Shrestha, G. Hamilton, E. O'Neill, S. Knapp, J.M. Elkins, Analysis of conditions affecting auto-phosphorylation of human kinases during expression in bacteria, Protein Expr. Purif. 81 (2012) 136–143.
[12] J. Cui, M. Holgado-Madruga, W. Su, H. Tsuiki, P. Wedegaertner, A.J. Wong, Identification of a specific domain responsible for JNK2α2 autophosphorylation, J. Biol. Chem. 280 (2005) 9913–9920.
[13] L. Yang, Z.R. Liu, Bacterially expressed recombinant p68 RNA helicase is phosphorylated on serine, threonine, and tyrosine residues, Protein Expr. Purif. 35 (2004) 327–333.
[14] B. Macek, I. Mijakovic, Site-specific analysis of bacterial phosphoproteomes, Proteomics 11 (2011) 3002–3011.
[15] C. Oudot, J.C. Cortay, C. Blanchet, D.C. Laporte, A. Di Pietro, A.J. Cozzone, J.M. Jault, The "catalytic" triad of isocitrate dehydrogenase kinase/phosphatase from *E. coli* and its relationship with that found in eukaryotic protein kinases, Biochemistry 40 (2001) 3047–3055.
[16] R. Kinstrie, N. Luebbering, M.-S. Diego, G. Sibbet, J. Han, P.A. Lochhead, V. Cleghon, Characterization of a domain that transiently converts class 2 DYRKs into intramolecular tyrosine kinases, Sci. Signal. 3 (2009) ra16.
[17] A. Quan, J. Xue, J. Wielens, K.J. Smillie, V. Anggono, M.W. Parker, M.A. Cousin, M.E. Graham, P.J. Robinson, Phosphorylation of syndapin I F-BAR domain at two helix-capping motifs regulates membrane tubulation, Proc. Natl. Acad. Sci. USA 109 (2012) 3760–3765.
[18] S.D. Chamberlain, A.M. Redman, J.W. Wilson, F. Deanda, J.B. Shotwell, R. Gerding, H. Lei, B. Yang, K.L. Stevens, A.M. Hassell, L.M. Shewchuk, M.A. Leesnitzer, J.L. Smith, P. Sabbatini, C. Atkins, A. Groy, J.L. Rowand, R. Kumar, R.A.J. Mook, G. Moorthy, S. Patnaik, Optimization of 4,6-bis-anilino-1H-pyrrolo[2,3-d]pyrimidine IGF-1R tyrosine kinase inhibitors towards JNK selectivity, Bioorg. Med. Chem. Lett. 19 (2009) 360–364.

JNK1β1 is phosphorylated during expression in *E. coli* and *in vitro* by MKK4 at three identical novel sites

GAVIN R. OWEN[a], STOYAN STOYCHEV[b], IKECHUKWU ACHILONU[a], AND HEINI W. DIRR[a]

[a]Protein Structure-Function Research Unit, School of Molecular and Cell Biology, University of the Witwatersrand, Johannesburg 2050, South Africa.

[b]Council for Scientific and Industrial Research, Biosciences, Pretoria, 0001, South Africa.

APPENDIX A.

SUPPLEMENTARY MATERIAL

- Table of Contents -

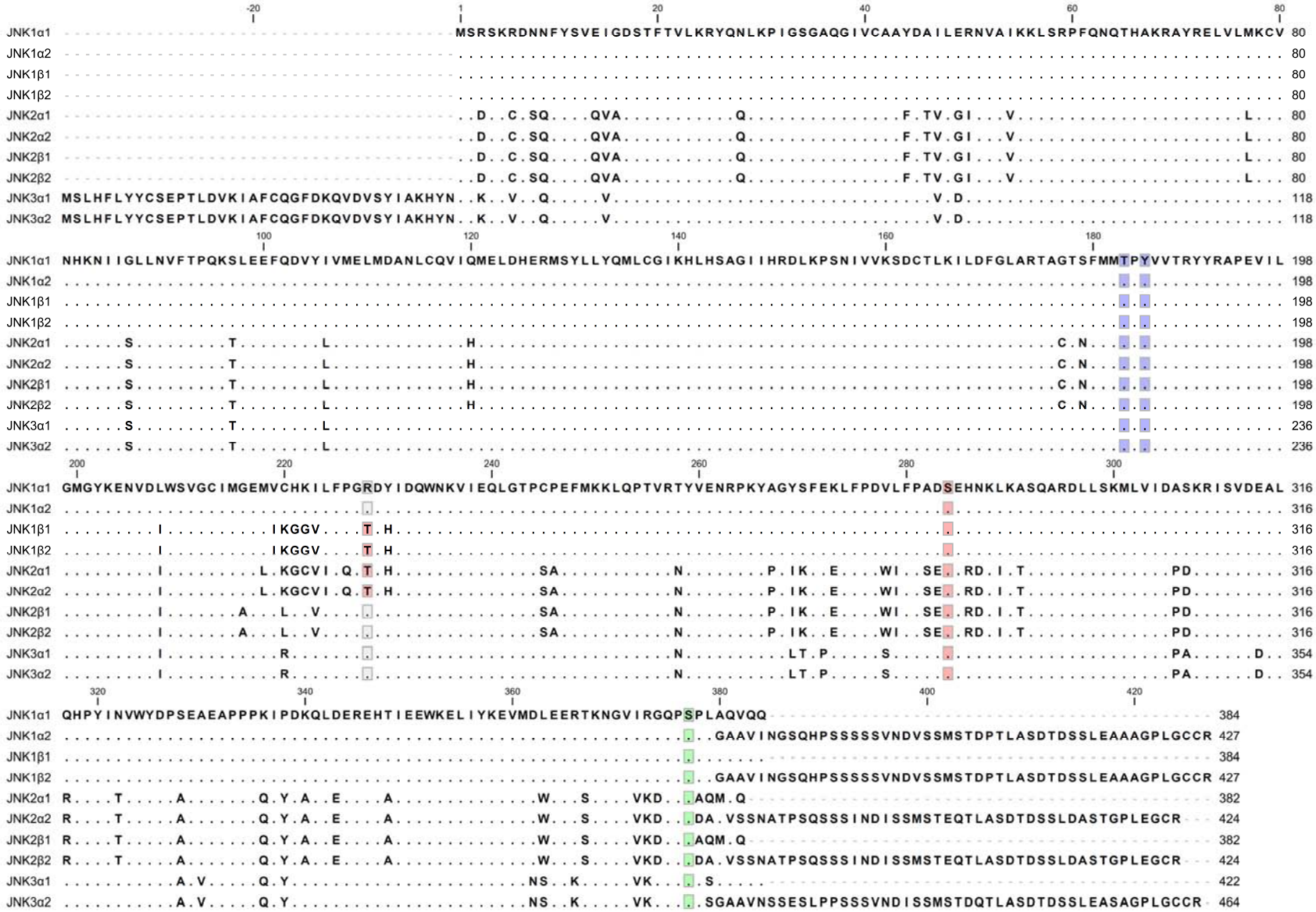

Fig. S1. Protein sequence alignment of the 3 JNK isoforms and their related splice variants. The canonical T183 and Y185 phospho-residues are indicated in blue, while the newly identified phospho-sites, T228 (not fully conserved) and S284 (conserved), are indicated in red. The previously identified yet uncharacterised and conserved phospho-residue, S377, is indicated in green. Identical residues are indicated as dots.

Table S1. JNK residues found previously to be additional sites of phosphorylation. The canonical T183 and Y185 residues (T221 and Y223 in JNK3), the phosphorylation of which is known to induce JNK activation, have not been included.

Phospho-residue	JNK isoform found to be phosphorylated	Residue conservation in JNKs	Phosphory-lation catalysed by	Effect of phosphory-lation	Site assigned by	Reference/s
S129	JNK1,2	All	PKC	augments JNK phospho-activation by MKK4/MKK7	SS[a]	[1,2,3]
T131	JNK3	All (T93 in JNK1,2)	cdk5	inhibits the kinase activity of JNK3	SS	[4]
S155	JNK1	All	—[c]	—	MS[b]	[5]
T178	All	All (T216 in JNK3)	—	—	SS, MS	[6,7]
S179	JNK1,3	JNK1,3	—	—	MS	[7,8]
T188	All	All (T226 in JNK3)	—	—	MS	[8]
T255	JNK1	All	—	—	MS	[9]
T258	JNK1	JNK1	—	—	MS	[9]
Y259	JNK1	All	—	—	MS	[9]
Y357	JNK1	All	—	—	MS	[9]
T367	JNK1	JNK1,3	—	—	MS	[9]
S377	JNK1,3	All (S415 in JNK3)	—	—	MS	[5,10-16]
T404	JNK2	JNK1α2, JNK1β2, JNK2α2, JNK2β2	MKK7	—	SS, MS	[5,17]
S407	JNK2	JNK2α2, JNK2β2	MKK7	—	SS	[17]
S417	JNK3	JNK3	—	—	MS	[5]

[a] "SS" denotes phospho-sites that have been unambiguously determined by site-specific methods, including specific MS strategies, amino acid sequencing, phosphorylated site-specific antibodies, and site-directed mutagenesis.

[b] "MS" indicates phospho-sites that were assigned by proteomic-based discovery-mode mass spectrometry only.

[c] "**—**" refers to that which is currently unknown.

SUPPLEMENTARY METHODS

Enzymatic assays of JNK1β1

To approximate the relative catalytic activity of each JNK1β1 phospho-form, the rate at which they phosphorylate the substrate, ATF2, was tested. This was achieved by monitoring the electrophoretic shift observed in ATF2 over time upon single and dual phosphorylation by JNK1β1 when subjected to Tricine–SDS-PAGE. The ATF2 phosphorylation assays were conducted as follows: 1 µM JNK1β1 (of each specific form), 30 µM ATF2, 0.2 mg/ml BSA, 10 mM $MgCl_2$, and 1 mM ATP, in Kinase-Reaction Buffer (10 mM Tris-HCl, pH 8.0, comprising 150 mM NaCl, 1 mM DTT, 0.02% (v/v) Triton X-100, and 0.02% (w/v) NaN_3) was incubated at 25 °C for 3 h. Samples were taken at regular intervals and immediately treated for reducing SDS-PAGE. The ATF2 samples were then resolved by Tricine–SDS-PAGE on a 16% Tris-Tricine gel [18] and stained with Coomassie Blue R-250.

Intact protein LC-MS

Intact JNK1β1 samples were analysed using a Dionex Ultimate 3000 RSLC system coupled to a QSTAR ELITE mass spectrometer. Proteins were loaded on a Jupiter C4 column (1 × 150 mm, 5 µm particle size) and eluted using a flow-rate of 200 µl/min with a gradient: 5-60% B in 25 min (A: 0.1% formic acid; B: 80% MeOH/0.1% formic acid). An electrospray voltage of 5.5 kV was applied and MS scans were acquired from *m/z* 700-2000. The multiply charged protein envelopes were deconvoluted using Bayesian Protein Reconstruct tool of AB Sciex, Analyst QS 2.0 using mass ranges of 10,000-70,000 Da, an S/N threshold of 20 and 3% minimum spectral intensity.

LC-MS/MS-based peptide sequencing

JNK1β1 samples were digested by incubation with trypsin (ratio of 1:50, trypsin:JNK1β1) in Kinase-Reaction Buffer supplemented with 1 mM $CaCl_2$ and 25 mM NH_4HCO_3, pH 8.0, for 18 h at 37 °C. After quenching the reaction with 0.5% formic acid and vacuum drying each sample, the JNK1β1 digests were resuspended in 35 µl, 2% acetonitrile/0.2% formic acid and analysed using a Dionex Ultimate 3000 RSLC system coupled to a QSTAR ELITE mass spectrometer. Peptides were first de-salted on an Acclaim PepMap C18 trap column (75 µm × 2 cm) for 8 min at 5 µl/min using 2% acetonitrile/0.2% formic acid, than separated on Acclain PepMap C18 RSLC column (75 µm × 15 cm, 2 µm particle size). Peptide elution was achieved using a flow-rate of 500 nl/min with a gradient: 4-60% B in 30 min

(A: 0.1% formic acid; B: 80% acetonitrile/0.1% formic acid). Nano-spray was achieved using a MicroIonSpray head assembled with a New Objective, PicoTip emitter. An electrospray voltage of 2.0-2.8 kV was applied to the emitter. The QSTAR ELITE mass spectrometer was operated in Information Dependant Acquisition using an Exit Factor of 7.0 and Maximum Accumulation Time of 2.5 sec. MS scans were acquired from *m/z* 400-1500 and the three most intense ions were automatically fragmented in Q2 collision cells using nitrogen as the collision gas. Collision energies were chosen automatically as function of *m/z* and charge.

Protein and peptide identification was performed using NCBI's msdb database and the Paraghon^{TM} algorithm *Thorough* search in Protein Pilot. An identification confidence of 95% was selected during searches.

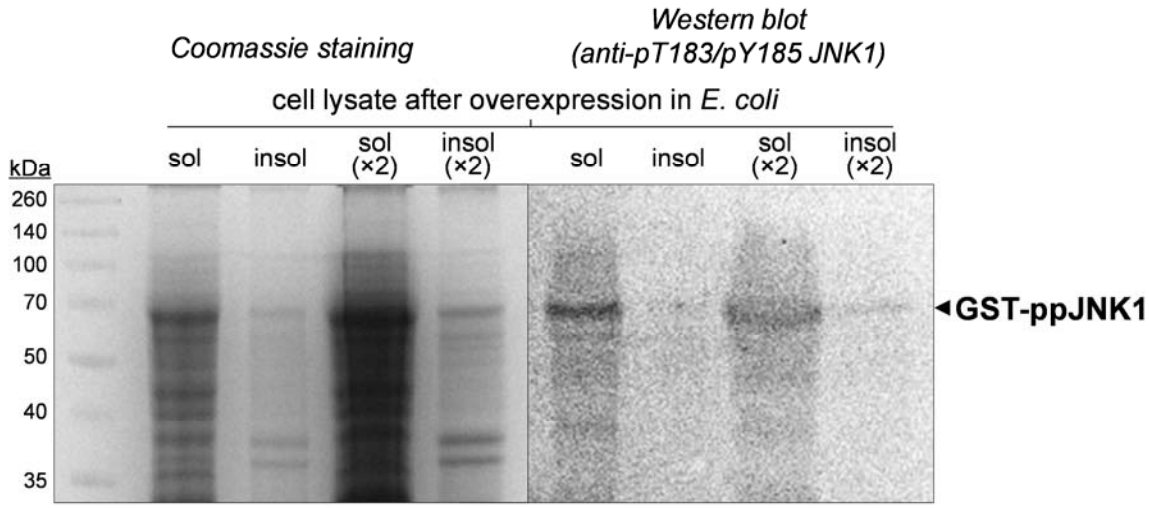

Fig. S2. Phosphorylated JNK1β1 is present predominantly in the soluble cell fraction of *E. coli* BL21(DE3)pLysS after its overexpression. Western blot analyses (using anti-pT183/pY185 JNK1 antibodies) of the soluble and insoluble bacterial cell lysates after overexpression of GST-JNK1 (subsequently processed and purified as JNK1β1 as described in [19]) demonstrates the large quantity of phosphorylated, soluble JNK1β1 expressed. Conversely, only a small degree of the insoluble JNK1β1 expressed displayed phosphorylation.

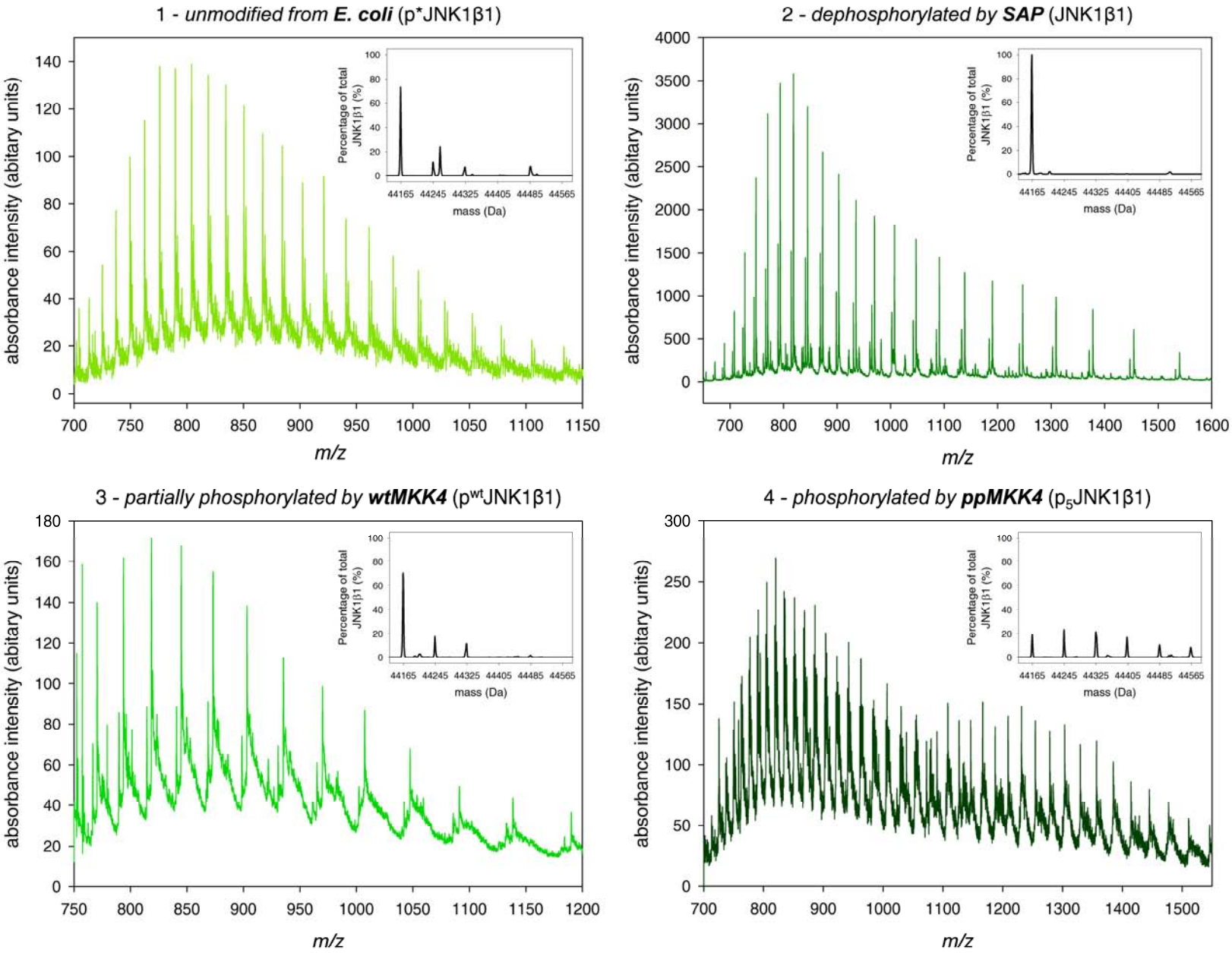

Fig. S3. Electrospray ionisation charge state envelopes of the JNK1β1 phospho-forms. Insets show the corresponding deconvoluted intact mass spectra presented in Fig. 1. Spectra were obtained and deconvoluted as described in the supplementary materials and methods.

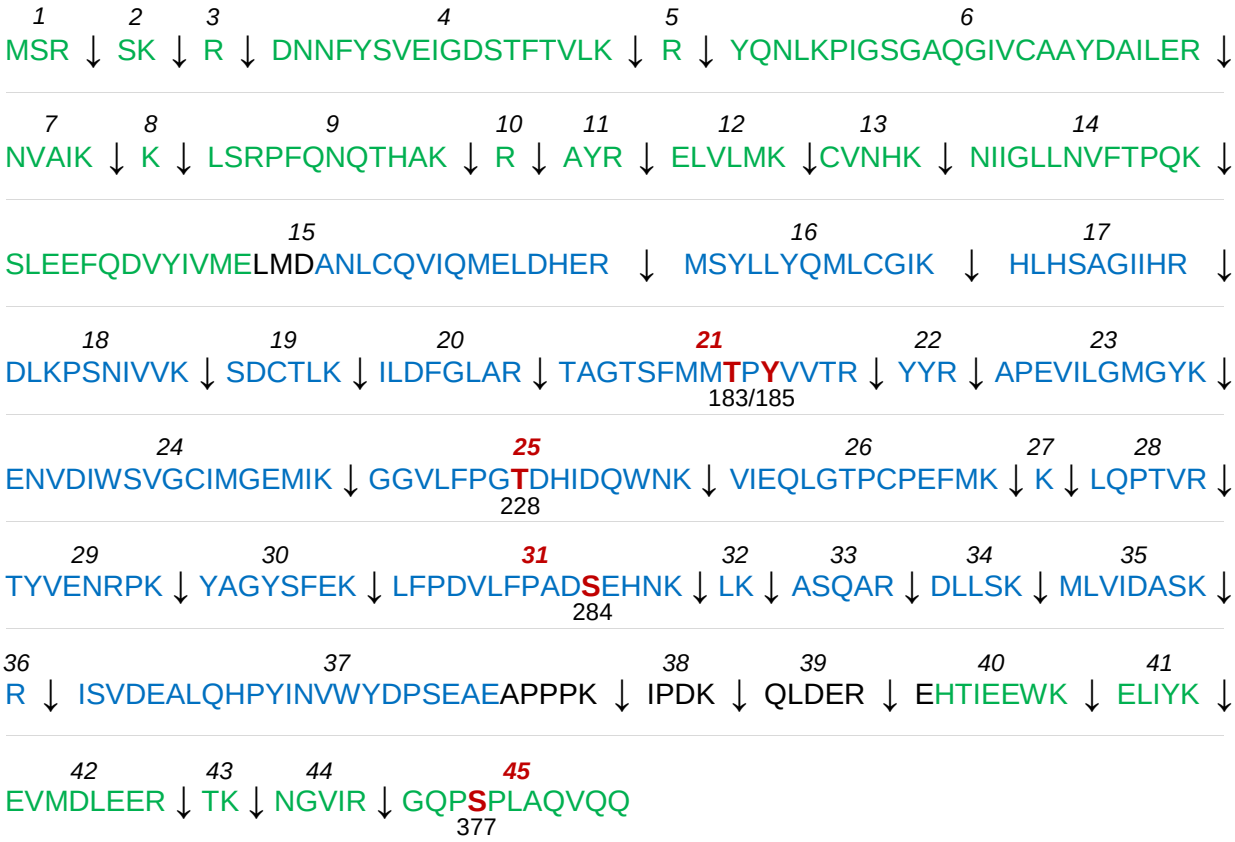

Fig. S4. Simulated trypsin digest of JNK1β1. The location of trypsin cleavage sites (↓) in JNK1β1 generate a theoretical cleavage pattern that contains 45 candidate peptide fragments (numbered above in italics) of varying length. The fragments and their specific residues found to be phosphorylated upon sequencing of the resulting tryptic peptides of JNK1β1 (phosphorylated both during expression in *E. coli* and *in vitro* by MKK4) are indicated in red. The amino acids that constitute the N- and C-terminal domains of JNK1β1 are indicated in green and blue, respectively.

- Supplementary Figure S5 -

Page 1 of 4

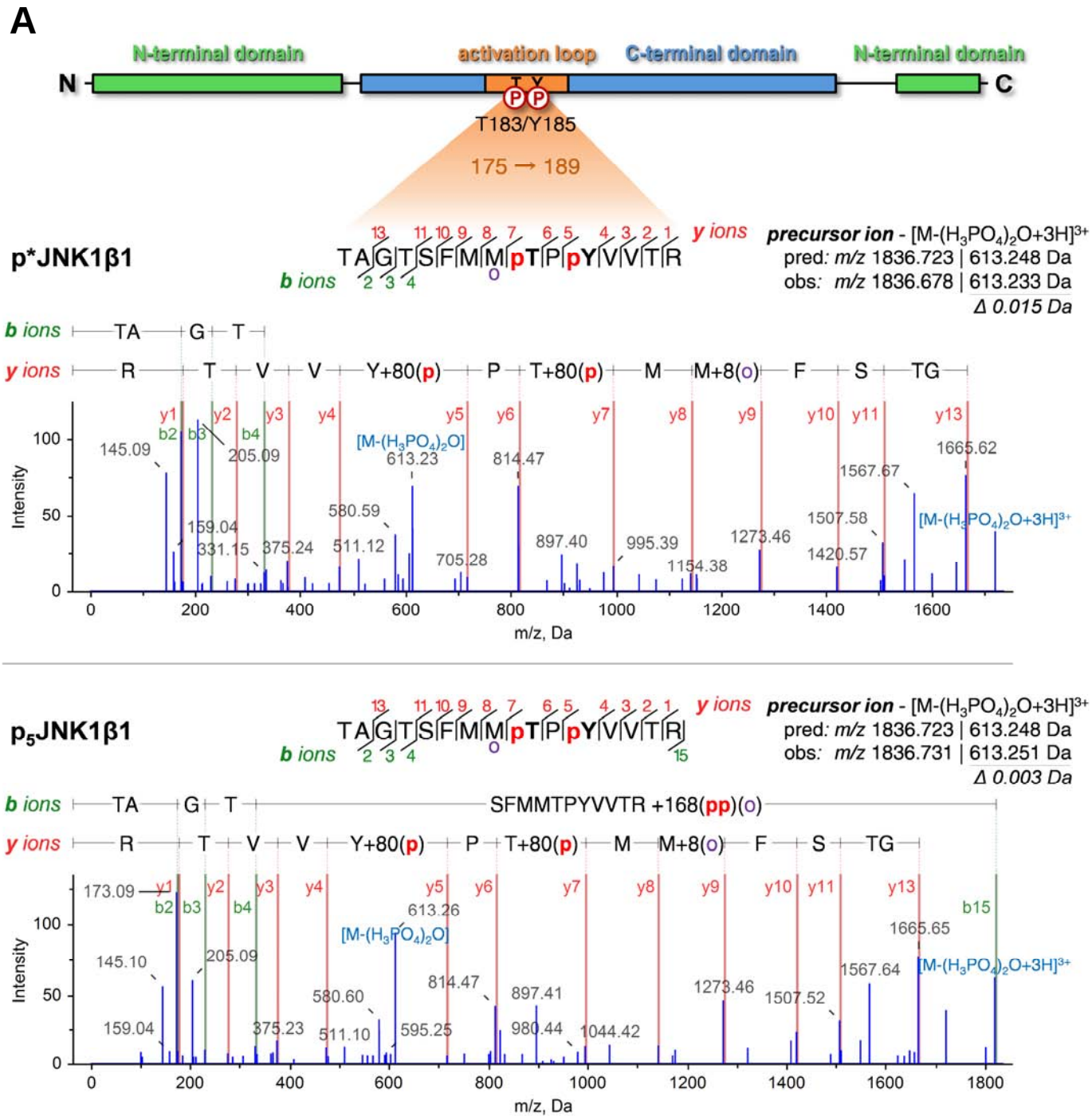

(*Figure S5 continues onto the next page; see page xii for its legend*)

- Supplementary Figure S5 -

Page 2 of 4

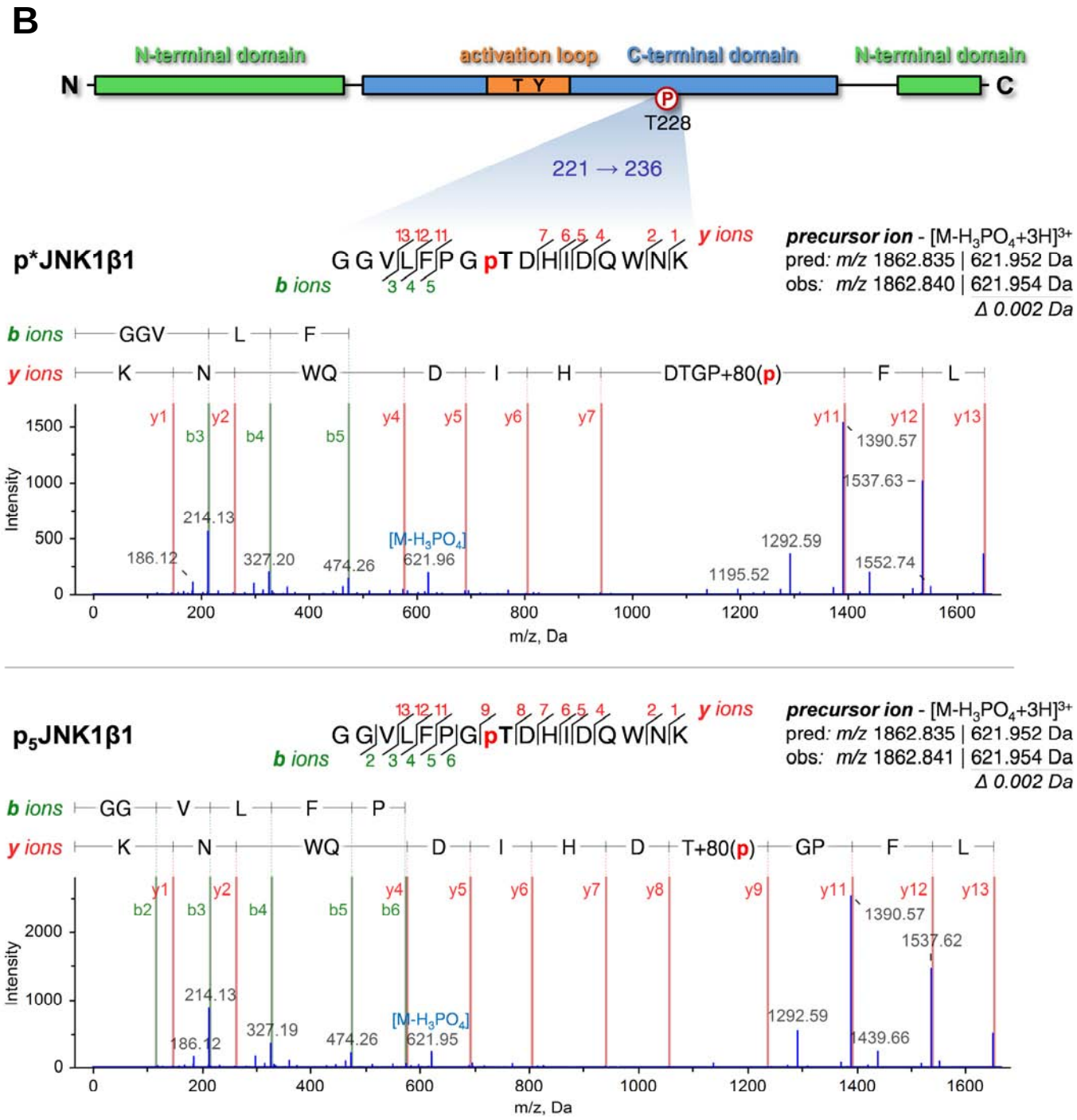

(*Figure S5 continues onto the next page; see page xii for its legend*)

- Supplementary Figure S5 -

Page 3 of 4

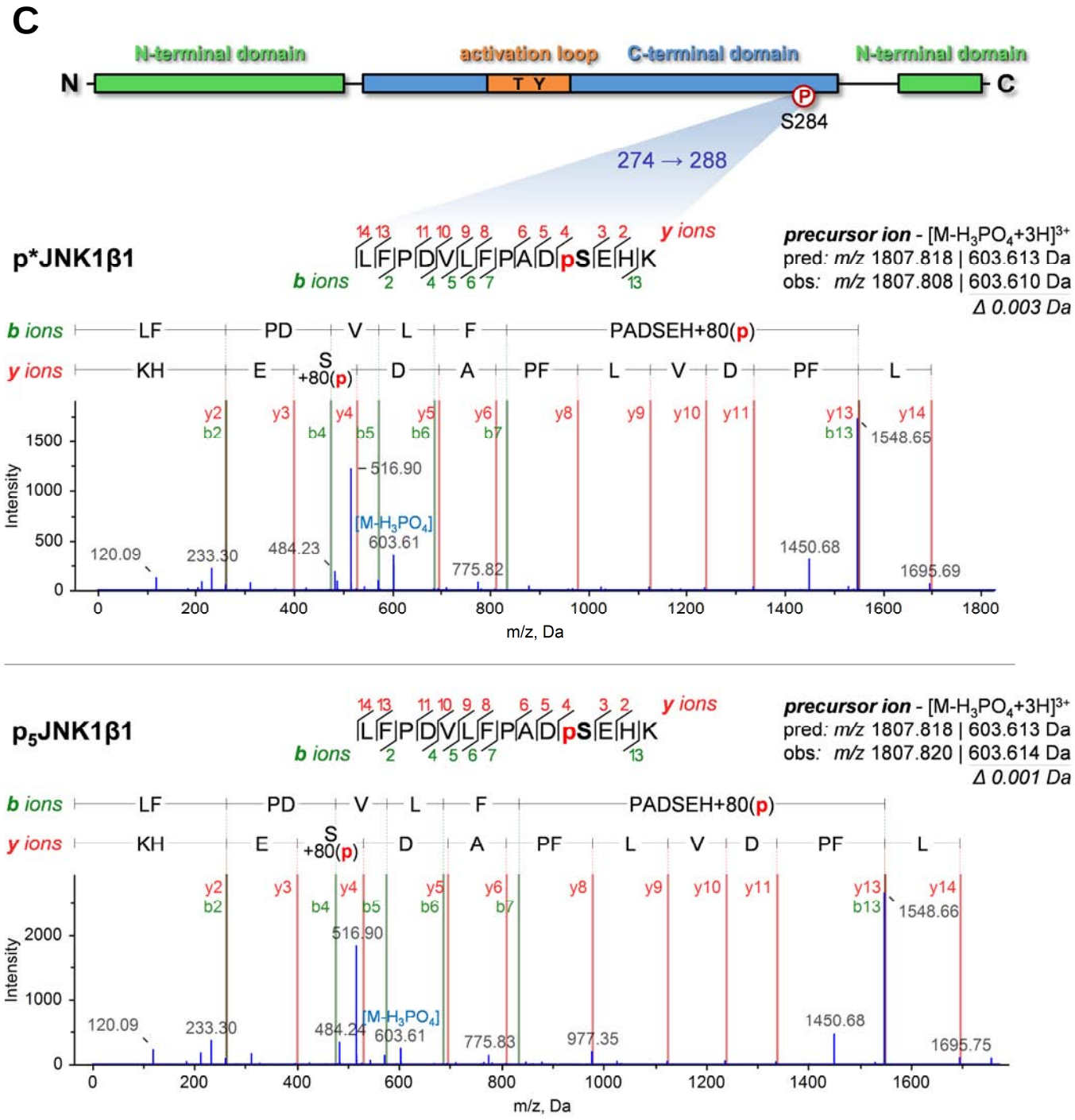

(*Figure S5 continues onto the next page; see page xii for its legend*)

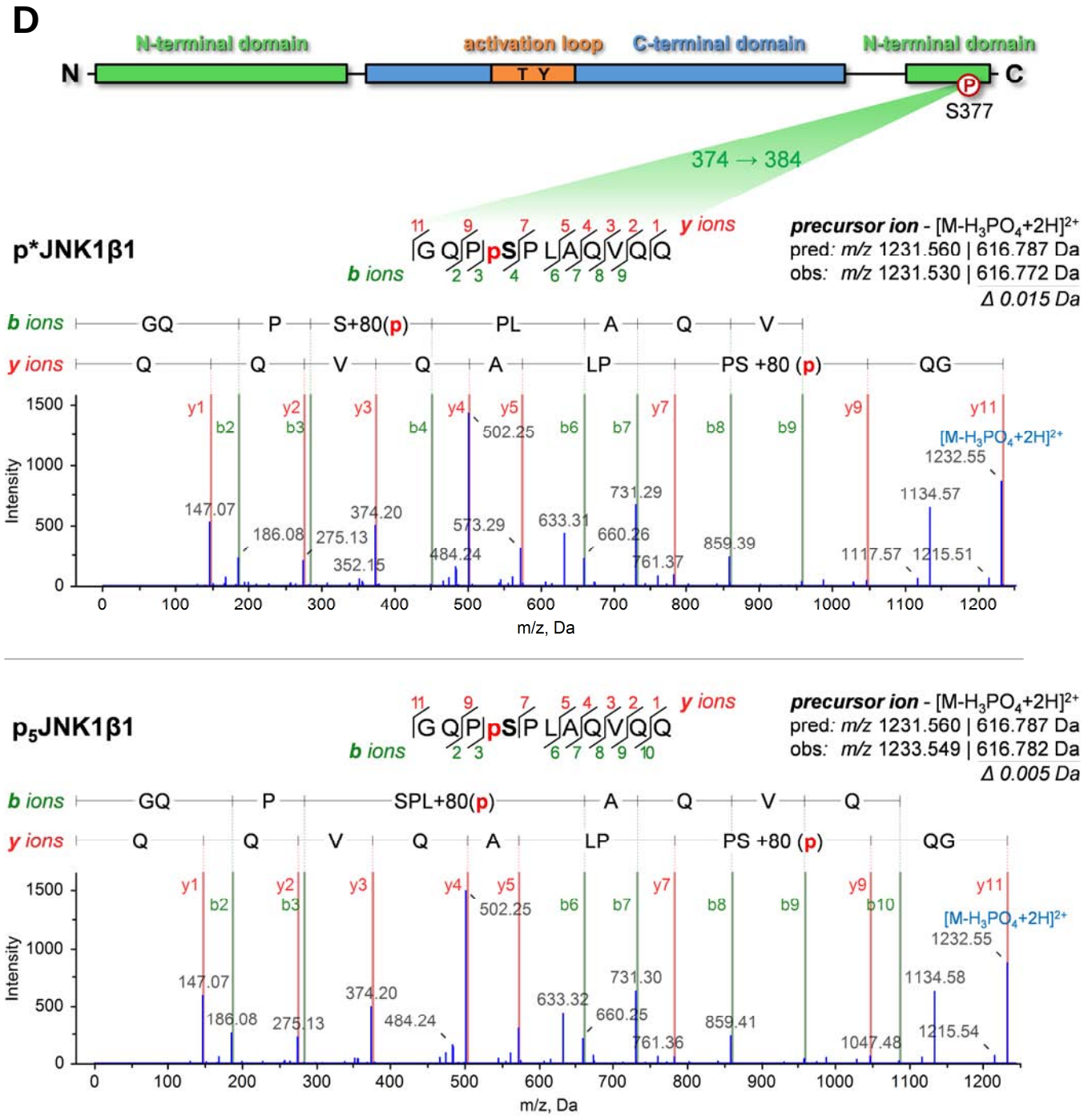

Fig. S5 (Page 4 of 4). Representative product ion MS/MS spectra of each tryptic phospho-peptide identified for JNK1β1 phosphorylated both during expression in *E. coli* (p*JNK1β1) and *in vitro* by MKK4 (p$_5$JNK1β1). A – triply charged ^{175}TAGTSFM**oMpT**P**pY**VVTR^{189} (doubly phosphorylated (**p**) at T183 and Y185, with M182 oxidised (**o**)); B – triply charged ^{221}GGVLFPG**pT**DHIDQWNK^{236} (phosphorylated at T228); C – triply charged ^{274}LFPDVLFPAD**pS**EHK^{288} (phosphorylated at S284); D – doubly charged ^{374}GQP**pS**PLAQVQQ^{384} (phosphorylated at S377). Identified b and y ions are annotated above each spectrum, with the amino acids determined unequivocally to be phosphorylated indicated with a red **p**. The predicted (pred) and observed (obs) *m/z* of each precursor ion and their monoisotopic masses, as well as the mass differences are indicated on the top right. All phospho-peptides were determined with >99% confidence.

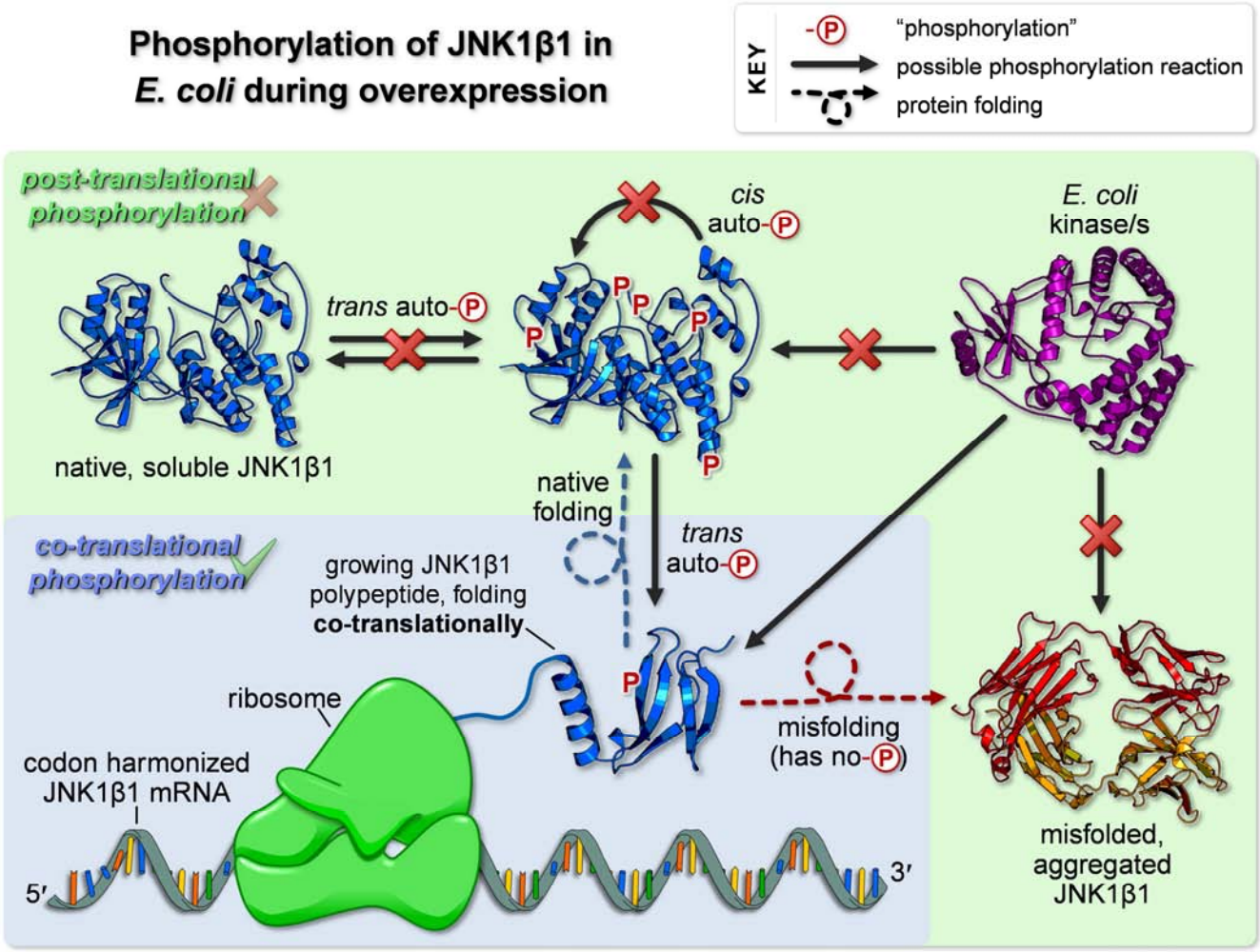

Fig. S6. Model for the phosphorylation of codon-harmonised JNK1β1 during expression in *E. coli*. Red crosses denote possible phosphorylation reactions that can be excluded based on evidence to the contrary from the literature. Refer to article text for details of the proposed model.

SUPPLEMENTARY RESULTS AND DISCUSSION

Phosphorylation propensity of each JNK1β1 phospho-site

To evaluate the propensity that the JNK1β1 phospho-residues have to be phosphorylated by ppMKK4 *in vitro*, the relative abundance of the phosphorylated and non-phosphorylated populations of each relevant precursor phospho-peptide of p_5JNK1β1 was compared. The area under the peaks of the mass chromatogram corresponding to the phosphorylated and non-phosphorylated states of both the +2 and +3 ion species of each phospho-peptide fragment was integrated, giving the total number of ions of the particular type in each sample.

To compare the levels of the phosphorylated and non-phosphorylated forms of each phospho-peptide in different replicate samples, the levels of the +2 and +3 ion species of each phosphorylated fragment were expressed as a percentage of the combined ion count of both the phosphorylated and non-phosphorylated forms of that fragment in that sample, where;

$$\%\ \text{phosphorylated} = \frac{\left(\text{phospho-peptide}^{+2/+3}\ \text{peak area}\right)}{\left(\text{unmodified peptide}^{+2/+3}\ \text{peak area}\right) + \left(\text{phospho-peptide}^{+2/+3}\ \text{peak area}\right)} \times 100$$

This process was repeated for all JNK1β1 phospho-peptide products of trypsin digestion, allowing us to compare the level at which each residue is phosphorylated as an indication of its relative propensity to be phosphorylated.

The average degrees of phosphorylation of each JNK1β1 residue found to be phosphorylated are presented in Supplementary Table S2. Residues T183/Y185 are undoubtedly the most highly phosphorylated residues, with over 60% of the precursor fragments in which they are situated being phosphorylated. Residue S377 is phosphorylated to less than half (33%) the extent of the canonical phosphorylatable residues, with T228 and S284 phosphorylated to a lesser but significant degree (similarly at ±10% each) (Table S2). Thus, the order of their propensity to be phosphorylated by ppMKK4 is: T183/Y185 > S377 > T228 ≥ S284.

Unsurprisingly, these findings confirm that the canonical activation residues of JNK1β1, T183/Y185, have the greatest predisposition to be phosphorylated, and that they are likely to be phosphorylated first. With this, it can be claimed with confidence that p_5JNK1β1 comprises approximately 60% kinase phosphorylated on at least T183 and Y185 (calculated by addition of the 2× to 5× phosphorylated kinase population percentages described in profile 4 of Fig. 1).

Table S2. The degree to which each tryptic phospho-peptide fragment of JNK1β1 is phosphorylated after incubation of the intact kinase with ppMKK4 for ≥3 h. Percentages are an average of the values obtained for both the +2 and +3 species of each phospho-peptide, generated from at least two independent experiments.

Sequence of JNK1β1 tryptic peptide fragment found to be phosphorylated	**Phosphorylated residue/s**	**Residues of JNK1β1 in fragment**	**Percentage (%) of fragment population that is phosphorylated (± SD), $n \geq 2$**
TAGTSFMM**pT**P**pY**VVTR	T183/Y185	175-189	61.2 (± 8.4)
GGVLFPG**pT**DHIDQWNK	T228[a]	221-236	10.4 (± 5.5)
LFPDVLFPAD**pS**EHNK	S284[a]	274-288	9.6 (± 2.7)
GQP**pS**PLAQVQQ	S377[b]	374-384	33.4 (± 8.5)

[a] newly identified JNK1β1 phospho-site

[b] previously identified but uncharacterised JNK1β1 phospho-site

SUPPLEMENTARY REFERENCES

[1] P. López-Bergami, H. Habelhah, A. Bhoumik, W. Zhang, L.H. Wang, Z. Ronai, RACK1 mediates activation of JNK by protein kinase C, Mol. Cell 19 (2005) 309-320.

[2] J. Liu, D. Yang, Y. Minemoto, M. Leitges, M.R. Rosner, A. Lin, NF-kappaB is required for UV-induced JNK activation via induction of PKCdelta., Mol. Cell 21 (2006) 467-480.

[3] P. Lopez-Bergami, Z. Ronai, Requirements for PKC-augmented JNK activation by MKK4/7, Int. J. Biochem. Cell Biol. 40 (2008) 1055-1064.

[4] B.S. Li, L. Zhang, S. Takahashi, W. Ma, H. Jaffe, A.B. Kulkarni, H.C. Pant, Cyclin-dependent kinase 5 prevents neuronal apoptosis by negative regulation of c-Jun N-terminal kinase 3, EMBO J. 21 (2002) 324-333.

[5] F.S. Oppermann, F. Gnad, J.V. Olsen, R. Hornberger, Z. Greff, G. Keri, M. Mann, H. Daub, Large-scale proteomics analysis of the human kinome, Mol. Cell. Proteomics 8 (2009) 1751-1764.

[6] C.S. Shi, N.N. Huang, K. Harrison, S.B. Han, J.H. Kehrl, The mitogen-activated protein kinase kinase kinase kinase GCKR positively regulates canonical and noncanonical Wnt signaling in B lymphocytes, Mol. Cell Biol. 26 (2006) 6511-6521.

[7] J. Wissing, L. Jänsch, M. Nimtz, G. Dieterich, R. Hornberger, G. Kéri, J. Wehland, H. Daub, Proteomics analysis of protein kinases by target class-selective prefractionation and tandem mass spectrometry, Mol. Cell Proteomics 6 (2007) 537-547.

[8] M.P. Stokes, C.L. Farnsworth, A. Moritz, J.C. Silva, X. Jia, K.A. Lee, A. Guo, R.D. Polakiewicz, M.J. Comb, PTMScan Direct: Identification and Quantification of Peptides from Critical Signaling Proteins by Immunoaffinity Enrichment Coupled with LC-MS/MS, Mol. Cell Proteomics 11 (2012) 187-201.

[9] L.-R. Yu, Z. Zhu, K.C. Chan, H.J. Issaq, D.S. Dimitrov, T.D. Veenstra, Improved titanium dioxide enrichment of phosphopeptides from HeLa cells and high confident phosphopeptide identification by cross-validation of MS/MS and MS/MS/MS spectra, J. Proteome Res. 6: (2007) 4150-4162.

[10] S.A. Beausoleil, J. Villén, S.A. Gerber, J. Rush, S.P. Gygi, A probability-based approach for high-throughput protein phosphorylation analysis and site localization, Nat. Biotechnol. 24 (2006).

[11] N. Dephoure, C. Zhou, J. Villen, S.A. Beausoleil, C.E. Bakalarski, S.J. Elledge, S.P. Gygi, A quantitative atlas of mitotic phosphorylation, Proc. Natl. Acad. Sci. USA 105 (2008) 10762-10767.

[12] H. Daub, J.V. Olsen, M. Bairlein, F. Gnad, F.S. Oppermann, R. Korner, Z. Greff, G. Keri, O. Stemmann, M. Mann, Kinase-selective enrichment enables quantitative phosphoproteomics of the kinome across the cell cycle, Mol. Cell 31 (2008) 438-448.

[13] G.L. Christensen, C.D. Kelstrup, C. Lyngsø, U. Sarwar, R. Bøgebo, S.P. Sheikh, S. Gammeltoft, J.V. Olsen, J.L. Hansen, Quantitative phosphoproteomics dissection of seven-transmembrane receptor signaling using full and biased agonists, Mol. Cell Proteomics 9 (2010) 1540-1553.

[14] K.T.G. Rigbolt, T.A. Prokhorova, V. Akimov, J. Henningsen, P.T. Johansen, I. Kratchmarova, M. Kassem, M. Mann, J.V. Olsen, B. Blagoev, System-wide temporal characterization of the proteome and phosphoproteome of human embryonic stem cell differentiation, Sci. Signal 4 (2011) rs3.

[15] C. Weber, T.B. Schreiber, H. Daub, Dual phosphoproteomics and chemical proteomics analysis of erlotinib and gefitinib interference in acute myeloid leukemia cells, J. Proteomics 75 (2012) 1343-1356.

[16] J.R. Wiśniewski, N. Nagaraj, A. Zougman, F. Gnad, M. Mann, Brain phosphoproteome obtained by a FASP-based method reveals plasma membrane protein topology, J. Proteome Res. 9 (2010) 3280-3289.

[17] Y. Fleming, C.G. Armstrong, N. Morrice, A. Paterson, M. Goedert, P. Cohen, Synergistic activation of stress-activated protein kinase 1/c-Jun N-terminal kinase (SAPK1/JNK) isoforms by mitogen-activated protein kinase kinase 4 (MKK4) and MKK7, Biochem. J. 352 (2000) 145–154.

[18] H. Schägger, G. von Jagow, Tricine-sodium dodecyl sulfate-polyacrylamide gel electrophoresis for the separation of proteins in the range from 1 to 100 kDa, Anal. Biochem. 166 (1987) 368-379.

[19] G.R. Owen, I. Achilonu, H.W. Dirr, High yield purification of JNK1β1 and activation by *in vitro* reconstitution of the MEKK1 → MKK4 → JNK MAPK phosphorylation cascade, Protein Expr. Purif. 87 (2013) 87-99.

CHAPTER 4

PUBLICATION 3

Phosphorylation- and nucleotide-binding-induced changes to the stability and hydrogen exchange patterns of JNK1β1 provide insight into its mechanisms of activation

GAVIN R. OWEN, STOYAN STOYCHEV, IKECHUKWU ACHILONU, AND HEINI W. DIRR

Journal of Molecular Biology 426, 3569-3589 (2014)

In this publication, the consequences of phosphorylation and nucleotide substrate binding to the structure, stability, and dynamics of JNK1β1 were established.

Author contributions: Gavin R. Owen performed all experimental work, analysed the data, and wrote the manuscript. Stoyan Stoychev assisted with the HX MS experiments. Ikechukwu Achilonu and Heini W. Dirr supervised the project and assisted in data analysis and interpretation.

GRAPHICAL ABSTRACT

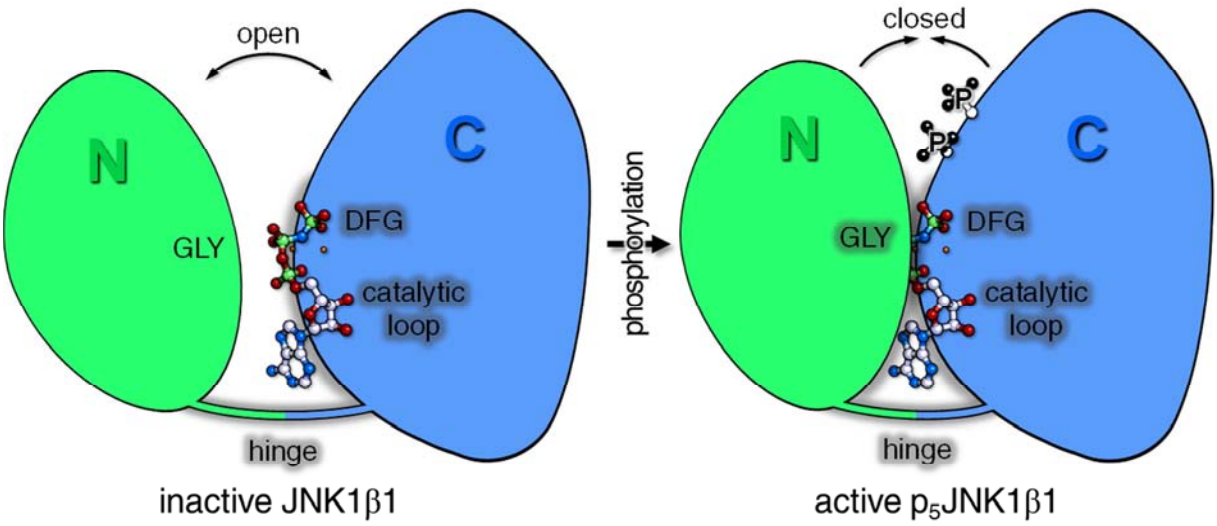

Phosphorylation- and Nucleotide-Binding-Induced Changes to the Stability and Hydrogen Exchange Patterns of JNK1β1 Provide Insight into Its Mechanisms of Activation

Gavin R. Owen [1], Stoyan Stoychev [2], Ikechukwu Achilonu [1] and Heini W. Dirr [1]

*1 - **Protein Structure–Function Research Unit,** School of Molecular and Cell Biology, University of the Witwatersrand, Johannesburg 2050, South Africa*
*2 - **Biosciences,** Council for Scientific and Industrial Research, Pretoria 0001, South Africa*

Correspondence to Heini W. Dirr: *heinrich.dirr@wits.ac.za*
http://dx.doi.org/10.1016/j.jmb.2014.08.019
Edited by P. Griffin

Abstract

Many studies have characterized how changes to the stability and internal motions of a protein during activation can contribute to their catalytic function, even when structural changes cannot be observed. Here, unfolding studies and hydrogen–deuterium exchange (HX) mass spectrometry were used to investigate the changes to the stability and conformation/conformational dynamics of JNK1β1 induced by phosphorylative activation. Equivalent studies were also employed to determine the effects of nucleotide binding on both inactive and active JNK1β1 using the ATP analogue, 5′-adenylyl-imidodiphosphate (AMP-PNP). JNK1β1 phosphorylation alters HX in regions involved in catalysis and substrate binding, changes that can be ascribed to functional modifications in either structure and/or backbone flexibility. Increased HX in the hinge between the N- and C-terminal domains implied that it acquires enhanced flexibility upon phosphorylation that may be a prerequisite for interdomain closure. In combination with the finding that nucleotide binding destabilizes the kinase, the patterns of solvent protection by AMP-PNP were consistent with a novel mode of nucleotide binding to the C-terminal domain of a destabilized and open domain conformation of inactive JNK1β1. Solvent protection by AMP-PNP of both N- and C-terminal domains in active JNK1β1 revealed that the domains close around nucleotide upon phosphorylation, concomitantly stabilizing the kinase. This suggests that phosphorylation activates JNK1β1 in part by increasing hinge flexibility to facilitate interdomain closure and the creation of a functional active site. By uncovering the complex interplay that occurs between nucleotide binding and phosphorylation, we present new insight into the unique mechanisms by which JNK1β1 is regulated.

Introduction

The c-Jun N-terminal kinases (JNKs) are mitogen-activated protein (MAP) kinases that mediate physiological responses to a number of extracellular stimuli, including cytokines and UV irradiation [1]. By phosphorylating a variety of target proteins, the diverse JNK signaling pathways regulate transcriptional events implicated in cellular processes such as proliferation, differentiation, and apoptosis [1].

Ten unique variants of JNK that are encoded by three alternatively spliced genes (*JNK1*, *JNK2*, and *JNK3*) have been identified [2]. They are distinguished by the length of their termini and the residues that form their substrate binding sites, as well as by the tissues in which they are predominantly expressed.

Although other sites of phosphorylation have been discovered, JNK1s are activated primarily through the dual phosphorylation of the canonical T183 and Y185 residues located in the activation lip. Phosphorylation induces greatly enhanced kinase activity, leading to the increased phosphorylation of transcription factors and other downstream target proteins [3].

The structure of JNK1β1 displays a conserved bilobal kinase core comprising an active site situated between an N-terminal domain and a C-terminal

domain [4]. The two domains are connected by a loop referred to as the hinge as it has been shown to act as the pivot point for interdomain closure, a conformational change required in many kinases for the formation of catalytically competent active site [5].

Phosphorylative activation leads to dramatic structural rearrangements within kinases. The changes that take place in MAP kinases are best understood for ERK2, as it is the only member that has had both its inactive and its active conformations elucidated [6,7]. Within ERK2, phosphorylation induces extensive remodeling of the activation lip that causes a high-affinity substrate binding groove to form and the repositioning of active-site residues into orientations that facilitate phosphoryl transfer [7].

Complementary studies employing hydrogen–deuterium exchange (HX) mass spectrometry (MS) has revealed that regulation of kinases is mediated through changes to both conformation and conformational mobility [8]. Even in the absence of structural changes, alterations in protein fluctuations and flexibility have been shown to impact protein functioning. Studies of ERK2 have illustrated that activation leads to significantly enhanced HX at backbone amides within the hinge, and since conformer interconversions in this regions were not observable by X-ray crystallography, the change could only be ascribed to the activation-dependent regulation of protein motions, particularly enhanced backbone flexibility [9]. A function for this mediation of hinge flexibility was initially suggested by measurements of steric protection from HX by 5′-adenylyl-imidodiphosphate (AMP-PNP), a non-hydrolyzable ATP analogue. The patterns of solvent protection describe a model in which the N- and C-terminal domains of inactive ERK2 is constrained from interdomain closure and thus occupy an open conformation, whereas the domains of active ERK2 instead adopt a closed conformation around the nucleotide [10]. These results illustrated that patterns of solvent protection upon nucleotide binding provide a means to detect domain closure and suggested that the enhanced flexibility of the hinge following activation of ERK2 may enable the interdomain interactions that close and functionalize the catalytic cleft. More recent studies have shown that increasing the conformational mobility of the hinge through mutations leads to activation of mono-phosphorylated ERK2 and phosphorylation-independent changes in the mode of nucleotide binding that is consistent with interdomain closure [11].

Despite the large diversity in activation lip conformations between the various inactive forms of the MAP kinases, the similarity found in the structure of phosphorylated activation lips reveals that the varied inactive conformers converge toward a comparable form upon activation [4,7,12,13]. One could expect that, due to the similarities in these characteristics of activation, as well as the conserved sequence and tertiary structure that the MAP kinases share, the members of this family would exhibit equivalent mechanisms of regulation. However, when comparing the information available for the activation-induced changes in the conformational dynamics of ERK1 [14], ERK2 [9,10], and p38α [15], it is clear that the small differences in the MAP kinase sequences result in significant distinctions in their phosphorylation-dependent regulation of regional protein mobility. Therefore, there is increasing evidence that the closely related MAP kinases diverge with respect to the mechanisms by which changes to internal protein motions contribute to regulating their activity. Due to the differential and pleiotropic effects of MAP kinase misfunction, fully understanding their distinct activation mechanisms is crucial if we are to explore each as potential individual therapeutic targets.

We have previously succeeded in producing high yields of active, phosphorylated JNK1β1 by reconstituting the MEKK1 → MKK4 → JNK MAPK (*m*itogen-*a*ctivated *p*rotein *k*inase) phosphorylation cascade *in vitro* [16]. Upon mass spectrometric analysis of the active JNK1β1, it was revealed that the kinase is phosphorylated by MKK4 at no less than five sites, albeit to varying degrees [17]. These phospho-sites comprised the canonical activation loop phosphorylation residues (T183 and Y185), as well as a recognized yet uncharacterized phospho-site (S377) and two novel phospho-residues (T228 and S284). Although we henceforth refer to the fully phosphorylated kinase as "p_5JNK1β1" due to the five phosphate groups that are added upon *in vitro* activation by MKK4, we do not imply that each phosphorylated residue is present in the population to the same extent. Nonetheless, we have shown that p_5JNK1β1 is highly active, possessing a specific activity of 3.3 ± 0.4 μmol/min per milligram of ATF2 [16].

In this study, we investigate the effect that phosphorylative activation has on the stability and conformational dynamics of the most abundant JNK isoform, JNK1β1 [18]. Comparing the changes in the HX behavior of peptides derived from inactive and active JNK1β1, we demonstrate how patterns of exchange may reflect changes in regional conformational mobilities upon phosphorylation, suggesting that activation regulates protein dynamics in regions important for catalysis and substrate binding. Additionally, we examined variations in steric protection from HX upon nucleotide substrate binding in both forms of JNK1β1 to explore possible changes in the extent of domain rotation following activation and to ascertain whether interdomain closure is required for catalysis. These data provide novel insight into the distinct mechanisms by which JNK1β1 is activated and expose the unique interplay that exists between nucleotide binding and phosphorylation for the regulation of its activity.

Results

Phosphorylative activation does not alter the structure of JNK1β1 extensively but increases the stability of the kinase

We investigated the effect that the addition of the five phosphate groups (Fig. 1a) has on the global structure of JNK1β1 using a number of spectroscopic methods. Fluorescence spectral data for unmodified and phosphorylated JNK1β1 are essentially identical (Fig. 1b), indicating that phosphorylation has little net effect on the tertiary structure and local environment of the many tyrosine and tryptophan residues of JNK1β1 (Fig. 1a). Overlaying circular dichroism spectra (Fig. 1c) also indicate that no significant change to the secondary structure of the protein occurs upon phosphorylation.

We carried out several experiments to examine the effect that phosphorylation has on the stability of JNK1β1. Temperature-induced denaturation, as well as urea-induced equilibrium and kinetic unfolding experiments, revealed that phosphorylation distinctly increases the thermal, conformational, and kinetic stability of JNK1β1 (Fig. 2).

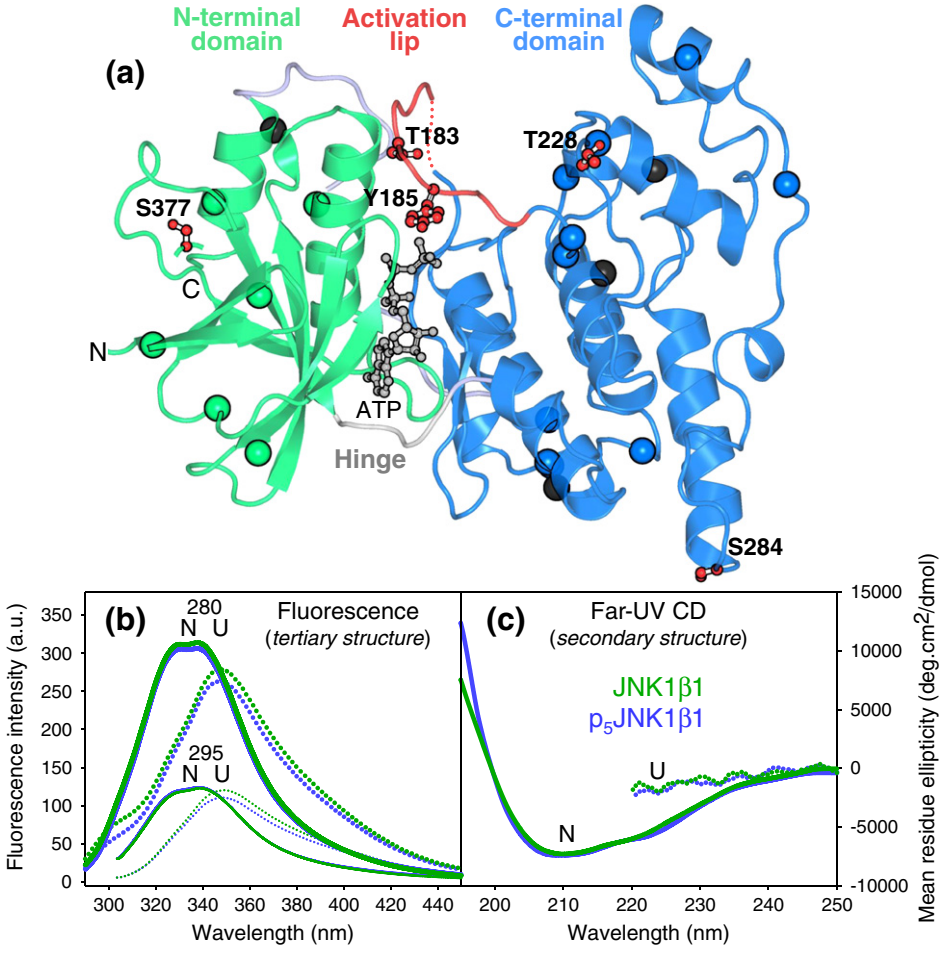

Fig. 1. Phosphorylative activation does not alter the structure of JNK1β1 extensively. (a) The location of the canonical (T183 and Y185) and novel (T228, S184, and S377) phosphorylation sites are shown, as well as the locations of the many tryptophan (black spheres) and tyrosine residues (green and blue spheres). As the C-terminal residues L364-Q384 were not resolved in the crystal structure, an additional serine has been used to indicate the position of S377. ATP (ball-and-stick model) binds within the catalytic cleft situated between the N-terminal (green) and the C-terminal (blue) domains. The protein structure was rendered using PyMOL™ v. 0.99 (DeLano Scientific, San Carlos, CA, USA) using the PDB entry 1JNK [4]. (b) Fluorescence spectra of unmodified and phosphorylated JNK1β1 using λ_{ex} of 280 nm and 295 nm, for both native (N) and unfolded (U) state of the kinase, indicate that the local environment of the tryptophan residues is largely unaltered by phosphorylated. (c) Circular dichroism spectra for unmodified and phosphorylated JNK1β1, both in their native and unfolded states, reveal that the secondary structure of the kinase does not change substantially upon activation.

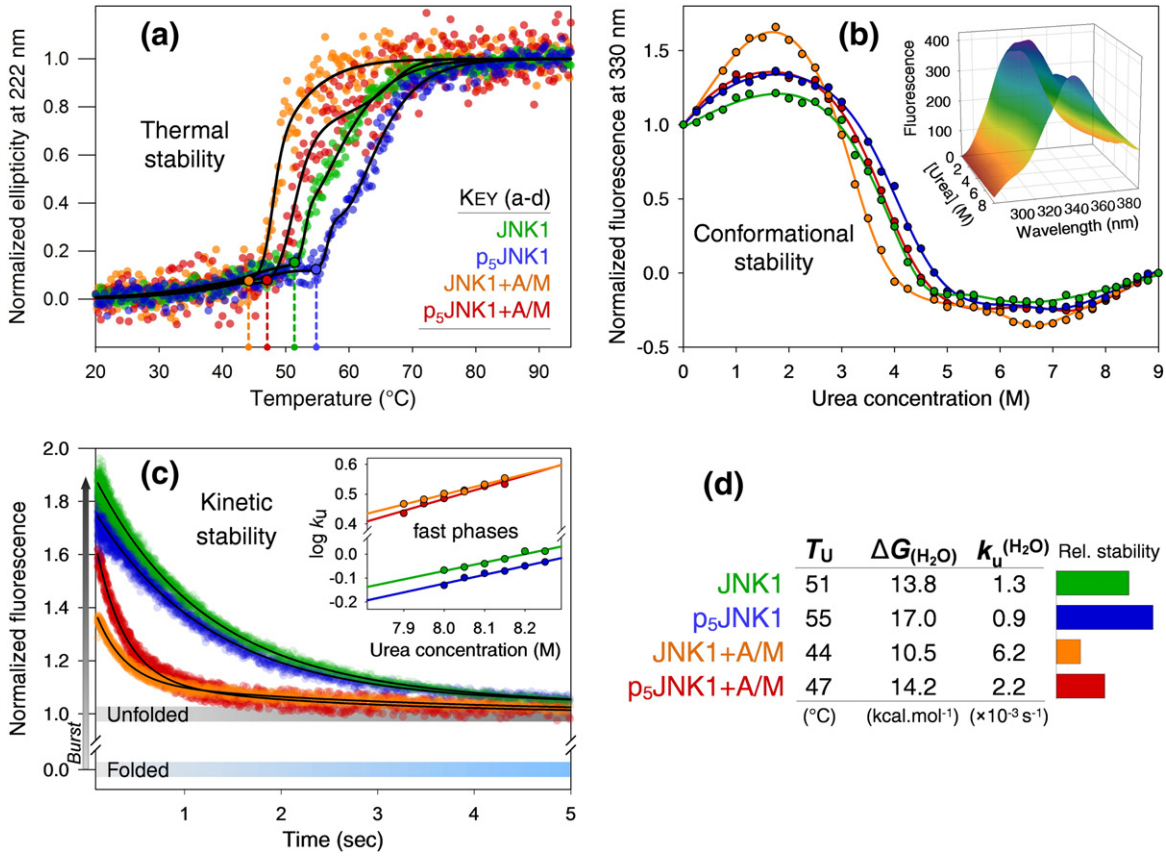

Fig. 2. Phosphorylation increases the stability of JNK1β1, whereas AMP-PNP/Mg^{2+} binding decreases the stability of both its unmodified and its phosphorylated forms. (a) Temperature-induced unfolding of JNK1β1 (green) and p_5JNK1β1 (blue), as well as their AMP-PNP/Mg^{2+}-bound forms [JNK1 + A/M (orange) and p_5JNK1 + A/M (red), respectively], was monitored by measuring ellipticity at 222 nm. The unfolding data are the average of three replicates and normalized such that 0 represents the native state and 1 represents the unfolded state. Lines of best fit are presented for clarity, while drop lines indicate the temperature at which each form begins to unfold (T_U). (b) Urea-induced equilibrium unfolding of the unbound and nucleotide-bound forms of both unmodified and phosphorylated JNK1β1, monitored by tryptophan fluorescence intensity at 330 nm using an λ_{ex} of 280 nm. Data points are the average of three replicates and were globally fitted to an equilibrium four-state monomer model together with the data from other unfolding probes to obtain $\Delta G^{\circ}_{H_2O}$ values (see Fig. S3). The inset shows the total set of fluorescence emission spectra recorded at different urea concentrations. (c) Unfolding kinetics traces for the JNK1β1 forms, averaged from three unfolding reactions in 8.1 M urea (see Fig. S2 for the residual plots for each fit). The baselines for the folded and unfolded states are indicated. The inset displays the urea dependence of the unfolding rate of the fast phase of each kinase form. Data points are the average of three replicates and were fit to a linear function to produce the kinetic parameters ($k_u^{H_2O}$) tabulated in (d). (d) Comparison of the parameters for the thermal (T_U), conformational ($\Delta G^{\circ}_{H_2O}$), and kinetic ($k_u^{H_2O}$) stability of each form of JNK1β1, obtained by fitting the unfolding datasets as described for each method. The overall relative stability of unmodified and phosphorylated JNK1β1, in both their apo and AMP-PNP/Mg^{2+}-bound forms, is represented as bars in summary.

During temperature-induced denaturation, all forms of JNK1β1 unfold in a cooperative and irreversible manner, yet each shows distinct and complex multi-state unfolding mechanisms as revealed by the line of best fit describing each dataset (Figs. 2a and S2a). As a result, single representative T_m values cannot be accurately assigned to each profile due to the complex transitions displayed among each apparent intermediate species. Nevertheless, the temperatures over which each protein unfolds completely are distinct and can thus be used as clear indicators of relative protein stability. The thermal unfolding profile of p_5JNK1β1 exhibits a roughly 5 °C increase in the temperature at which the modified kinase starts to unfold compared to JNK1β1 (Fig. 2a), illustrating a clear stabilization by phosphorylation.

By monitoring the urea-induced equilibrium unfolding of JNK1β1 using fluorescence spectroscopy [as well as by circular dichroism and 8-anilino-1-naphthalenesulfonate (ANS) binding as detailed in the Fig. S3], we could also assess the effect that phosphorylation has on its conformational stability.

The reversibility of the chemical denaturation by urea of all forms of JNK1β1 was first confirmed (see Fig. S3a), allowing a thermodynamic explanation of the overall structural transitions to be made. It is evident that the equilibrium unfolding curves of the various forms of JNK1β1 are not simple, monophasic sigmoidal curves but display complex multi-state characteristics, similarly to its thermal unfolding profiles. The unfolding data monitored by fluorescence and circular dichroism also do not coincide throughout all transitions for each form (Fig. S3d), reaffirming the suggestion that intermediate species exist along their equilibrium unfolding pathways. In further support to this, ANS binding experiments illustrated that all forms of JNK1β1 exhibit differential binding patterns to the amphipathic dye at the varying urea concentrations as the proteins unfold (Fig. S3c), confirming that significant populations of differing intermediate species with unique solvent-exposed hydrophobic patches accumulate at equilibrium under mild denaturing conditions.

As the precise number of intermediates that exist during equilibrium unfolding is not immediately apparent by examining the transitions displayed in the unfolding curves, we globally fit the intrinsic fluorescence intensities at various wavelengths and the ellipticity at 222 nm data to three-, four-, and five-state monomeric models. While the attempts to fit the data to a three-state model were not satisfactory, the data fit equally well to both four- and five-state models. We thus selected the simpler model with fewer assumed intermediate states to describe the physical and thermodynamic nature of JNK1β1 denaturation. The analysis and interpretation of the conformational stability parameters ($\Delta G^{\circ}_{H_2O}$ and m values) generated for each transition by global fitting of the unfolding data to the proposed four-state monomer model ($N \leftrightarrow I_1 \leftrightarrow I_2 \leftrightarrow U$) is intricate and will be published independently, but the overall $\Delta G^{\circ}_{H_2O}$ values for the complete unfolding ($N \leftrightarrow U$; ΔG°_{NU}) of each form of JNK1β1 are used here to describe the effects that phosphorylation has on their global conformational stability. Nonetheless, the distinctive patterns displayed by each equilibrium unfolding curve (Fig. 2b) highlight that, while each form of JNK1β1 unfolds via two apparent intermediate states, the extent and cooperativity of the structural changes (presented by changes in fluorescent intensity/ellipticity) and the changes in free energy that occur between the intermediates are clearly influenced by the presence of AMP-PNP/Mg^{2+} and the phosphorylation state of the kinase.

The overall ΔG°_{NU} of phosphorylated JNK1β1 (17.0 ± 2.2 kcal/mol) was increased relative to that of the unmodified kinase (13.8 ± 1.4 kcal/mol), with the range of the predominant unfolding transition shifted to a higher urea concentration when compared to the same transition of inactive JNK1β1. Therefore, as p_5JNK1β1 is more thermodynamically stable than JNK1β1, phosphorylation increases the global conformational stability of the kinase.

Determining the rates of unfolding of JNK1β1 using a stopped-flow instrument that measures tryptophan fluorescence allowed understanding of the effect that phosphorylation has on its kinetic stability. The unfolding of all forms of JNK1β1 shows tri-phasic kinetics comprising an initial positive-amplitude burst phase, followed by two consecutive negative-amplitude phases (Fig. 2c). As the burst phase occurs within the dead time of the instrument and is wholly unresolved, it was excluded when fitting the kinetics data. The phases that follow are well-defined and fit well to a double-exponential decay function, producing a distinct fast and slow phase (Fig. 2c).

The two intermediates observed during the kinetic unfolding reactions, as well as the changes in amplitude that exist between each species, are consistent with that predicted by the equilibrium unfolding studies and the proposed four-state monomer model ($N \leftrightarrow I_1 \leftrightarrow I_2 \leftrightarrow U$). While the formation of the kinetic unfolding intermediates may represent the same structural events that are described by the equilibrium unfolding model, they cannot be directly compared as we are yet to establish whether the three kinetic unfolding phases occur sequentially or in parallel. Comprehensive analyses of the rates of unfolding of each intermediate and the associated kinetic cooperativity (m values) for each phase, specifically in relation to their corresponding thermodynamic parameters determined during equilibrium unfolding experiments, will also be published elsewhere. Nevertheless, we can use the rate constants for the resolvable phases of unfolding determined as a function of urea concentration to characterize the impact of phosphorylation on unfolding kinetics. The logarithms of the rate constants for the fast phase increase linearly with urea concentration (Fig. 2c, inset), while those for the slow phase are independent of urea (data not shown). Fitting the unfolding data to the linear equation described (see Materials and Methods) yielded $k_u^{H_2O}$ values of (1.3 ± 0.03) × 10^{-3} and (0.9 ± 0.1) × 10^{-3} s^{-1} for the fast phases of JNK1β1 and p_5JNK1β1, respectively, with no significant difference existing between their kinetic cooperativities (slope of each curve, inset of Fig. 2c). A similar reduction in the rate of unfolding upon phosphorylation was seen when comparing the slow unfolding phases of each species (data not shown). Phosphorylation therefore reduces the overall rate of unfolding of JNK1β1, reiterating our findings that the kinase is stabilized upon activation.

AMP-PNP/Mg^{2+} binding decreases the stability of both unmodified and phosphorylated JNK1β1

To investigate the effect that AMP-PNP/Mg^{2+} binding has on the stability of both inactive and active JNK1β1, we subjected ligand-bound JNK1β1

and p_5JNK1β1 to the same thermal, thermodynamic, and kinetic stability experiments. Surprisingly, we found that the presence of AMP-PNP/Mg^{2+} significantly destabilized the global conformational state of the kinase.

Ligand binding decreased the thermostability of both JNK1β1 and p_5JNK1β1 to a similar degree, lowering the temperature at which each form begins to unfold by ±8 °C (Fig. 2a). With respect to changes to the thermodynamic stability of the kinase, the equilibrium unfolding profiles suggest that, while the binding of AMP-PNP/Mg^{2+} may stabilize the first unfolding intermediate of unmodified JNK1β1, it appears to destabilize the second intermediate species substantially, with the transition between the intermediates displaying both an increase in cooperativity and a shift to a lower urea concentration (Fig. 2b). The effect of ligand binding on p_5JNK1β1 is less distinct, yet it is evident from its unfolding profile that the $I_1 \leftrightarrow I_2$ transition is also shifted to a lower range of urea concentrations. Global fitting of the unfolding data generated ΔG°_{NU} values of 10.5 ± 1.3 and 14.2 ± 1.8 kcal/mol for the JNK1β1 + AMP-PNP/Mg^{2+} and p_5JNK1β1 + AMP-PNP/Mg^{2+} complexes, respectively. When we compare these changes in free energy to that measured for the complete unfolding of its unbound forms (larger ΔG°_{NU} values of 13.8 kcal/mol for JNK1β1 and 17.0 kcal/mol for p_5JNK1β1), it is clear that the presence of AMP-PNP/Mg^{2+} thermodynamically destabilizes both forms of the kinase.

While the unfolding kinetics of the ligand-bound JNK1β1 forms display the same characteristic phases exhibited by the uncomplexed kinase (Fig. 2c), AMP-PNP/Mg^{2+} binding increases the rate of the fast phase by ~5- and ~3-fold for JNK1β1 and p_5JNK1β1, yielding $k_u^{H_2O}$ values of (6.2 ± 2.4) × 10^{-3} and (2.2 ± 1.2) × 10^{-3} s^{-1}, respectively. Despite the decrease in kinetic stability, ligand binding does not alter the kinetic cooperativity of each fast phase significantly (Fig. 2c, inset). Additionally, the slow unfolding phase of each form also experienced an increase in their rate upon ligand binding (data not shown), reinforcing the indication of global kinetic destabilization suggested by the increases in the rate of each fast phase.

All findings considered, it is evident that the binding of AMP-PNP/Mg^{2+} destabilizes the global conformational state of both unmodified and phosphorylated forms of JNK1β1. Nonetheless, even in the presence of AMP-PNP/Mg^{2+}, the phosphorylated kinase is still more stable than its unmodified form.

Conformational dynamics of JNK1β1 as revealed by HX

To uncover the dynamic changes that occur as a result of both activation and ATP/Mg^{2+} binding, as well as to help rationalize the effect that these events have on the stability of JNK1β1, we used amide HX MS. HX measurements for JNK1β1 and p_5JNK1β1 were made by incubating the kinase in D_2O for varying times, both in the absence and in the presence of AMP-PNP and Mg^{2+} ions. After pepsin proteolysis, 103 and 80 peptides reporting exchange were identified at 1% false detection rate for JNK1β1 and p_5JNK1β1, respectively, accounting for 98% coverage (at least 381 of 384 residues) of their primary sequence (the peptides are annotated onto the sequence of JNK1β1 in Fig. 3). The extent of back-exchange that occurred during the experiment, averaged over all peptides, was 26 ± 2.7%.

Firstly, the level of deuteration after 50 min was used to examine the degree of exchange in localized regions of JNK1β1, revealing the global conformational dynamics of the kinase by mapping the data to its crystal structure (Fig. 4). Generally, HX measurements revealed buried regions within the core of both N- and C-terminal domains that exhibited slow exchange, with loops and secondary structure in the periphery of the kinase displaying much faster exchange. In the C-terminal domain, regions of low HX (0–40%) include the catalytic loop (containing the conserved catalytic base, D152), strand β8, and the solvent-inaccessible parts of the solid helical core comprising αE, αF, αG, and αI; these elements form a network of interactions that extends to the active site. Low-exchanging regions in the N-terminal domain were observed in parts of strands β3, β4, and β5, as well as in helices αC and αL16 with which the aforementioned strands interact, forming a hydrophobic core. In contrast, regions displaying high levels of HX comprise the MAPK insert and helix αH (as well as their intervening loops), in addition to several other loops that include the highly flexible activation lip, the DFG motif, and the Gly-rich flap, all of which possess high solvent accessibility. Overall, the local patterns of HX and the implied regional conformational mobility of the kinase are consistent with that which can be expected from the tertiary structure of JNK1β1.

Changes to the regional conformational dynamics of JNK1β1 upon phosphorylative activation

To identify the regions of JNK1β1 that undergo changes in their dynamics upon phosphorylation and to possibly shed light on the mechanism by which these changes induce kinase activation, we compared HX measurements of unmodified JNK1β1 to those of fully phosphorylated p_5JNK1β1. Proteolytic cleavage sites in the two forms were very similar, with only a few additional peptides identified for JNK1β1 (Fig. 3). These differing patterns of cleavage may be due to phosphorylation-induced changes in proteolytic specificity. Nonetheless, in the context of the large pool of shared peptides and

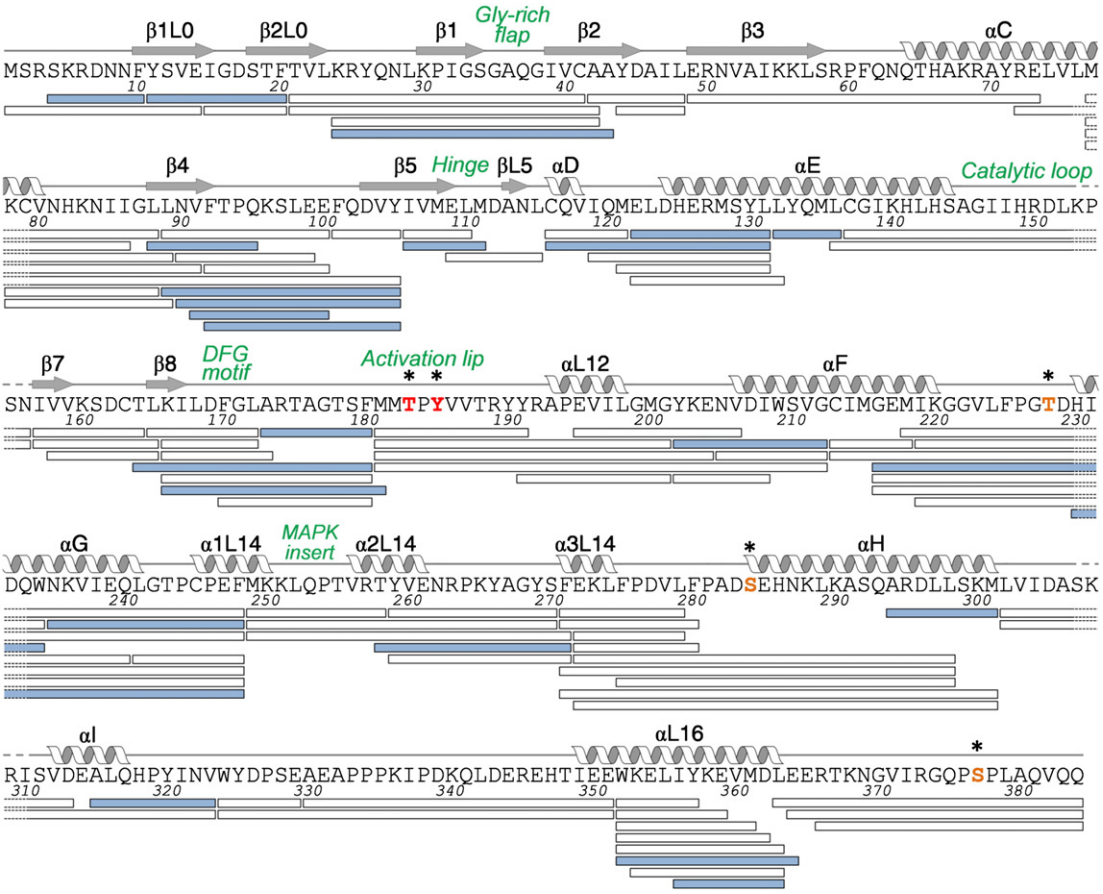

Fig. 3. Peptic fragment coverage map of JNK1β1. Sequence coverage of JNK1β1 by the peptides analyzed in this study, with residue numbering and secondary-structure elements labeled as previously described by Zhang *et al.* [6]. The peptides observed only in the p_5JNK1β1 datasets and not in those from unmodified JNK1β1 are shown in blue, reflecting the differences in pepsin proteolysis caused by phosphorylation. The canonical (T183/Y185) and novel (T228/S184/S377) phosphorylated residues of p_5JNK1β1 are indicated in red and orange, respectively, as well as by asterisks.

the comparable peptides that were generated, the additional peptides do not contribute substantially to the coverage and resolution of the regional HX data.

We do not yet fully understand the structural changes that take place following JNK activation, as a crystal or solution structure of the phosphorylated kinase that could reveal these modifications has not yet been solved. It is thus important to note that, since there is no established structural information to compare the HX data with, we are unable to assign the differences observed in HX induced by JNK1β1 activation specifically either to distinct structural modifications that lead to changes in solvent accessibility or to changes to the conformational flexibility and internal motions of the native protein. Be that as it may, several peptides demonstrated significant differences in their level of deuteration when comparing JNK1β1 and p_5JNK1β1. As many of these peptides share sequence overlap, regional changes in HX can be represented by examining specific characteristic peptides. Regions in JNK1β1 that were responsive to phosphorylation and that exhibited altered HX behavior following activation are those known to be involved in substrate binding and catalysis. These include the Gly-rich flap, the hinge region, the catalytic loop, the DFG motif and activation lip, helices αG/αH and the intervening α1L14/α2L14 MAPK insert, and helices αE/αF and strands β7/β8.

The Gly-rich flap and the flanking β1 and β2 strands, an important site for interaction with nucleotide triphosphates that is represented well by peptide K30-A42 (KRYQNLKPIGSGAQGIVCA), experienced an increase in solvent accessibility upon phosphorylation (Fig. 5). It has been proposed that gating motions of this loop are essential for the association and dissociation of nucleotide substrates [19,20]. Increased protein mobility in this region following JNK1β1 activation may thus facilitate ATP binding and/or ADP release, thereby enhancing catalysis in p_5JNK1β1.

The hinge region that separates the N- and C-terminal domains of JNK1β1 also underwent an

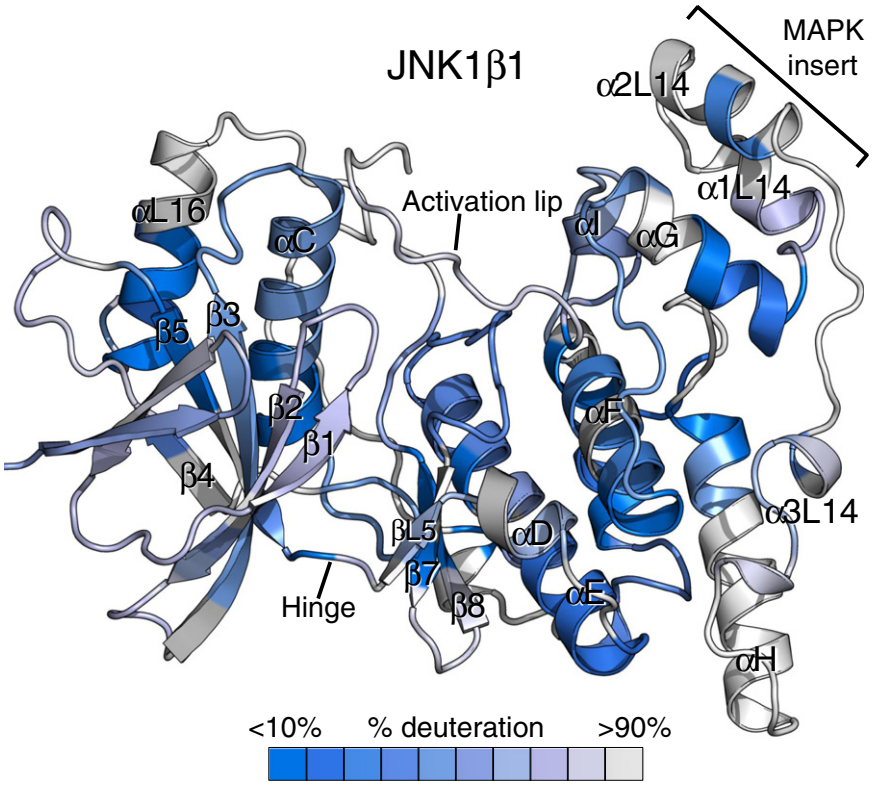

Fig. 4. Conformational dynamics of JNK1β1 as indicated by regional patterns of HX. The extent of deuteration of unmodified JNK1β1 after 50 min in deuterium is shown, expressed as a percentage of the total number of exchangeable amides in each region. Percentages are mapped onto the structure (PDB entry 1JNK) as colors that correspond to the accompanying color bar.

increase in flexibility upon phosphorylation, illustrated by the increased deuterium incorporation in peptide E109-L115 (ELMDANL) (Fig. 5). In many kinases, the hinge represents both a site of contact for the adenosine ring of ATP [6,21] and the pivot point at which ridged-body rotations allow interdomain closure to occur, facilitating the formation of the active site [19,22]. In a manner similar to ERK2 [11], it is possible that enhanced conformational mobility in the hinge following activation permits interdomain interactions that promote domain closure that may be vital for p_5JNK1β1 catalysis.

Phosphorylation resulted in a marked decrease in HX in peptide L136-N156 (LCGIKHLHSAGIIHRDLKPSN), which encompasses both the catalytic loop and much of helix αE (Fig. 5). The catalytic loop of kinases is a central part of their active site as it forms ion-pair interactions with the activation lip upon phosphorylation, bridging the phosphates with the catalytic base [23]. These interactions may limit flexibility in the catalytic loop to constrain the catalytic residue into the correct orientation for catalysis, which may concomitantly decrease the conformational mobility of helix αE through the side-chain interactions that exist between the two elements. Reduced mobility was also detected at a few additional sites within the α-helix core of the C-terminal domain following phosphorylation (see Fig. S4 for their corresponding peptides), which likely arises from the network of helix interactions that extends throughout the core from the constrained catalytic loop and helix αE. This broad reduction in the conformational mobility of the core would undoubtedly increase the stability of the C-terminal domain, contributing significantly to the global stabilization of JNK1β1 that we have observed upon phosphorylation (Fig. 2).

The entire length of the extended loop spanning the DFG motif and activation lip displayed a decrease in HX in p_5JNK1β1 when compared to its inactive form, as shown by the representative peptides L165-L172 (LKILDFGL) and M181-Y191 (MMTPYVVTRYY) (Fig. 5). As reported for many other kinases, the activation lip of inactive JNK1β1 presumably fluctuates between multiple conformations in solution. Dual phosphorylation of kinases at the Thr-Xxx-Tyr activation residues initiates new ion-pair interactions between the phosphates and neighboring side chains that induce substantial conformational remodeling of the activation lip. Despite the lack of understanding regarding the conformation of the activation lip in phosphorylated JNKs, a dramatic

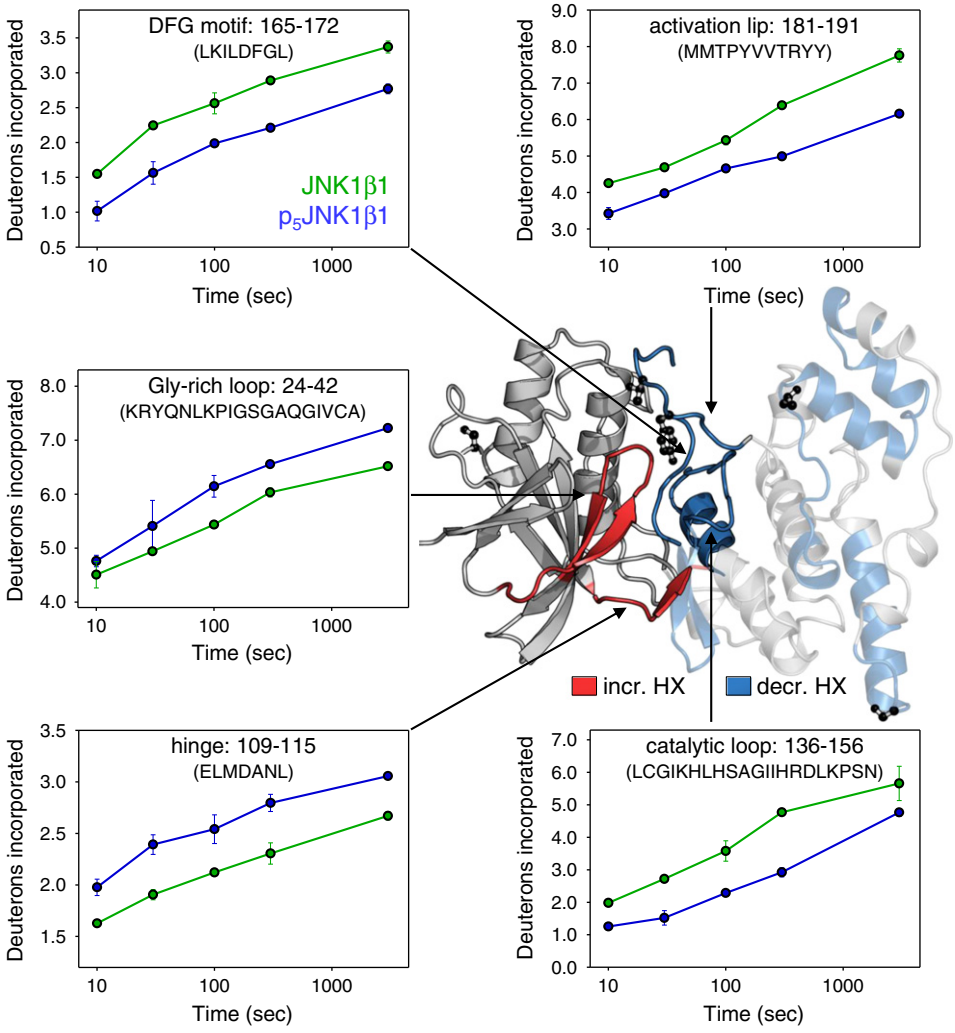

Fig. 5. Changes in HX in the active site of JNK1β1 induced by phosphorylative activation. Peptides representing the regions of the catalytic cleft that experienced an increase (red) or decrease (blue) in HX following activation of JNK1β1 by phosphorylation are mapped onto its structure. The residues phosphorylated in p_5JNK1β1 are shown as ball-and-stick models. The deuteron uptake plot for each representative peptide compares the deuteron incorporation of unmodified JNK1β1 (green) and p_5JNK1β1 (blue) over time. Lines through the points are presented only as guides for the eye. Error bars represent standard error of the mean of at least three independent experiments, and error bars may be smaller than the symbol used. Peptides displaying increases in HX upon phosphorylation comprise those derived from the Gly-rich loop and the hinge region, whereas peptides from the activation lip, DFG motif, and catalytic loop displayed decreased HX.

restructuring of this region would also be expected to occur upon activation of JNK1β1. The conserved DFG motif (residues Asp169-Phe170-Gly171) is also an indicator of the functional state of many protein kinases, as it is essential in forming metal coordination interactions with Mg^{2+}-ATP [24–27]. The predictable structural changes and the accompanying loss of the high flexibility of the activation lip upon formation of a more rigid functional conformation easily account for the decreased HX detected in this region of p_5JNK1β1. It is also probable that these events participate in the observed stabilization of the phosphorylated kinase.

Helices αG and αH, as well as the intervening helices α1L14 and α2L14 that form the MAPK insert, are another major region in which a decrease in deuteration levels may reflect that an expansive reduction in conformational mobility occurs upon phosphorylation. The four peptides G216-Q240 (GEMIKGGVLFPGTDHIDQWNKVIEQ), L241-F248 (LGTPCPEF), M249-T258 (MKKLQPTVRT), and F280-L298 (FPDVLFPADSEHNKLKASQARDLL) represent the general decrease in HX displayed by the many p_5JNK1β1 peptides identified for this region (Fig. 6). Other MAP kinases have shown either no change (ERK1 [14] and p38α [15]) or an increase in

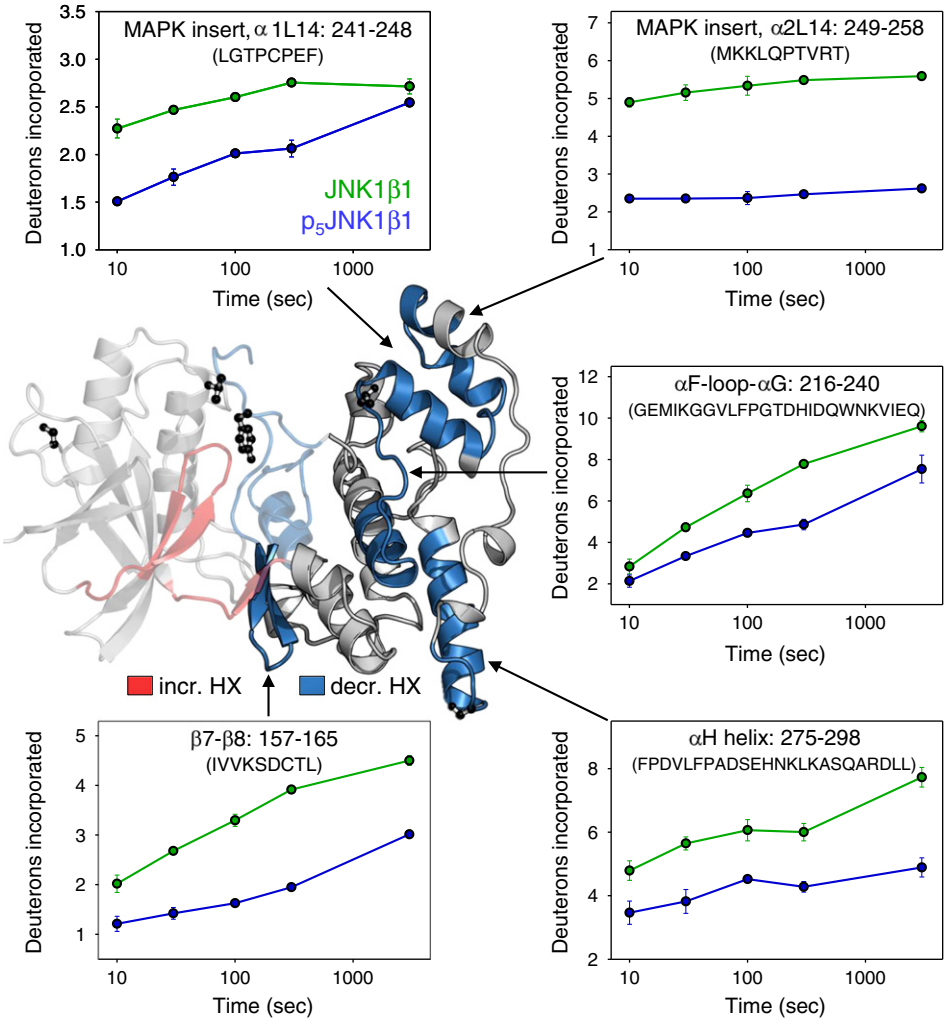

Fig. 6. HX changes in the C-terminal domain of JNK1β1 induced by phosphorylative activation. Representative peptides of the C-terminal domain show the regions outside of the active site that experienced a decrease in HX upon phosphorylation, mapped in blue onto the ribbon structure. The phosphorylated residues of p_5JNK1β1 are indicated as ball-and-stick models. Deuteron uptake plots compare the deuteron incorporation into the relevant peptides of unmodified JNK1β1 (green) and p_5JNK1β1 (blue) over time. Lines through the points are a guide for the eye only, while the error bars represent standard error of the mean of at least three independent experiments. C-terminal domain peptides exhibiting decreased HX following activation include those from the MAPK insert and helix αH, as well as the αF-loop-αG and β7-β8 structural elements.

HX (ERK2 [9]) in the MAPK insert following activation, the latter being attributed to disrupted interactions between the insert and the activation lip after the structural reorganizations that are triggered by activation. While the analogous contacts in JNK1β1 may be similarly disrupted, we hypothesize that the potential increase in the flexibility of the MAPK insert and the surrounding regions is overturned by the presence of the phosphate group that we have recently identified on T228 of p_5JNK1β1 [17]. This novel JNK1β1 phospho-site neighbors the N-capping motif of helix αG (N229-L241). Since helix-capping motifs (and the modifications thereof) are known to influence the stability of the helix and the protein in which they are located (e.g., see Ref. [28]), it is conceivable that the phosphorylation of T228 stabilizes the adjacent helix αG, which by extension reduces the conformational mobility of the MAPK insert through the helix interactions that the structures share. Likewise, it appears that helix αH (S284-M301) may be stabilized in a similar manner in p_5JNK1β1, as the additional novel phospho-site we have identified, S284, also forms part of the N-capping motif of this helix. The MAPK insert has been shown in other MAP kinases to be required for interactions with upstream kinases and additional regulatory proteins [29]. With the JNKs possessing more than 50 binding partners [3], it would not be

surprising if several regulatory proteins also interacted with the MAPK insert of JNK1β1. Decreased flexibility at these potential sites of interaction upon phosphorylation might affect the binding of the appropriate regulatory elements, acting to either enhance or inhibit the activity of p_5JNK1β1 *in vivo*.

In addition to helix αG, part of helix αF and their interconnecting loop, as well as strands β7 and β8, all exhibit decreased solvent accessibility after kinase activation. The changes in helix αF and its adjoining loop are depicted in the many peptides akin to G216-Q240 mentioned above (see Fig. S4), while the reduced HX in strands β7 and β8 is illustrated in peptide I157-L165 (IVVKSDCTL) (Fig. 6). These regions constitute an extended peptide-substrate binding site, in which the αF-loop-αG and β7-loop-β8 structures respectively interact with, for example, the D-domain and DEJL docking motif of c-Jun [30,31]. The decrease in HX implies that the conformational mobility of the binding site decreases upon JNK1β1 phosphorylation, which may act to promote substrate binding, enhancing catalytic turnover.

Solvent protection and changes to JNK1β1 conformational dynamics upon AMP-PNP/Mg^{2+} binding

The activation of many kinases is dependent on the formation of a functional active site by interdomain closure of the conserved N- and C-terminal domains upon phosphorylation. Since the "hinge region" that exists between two domains represents the pivot point at which these ridged-body rotations occur [19,22], the observed increase in the HX and conformational flexibility of JNK1β1 in this region following phosphorylation (see Fig. 5) suggests that activation of this MAP kinase may also require interdomain closure to form a competent catalytic site. To test this hypothesis, we investigated variations in interdomain interactions between JNK1β1 and p_5JNK1β1 by measuring the HX of each form in the presence of the non-hydrolyzable ATP analogue, AMP-PNP. Alterations in steric exclusion of bulk solvent following ligand interactions can be detected by HX [8], and thus, regions with reduced rates of HX likely signify protein–ligand binding interfaces. Since ATP is able to interact with parts of both N- and C-terminal domains within the catalytic cleft formed between the two, changes in steric protection from HX upon nucleotide binding provide a means to detect possible domain closure. Additional changes to regional conformational motilities revealed by HX will also assist in rationalizing the destabilizing effect that ATP binding has been shown to have on JNK1β1 (Fig. 2).

Four distinct regions within unmodified JNK1β1 displayed significant changes in HX upon ligand binding. Surprisingly, the patterns of solvent protection and/or changes in protein mobility correspond to a novel mode of ATP binding that is not present in the other MAP kinases, ERK and p38. The regions in ligand-bound JNK1β1 that demonstrated decreased HX and hence solvent protection relative to its unbound form comprised the hinge region and the adjacent strands β5 and βL5 (represented by the overlapping peptides I106-L110 and E109-L115), the catalytic loop (peptide L136-N156), and the DFG motif (peptide L165-L172) (Fig. 7). Conversely, the C-terminal end of helix αC shows a marked increase in HX in JNK1β1 upon AMP-PNP/Mg^{2+} binding. As direct interactions between the nucleotide and helix αC are not apparent in the available structures, the increased HX is most likely due to increases in conformational mobility induced upon occupancy of the active site. The changes can be observed in peptide R72-I86 (RELVLMKCVNHKNII) (Fig. 7); since its overlapping peptides (beginning from M77) do not exhibit a change (Fig. S4), the enhanced HX can be localized to amide residues R72-L76 (RELVL) within helix αC.

Active p_5JNK1β1 presented decreased HX by solvent protection in four discrete regions upon ligand binding. Three of these regions included the hinge region, the catalytic loop, and the DFG motif, similarly to that observed in inactive JNK1β1 following binding (Fig. 7). Significant solvent protection was additionally found in the Gly-rich flap and the adjoining β1 and β2 strands of p_5JNK1β1 (displayed in peptide K30-A42), protection that was not observed in JNK1β1. Unlike JNK1β1, residues R72-L76 (RELVL) of helix αC of p_5JNK1β1 experienced only a small increase in its degree of HX following AMP-PNP/Mg^{2+} binding (Fig. 7). The extent at which HX decreases in p_5JNK1β1 as a result of solvent protection by nucleotide binding appears to supplement the reduction in HX caused by the lowered solvent accessibility/conformational flexibility that is induced in these regions by phosphorylation. The differences seen in HX in the C-terminal domain contact surface when comparing the ligand-bound forms of JNK1β1 and p_5JNK1β1 can thus be attributed to the decreased exchange into unbound p_5JNK1β1 compared to JNK1β1, rather than disparities in solvent protection by ligand binding.

All of these regions contain amino acids that are known across protein kinases to form direct interactions with nucleotide substrates (see Ref. [23] for review). These contacts are consistent with the protein–ligand interactions that have been observed in the co-crystal structure of AMP-PNP bound to inactive JNK3 (PDB ID: 1JNK) [4]. To understand the nature of the JNK1β1–nucleotide binding interface suggested by the steric exclusion of bulk solvent upon binding, we examined the HX results against the JNK3-AMP-PNP/Mg^{2+} co-crystal structure. As it is the only structure of JNK that has been solved in the absence of a stabilizing inhibitory peptide (such as a JIP1 peptide) and as the residues involved in

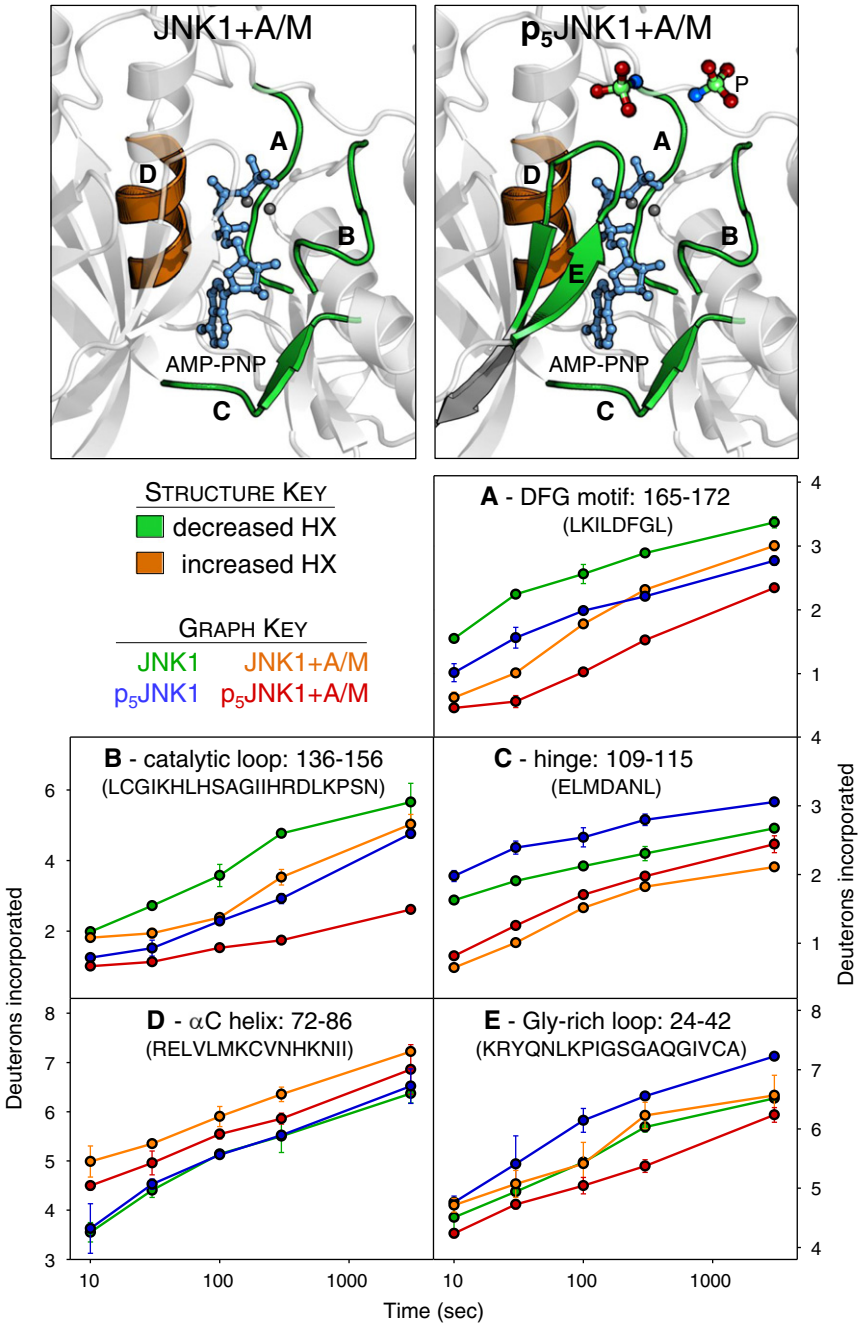

Fig. 7. Patterns of altered HX in the active site of JNK1β1 and p_5JNK1β1 upon AMP-PNP binding reflect differential sites at which unmodified and phosphorylated kinase interacts with nucleotide. The top panels indicate the location of the peptides derived from the active site of unmodified JNK1β1 (left structure) and p_5JNK1β1 (right structure) in which HX was reduced (green) or enhanced (orange) upon binding of AMP-PNP. AMP-PNP is indicated as a ball-and-stick model. Time courses of HX for the peptides representing each region display the distinct effects of AMP-PNP binding to JNK1β1 and p_5JNK1β1. HX data for the unbound forms of JNK1β1 (green) and p_5JNK1β1 (blue) are compared to their nucleotide-bound forms, JNK1 + A/M in orange and p_5JNK1 + A/M in red. Error bars represent standard error of the mean of at least three independent experiments. Both JNK1β1 and p_5JNK1β1 showed protection from HX upon AMP-PNP binding in peptides from A (the DFG motif), B (the catalytic loop), and C (the hinge region). p_5JNK1β1 exhibited additional HX protection by nucleotide compared to JNK1β1 in peptides from E (the Gly-rich loop), suggesting that interdomain closure occurs in the active kinase upon ATP binding. Peptides with enhanced HX upon nucleotide binding in both JNK1β1 and p_5JNK1β1 represent D (a C-terminal section of helix αC).

ATP binding are conserved across the various JNK isoforms [2], we feel that it best represents the native conformation and interactions present in the ATP-bound active site. This is primarily because the inhibitors are well-known to drastically distort the catalytic cleft such that ligand interactions are disrupted [32]. Additionally, the crystal structures of JNK1β1–AMP-PNP–inhibitory peptide ternary complexes that have been solved [33] share similar ligand binding characteristics with JNK3, supporting the validity of using this co-crystal structure. Nonetheless, significant differences may still exist between JNK3 and JNK1β1 with respect to the nature of their individual interactions with ATP.

The hinge region, the catalytic loop, and the DFG motif represented by the solvent-protected peptides described above all form key contacts with AMP-PNP within the C-terminal domain of inactive JNK3 (see Supplementary Information for a detailed description of these interactions). The comparable decreases in deuterium incorporation at the C-terminal domain side of the ligand–protein interface upon AMP-PNP binding in JNK1β1 and p_5JNK1β1 indicate that stable interactions between the nucleotide and the hinge region, the catalytic loop, and the DFG motif occur in both inactive and active JNK1β1.

In contrast, the N-terminal domain half of the nucleotide binding interface, particularly the Gly-rich flap, displayed differences in protection from HX by AMP-PNP binding between inactive and active JNK1β1 (the potential interactions of nucleotide with the N-terminal domain, as illustrated by JNK3, are detailed in Supplementary Information). As solvent protection of the Gly-rich flap was exhibited to a much greater degree in the relevant peptides of p_5JNK1β1, it is implied that residues in the flap of the active kinase establish more stable interactions with AMP-PNP than the equivalent residues in inactive JNK1β1. The finding that p_5JNK1β1 is able to interact productively with AMP-PNP at both N- and C-terminal domain faces of the catalytic cleft, while unmodified JNK1β1 makes contact with the nucleotide predominantly through the C-terminal domain, suggests that the ATP-bound conformation of active, phosphorylated JNK1β1 adopts interdomain interactions that lead to greater domain closure when compared to its inactive form.

Discussion

By measuring the stability and HX behavior of inactive and active JNK1β1 in solution, we provide the first insight into the mechanisms by which phosphorylation regulates the conformational dynamics of the kinase to induce its activation. Complementary studies with AMP-PNP/Mg^{2+}-bound kinase revealed a novel mode of nucleotide binding to the inactive form of JNK1β1, validating the intriguing destabilizing effect that nucleotide binding was shown to have on the kinase and supporting the mechanisms of activation proposed by the HX measurements of unbound JNK1β1.

The interpretation of HX data can be assisted greatly by atomic structural information. However, while numerous X-ray structures of non-phosphorylated and inactive JNK1 have been published (e.g., see Ref. [34]), a structure of the phosphorylated, active kinase has not yet been solved. Although insufficient structural information exists to conclude unambiguously that the changes in HX upon activation reflect changes in specifically the structure or internal motions of the protein, our HX measurements nevertheless describe the effects that phosphorylation and nucleotide binding have on the conformational state of JNK1β1.

Initial HX analysis of JNK1β1 indicates slow-exchanging core regions in both N- and C-terminal domains, with higher degrees of HX in peripheral elements such as loops and solvent-exposed secondary structure. The regional patterns of HX in JNK1β1 are thus consistent with its known tertiary structure and, expectedly, are similar to the HX patterns displayed by the inactive forms of both ERK2 [9] and p38α [15]. It is unsurprising that regional conformational flexibilities are conserved among the MAP kinases given that they share a well-conserved tertiary structure.

Phosphorylation-induced changes to the HX patterns of JNK1β1 provide insight into its activation mechanisms

HX experiments revealed that, upon phosphorylative activation of JNK1β1, significant changes to the structure and/or internal motions occur in localized regions of the protein that are associated with kinase regulation, catalysis, and substrate binding. Increased HX in the Gly-rich flap upon activation likely reflects increased flexibility that may enhance activity by facilitating nucleotide binding or release, as observed in PKA where flap flexibility is thought to enhance the rate-limiting release of ADP [19,20]. The hinge region also experienced enhanced HX, and since it permits the interdomain closure required for the formation of a functional active site in many kinases, increased mobility here following phosphorylation may facilitate this event [11]. Decreased HX within the activation lip, the DFG motif, and the catalytic loop is consistent with the structural reconfiguration of the catalytic cleft into its active conformation that is expected upon phosphorylation of JNK1β1. It is probable that reduced mobility and/or remodeling of the DFG motif is necessary for it to assist in binding and correctly orienting the nucleotide β- and γ-phosphates for phosphoryl transfer. The extended peptide-substrate binding site (αF-αG, strands β7-β8, and the loops between them) also

showed reduced HX in active JNK1β1. Decreased protein motions at the interface for docking-motif recognition could contribute to kinase activation and catalytic turnover by reducing the entropic cost of substrate binding. A reduction in HX in helices αG-αH and the intervening helices of the MAPK insert indicates that it also undergoes a possible decrease in mobility following activation. It is plausible that the phosphorylation of the novel JNK1β1 phospho-sites, T228 and S284, stabilizes these helices through their capacity as helix-capping residues, which may affect the binding of the potential regulatory proteins that have been shown to interact with the MAPK insert in other MAP kinases [29].

When comparing the patterns of regional HX of JNK1β1 with ERK2 and p38α, we reveal both similarities and significant differences. Expectedly, the MAP kinases all display modifications in their activation lip and DFG motifs upon phosphorylative activation as a result of active-site remodeling. The kinases additionally all exhibit decreased HX in the extended peptide-substrate binding site formed by the αF-loop-αG and β7-loop-β8 elements, at which reduced conformational mobility may modulate binding of substrate or regulatory proteins. Disparities in their response to phosphorylation begin at the hinge and Gly-rich flap, where only JNK1β1 and ERK2 share patterns of enhanced HX while p38α remains unaltered. Interestingly, it is within the HX behavior of the MAPK insert where the active MAP kinases diverge the most. While activation leads to enhanced HX in the MAPK insert of ERK2, the insert of p38α shows no change. Conversely, the insert of JNK1β1 experiences reduced HX following phosphorylation.

The differences in the changes to HX in these regions upon phosphorylation likely represent the differences in the mechanisms by which each kinase is activated. Firstly, modulating hinge flexibility in ERK2 acts to regulate the interdomain closure required for the creation of the active site [10,11], a means of activation that we now propose to also take place in JNK1β1 (as discussed below). In contrast, p38α is known to remain in an open conformation whether it has been activated by phosphorylation or bound by ATP-competitive inhibitors [35,36]. Thus, while increased hinge flexibility may be necessary for the domain rotations associated with the activation of JNK1β1 and ERK2, structural constraints in the hinge of p38α limit its flexibility and preclude interdomain closure as a contributor to its state of activity.

The opposing behaviors displayed by the MAPK insert of each kinase reflect further dissimilarities in the mechanisms contributing to their regulation. Enhanced HX and mobility in the ERK2 insert has been ascribed to the disruption of its interactions with the activation lip as the lip undergoes activation-induced remodeling, events that have been proposed to affect phosphorylation-dependent interactions with other regulatory macromolecules [9]. We hypothesize that the distinctive decrease in the flexibility of the JNK1β1 insert implied by the reduced HX is caused by the helix stabilizing ability of the uniquely phosphorylated N-capping motifs. Phosphorylation at these novel sites of modification (T228 and S284 in JNK1β1) has not been found in other members of the MAP kinase family, suggesting that they could act to differentially shift the binding free-energy landscape of active JNK1β1 to either permit exclusive binding modes of common regulatory macromolecules to occur at the less dynamic MAPK insert or stabilize the previously energetically unfavorable binding of unique regulatory elements that would otherwise not bind to the more flexible inserts of ERK2 or p38α. Like most unique post-translational modifications, these effects would contribute to forms of phosphorylation-dependent regulation of JNK1β1 that are distinct from the other MAP kinases and thereby assist in mediating their divergent functions.

All considered, the distinguishing HX behaviors of JNK1β1, ERK2, and p38α reveal that, while the patterns of solvent accessibility of their inactive forms are well-conserved, the character of activation-induced changes in conformational mobility is not fully conserved among MAP kinases despite the enzymes being closely related in both sequence and tertiary structure. We therefore echo previous findings that closely related MAP kinases diverge with respect to their constraints to activation, as well as the phosphorylation-dependent regulation of the internal motions that induce activation.

Steric protection of JNK1β1 by AMP-PNP reveals that interdomain closure is required for activation

Monitoring HX in the active site of AMP-PNP-bound JNK1β1 and p_5JNK1β1 revealed a novel mode of nucleotide binding to inactive kinase that differs from that of its active form. Patterns of decreased HX following binding in each kinase form were, in part, compatible with the steric exclusion of solvent expected to take place at residues thought to interact directly with the nucleotide. Both inactive and active JNK1β1 exhibited solvent protection in the hinge region, the catalytic loop, and the DFG motif. These regions represent the C-terminal side of the active site with which nucleotide has been shown to form hydrogen bonds in co-crystal structures of AMP-PNP bound to JNK3, PKA, and other kinases. The comparable HX between JNK1β1 and p_5JNK1β1 in these regions indicates that nucleotide forms binding interactions to the C-terminal domain that are similar in both inactive and active enzymes.

In contrast, disparities in the nature of nucleotide binding to the N-terminal domain between JNK1β1

and p_5JNK1β1 were revealed by the finding that only active kinase displays reduced HX at its Gly-rich flap, suggesting that AMP-PNP does not form stable interactions with the N-terminal domain of inactive JNK1β1. These results are surprising in that it has been shown in many other kinases that ATP interacts more productively with the N-terminal domain Gly-rich "ATP-binding" flap than with the residues of their C-terminal domain. This purportedly conserved site of interaction has led to the bilobed structure of kinases being characterized as comprising an N-terminal "ATP-binding" domain and a C-terminal "substrate-binding" domain [37]. Consistent with this characterization, studies of steric protection from HX in the MAP kinase ERK2 have revealed that AMP-PNP binding protects both N- and C-terminal domains of the nucleotide-binding pocket in active kinase, whereas in the inactive ERK2 form, AMP-PNP protects only the N-terminal domain [10]. While this suggested that ERK2 undergoes interdomain closure upon phosphorylation and ATP binding, it illustrated that, in the open domain conformation of the inactive MAP kinase, the nucleotide interacts more stably with the N-terminal domain.

Despite these findings and presumptions about the nature of ATP binding to kinases, there is also significant evidence indicating that the residues within the N-terminal domain of the active-site cleft of many kinases contribute less to nucleotide binding than initially expected. Measuring the nucleotide binding affinities and rates at which the γ-phosphate group is transferred in several Gly-rich flap mutants of PKA revealed that the flap functions primarily in stabilizing the transition state required for phosphoryl group transfer, indicating that, oddly enough, it is more important in facilitating catalysis than the anchoring of either ATP or ADP (Refs. [38] and [39] and see Ref. [23] for a review). Additional mutagenesis studies of Lys72 in both human and yeast PKA (Lys93 and Lys55 in JNK3 and JNK1β1, respectively), a residue located within the N-terminal domain that interacts with and stabilizes the α- and β-phosphates of ATP (Fig. S5), indicated that its primary function is also to enable phosphoryl group transfer without affecting the binding of ATP [40]. Conservative substitutions of this highly conserved Lys residue in Lck and ERK2 created mutant kinases in which changes in ATP binding could not be detected despite the proteins displaying drastically reduced turnover numbers [41,42]. Perhaps most relevantly, the affinities of adenosine, ADP, and ATP for PKA have been found to be incredibly similar [38]. This suggests that the electrostatic interactions that arise between the phosphate groups and residues within either the N- and or the C-terminal domain of the active site do not exist exclusively to reduce the ground-state energy level of the ligand–enzyme complex but instead to finely orient the γ-phosphoryl group for nucleophilic attack.

From the evidence mentioned above, it is clear that the domain surface with which ATP interacts most stably in the inactive form of kinases is functionally unimportant, provided that, upon kinase activation, conformational changes that allow the nucleotide to form stable interactions with the catalytically relevant residues in both N- and C-terminal domain halves of the active site occur, thereby enabling phosphoryl transfer. The finding that AMP-PNP interacts minimally with the Gly-rich flap in unmodified JNK1β1 is therefore not inconceivable, but it is compatible with the kinase occupying an open conformation in its inactive form. The simultaneous steric protection of both N- and C-terminal domains of active kinase by AMP-PNP then suggests that JNK1β1 adopts a closed conformation following phosphorylation and nucleotide binding.

Support for the apparent open conformation of the domains of inactive JNK1β1 is provided by the examination of the JNK3–AMP-PNP co-crystal structure [4]. When compared to the canonical structure of active PKA C-subunit, it was revealed that the domains of JNK3 are rotated apart, resulting in the misalignment of the two halves of the catalytic site. While residue Lys93 of the N-terminal domain is oriented similarly to its corresponding residue in PKA, residue Asp189 in the catalytic loop and residue Asp207 in the DFG motif of the C-terminal domain are misaligned [4]. As the conserved Asp189 and Asp207 are thought to be critical for protein kinase activity, their misalignment suggests that the open conformation of the domains of JNK3 plays a role in the low activity on the non-phosphorylated form of the kinase.

Combining the HX data and comparing the dynamic motions of inactive and active JNK1β1 with that of the studies of solvent accessibility in their nucleotide-bound forms, we propose a model explaining the differential HX protection of the Gly-rich loop between JNK1β1 and p_5JNK1β1. This model sees that both JNK1β1 and p_5JNK1β1 form stable interactions with ATP/Mg^{2+} through the C-terminal domain contact surface of the active site (comprising the hinge, the DFG motif, and catalytic loop) (Fig. 8). Interactions between ATP/Mg^{2+} and the Gly-rich flap of the N-terminal domain are transient in the inactive, non-phosphorylated kinase, consistent with an open solution conformation in which constraints in the hinge of the kinase prevent domain closure. Upon phosphorylative activation, we believe that an increase in the conformational dynamics of the hinge reflects an increase in its backbone flexibility that releases the constraints to interdomain closure and provides the domains a greater degree of freedom to rotate. The active kinase is thus able to form interdomain interactions that lead to greater domain closure, either prior to nucleotide binding or as a result of contributions by bridging interactions by the nucleotide itself, inducing

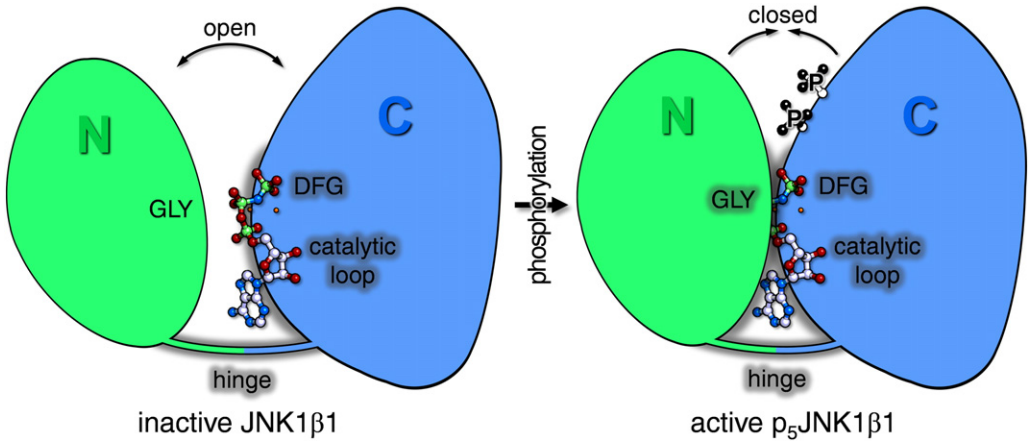

Fig. 8. Model describing the distinct patterns of steric protection from HX between JNK1β1 and p_5JNK1β1 upon AMP-PNP binding. The model proposes that AMP-PNP (ball-and-stick) interacts with the hinge and C-terminal domain (the DFG motif and catalytic loop) of both JNK1β1 and p_5JNK1β1, producing comparable patterns of solvent protection in these regions between the inactive and active kinase forms. The lack of protection from HX in the Gly-rich loop of unmodified JNK1β1 upon binding indicates that little interaction takes place between AMP-PNP and this region of inactive kinase. Increased solvent protection and accordingly more stable interactions occur between nucleotide and the Gly-rich loop of p_5JNK1β1, likely as a result of interdomain closure made possible through the enhanced flexibility in the hinge induced upon phosphorylation.

a closed conformation that is necessary for catalysis (Fig. 8). We cannot however exclude the possibility of models in which structural differences in the active site between JNK1β1 and p_5JNK1β1 cause differential hydrogen bonding interactions with ATP/Mg^{2+}.

A similar proposition has been made for both p38γ and ERK2, yet as described with respect to the latter, AMP-PNP has been shown contrastingly to interact more productively with the N-terminal domain of the inactive, open form of this MAP kinase prior to the interdomain closure that accompanies phosphorylation [10]. Even more divergently, the closely related ERK1 displays HX behavior suggesting that hinge flexibility is not regulated by activation and that both inactive and active forms of this MAP kinase permit domain closure and creation of a closed active site upon nucleotide binding [14]. These findings reiterate that these enzymes differ with respect to the regulation of interdomain closure and their mechanisms of activation although the related MAP kinases are structurally similar.

A conserved active-site helix displays activation-dependent changes in its response to nucleotide binding

It has become evident that regulation via phosphorylation-induced refolding of the activation loop incorporates conformational and/or dynamic changes in other distinct structural elements distal from the phosphorylation site. One such well-understood element is helix αC, the only conserved helix in the N-terminal domain and whose state is directly associated with kinase activity. In most inactive kinase structures, helix αC is displaced from its active alignment largely as a rigid unit such that important stabilizing interactions within the active site are disrupted. For example, phosphorylative activation of ERK2, cdk2, and InRK (and many others) triggers a distinct repositioning of helix αC so that the conserved Glu (located at the center of the helix) is oriented correctly to stabilize and form a salt bridge with the conserved Lys (of strand β3) that interacts with the α- and β-phosphoryl groups of ATP (see Ref. [23] for an extensive review). Most active kinases have an intact Glu-Lys salt bridge as a result of an aligned αC helix, indicating that the formation of the dyad is a significant contributor to the enhanced rate of phosphoryl transfer that is incurred following phosphorylation. Although mutagenesis studies have shown that substitutions at the Glu residue creates mutant kinases with drastically reduced activity, it is important to note again that, while the replacements resulted in a loss of cooperativity in binding of cofactor and substrate, nucleotide binding affinities were not affected [43]. This reiterates the finding that residues in the N-terminal of the active site may contribute more to catalysis than nucleotide binding.

While the positioning of αC helix appears to be critical for the functioning of most protein kinases, as its displacement is nearly always involved in kinase inactivation, the mechanism by which each kinase repositions the helix is not conserved. The structural changes in αC can be linked to the phosphorylation of the activation residues through numerous interactions, but its position has also been shown to be affected by nucleotide binding. Additional HX studies of PKA have illustrated that binding of ADP is sufficient

to alter the environment of helix αC to display decreased HX [44]. The finding by Resing and Ahn that active MKK1 demonstrates increased mobility in helix αC compared to its inactive form [45] further attests to the dynamic flexibility of this helix in different kinases and reveals that its behavior can depend on both phosphorylation and nucleotide-bound state of the kinase.

We found that, in JNK1β1, a C-terminal fragment of helix αC containing the catalytic Glu73 experiences a distinct increase in conformational mobility upon AMP-PNP binding. This suggests that either nucleotide binding induces changes to the structure and/or conformational mobility of the helix through the interactions that exist between the C-terminal domain of the active site and helix αC or the nucleotide preferentially binds a conformer or native-like intermediate species of JNK1β1 in which helix αC is more flexible or oriented such that it is more solvent exposed. The potential conformational selection and stabilization of an intermediate state was suggested initially in the equilibrium unfolding experiments by a much greater signal produced by the first intermediate when compared to unbound JNK1β1 (Fig. 2).

In the inactive form of JNK1β1, the orientation of helix αC may place catalytically relevant/irrelevant residues into unknown positions that have enthalpically unfavorable binding energies to nucleotide, thus causing subtle structural shifts and/or enhanced conformational mobility to occur in helix αC upon ATP binding that produces a favorable contribution to entropy. Energetically unfavorable ATP binding and the resulting distortions of the phosphate groups and of active-site residues from catalytic geometries is a common means of kinase inactivation [43].

With respect to the alternative possibility of conformational selection by nucleotide (preferential binding to one of the ensemble of exchanging protein conformers in equilibrium), helix αC may first need to adopt a less rigid structure prior to ATP binding to reduce the local entropic penalties of association. This may be necessary because the proposed open conformation of the inactive kinase permits less favorable contributions to enthalpy upon binding as a result of the nucleotide being able to interact with only a single side of the active site. A protein conformer with a more flexible αC helix may also allow the transient opening of the Gly-rich flap thought to be necessary for access to the nucleotide-binding pocket, an effect possibly transmitted through strand β3 with which each structural element interacts. The catalytically relevant Glu73 is also situated in the segment of helix αC that undergoes increased HX in inactive JNK1β1 following nucleotide binding, suggesting that the changes in this region may hold or further displace Glu73 away from its catalytically aligned orientation, preserving the kinase in its inactive form until it is activated by phosphorylation. In support of these suggestions, Vogt and Di Cera have recently argued that this form of conformational selection can in fact account for the behavior of almost all ligand binding events [46].

The R72-L76 fragment of helix αC in p_5JNK1β1 experiences a much smaller increase in HX upon nucleotide binding when compared to unmodified JNK1β1. While the presence of AMP-PNP may cause increases to the conformational mobility of helix αC in p_5JNK1β1 in a manner similar to that proposed for non-phosphorylated kinase, the expected repositioning of the helix into catalytic alignment following activation is also likely to stabilize it through the catalytically important interactions that arise (such as the newly formed Glu73–Lys55 dyad, as well as their interaction with the α- and β-phosphates of AMP-PNP). The changes to helix αC that are triggered by nucleotide in JNK1β1 may therefore also occur in p_5JNK1β1 but would take place to a much lesser degree.

Regardless of the means by which the enhanced flexibility of helix αC arises in nucleotide-bound JNK1β1 and p_5JNK1β1, it is highly probable that it disturbs the network of interactions that extend from the helix throughout the core of the N-terminal domain and into the Gly-rich flap. As the helix is the only major structural element that has a marked increase in its conformational mobility upon nucleotide binding, it is likely to be the main source of the destabilization observed in AMP-PNP-bound kinase. The enhanced dynamic motions in helix αC could be coupled by a network of contacts to the N-terminal β-sheet and helix αL16, inducing a "loosening" of the internal structure of the entire N-terminal domain. The dynamics of the individual structural elements may not increase significantly enough to be detected unambiguously by the HX experiments, but in combination, they conceivably decrease the overall stability of the domain.

Since the N-terminal domain of the active kinase provides catalytically important interactions with ATP, increased dynamics in this domain of p_5JNK1β1 upon nucleotide binding could enable the conformational changes that take place during phosphoryl transfer and ADP release. Again, the finding that ADP release is the rate-limiting step during catalysis in PKA supports this hypothesis [47]. Activation-induced increases in the conformational mobility of domains are not uncommon in protein kinases. For example, phosphorylation of InRK destabilizes the kinase toward guanidine-induced unfolding [48], while HX experiments in MKK1 indicates that its N-terminal domain becomes more flexible following phosphorylative activation [45].

In an independent publication, we will be exploring the implications of the conformational stability parameters ($\Delta G^{\circ}_{H_2O}$ and m values) measured for the formation of each observed intermediate in terms of the stabilizing or destabilizing effect that nucleotide binding and phosphorylation has on each species, all

in order to establish the significance of these events in the activation and catalytic functioning of JNK1β1.

Nevertheless, our findings indicate that nucleotide alone can induce far-reaching structural effects that include altering the position and/or conformational dynamics of a critical active-site helix, and in doing so, it reduces the thermal, conformational, and kinetic stability of the kinase. Further studies will be required to fully understand the mechanisms by which binding triggers these events or their exact functional relevance, but since similar effects of nucleotide binding on helix αC have been reported in other kinases, including PKA [44], this behavior is not a completely isolated or unique phenomenon.

Conclusion

The effects of nucleotide binding on the stability of JNK1β1, as well as the associated patterns of solvent protection and/or changes in protein mobility, correspond to a novel mode of ATP binding that is, in some part, incompatible with what we think we understand about the nature of binding and of the sites that inactive kinases use to make contact with nucleotides. The JNK1β1 HX data are nonetheless consistent with the prevailing model for protein kinase activation in which interdomain closure through rotation of the N-terminal domain with respect to the C-terminal domain produces a functional active site. However, nucleotide-dependent destabilization and the concomitant detection of enhanced HX in a conserved active-site helix within the interface between the two domains revealed that the model for the activation of JNK1β1 is much more intricate. In the inactive form of JNK1β1, nucleotide may possibly select for a kinase conformation in which the domains are more open and the N-terminal domain is transiently destabilized, preventing the domain from forming a more stable, catalytically functional structure until the kinase is phosphorylated. Ultimately, it is clear that there exists complex and unique interplay between the effects of phosphorylation and nucleotide substrate binding for the regulation of JNK1β1 activity.

Materials and Methods

Expression, purification, and phosphorylation of JNK1β1

Overexpression and purification of JNK1β1 from *Escherichia coli* and preparation of its non-phosphorylated and fully phosphorylated forms were achieved as previously described [16].

Spectroscopic measurements

Fluorescence emission spectra were measured in triplicate with a Jasco FP-6300 fluorescence spectrophotometer at 20 °C, using an excitation wavelength of 280 and 295 nm. Far-UV circular dichroism measurements were recorded using a Jasco J-810 circular dichroism spectropolarimeter and represent an average of 10 accumulations. Measurements were performed at 20 °C with 2 μM JNK1β1 in "Characterization Buffer" [10 mM Tris–HCl buffer, pH 8.0, comprising 150 mM NaCl, 1 mM DTT, and 0.02% (w/v) NaN_3] for both methods. All spectra were corrected for solvent. Circular dichroism data were averaged and normalized by calculating the mean residue ellipticity, [θ] (degrees square centimeters per decimole) using the equation:

$$[\theta] = \frac{100\theta}{Cnl}$$

where θ is the measured ellipticity (millidegrees), C is the protein concentration (millimolar), n is the number of residues in the protein, and l is the path length (centimeters).

Stability studies

Temperature-induced unfolding

Temperature-induced denaturation of protein was monitored by measuring the amount of α-helical structure present using ellipticity at 222 nm, employing a Jasco J-810 circular dichroism spectropolarimeter over a temperature range of 20–95 °C. Thermal unfolding profiles were recorded using 5 μM JNK1β1 in Characterization Buffer, both with and without the addition of 1 mM AMP-PNP and 10 mM $MgCl_2$ (protein solutions with ligand added were pre-equilibrated at 20 °C for 30 min before unfolding to allow binding). The temperature was increased at a rate of 1 °C/min, which was controlled by a Jasco PTC-423S Peltier-type temperature control system. The temperature unfolding profiles were performed in triplicate, averaged, and normalized by converting the data to mean residue ellipticity. To describe the thermal unfolding profiles, we calculated lines of best fit using SigmaPlot v11.0 (SPSS Science, Chicago, IL, USA).

Urea-induced equilibrium unfolding and refolding

Equilibrium unfolding experiments were performed by incubating 1 μM protein (in Characterization Buffer) with 0–9 M urea, either with or without the addition of ligand (1 mM AMP-PNP and 10 mM $MgCl_2$). Refolding and reversibility experiments were conducted by diluting 10 μM protein unfolded in 8 M urea (with and without ligand added) to 1 μM containing 0.8–7.9 M urea. After allowing the solutions (prepared in triplicate) to equilibrate for 30 min at 20 °C, we monitored the changes to the global structure of JNK1β1 that occur upon unfolding and refolding using three different probes: (i) fluorescence spectroscopy to monitor the tertiary structure (λ_{ex} = 280 nm and λ_{em} = 310–347 nm), (ii) far-UV circular dichroism at 222 nm to monitor the secondary structure, and (iii) ANS binding to monitor the environment of the proposed ANS binding sites determined in this study (see Fig. S1). Measurements of ANS binding were conducted by adding 200 μM ANS to protein unfolded in 0–9 M urea and determining the fluorescence of ANS excited at 390 nm and emitting at 475 nm. To ensure the absence of aggregation during unfolding and refolding experiments, we monitored

Rayleigh scattering by setting both excitation and emission wavelengths at 340 nm. Fluorescence and circular dichroism equilibrium unfolding data were globally fit [49] to a four-state monomer model ($N \leftrightarrow I \leftrightarrow I_2 \leftrightarrow U$) using the linear extrapolation method [50] provided by Savuka version 6.2.26 [51] to calculate the conformational stability parameters, $\Delta G^{\circ}_{H_2O}$ (free energy of unfolding in the absence of urea, in kilocalories per mole) and m value [cooperativity factor (kcal mol^{-1} M^{-1})].

Urea-induced unfolding kinetics

Unfolding kinetics data were measured by intrinsic fluorescence at 20 °C using a stopped-flow mixing instrument with a 2-ms dead time (Applied Photophysics SX-18MV). Protein was excited at 280 nm, and the emission was monitored using a 320-nm-longpass filter. JNK1β1 in characterization buffer was diluted 6-fold with urea in buffer, producing a final protein concentration of 0.4 μM in 7.8–8.3 M urea. For ligand-bound protein unfolding experiments, 1 mM AMP-PNP and 10 mM $MgCl_2$ were added to both urea and protein solutions and allowed to equilibrate prior to unfolding. No less than three kinetic traces were recorded and averaged at each urea concentration, which were then analyzed and fit to a triple exponential equation by the nonlinear least-squares method using the Applied Photophysics software version 4.47. The dependence of the observed rate constants on urea concentration was fit to the equation:

$$\log k_u = \log k_u^{H_2O} + \frac{m_u^{\ddagger}[\text{urea}]}{2.303RT}$$

where k_u is the observed unfolding rate constant, $k_u^{H_2O}$ is the unfolding rate constant in the absence of urea, and $m_u^{\ddagger}$ is the m value for the unfolding of the native state to form the transition state.

Hydrogen–deuterium exchange mass spectrometry

To conduct the HX reactions, we diluted 15 μL of unmodified or phosphorylated JNK1β1 at a concentration of 2.8 mg/mL [in 20 mM phosphate buffer (pH 7.8) with 150 mM NaCl, 1 mM DTT, and 0.02% NaN_3] with 35 μL of 100% D_2O at 20 °C for 10, 30, 100, 300, or 3000 s before the simultaneous quenching of exchange and proteolysis of the protein. Ligand-bound protein exchange reactions were conducted similarly, except that 1 mM AMP-PNP and 10 mM $MgCl_2$ were added to both D_2O and protein solutions. An equal volume (50 μL) of ice-cold quench buffer [20 mM phosphate buffer (pH 2.2) with 150 mM NaCl, 1 mM DTT, and 0.02% NaN_3] containing 4 M guanidinium chloride and 0.5 mg/mL pepsin (Sigma) was added to the reaction buffer. A fully deuterated control was achieved by allowing deuteration to occur overnight, while a non-deuterated control experiment was performed by replacing the D_2O with MilliQ H_2O. Proteolysis was allowed to proceed for 5 min on ice upon addition of the quench buffer, after which the samples were injected onto an Aeris PEPTIDE 3.6-μm XB-C18 RP column (Phenomenex) that was submerged in ice and coupled to an AB SCIEX QSTAR Elite mass spectrometer. Peptides were eluted at a rate of 300 μL/min with a linear acetonitrile gradient (5–95%) over 15 min. Collision-induced dissociation was performed for the initial identification of peptides, while all subsequent samples were analyzed in MS mode. MS resolution was in the range 13,000–15,000 full width at half maximum, and all exchange reactions were performed at least in duplicate. PEAKS 6 (Bioinformatics Solutions, Inc.) was used to sequence the initial peptide pool, and HDExaminer 1.3 (Sierra Analytics) was used to process the deuterium exchange data. Statistically significant differences in deuteration behavior between the JNK1β1 forms were established by calculating a Student's *t*-distribution at a 95% confidence level using all of the replicates and charge states available.

Acknowledgment

This work was supported by the University of the Witwatersrand, South African National Research Foundation (Grants: 60810, 65510, and 68898 to H.W.D.) and South African Research Chairs Initiative of the Department of Science and Technology and National Research Foundation (Grant 64788 to H.W.D.).

Appendix A. Supplementary data

Supplementary data to this article can be found online at http://dx.doi.org/10.1016/j.jmb.2014.08.019.

Received 23 June 2014;
Received in revised form 22 August 2014;
Accepted 25 August 2014
Available online 29 August 2014

Keywords:
c-Jun N-terminal kinase;
MAP kinases;
hydrogen exchange;
mass spectrometry;
protein dynamics

Abbreviations used:
ANS, 8-anilino-1-naphthalenesulfonate; AMP-PNP, 5′-adenylyl-imidodiphosphate; HX, hydrogen–deuterium exchange; JNK, c-Jun N-terminal kinase; MS, mass spectrometry; MAP, mitogen-activated protein.

References

[1] Davis RJ. Signal transduction by the JNK group of MAP kinases. Cell 2000;103:239–52.
[2] Gupta S, Barrett T, Whitmarsh AJ, Cavanagh J, Sluss HK, Derijard B, et al. Selective interaction of JNK protein kinase isoforms with transcription factors. EMBO J 1996;15:2760–70.

[3] Bogoyevitch MA, Kobe B. Uses for JNK: the many and varied substrates of the c-Jun N-terminal kinases. Microbiol Mol Biol Rev 2006;70:1061–95.
[4] Xie X, Gu Y, Fox T, Coll JT, Fleming MA, Markland W, et al. Crystal structure of JNK3: a kinase implicated in neuronal apoptosis. Structure 1998;6:983–91.
[5] Goldsmith EJ, Cobb MH. Protein kinases. Curr Opin Struct Biol 1994;4:833–40.
[6] Zhang F, Strand A, Robbins D, Cobb MH, Goldsmith EJ. Atomic structure of the MAP kinase ERK2 at 2.3 Å resolution. Nature 1994;367:704–11.
[7] Canagarajah BJ, Khokhlatchev A, Cobb MH, Goldsmith EJ. Activation mechanism of the MAP kinase ERK2 by dual phosphorylation. Cell 1997;90:859–69.
[8] Hoofnagle AN, Resing KA, Ahn NG. Protein analysis by hydrogen exchange mass spectrometry. Annu Rev Biophys Biomol Struct 2003;32:1–25.
[9] Hoofnagle AN, Resing KA, Goldsmith EJ, Ahn NG. Changes in protein conformational mobility upon activation of extracellular regulated protein kinase-2 as detected by hydrogen exchange. Proc Natl Acad Sci USA 2001;98:956–61.
[10] Lee T, Hoofnagle AN, Resing KA, Ahn NG. Hydrogen exchange solvent protection by an ATP analogue reveals conformational changes in ERK2 upon activation. J Mol Biol 2005;353:600–12.
[11] Sours KM, Xiao Y, Ahn NG. Extracellular-regulated kinase 2 is activated by the enhancement of hinge flexibility. J Mol Biol 2014;426:1925–35.
[12] Wang Z, Harkins PC, Ulevitch RJ, Han J, Cobb MH, Goldsmith EJ. The structure of mitogen-activated protein kinase p38 at 2.1-Å resolution. Proc Natl Acad Sci USA 1997; 94:2327–32.
[13] Bellon S, Fitzgibbon MJ, Fox T, Hsiao HM, Wilson KP. The structure of phosphorylated p38gamma is monomeric and reveals a conserved activation-loop conformation. Structure 1999;7:1057–65.
[14] Ring AY, Sours KM, Lee T, Ahn NG. Distinct patterns of activation-dependent changes in conformational mobility between ERK1 and ERK2. Int J Mass Spectrom 2011;302: 101–9.
[15] Sours KM, Kwok SC, Rachidi T, Lee T, Ring A, Hoofnagle AN, et al. Hydrogen-exchange mass spectrometry reveals activation-induced changes in the conformational mobility of p38alpha MAP kinase. J Mol Biol 2008;379:1075–93.
[16] Owen GR, Achilonu I, Dirr HW. High yield purification of JNK1β1 and activation by *in vitro* reconstitution of the MEKK1 → MKK4 → JNK MAPK phosphorylation cascade. Protein Expression Purif 2013;87:87–99.
[17] Owen GR, Stoychev S, Achilonu I, Dirr HW. JNK1beta1 is phosphorylated during expression in *E. coli* and *in vitro* by MKK4 at three identical novel sites. Biochem Biophys Res Commun 2013;432:683–8.
[18] Dreskin SC, Thomas GW, Dale SN, Heasley LE. Isoforms of Jun kinase are differentially expressed and activated in human monocyte/macrophage (THP-1) cells. J Immunol 2001;166:5646–53.
[19] Narayana N, Cox S, Nguyen-huu X, Ten Eyck LF, Taylor SS. A binary complex of the catalytic subunit of cAMP-dependent protein kinase and adenosine further defines conformational flexibility. Structure 1997;5:921–35.
[20] Taylor SS, Radzio-Andzelm E, Madhusudan Cheng X, Ten Eyck L, Narayana N. Catalytic subunit of cyclic AMP-dependent protein kinase: structure and dynamics of the active site cleft. Pharmacol Ther 1999;82:133–41.
[21] Fox T, Coll JT, Xie X, Ford PJ, Germann UA, Porter MD, et al. A single amino acid substitution makes ERK2 susceptible to pyridinyl imidazole inhibitors of p38 MAP kinase. Protein Sci 1998;7:2249–55.
[22] Tsigelny I, Greenberg JP, Cox S, Nichols WL, Taylor SS, Ten Eyck LF. 600 ps molecular dynamics reveals stable substructures and flexible hinge points in cAMP dependent protein kinase. Biopolymers 1999;50:513–24.
[23] Adams JA. Kinetic and catalytic mechanisms of protein kinases. Chem Rev 2001;101:2271–90.
[24] Kornev AP, Haste NM, Taylor SS, Eyck LF. Surface comparison of active and inactive protein kinases identifies a conserved activation mechanism. Proc Natl Acad Sci USA 2006;103:17783–8.
[25] Levinson NM, Kuchment O, Shen K, Young MA, Koldobskiy M, Karplus M, et al. A Src-like inactive conformation in the abl tyrosine kinase domain. PLoS Biol 2006;4:2.
[26] Vogtherr M, Saxena K, Hoelder S, Grimme S, Betz M, Schieborr U, et al. NMR characterization of kinase p38 dynamics in free and ligand-bound forms. Angew Chem Int Ed Engl 2006;45:993–7.
[27] Kannan N, Neuwald AF. Did protein kinase regulatory mechanisms evolve through elaboration of a simple structural component? J Mol Biol 2005;351:956–72.
[28] Quan A, Xue J, Wielens J, Smillie KJ, Anggono V, Parker MW, et al. Phosphorylation of syndapin I F-BAR domain at two helix-capping motifs regulates membrane tubulation. Proc Natl Acad Sci USA 2012;109:3760–5.
[29] Robinson FL, Whitehurst AW, Raman M, Cobb MH. Identification of novel point mutations in ERK2 that selectively disrupt binding to MEK1. J Biol Chem 2002;277: 14844–52.
[30] Kallunki T, Su B, Tsigelny I, Sluss HK, Derijard B, Moore G, et al. JNK2 contains a specificity-determining region responsible for efficient c-Jun binding and phosphorylation. Genes Dev 1994;8:2996–3007.
[31] Jacobs D, Glossip D, Xing H, Muslin AJ, Kornfeld K. Multiple docking sites on substrate proteins form a modular system that mediates recognition by ERK MAP kinase. Genes Dev 1999;13:163–75.
[32] Heo YS, Kim SK, Seo CI, Kim YK, Sung BJ, Lee HS, et al. Structural basis for the selective inhibition of JNK1 by the scaffolding protein JIP1 and SP600125. EMBO J 2004;23: 2185–95.
[33] Garai A, Zeke A, Gogl G, Toro I, Fordos F, Blankenburg H, et al. Specificity of linear motifs that bind to a common mitogen-activated protein kinase docking groove. Sci Signaling 2012;5:2003004.
[34] Nakaniwa T, Fukada H, Inoue T, Gouda M, Nakai R, Kirii Y, et al. Seven cysteine-deficient mutants depict the interplay between thermal and chemical stabilities of individual cysteine residues in mitogen-activated protein kinase c-Jun N-terminal kinase 1. Biochemistry 2012;51:8410–21.
[35] ter Haar E, Prabhakar P, Liu X, Lepre C. Crystal structure of the p38 alpha-MAPKAP kinase 2 heterodimer. J Biol Chem 2007;282:9733–9.
[36] White A, Pargellis CA, Studts JM, Werneburg BG, Farmer BT. Molecular basis of MAPK-activated protein kinase 2:p38 assembly. Proc Natl Acad Sci USA 2007;104:6353–8.
[37] Johnson DA, Akamine P, Radzio-Andzelm E, Madhusudan M, Taylor SS. Dynamics of cAMP-dependent protein kinase. Chem Rev 2001;101:2243–70.
[38] Hoppe J, Freist W, Marutzky R, Shaltiel S. Mapping the ATP-binding site in the catalytic subunit of adenosine-3′:5′-

monophosphate-dependent protein kinase. Spatial relationship with the ATP site of the undissociated enzyme. Eur J Biochem 1978;90:427–32.
[39] Grant BD, Hemmer W, Tsigelny I, Adams JA, Taylor SS. Kinetic analyses of mutations in the glycine-rich loop of cAMP-dependent protein kinase. Biochemistry 1998;37: 7708–15.
[40] Gibbs CS, Zoller MJ. Rational scanning mutagenesis of a protein kinase identifies functional regions involved in catalysis and substrate interactions. J Biol Chem 1991;266: 8923–31.
[41] Robinson MJ, Harkins PC, Zhang J, Baer R, Haycock JW, Cobb MH, et al. Mutation of position 52 in ERK2 creates a nonproductive binding mode for adenosine 5′-triphosphate. Biochemistry 1996;35:5641–6.
[42] Carrera AC, Alexandrov K, Roberts TM. The conserved lysine of the catalytic domain of protein kinases is actively involved in the phosphotransfer reaction and not required for anchoring ATP. Proc Natl Acad Sci USA 1993;90:442–6.
[43] Engh RA, Bossemeyer D. Structural aspects of protein kinase control-role of conformational flexibility. Pharmacol Ther 2002;93:99–111.
[44] Andersen MD, Shaffer J, Jennings PA, Adams JA. Structural characterization of protein kinase A as a function of nucleotide binding. Hydrogen-deuterium exchange studies using matrix-assisted laser desorption ionization-time of flight mass spectrometry detection. J Biol Chem 2001;276: 14204–11.
[45] Resing KA, Ahn NG. Deuterium exchange mass spectrometry as a probe of protein kinase activation. Analysis of wild-type and constitutively active mutants of MAP kinase kinase-1. Biochemistry 1998;37:463–75.
[46] Vogt AD, Di Cera E. Conformational selection is a dominant mechanism of ligand binding. Biochemistry 2013;52:5723–9.
[47] Adams JA, Taylor SS. Energetic limits of phosphotransfer in the catalytic subunit of cAMP-dependent protein kinase as measured by viscosity experiments. Biochemistry 1992;31: 8516–22.
[48] Bishop SM, Ross JB, Kohanski RA. Autophosphorylation dependent destabilization of the insulin receptor kinase domain: tryptophan-1175 reports changes in the catalytic cleft. Biochemistry 1999;38:3079–89.
[49] Beechem JM. Global analysis of biochemical and biophysical data. Methods Enzymol 1992;210:37–54.
[50] Pace CN. Determination and analysis of urea and guanidine hydrochloride denaturation curves. Methods Enzymol 1986; 131:266–80.
[51] Bilsel O, Zitzewitz JA, Bowers KE, Matthews CR. Folding mechanism of the alpha-subunit of tryptophan synthase, an alpha/beta barrel protein: global analysis highlights the interconversion of multiple native, intermediate, and unfolded forms through parallel channels. Biochemistry 1999;38: 1018–29.

Phosphorylation and nucleotide-binding induced changes to the stability and hydrogen exchange patterns of JNK1β1 provide insight into its mechanisms of activation

GAVIN R. OWEN[1], STOYAN STOYCHEV[2], IKECHUKWU ACHILONU[1], AND HEINI W. DIRR[1]

[1]Protein Structure-Function Research Unit, School of Molecular and Cell Biology, University of the Witwatersrand, Johannesburg 2050, South Africa.

[2]Council for Scientific and Industrial Research, Biosciences, Pretoria, 0001, South Africa.

APPENDIX A.

SUPPLEMENTARY MATERIAL

- Table of Contents -

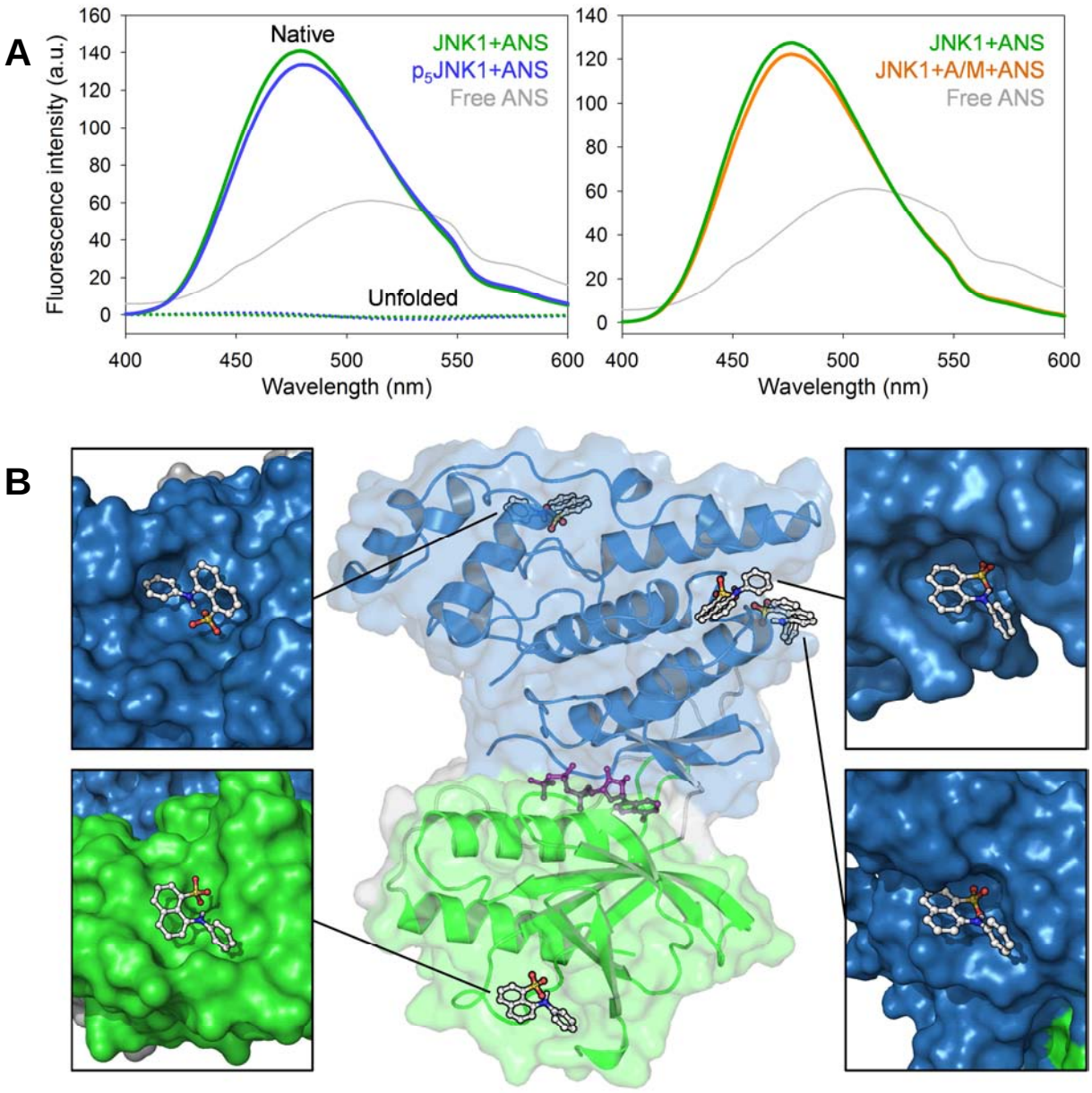

Fig. S1. ANS binding to JNK1β1 and p_5JNK1β1. (A) Emission spectra of ANS bound to JNK1β1 (green) and p_5JNK1β1 (blue) indicates that the dye interacts similarly with the inactive and active form of the native kinase (the emission spectra display equivalent increases in fluorescence intensity and hypsochromic shifts relative to free ANS in grey), but the dye does not interact with their unfolded states (left panel). Although we do not yet fully understand the nature or location/s of the JNK1β1-ANS interaction, the finding that the presence of AMP-PNP/Mg^{2+} (+A/M) does not affect ANS binding (indicated by the overlaying ANS emission spectra shown in the right panel), reveals that the dye does not interact within the active site of the kinase. (B) *In silico* molecular docking of ANS to determine potential sites at which the dye interacts with JNK1β1. ANS was docked to the crystal structure of JNK1β1 (PDB entry 2SX0) using AutoDock Vina 1.1.2 [1] to perform the docking calculations. Polar H-atoms were computed and added to JNK1β1 using AutoDock Tools 1.5.6 [2] prior to performing the docking calculations. The search space comprised a large, XYZ-coordinates aligned box with margin sizes of 54 Å (X) × 64 Å (Y) × 88 Å (Z) that encompassed the entire protein. The exhaustiveness of the search was set to 20, whilst all other parameters were kept at their default values. ANS was allowed to be fully flexible with all bonds rotatable, while JNK1β1 was treated as rigid during docking. To evaluate the interaction of the flexible ligand with the protein and identify its putative binding modes, the resulting docked structures were ranked according to their calculated docking energies and inspected. Four potential sites of interaction were identified.

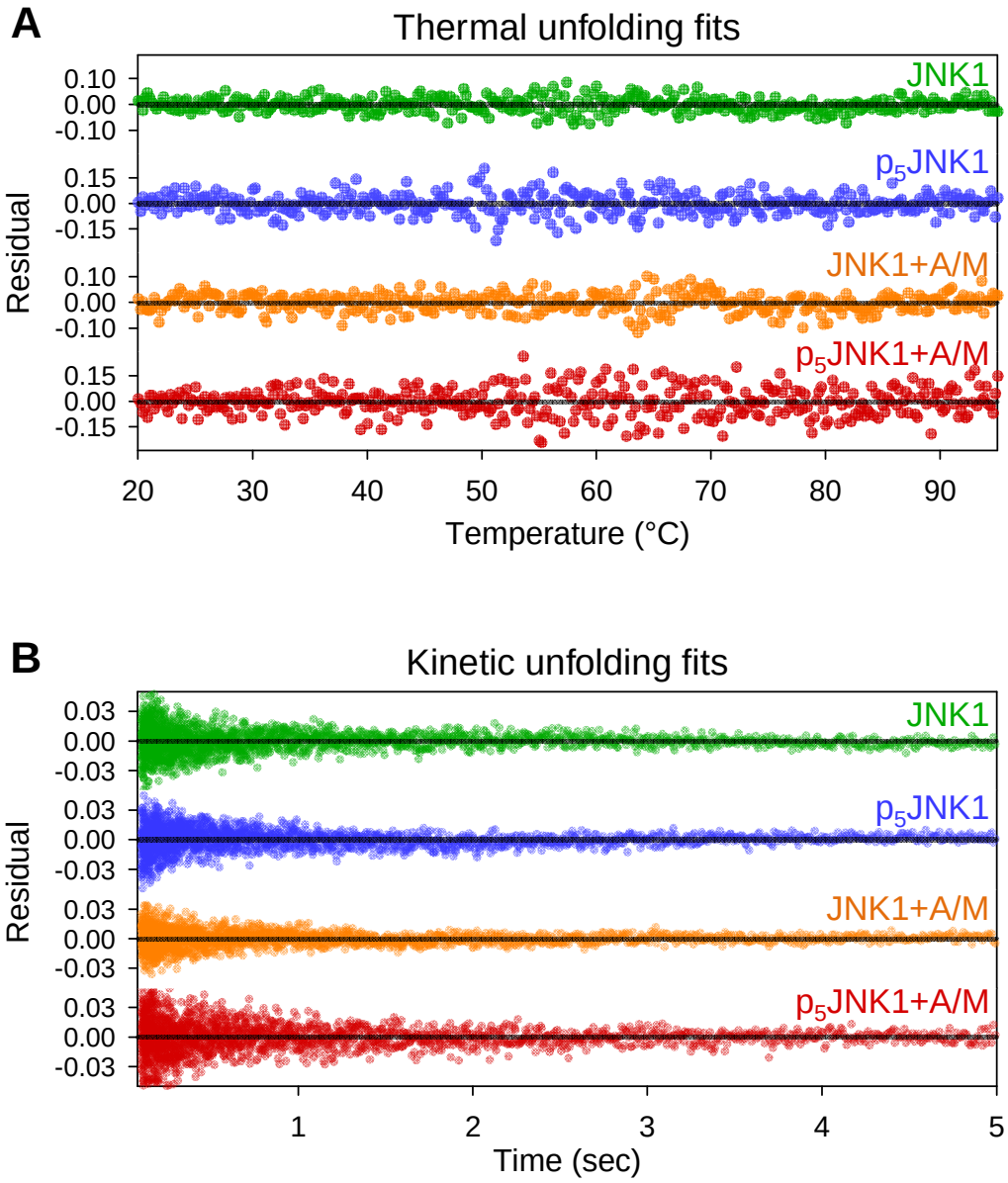

Fig. S2. Residual plots for the fits to the thermal (A) and kinetic (B) unfolding data of the apo and AMP-PNP/Mg^{2+} bound forms of JNK1β1 and p_5JNK1β1. The residuals show excellent fits to the unfolding data illustrated in Figure 2.

- Supplementary Figure S3 -

Page 1 of 5

JNK1β1

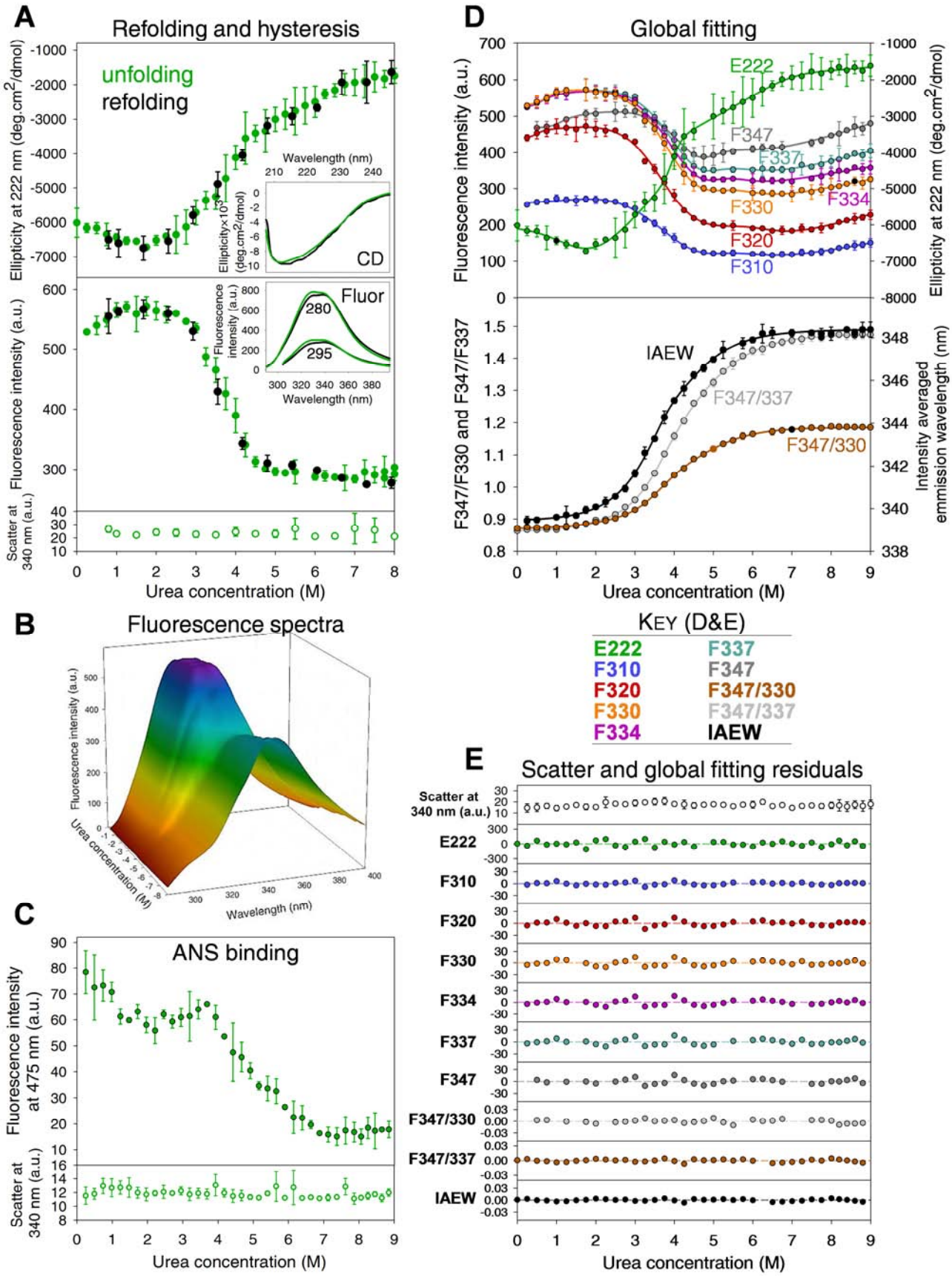

(*Figure S3 continues onto the next page; see page viii for its legend*)

- Supplementary Figure S3 -

Page 2 of 5

p_5JNK1β1

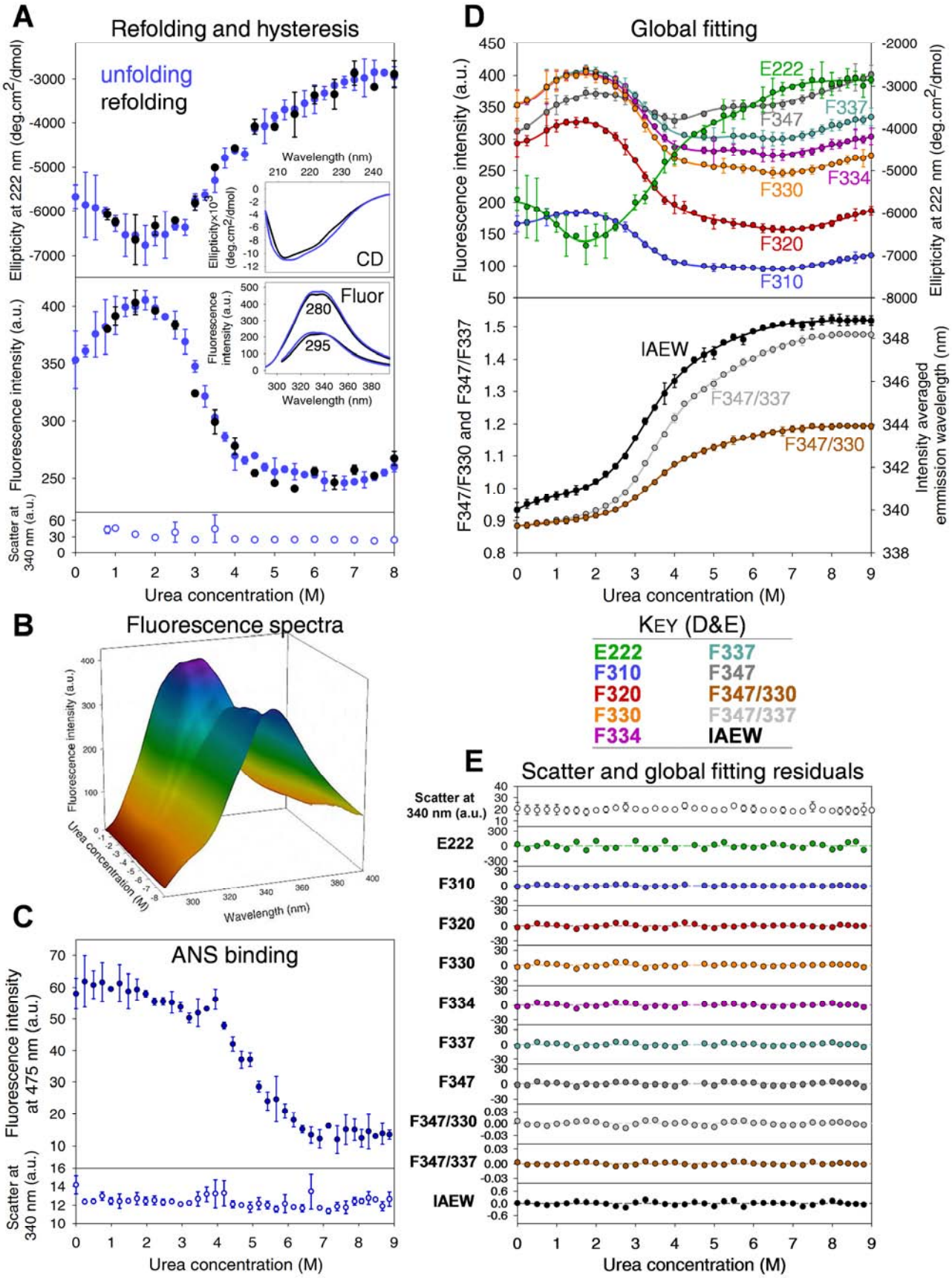

(*Figure S3 continues onto the next page; see page viii for its legend*)

- Supplementary Figure S3 -

Page 3 of 5

JNK1β1 + AMP-PNP/Mg^{2+}

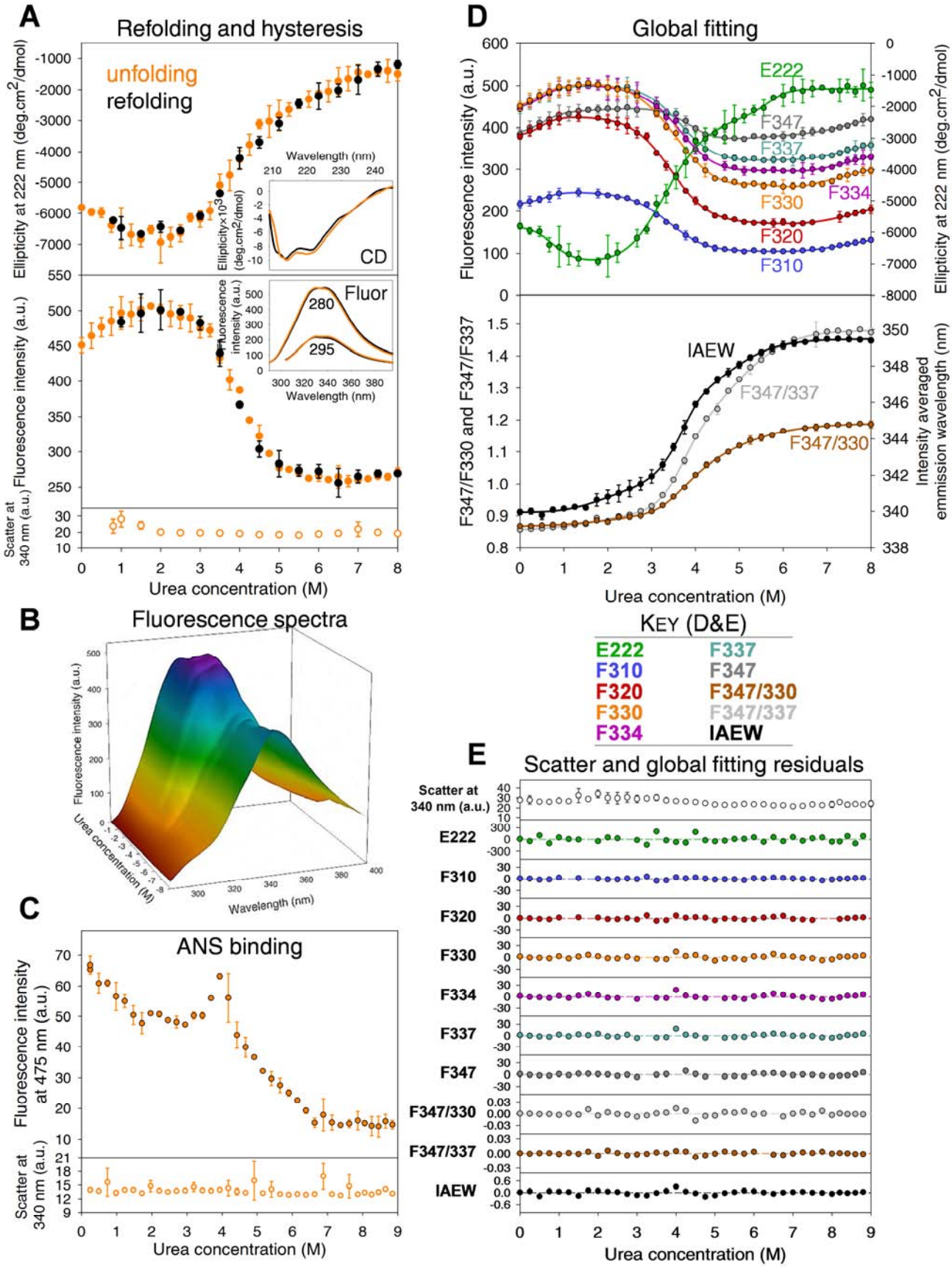

(*Figure S3 continues onto the next page; see page viii for its legend*)

- Supplementary Figure S3 -

Page 4 of 5

p_5JNK1β1 + AMP-PNP/Mg^{2+}

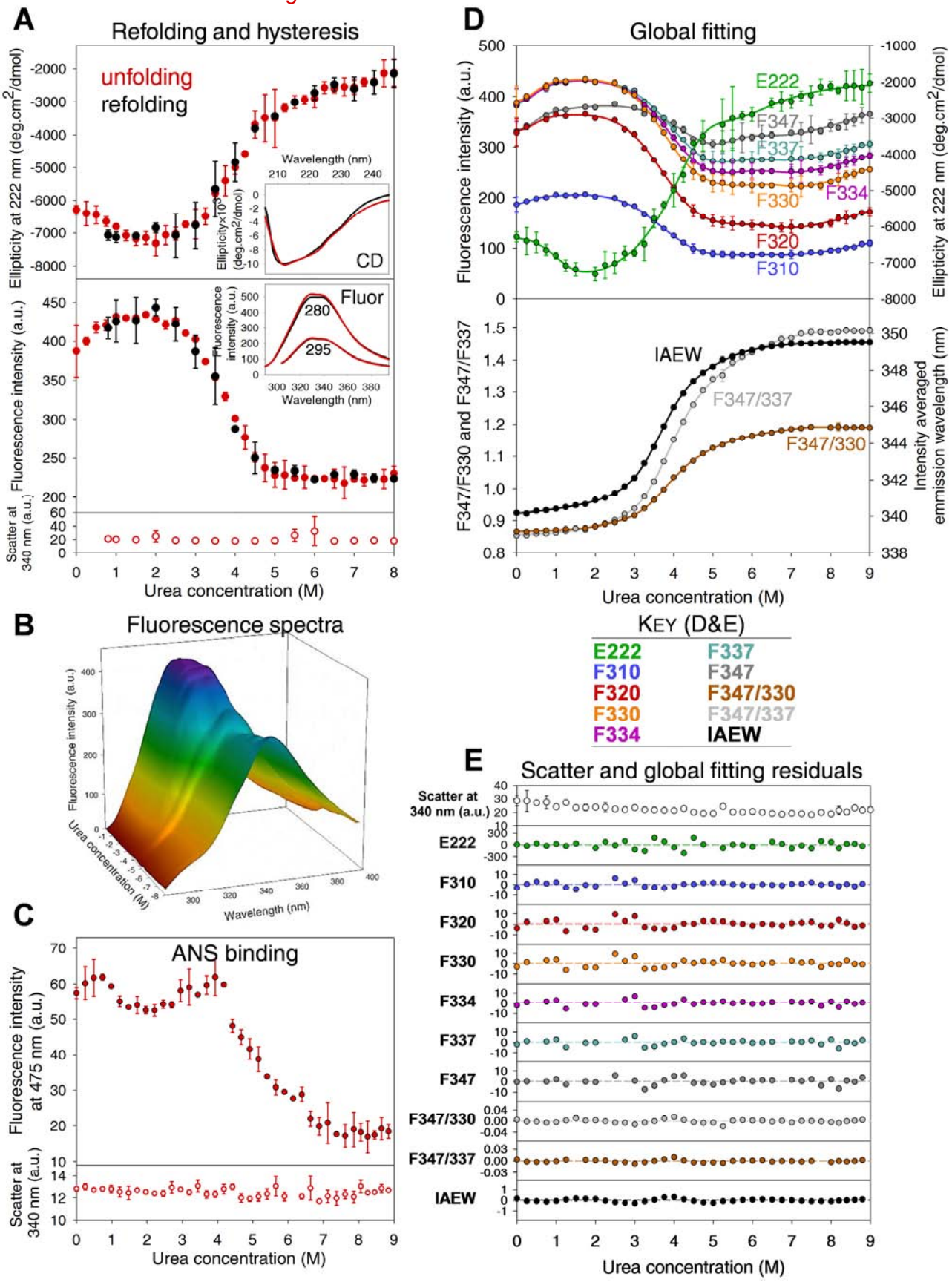

(*See the following page, page viii, for the legend of Figure S3*)

Fig. S3 (Page 5 of 5). Complete urea-induced equilibrium unfolding analysis of the apo and nucleotide bound forms of JNK1β1 and p_5JNK1β1.

(A) Confirming that the unfolding process of the JNK1β1 forms attain equilibrium and do not exhibit unfolding-refolding hysteresis (allowing definition of the thermodynamic parameters, $\Delta G°_{H2O}$ and *m*-value, for the structural transitions), the equilibrium unfolding and refolding pathways were coincident and thus reversible when monitored by both circular dichroism (top panel) and fluorescence (middle panel). The native states were also completely recoverable once they had been unfolded in urea, as the insets show that both the circular dichroism and fluorescence spectra of the refolded proteins, recovered upon dilution of the denaturant, overlay with the spectra of the native states. The lack of protein aggregation was determined using fluorescence scatter at 340 nm (bottom panel). Data points are an average of three replicates.

(B) The complete set of fluorescence emission spectra (λ_{ex} of 280 nm) for the protein unfolded in the various urea concentrations, illustrating that there is both a significant decrease in fluorescence intensity and a ±13 nm shift in λ_{max} when JNK1β1 is unfolded in urea.

(C) Varying degrees of ANS fluorescence during urea-induced unfolding of the JNK1β1 forms indicate that ANS binds differentially to the kinases as they unfold, reaffirming that various and distinct intermediate species with solvent exposed hydrophobic patches exist along their unfolding pathway. The data are an average of three replicates and were corrected for the contribution of free ANS in buffer. Scatter data indicates that the ANS binding peaks were not due to protein aggregation occurring along the unfolding transition (bottom panel).

(D) Global fitting of equilibrium unfolding data obtained using fluorescence and circular dichroism. The unfolding data that were analyzed were monitored using intrinsic fluorescence intensity (λ_{ex} of 280 nm) at 310 nm (blue - F310), 320 nm (red - F320), 330 nm (orange - F330), 334 nm (purple - F334), 337 nm (cyan - F337), and 347 nm (grey - F347), as well as by mean residue ellipticity at 222 nm (green - E222) (all presented in the top panel). Additional data derived from the fluorescence spectra, including the ratios of unfolded to folded protein (brown - F347/330, and light grey - F347/337) and the intensity averaged emission wavelength (black - IAEW, calculated using the equation: $IAEW = \Sigma\lambda i \times Fi / \Sigma Fi$, where λi is the wavelength and Fi is the fluorescence intensity), were also analyzed (bottom panel). Buffer-corrected data were plotted as the average of 3 replicates, and were globally fit using Savuka v. 6.2.26 [3]. The lines represent the best fits of the four-state model to the data.

(E) Light scatter data indicated the lack of protein aggregation (top panel), whilst residual plots for the fits of each of the data sets used for global analysis of equilibrium unfolding indicate good fits to the data.

- Supplementary Figure S4 -

Page 1 of 4

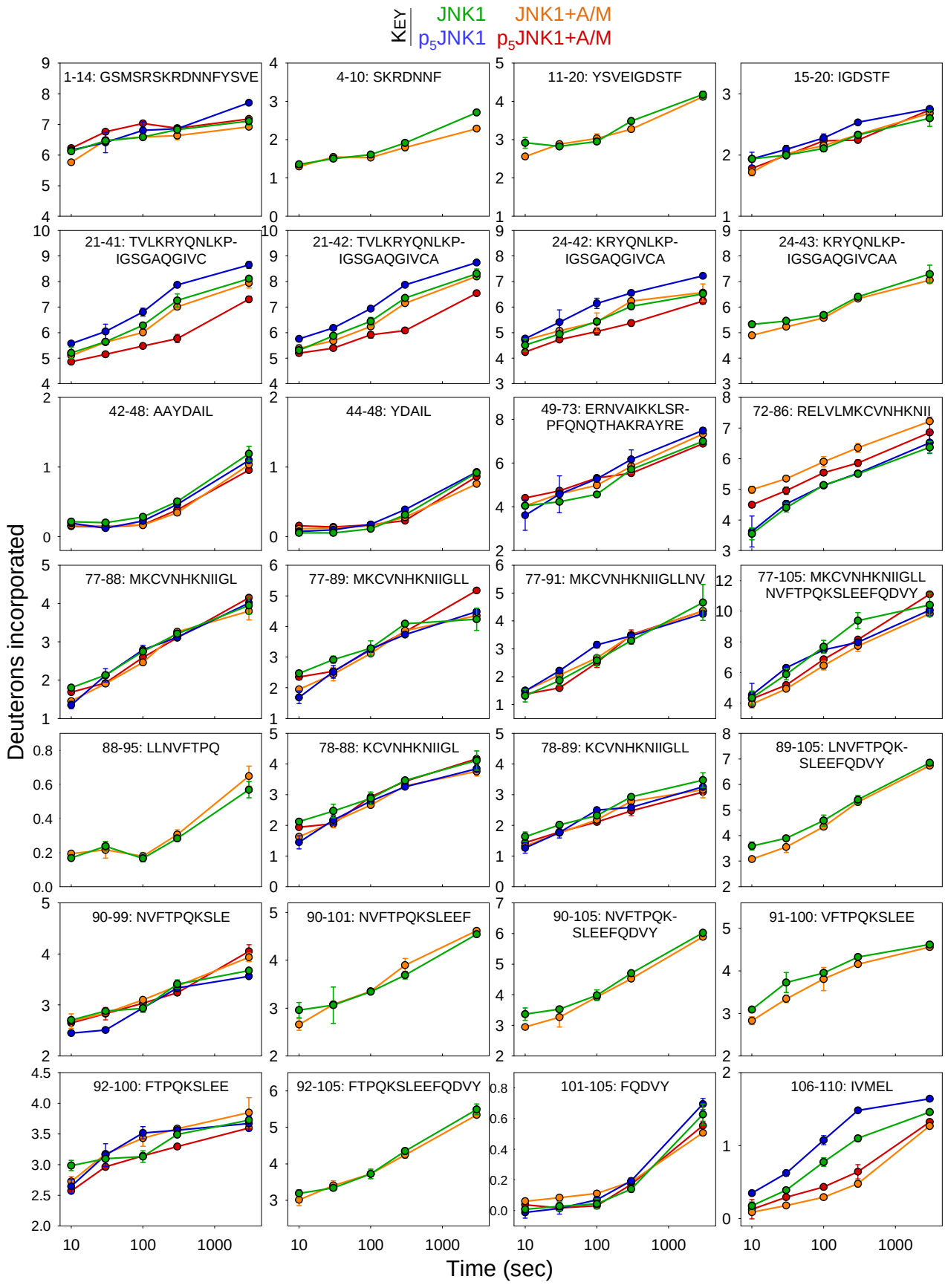

(*Figure S4 continues onto the next page; see page xii for its legend*)

- Supplementary Figure S4 -

Page 2 of 4

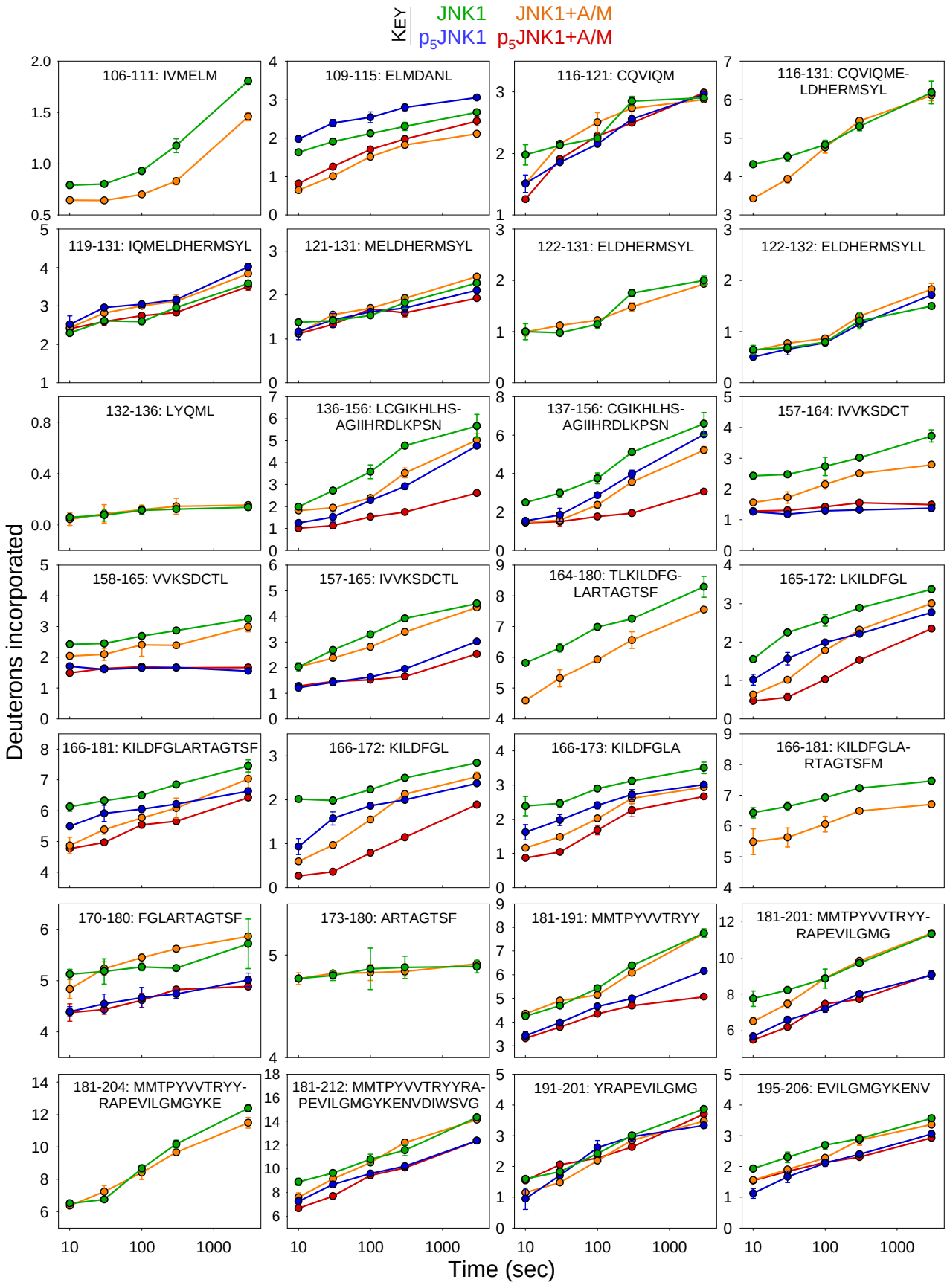

(*Figure S4 continues onto the next page; see page xii for its legend*)

- Supplementary Figure S4 -

Page 3 of 4

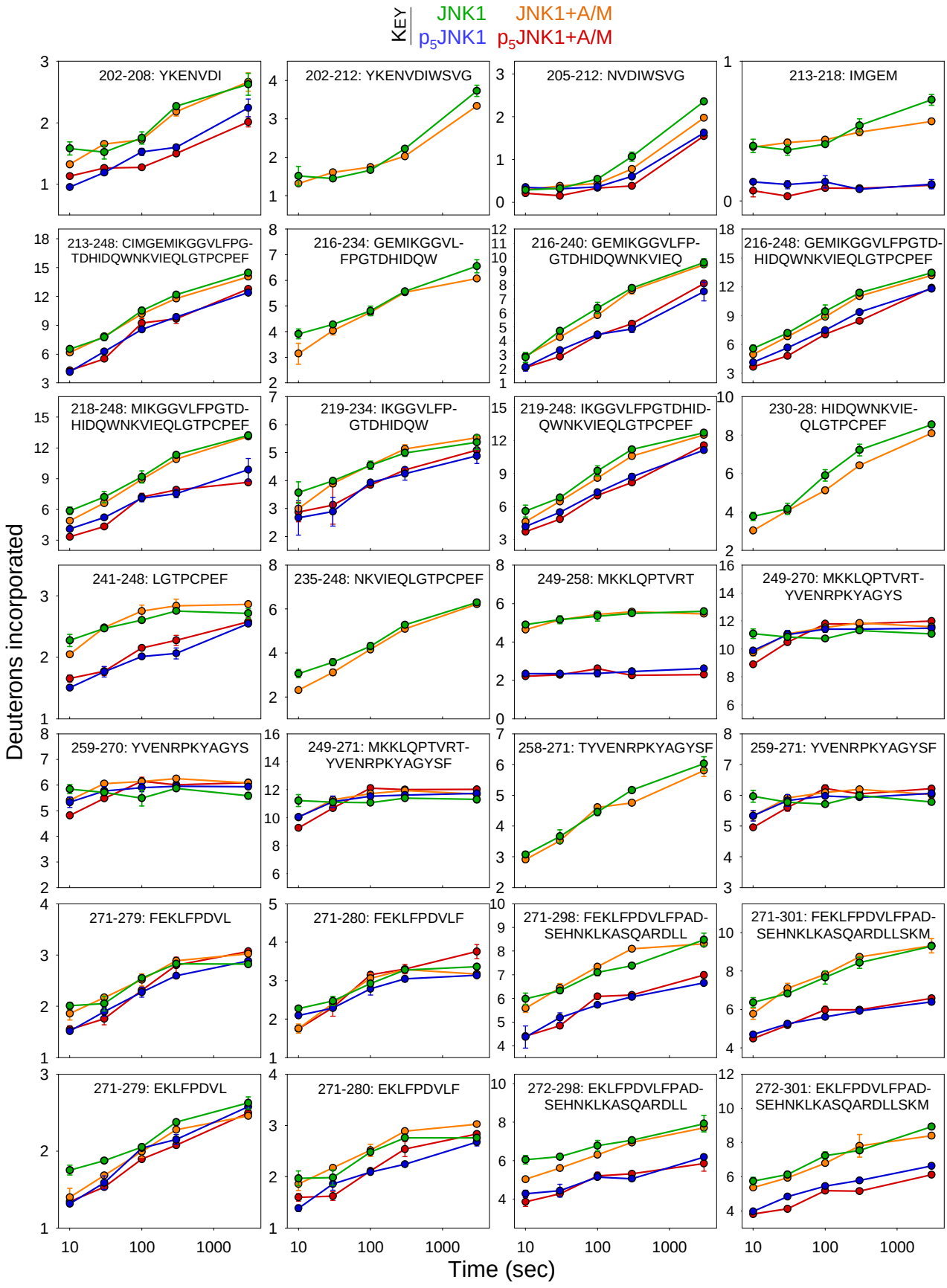

(*Figure S4 continues onto the next page; see page xii for its legend*)

- Supplementary Figure S4 -

Page 4 of 4

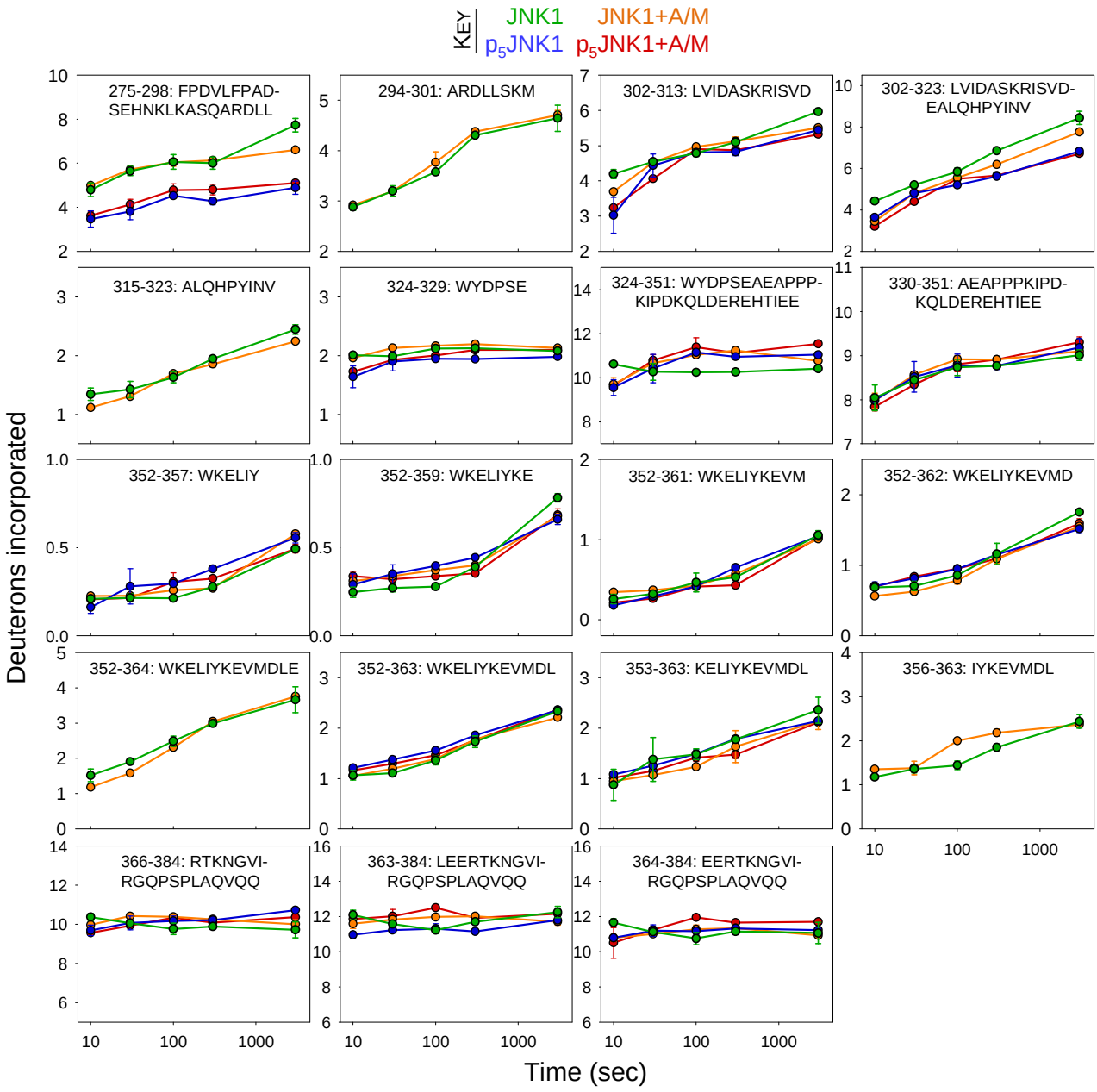

Fig. S4 (Page 4 of 4). Complete HX-MS analysis, illustrating the deuteron uptake plots for each of the peptides identified for apo and AMP-PNP/Mg^{2+} bound JNK1β1 and p_5JNK1β1. Peptides are labelled by their residue numbers, as well as by their corresponding amino acid sequence. The kinase forms are indicated as follows: JNK1β1 in green, p_5JNK1β1 in blue, JNK1β1+AMP-PNP/Mg^{2+} in orange, and p_5JNK1β1+AMP-PNP/Mg^{2+} in red. Lines are guides for the eye only. Error bars indicate the standard error of the mean of at least 3 independent experiments, and many error bars are smaller than the symbol used.

SUPPLEMENTARY INFORMATION

The interactions of AMP-PNP/Mg^{2+} nucleotide substrate within the active site of inactive, non-phosphorylated JNK3

The N6 and N1 atoms of the adenine base of the nucleotide interact with backbone elements of both Glu147 and Met149 (Figure S5), corresponding to Met109 and Glu111 in JNK1β1, located within the hinge and its preceding strand β5. The side chain of Asn152 and the carbonyl group of Ser193 (Asn114 and Ser155 in JNK1β1) situated in strand βL5 and the catalytic loop, respectively, from a hydrogen-bonding network to the O2′ and O3′ hydroxyls of the ribose sugar. Many other hydrogen bonds, both direct and indirect, are formed between the triphosphate group and residues found in the C-terminal domain half of the active site. Like most kinases, the JNK-ATP complex also requires two magnesium ions (M1 and M2) for functional binding. In JNK3, M2 make contact with the side chain of Asn194 (Asn156 in JNK1β1) within the catalytic loop, allowing it to bridge the oxygens of the α- and γ-phosphoryl groups of AMP-PNP, while M1 interacts via a water molecule with the carboxylate oxygens of Asp207 (corresponding to Asp169 in JNK1β1) of the DFG motif, allowing it to chelate the β- and γ-phosphoryl group oxygens (Figure S5). M1 also interacts with the carboxylate oxygen of Glu111 (Glu73 in JNK1β1) located in helix αC via an additional water molecule, chelating the β- and γ-phosphate groups in assistance to Asp207. The main chain amide and side chain carbonyl oxygen of Gln75 (Gln37 in JNK1β1) in the Gly-rich flap, as well as the side chain amine of the conserved Lys93 (Lys55 in JNK1β1) of strand β3, interact with the β- and α-phosphate oxygen atoms, respectively (Figure S5).

According to this JNK3–AMP-PNP co-crystal structure [4], the nucleotide is thus predicted to interact with the Gly-rich flap of inactive JNK3. Our HX measurements reveal however that interactions between these elements within inactive JNK1β1 do not occur stably in solution, or, at most, occur only transiently. JNK3 may then differ from JNK1β1 in the extent to which interdomain closure occurs in its inactive form, perhaps with JNK3 possessing a more closed active site that allows AMP-PNP to interact productively with both the N- and C-terminal domains. This is conceivable given the diversity seen in the constraints to activation among the closely related isoforms of other MAP kinases. Alternatively, the structure of the JNK3–AMP-PNP co-crystal might be complicated by crystal packing defects that may distort the conformation of the active site and misrepresent the solution structure of the kinase. Furthermore, since X-ray structures represent only one of the energetically favourable conformations the protein can occupy in solution, the potentially greater stability of a closed domain conformation may prevent crystallography from detecting an average open solution conformation.

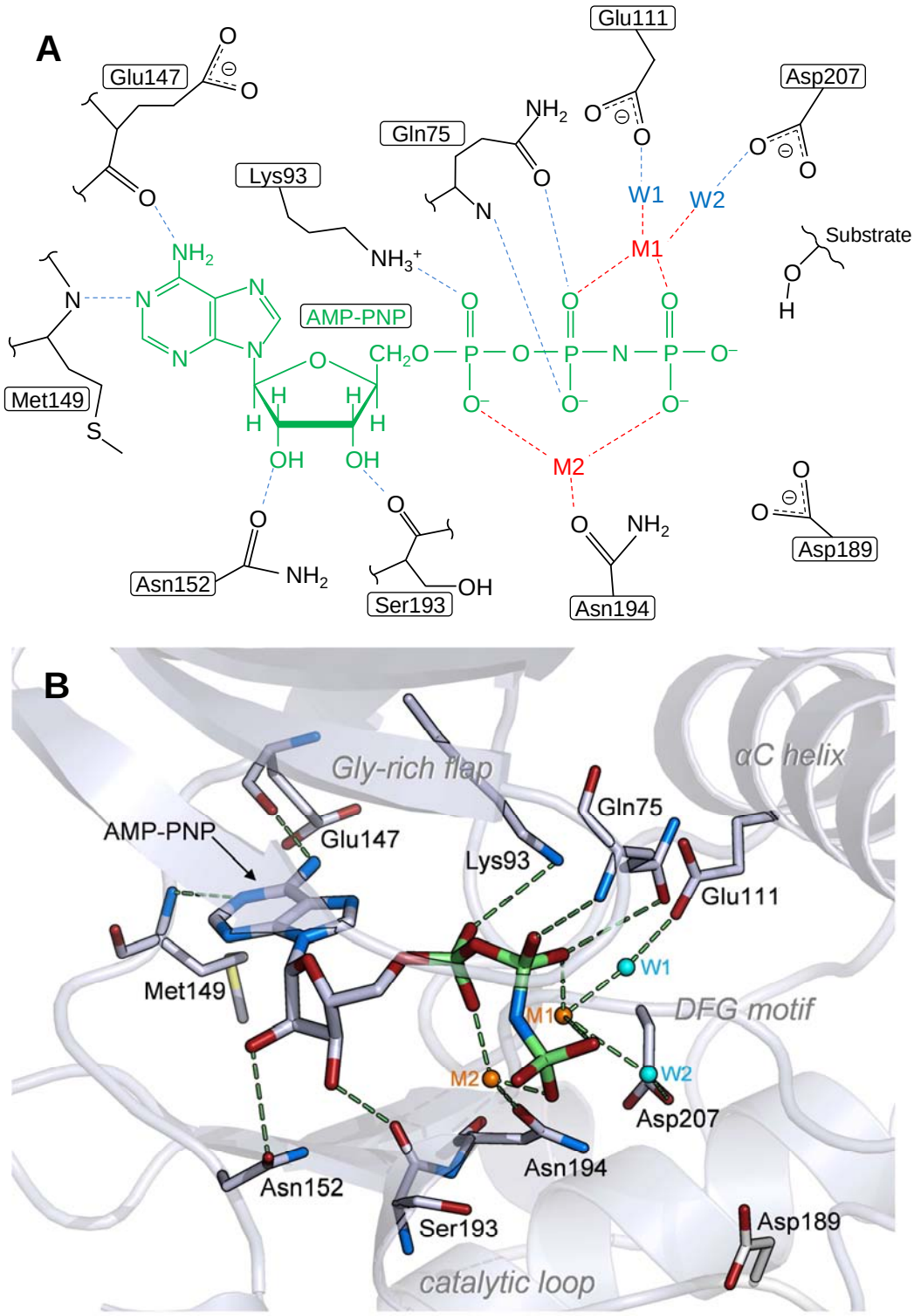

Fig. S5. The nucleotide-bound active site of JNK3. The residues of JNK3 that interact via hydrogen bonds and electrostatic forces with the ATP analogue, AMP-PNP, within the active site of inactive (non-phosphorylated) JNK3 are illustrated. The two essential divalent metal ions, Mg^{2+}, required for the coordination of the phosphoryl oxygen atoms of AMP-PNP are labelled M1 and M2 (A & B) and represented by orange spheres (B). The water molecules involved in the indirect hydrogen bonds formed between selected residues and AMP-PNP are indicated by W1 and W2 (A & B), and shown as cyan spheres (B). (A) A schematic representation of the binary complex formed between AMP-PNP (green) and non-phosphorylated JNK3 (PDB entry 1JNK [4]). Hydrogen bonds and electrostatic interactions are represented by blue and red dotted lines, respectively, yet are not drawn to scale. (B) A three-dimensional representation of the binary complex, in which the relevant interactions are indicated by green dashed lines. Oxygen, nitrogen, and phosphorus atoms are shown in red, blue, and green, respectively.

SUPPLEMENTARY REFERENCES

[1] Trott O, Olson AJ. AutoDock Vina: improving the speed and accuracy of docking with a new scoring function, efficient optimization, and multithreading. J Comput Chem. 2010;31:455-61.

[2] Morris GM, Huey R, Lindstrom W, Sanner MF, Belew RK, Goodsell DS, et al. AutoDock4 and AutoDockTools4: Automated docking with selective receptor flexibility. J Comput Chem. 2009;30:2785-91.

[3] Beechem JM. Global analysis of biochemical and biophysical data. Methods Enzymol. 1992;210:37-54.

[4] Xie X, Gu Y, Fox T, Coll JT, Fleming MA, Markland W, et al. Crystal structure of JNK3: a kinase implicated in neuronal apoptosis. Structure. 1998;6:983-91.

CHAPTER 5

GENERAL DISCUSSION

The improper or unregulated activation of the JNK signalling pathway has been discovered in several diseases, providing the justification for targeting this MAPK pathway for rational drug design. For example, the erosion of cartilage and bone associated with rheumatoid arthritis is induced by the excessive production of matrix metalloproteinases, a process that is mediated by the activation of AP-1 through the JNK signalling cascade [60-62]. The JNK pathway is also over stimulated in the susceptible neurons of individuals with Alzheimer's disease, implicating the MAPK in the pathophysiology and pathogenesis of the disease [63-66]. Moreover, the JNKs have been shown to be important mediators of insulin resistance and obesity, and have thus been proposed as possible targets for type II diabetes [31,67,68].

Although a number of JNK inhibitors targeting its inactive form have already been discovered [69], if we hope to find medical benefit in the therapeutic regulation of JNKs and potentially develop effective therapies against the diverse array of its associated diseases, we first need to understand the mechanisms by which JNK becomes activated. Since the effects that activation has on the structure, stability, and dynamics of the MAPK have not yet been elucidated, this investigation sought to characterise the changes that take place upon phosphorylation of the most abundant JNK isoform, JNK1β1.

5.1. Implications for the possible co-translational phosphorylation of JNK1β1

Previously, the soluble overexpression and efficient purification of the JNK isoforms for subsequent study had been notoriously difficult, with the various strategies used in attempt to acquire large yields of highly pure kinase proving to be largely unsuccessful [70]. Aiming then to first improve the soluble overexpression of JNK1β1, this study illustrated that by harmonising the codon usage frequencies of its open reading frame to those of the *E. coli* expression host (codon usage harmonisation), in combination with its expression as a fusion protein with the highly soluble GST as well as by altering the kinetics of its folding by reducing the cultivation temperature, large quantities of soluble JNK1β1 could be expressed (Chapter 2, [71]).

This effective and novel JNK1β1 expression strategy resulted however in unexpected and highly significant consequences to the modification state of the kinase post translation. It was revealed that under these expression conditions, JNK1β1 is partially activated by phosphorylation at five distinct sites in *E. coli*, an environment lacking the eukaryotic kinases thought necessary for its phosphorylative activation. These phospho-sites comprised the canonical T183 and Y185 activation residues, S377 (a previously recognised yet uncharacterised phospho-site), in addition to T228 and S284 (novel phospho-residues) (Chapter 3, [72]). The significance of these phospho-residues and the fact that they are not random artefacts of the recombinant expression of JNK1β1 became clear when the identical sites (following their complete dephosphorylation) were found to be phosphorylated *in vitro* by active MKK4 (Chapter 3, [72]).

After excluding the possibility of post-translational phosphorylation occurring in any form during expression, this study suggested that the unique yet natural kinetics of translation and folding of JNK1β1 imparted by the codon harmonisation facilitates the phosphorylation events that are proposed to take place during co-translational folding. Whether catalysed by co-translational *trans* auto-phosphorylation or by eukaryotic-like endogenous *E. coli* protein kinases, the systematic, "co-folding" phosphorylation of JNK1β1 in *E. coli* appeared to mimic the events that occur in its natural human host environment (Chapter 3, [72]). It has been established that altering the rate of production and folding of a protein can influence its degree of phosphorylation [73], and it indeed appears that JNK1β1 has a predisposition to be phosphorylated during co-translational folding when the kinetics of its translation are at their natural rate. It is therefore conceivable that during the natural expression of JNK1β1 in human cells, active MKK4 (and perhaps other modifiers of JNK1β1) recognises and interacts with the specific phosphorylatable motifs of JNK1β1 during its translation and subsequent folding (Figure 8), in a manner not unlike the events that were detected in *E. coli*.

Alternatively, fully folded and native JNK1β1 could possibly act upon the partially folded phosphorylatable motifs of newly synthesised JNK1β1 polypeptides in a co-translational *trans* auto-phosphorylation process (Figure 8). In this case, JNK1β1 could either be unmodified, or previously activated through phosphorylation by MKK4 or the aforementioned co-folding auto-phosphorylation process in a positive feedback loop (Figure 8).

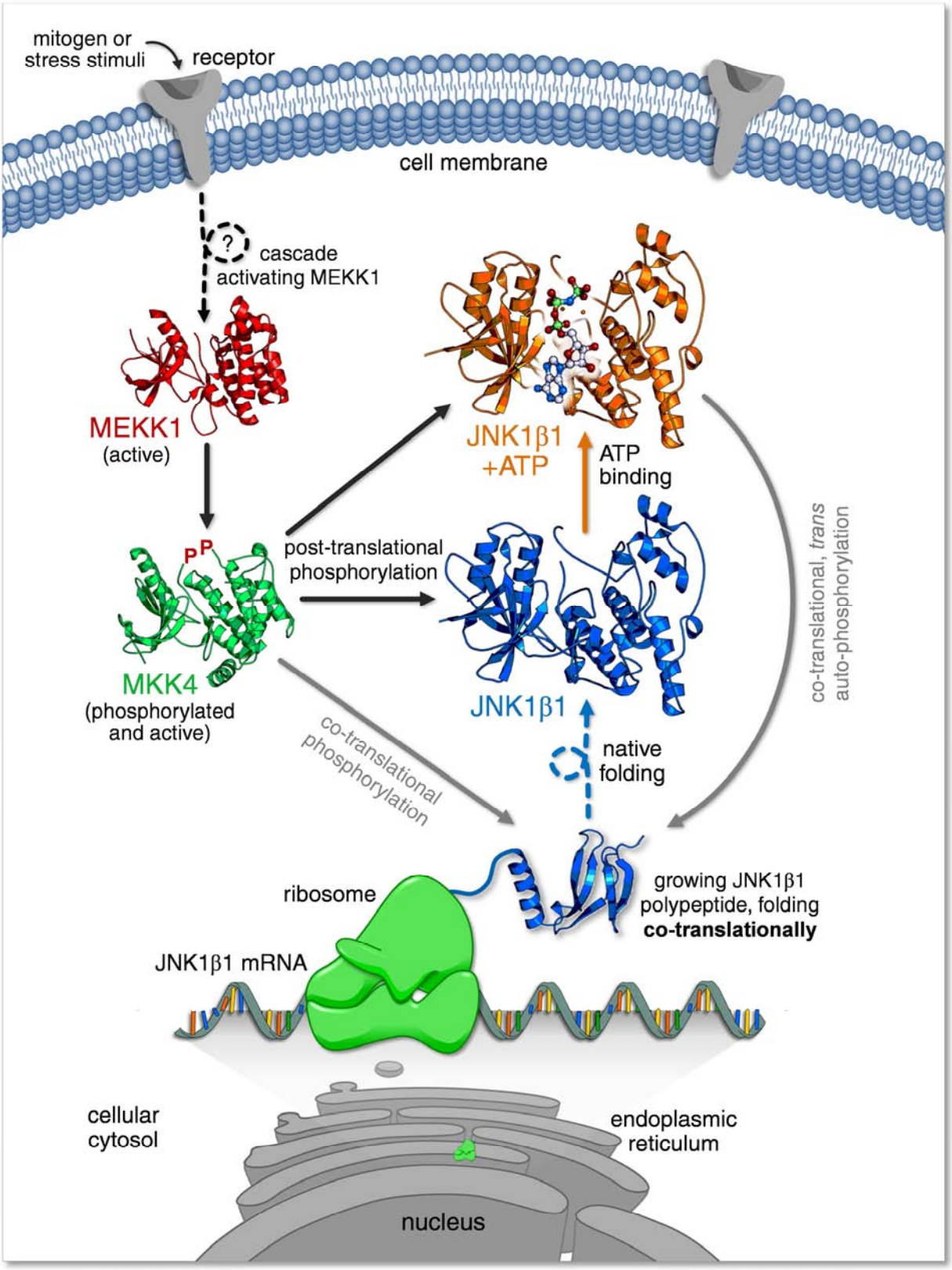

Figure 8. Possible means by which JNK1β1 may become phosphorylated in human cells. Evidence suggests that either active MKK4 or native, fully-folded JNK1β1 (unmodified or previously phosphorylated) is able to phosphorylate the nascent JNK1β1 polypeptide as it grows and folds co-translationally (grey arrows). Active MKK4 is also able to phosphorylate either unbound or ATP-bound native JNK1β1 post-translationally (black arrows).

Co-translational modification of nascent polypeptides is a well-documented phenomenon. Insights into the process have been gained predominantly through the study of secretory and membrane proteins, which undergo extensive co-translational glycosylation. Glycosylation represents a largely conserved protein modification that many mammalian cells employ co-translationally to facilitate the correct folding, processing, assembly, trafficking, and thus functioning of non-cytosolic proteins [74,75].

Mechanisms of co-translational modification of cytosolic proteins are however less understood. Nonetheless, phosphorylation during translation has recently been found to be important regulatory events in the cellular functioning of many kinases, including Akt and PKA. mTOR has been shown to mediate the constitutive phosphorylation of specific residues of Akt during its translation, modifications that enable the correct co-translational folding of the nascent Akt polypeptide [76]. These phospho-residues are thus critical for the newly synthesized kinase to attain its proper conformation, where after they are required for its subsequent maturation and stability [76]. Within PKA, *cis* auto-phosphorylation of the C-terminal Ser338 residue occurs co-translationally, an event that precedes and is a prerequisite to the activating post-translational auto-phosphorylation of the activation lip Thr197 [77]. Phosphorylation of Ser338 is also essential for the processing, maturation, and solubility of PKA, as the kinase is prone to aggregation in the absence of the modification [77].

Given that phosphorylated JNK1β1 was detected in large quantities only in the soluble cell fraction after recombinant overexpression (Chapter 2, [71]), it is possible that co-translational phosphorylation of one or more of the newly identified (non-activation lip) phospho-residues may occur in human cells to promote the correct folding, solubility, and stability of JNK1β1 in a means similar to Akt and PKA. The finding in this study that phosphorylation significantly stabilises JNK1β1 lends support to this possibility (Chapter 4, [78]). Indeed, the decrease in the flexibility of critical α-helices and the C-terminal domain as a whole upon phosphorylation of JNK1β1 appeared to be contributed to by the phosphorylation of the novel phospho-sites, T228 and S284 (Chapter 4, [78]).

With respect to the recognised phosphorylation of fully-folded, native JNK1β1 by active MKK4, it is probable that MKK4 would interact with and phosphorylate the nucleotide bound form of inactive JNK1β1. Although they may possess different affinities for ATP, if active MKK4 is to be bound by nucleotide in preparation for phosphorylating JNK1β1, it follows that the MAPK would also bind an ATP molecule from the pool of nucleotide

substrate likely to be in the vicinity of the two kinases. The concurrent binding of individual ATP molecules to both MKK4 and JNK1β1 may be a critical factor contributing to the efficient phosphorylation of the latter, because the presence of nucleotide significantly destabilises inactive JNK1β1 (Chapter 4, [78]). The accompanying increase in the dynamics and conformational mobility of JNK1β1 upon nucleotide binding may allow enthalpic contributions to the formation of the MKK4–JNK1β1 complex to be enhanced; a more rigid structure may either exclude kinase conformations that allow selective interactions to form, or may not allow interactions that could arise through an induced-fit mechanism. The destabilising effect that nucleotide has on JNK1β1 could thus also function to promote the binding of the kinase to MKK4, thereby increasing the catalytic turnover of JNK1β1 phosphorylation.

5.2. Mechanisms contributing to the activation of JNK1β1 upon phosphorylation

This study details the distinct changes in the stability and dynamics of JNK1β1 that take place upon both nucleotide binding and/or phosphorylation, providing insight into the mechanisms by which the kinase is activated. Firstly, the increased flexibility in the Gly-rich flap implied by the enhanced rate of hydrogen-deuterium exchange following phosphorylation reflects that which occurs in PKA, where high mobility in the corresponding flap is hypothesized to facilitate both ATP binding and the rate-limiting release of ADP product [79,80]. Additionally, the increased motions in the backbone of the hinge observed upon JNK1β1 activation, likely provides the flexibility required for the domain closure that occurs when nucleotide binds to the active form of the kinase, detected during HX protection studies using AMP-PNP. The effects of nucleotide binding and phosphorylation on JNK1β1 are summarised in Figure 9.

It is uncertain at present whether phosphorylation alone can induced any degree of domain closure without ATP binding, or if the presence of nucleotide within the active site cleft causes the rotation of the domains after the restraints to closure are removed by phosphorylation. The increased HX accompanying enhanced flexibility in the Gly-rich flap observed in the active form of unbound JNK1β1 could prevent the detection of any potential decreases in HX at the domain interface that would accompany domain closure. Nevertheless, the finding that AMP-PNP simultaneously protects residues in both the C-terminal domain and the Gly-rich flap in p_5JNK1β1 indicates that, at the very least, active kinase adopts a closed domain conformation around nucleotide upon binding (Figure 9).

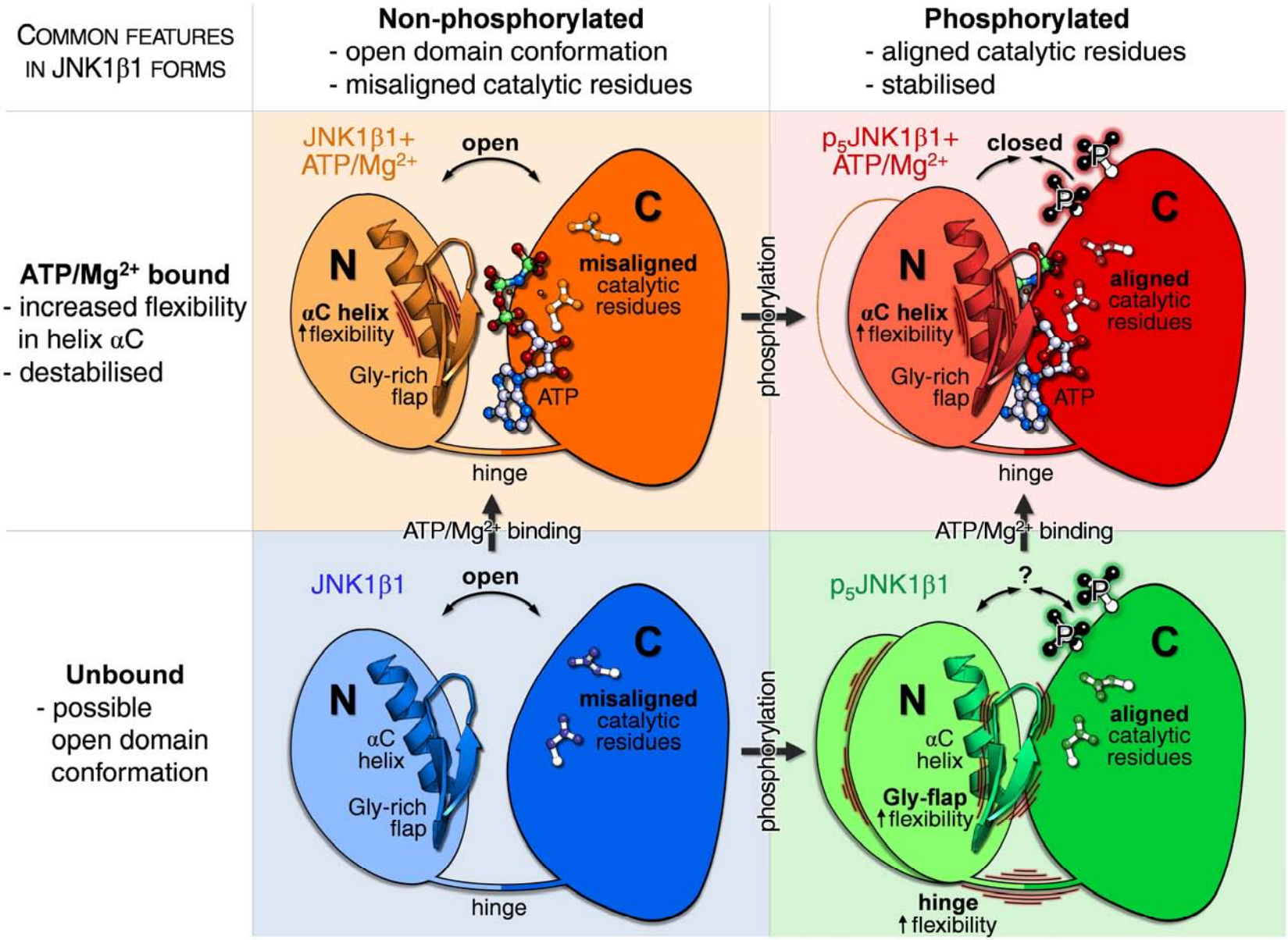

Figure 9. Summary of the major changes to JNK1β1 that occur upon nucleotide binding and/or phosphorylative activation. The open or closed state of the N- and C-terminal domains, as well as the effects to the structure and conformational flexibility of key kinase elements are indicated. Features common to specific forms of the kinase are stated.

The patterns of protection from HX observed when nucleotide is bound to active JNK1β1 are consistent with the closed domain conformation of co-crystal structures of ATP/ADP bound PKA (Figure 10). Similarly, the limited interactions detected between the Gly-rich flap and AMP-PNP in unmodified JNK1β1 are consistent with the open domain conformations observed in structures of unbound PKA (Figure 10) [81]. Although the catalytic subunit of PKA is constitutively active in the absence of its N-terminal regulatory subunit (in contrast to JNK1 and the other MAP kinases), the domain closure required for the formation of the active site is thought to be triggered by binary complex formation with nucleotide substrate [79,82,83]. These structures can thus be used in example to demonstrate the structural changes associated with the proposed JNK1β1 domain closure and the relative positions of its N- and C-terminal domains in their open and closed conformations (Figure 10). The dynamic and responsive nature of the two kinase domains and the Gly-rich flap can be further demonstrated by examining the co-crystal structure of PKA bound to ADP-AlF_3 (PDB: 1L3R) (Figure 10). This structure mimics the kinase reaction transition-state and represents the structural changes that the protein is likely to undergo during catalysis [84], emphasising the dynamic properties of these kinase conformers.

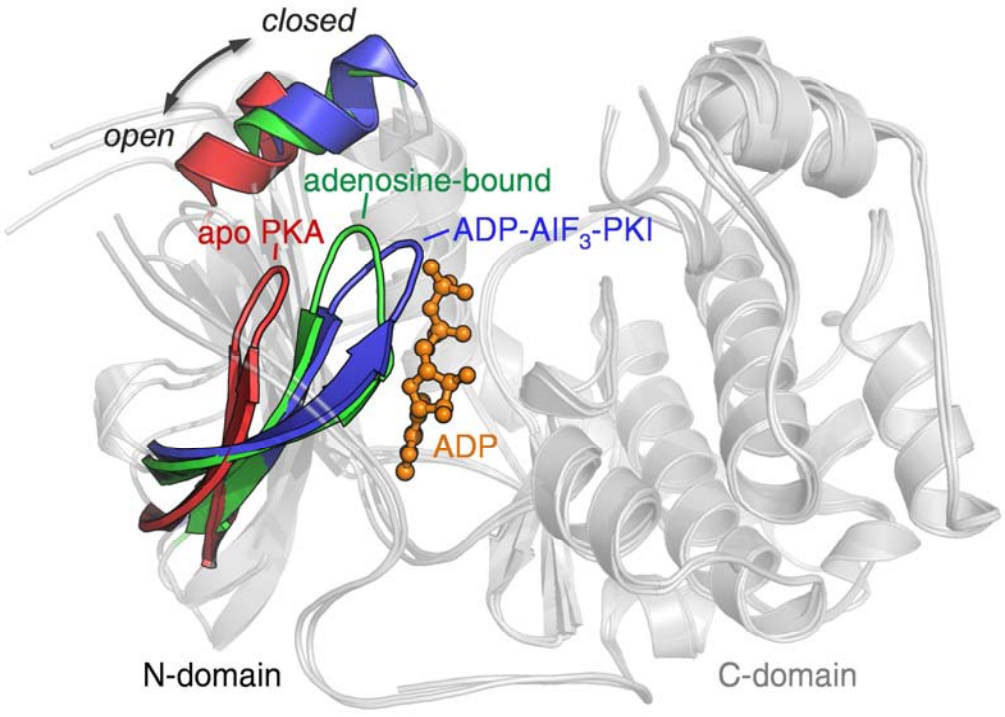

Figure 10. Crystal structures of the catalytic subunit of PKA in various forms, illustrating the conformational changes accompanying kinase domain closure and catalysis. Unbound PKA (PDB code: 1J3H) [81], adenosine-bound PKA (1BKX) [79], and the transition-state mimetic, ADP-AlF_3 bound form of PKA (1L3R) [84] were structurally fit using Swiss-Pdb Viewer [85]. The Gly-rich flap and helix αB of the PKA forms are coloured blue (1L3R), green (1BKX), and red (1J3H) to demonstrate the closure of the domains and changes to the dynamic flap that occur during nucleotide binding and catalysis. The position of ADP in the closed domain conformation of PKA is indicated (orange ball-and-stick structure).

5.2.1. Functional implications for nucleotide-binding induced destabilisation of JNK1β1

JNK1β1 was found to experience significant destabilisation upon binding to AMP-PNP/Mg^{2+} (Chapter 4, [78]), suggesting that the nucleotide binds with higher affinity to a partially folded intermediate state of the kinase. HX MS data revealed that AMP-PNP binding also leads to a related increase in the conformational mobility of the conserved active site helix, αC (Figure 9), whose disruption arguably causes destabilisation of the N-terminal domain and the kinase as a whole. The results indicate that the loss of stability in nucleotide bound JNK1β1 is most compatible with enhanced dynamic motion throughout the core of one domain of the protein, rather than large rigid body movements or significant unfolding events.

Enclosure of the catalytic cleft by the Gly-rich flap presents a clear disadvantage to the kinase as it restricts access to the active site. Since these and other steric factors play a crucial role in the access of substrates to the ATP binding pocket, decreased stability and increased mobility in the nucleotide-bound kinase could enable the conformational changes in its common docking-domain necessary for interaction with its regulators and protein substrates, as well as assist in phosphoryl transfer and ADP release. In support of this, Figuera-Losada and LoGrasso have shown that the presence of ATP significantly increases the affinity of both unmodified and phosphorylated JNK1β1 for protein substrates such as ATF2 and c-Jun [86]. Their study also proposes that, once the kinase has completed catalysing the phosphorylation of the immobilized protein substrate in the presence of bound ATP, decreased stability could facilitate the rapid dissociation of JNK1β1 from the substrate. The free energy difference of the nucleotide-bound form could conceivably also promote (or prevent) the binding and/or release of other regulatory elements involved in mediating JNK1β1 activity.

It is also probable that reduced stability and enhanced protein dynamics allow for the conformational changes, both large and small, that are required for the complete catalytic cycle to proceed. While it has been established that phosphorylation initiates changes to the structure and mobility of JNK1β1 to enable the enzymatic reaction it catalyses to take place, the changes in the conformational dynamics of its catalytic residues following phosphorylation and/or nucleotide binding may also be important for enhancing the rate of phosphoryl transfer itself. Changes in the rate of the chemical step of enzyme-catalysed reactions have long been correlated with alterations in the dynamics of the proteins in which they occur. For example, studies on glucose oxidase have shown that glycosylation-induced

reductions in conformational flexibility leads to decreases in the rate of hydrogen tunnelling during the hydrogen transfer step of the reaction [87]. This is due to the vibrational states of the hydrogen donor/acceptor atoms determining the degree to which the hydrogens are tunnelled [87].

Relatedly, the enhanced conformational mobility following nucleotide binding and the proposed concomitant loosening of the internal structure of the N-terminal domain, can also suggest that the molecular volume of JNK1β1 increases in the presence of nucleotide. Studies have shown that increases in molecular volume (referred to as increased enzyme compressibility) is associated with enhanced enzyme activity in several mutant proteins [88].

Thus, as fluctuational movements in enzymes are thought to contribute to the lowering of energy barriers that exist along reaction coordinates, it is not unreasonable to implicate the nucleotide-binding induced increases in flexibility within helix αC, containing the catalytically important Glu73, in enzyme catalysis. It also appears that helix αC may in effect act as an important transducing element, allowing modifications to the structure, stability, and/or conformational dynamics of the active site that are induced by nucleotide binding to alter the stability and dynamics of the N-terminal domain to assist in the enhancement of kinase activity upon phosphorylation.

5.3. Conclusions

Due to the diversity of signals and pathways that impinge upon the JNK signalling cascade and its consequent involvement in many human diseases, an understanding of the mechanisms that activate the MAP kinase has long been sought after. Previous difficulties in its acquisition and phosphorylation have however impeded its investigation, and as such, the mechanisms by which phosphorylation activates JNK is poorly understood. In this research, a novel and robust method that considerably improves upon the purification of highly pure and phosphorylated JNK1β1 is first described. Acquiring large yields of active JNK1β1, this study identified the exact sites at which its activator, MKK4, phosphorylates the kinase, revealing novel and uncharacterised phospho-residues that appear to have functional and biochemical significance. Concurrently, these findings raise unique questions that have significant implications for all heterologous protein expression, and highlight the important role of translation kinetics in the natural co-translational modification of kinases. The molecular and biophysical consequences of nucleotide binding and phosphorylative

activation of JNK1β1 were then established. The results indicate that the full activation of JNK1β1 is coupled to the regulation of its stability and conformational dynamics by both ATP binding and phosphorylation, and reveal that activation involves altering the flexibility of the hinge to allow the kinase to shift from an open to a closed domain conformation. In addition, the far-reaching changes to the mobility of the kinase detected upon activation provide novel insight into the dynamic motions necessary for initiating enzyme catalysis. This work thus offers a detailed characterisation of the regulation of JNK1β1 function by nucleotide binding and phosphorylation by MKK4, and represents the first step towards elucidating the mechanisms that contribute to inducing its activation.

REFERENCES

[1] Hunter, T. (1995) Protein kinases and phosphatases: the yin and yang of protein phosphorylation and signaling, *Cell 80*, 225-236.

[2] Ben-David, Y., Letwin, K., Tannock, L., Bernstein, A., and Pawson, T. (1991) A mammalian protein kinase with potential for serine/threonine and tyrosine phosphorylation is related to cell cycle regulators, *Embo J 10*, 317-325.

[3] Adams, J. A. (2001) Kinetic and catalytic mechanisms of protein kinases, *Chem Rev 101*, 2271-2290.

[4] Hardie, D. G. (1989) Protein phosphorylation and dephosphorylation, *Curr Opin Cell Biol 1*, 220-226.

[5] Hanks, S. K., and Hunter, T. (1995) Protein kinases 6. The eukaryotic protein kinase superfamily: kinase (catalytic) domain structure and classification, *Faseb J 9*, 576-596.

[6] Hunter, T. (1994) 1001 protein kinases redux--towards 2000, *Semin Cell Biol 5*, 367-376.

[7] Manning, G., Whyte, D. B., Martinez, R., Hunter, T., and Sudarsanam, S. (2002) The protein kinase complement of the human genome, *Science 298*, 1912-1934.

[8] Hunter, T. (1989) Protein modification: phosphorylation on tyrosine residues, *Curr Opin Cell Biol 1*, 1168-1181.

[9] Whitmarsh, A. J., and Davis, R. J. (1998) Structural organization of MAP-kinase signaling modules by scaffold proteins in yeast and mammals, *Trends Biochem Sci 23*, 481-485.

[10] Chen, Z., Gibson, T. B., Robinson, F., Silvestro, L., Pearson, G., Xu, B., Wright, A., Vanderbilt, C., and Cobb, M. H. (2001) MAP kinases, *Chem Rev 101*, 2449-2476.

[11] Graves, J. D., and Krebs, E. G. (1999) Protein phosphorylation and signal transduction, *Pharmacol Ther 82*, 111-121.

[12] Lew, J. (2003) MAP kinases and CDKs: kinetic basis for catalytic activation, *Biochemistry 42*, 849-856.

[13] Cui, J., Zhang, M., Zhang, Y., and Xu, Z. (2007) JNK pathway: diseases and therapeutic potential, *Acta Pharmacol Sin 28*, 601-608.

[14] Gupta, S., Barrett, T., Whitmarsh, A. J., Cavanagh, J., Sluss, H. K., Derijard, B., and Davis, R. J. (1996) Selective interaction of JNK protein kinase isoforms with transcription factors, *EMBO J 15*, 2760–2770.

[15] Davis, R. J. (2000) Signal transduction by the JNK group of MAP kinases, *Cell 103*.

[16] Weston, C. R., and Davis, R. J. (2002) The JNK signal transduction pathway, *Curr Opin Genet Dev 12*, 14-21.

[17] Kyriakis, J. M., Brautigan, D. L., Ingebritsen, T. S., and Avruch, J. (1991) pp54 microtubule-associated protein-2 kinase requires both tyrosine and serine/threonine phosphorylation for activity, *J Biol Chem 266*, 10043-10046.

[18] Dérijard, B., Hibi, M., Wu, I. H., Barrett, T., Su, B., Deng, T., Karin, M., and Davis, R. J. (1994) JNK1, a protein kinase stimulated by UV light and Ha-Ras that binds and phosphorylates the c-Jun activation domain, *Cell 76*, 1025-1037.

[19] Johnson, G. J. (2007) The c-Jun kinase/stress-activated pathway: regulation, function and role in human disease, *Biochim Biophys Acta 1773*, 1341-1348.

[20] Bogoyevitch, M. A., and Kobe, B. (2006) Uses for JNK: the many and varied substrates of the c-Jun N-terminal kinases, *Microbiol Mol Biol R 70*, 1061-1095.

[21] Barr, R. K., and Bogoyevitch, M. A. (2001) The c-Jun N-terminal protein kinase family of mitogen-activated protein kinases (JNK MAPKs), *Int J Biochem Cell Biol 33*, 1047-1063.

[22] Pulverer, B. J., Kyriakis, J. M., Avruch, J., Nikolakaki, E., and Wood-gett, J. R. (1991) Phosphorylation of c-jun mediated by MAP kinases, *Nature 353*, 670-674.

[23] Gupta, S., Campbell, D., Derijard, B., and Davis, R. J. (1995) Transcription factor ATF2 regulation by the JNK signal transduction pathway, *Science 267*, 389-393.

[24] Atzori, C., Ghetti, B., Piva, R., Srinivasan, A. N., Zolo, P., Delisle, M. B., Mirra, S. S., and Migheli, A. (2001) Activation of the JNK/p38 pathway occurs in diseases characterized by tau protein pathology and is related to tau phosphorylation but not to apoptosis, *J Neuropathol Exp Neurol 60*, 1190-1197.

[25] Okazawa, H., and Estus, S. (2002) The JNK/c-Jun cascade and Alzheimer's disease, *Am J Alzheimers Dis Other Demen 17*, 79-88.

[26] Peng, J., and Andersen, J. K. (2003) The role of c-Jun N-terminal kinase (JNK) in Parkinson's disease, *IUBMB Life 55*, 267-271.

[27] Zhu, X., Perry, G., and Smith, M. A. (2003) Amyotrophic lateral sclerosis: a novel hypothesis involving a gained 'loss of function' in the JNK/SAPK pathway, *Redox Rep 8*, 129-133.

[28] Lagalwar, S., Berry, R. W., and Binder, L. I. (2007) Relation of hippocampal phospho-SAPK/JNK granules in Alzheimer's disease and tauopathies to granulovacuolar degeneration bodies, *Acta Neuropathol 113*, 63-73.

[29] Zhang, W., Elimban, V., Nijjar, M. S., Gupta, S. K., and Dhalla, N. S. (2003) Role of mitogen-activated protein kinase in cardiac hypertrophy and heart failure, *Exp Clin Cardiol 8*, 173-183.

[30] Mitsuyama, K., Suzuki, A., Tomiyasu, N., Tsuruta, O., Kitazaki, S., Takeda, T., Satoh, Y., Bennett, B. L., Toyonaga, A., and Sata, M. (2006) Pro-inflammatory signaling by Jun-N-terminal kinase in inflammatory bowel disease, *Int J Mol Med 17*, 449-455.

[31] Lanuza-Masdeu, J., Arevalo, M. I., Vila, C., Barbera, A., Gomis, R., and Caelles, C. (2013) *In vivo* JNK activation in pancreatic beta-cells leads to glucose intolerance caused by insulin resistance in pancreas, *Diabetes 62*, 2308-2317.

[32] Xie, X., Gu, Y., Fox, T., Coll, J. T., Fleming, M. A., Markland, W., Caron, P. R., Wilson, K. P., and Su, M. S. (1998) Crystal structure of JNK3: a kinase implicated in neuronal apoptosis, *Structure 6*, 983-991.

[33] Heo, Y. S., Kim, S. K., Seo, C. I., Kim, Y. K., Sung, B. J., Lee, H. S., Lee, J. I., Park, S. Y., Kim, J. H., Hwang, K. Y., Hyun, Y. L., Jeon, Y. H., Ro, S., Cho, J. M., Lee, T. G., and Yang, C. H. (2004) Structural basis for the selective inhibition of JNK1 by the scaffolding protein JIP1 and SP600125, *Embo J 23*, 2185-2195.

[34] Zhang, F., Strand, A., Robbins, D., Cobb, M. H., and Goldsmith, E. J. (1994) Atomic structure of the MAP kinase ERK2 at 2.3 A resolution, *Nature 367*, 704-711.

[35] Ember, B., and LoGrasso, P. (2008) Mechanistic characterization for c-jun-N-Terminal Kinase 1α1, *Arch Biochem Biophys 477*, 324-329.

[36] Denu, J. M., Stuckey, J. A., Saper, M. A., and Dixon, J. E. (1996) Form and function in protein dephosphorylation, *Cell 87*, 361-364.

[37] Hanks, S. K., Quinn, A. M., and Hunter, T. (1988) The protein kinase family: conserved features and deduced phylogeny of the catalytic domains, *Science 241*, 42-52.

[38] Taylor, S. S., and Radzio-Andzelm, E. (1994) Three protein kinase structures define a common motif, *Structure 2*, 345-355.

[39] Johnson, L. N., Noble, M. E., and Owen, D. J. (1996) Active and inactive protein kinases: structural basis for regulation, *Cell 85*, 149-158.

[40] Resing, K. A., and Ahn, N. G. (1998) Deuterium exchange mass spectrometry as a probe of protein kinase activation. Analysis of wild-type and constitutively active mutants of MAP kinase kinase-1, *Biochemistry 37*, 463-475.

[41] Gibbs, C. S., and Zoller, M. J. (1991) Rational scanning mutagenesis of a protein kinase identifies functional regions involved in catalysis and substrate interactions, *J Biol Chem 266*, 8923-8931.

[42] Skamnaki, V. T., Owen, D. J., Noble, M. E., Lowe, E. D., Lowe, G., Oikonomakos, N. G., and Johnson, L. N. (1999) Catalytic mechanism of phosphorylase kinase probed by mutational studies, *Biochemistry 38*, 14718-14730.

[43] Adams, J. A., and Taylor, S. S. (1993) Phosphorylation of peptide substrates for the catalytic subunit of cAMP-dependent protein kinase, *J Biol Chem 268*, 7747-7752.

[44] Admiraal, S. J., and Herschlag, D. (1995) Mapping the transition state for ATP hydrolysis: implications for enzymatic catalysis, *Chem Biol 2*, 729-739.

[45] Zhou, J., and Adams, J. A. (1997) Is there a catalytic base in the active site of cAMP-dependent protein kinase?, *Biochemistry 36*, 2977-2984.

[46] Sondhi, D., Xu, W., Songyang, Z., Eck, M. J., and Cole, P. A. (1998) Peptide and protein phosphorylation by protein tyrosine kinase Csk: insights into specificity and mechanism, *Biochemistry 37*, 165-172.

[47] Madhusudan, Trafny, E. A., Xuong, N.-H., Adams, J. A., Eyck, L. F. T., Taylor, S. S., and Sowadski, J. M. (1994) cAMP-dependent protein kinase: crystallographic insights into substrate recognition and phosphotransfer, *Protein Science 3*, 176-187.

[48] Corbin, J. D., Sugden, P. H., West, L., Flockhart, D. A., Lincoln, T. M., and McCarthy, D. (1978) Studies on the properties and mode of action of the purified regulatory subunit of bovine heart adenosine 3':5'-monophosphate-dependent protein kinase, *J Biol Chem 253*, 3997-4003.

[49] Johnson, L. N., and Lewis, R. J. (2001) Structural basis for control by phosphorylation, *Chem Rev 101*, 2209-2242.

[50] Jeffrey, P. D., Russo, A. A., Polyak, K., Gibbs, E., Hurwitz, J., Massague, J., and Pavletich, N. P. (1995) Mechanism of CDK activation revealed by the structure of a cyclinA-CDK2 complex, *Nature 376*, 313-320.

[51] Hubbard, S. R. (1997) Crystal structure of the activated insulin receptor tyrosine kinase in complex with peptide substrate and ATP analog, *Embo J 16*, 5572-5581.

[52] Mohammadi, M., Schlessinger, J., and Hubbard, S. R. (1996) Structure of the FGF receptor tyrosine kinase domain reveals a novel autoinhibitory mechanism, *Cell 86*, 577-587.

[53] Cobb, M. H., and Goldsmith, E. J. (1995) How MAP kinases are regulated, *J Biol Chem 270*, 14843-14846.

[54] Lee, T., Hoofnagle, A. N., Resing, K. A., and Ahn, N. G. (2005) Hydrogen exchange solvent protection by an ATP analogue reveals conformational changes in ERK2 upon activation, *J Mol Biol 353*, 600-612.

[55] Sours, K. M., Xiao, Y., and Ahn, N. G. (2014) Extracellular-regulated kinase 2 is activated by the enhancement of hinge flexibility, *J Mol Biol 426*, 1925-1935.

[56] Knighton, D. R., Zheng, J. H., Ten Eyck, L. F., Ashford, V. A., Xuong, N. H., Taylor, S. S., and Sowadski, J. M. (1991) Crystal structure of the catalytic subunit of cyclic adenosine monophosphate-dependent protein kinase, *Science 253*, 407-414.

[57] Knighton, D. R., Zheng, J. H., Ten Eyck, L. F., Xuong, N. H., Taylor, S. S., and Sowadski, J. M. (1991) Structure of a peptide inhibitor bound to the catalytic subunit of cyclic adenosine monophosphate-dependent protein kinase, *Science 253*, 414-420.

[58] Bossemeyer, D., Engh, R. A., Kinzel, V., Ponstingl, H., and Huber, R. (1993) Phosphotransferase and substrate binding mechanism of the cAMP-dependent protein kinase catalytic subunit from porcine heart as deduced from the 2.0 A structure of the complex with Mn^{2+} adenylyl imidodiphosphate and inhibitor peptide PKI(5-24), *Embo J 12*, 849-859.

[59] Dreskin, S. C., Thomas, G. W., Dale, S. N., and Heasley, L. E. (2001) Isoforms of Jun kinase are differentially expressed and activated in human monocyte/macrophage (THP-1) cells, *J Immunol 166*, 5646-5653.

[60] Gum, R., Wang, H., Lengyel, E., Juarez, J., and Boyd, D. (1997) Regulation of 92 kDa type IV collagenase expression by the jun aminoterminal kinase- and the extracellular signal-regulated kinase-dependent signaling cascades, *Oncogene 14*, 1481-1493.

[61] Han, Z., Chang, L., Yamanishi, Y., Karin, M., and Firestein, G. S. (2002) Joint damage and inflammation in c-Jun N-terminal kinase 2 knockout mice with passive murine collagen-induced arthritis, *Arthritis Rheum 46*, 818-823.

[62] Chambers, M., Kirkpatrick, G., Evans, M., Gorski, G., Foster, S., and Borghaei, R. C. (2013) IL-4 inhibition of IL-1 induced Matrix metalloproteinase-3 (MMP-3) expression in human fibroblasts involves decreased AP-1 activation via negative crosstalk involving of Jun N-terminal kinase (JNK), *Exp Cell Res 319*, 1398-1408.

[63] Troy, C. M., Rabacchi, S. A., Xu, Z., Maroney, A. C., Connors, T. J., Shelanski, M. L., and Greene, L. A. (2001) beta-Amyloid-induced neuronal apoptosis requires c-Jun N-terminal kinase activation, *J Neurochem 77*, 157-164.

[64] Bozyczko-Coyne, D., Saporito, M. S., and Hudkins, R. L. (2002) Targeting the JNK pathway for therapeutic benefit in CNS disease, *Curr Drug Targets CNS Neurol Disord 1*, 31-49.

[65] Zhu, X., Lee, H. G., Raina, A. K., Perry, G., and Smith, M. A. (2002) The role of mitogen-activated protein kinase pathways in Alzheimer's disease, *Neurosignals 11*, 270-281.

[66] Wang, D., Fu, Q., Zhou, Y., Xu, B., Shi, Q., Igwe, B., Matt, L., Hell, J. W., Wisely, E. V., Oddo, S., and Xiang, Y. K. (2013) b2 adrenergic receptor, protein kinase A (PKA) and c-Jun N-terminal kinase (JNK) signaling pathways mediate tau pathology in Alzheimer disease models, *J Biol Chem 288*, 10298-10307.

[67] Waeber, G., Delplanque, J., Bonny, C., Mooser, V., Steinmann, M., Widmann, C., Maillard, A., Miklossy, J., Dina, C., Hani, E. H., Vionnet, N., Nicod, P., Boutin, P., and Froguel, P. (2000) The gene MAPK8IP1, encoding islet-brain-1, is a candidate for type 2 diabetes, *Nat Genet 24*, 291-295.

[68] Hirosumi, J., Tuncman, G., Chang, L., Gorgun, C. Z., Uysal, K. T., Maeda, K., Karin, M., and Hotamisligil, G. S. (2002) A central role for JNK in obesity and insulin resistance, *Nature 420*, 333-336.

[69] Bogoyevitch, M. A., Ngoei, K. R., Zhao, T. T., Yeap, Y. Y., and Ng, D. C. (2010) c-Jun N-terminal kinase (JNK) signaling: recent advances and challenges, *Biochim Biophys Acta 3*, 463-475.

[70] Thévenin, A. F., Zony, C. L., Bahnson, B. J., and Colman, R. F. (2011) Activation by phosphorylation and purification of human c-Jun N-terminal kinase (JNK) isoforms in milligram amounts, *Protein Expr Purif 75*, 138–146.

[71] Owen, G. R., Achilonu, I., and Dirr, H. W. (2013) High yield purification of JNK1β1 and activation by *in vitro* reconstitution of the MEKK1 → MKK4 → JNK MAPK phosphorylation cascade, *Protein Expr Purif 87*, 87-99.

[72] Owen, G. R., Stoychev, S., Achilonu, I., and Dirr, H. W. (2013) JNK1β1 is phosphorylated during expression in *E. coli* and *in vitro* by MKK4 at three identical novel sites, *Biochem Biophys Res Commun 432*, 683-688.

[73] Shrestha, A., Hamilton, G., O'Neill, E., Knapp, S., and Elkins, J. M. (2012) Analysis of conditions affecting auto-phosphorylation of human kinases during expression in bacteria, *Protein Expr Purif 81*, 136-143.

[74] Weerapana, E., and Imperiali, B. (2006) Asparagine-linked protein glycosylation: from eukaryotic to prokaryotic systems, *Glycobiology 16*, 1.

[75] Bas, T., Gao, G. Y., Lvov, A., Chandrasekhar, K. D., Gilmore, R., and Kobertz, W. R. (2011) Post-translational N-glycosylation of type I transmembrane KCNE1 peptides: implications for membrane protein biogenesis and disease, *J Biol Chem 286*, 28150-28159.

[76] Oh, W. J., Wu, C. C., Kim, S. J., Facchinetti, V., Julien, L. A., Finlan, M., Roux, P. P., Su, B., and Jacinto, E. (2010) mTORC2 can associate with ribosomes to promote cotranslational phosphorylation and stability of nascent Akt polypeptide, *Embo J 29*, 3939-3951.

[77] Keshwani, M. M., Klammt, C., von Daake, S., Ma, Y., Kornev, A. P., Choe, S., Insel, P. A., and Taylor, S. S. (2012) Cotranslational cis-phosphorylation of the COOH-terminal tail is a key priming step in the maturation of cAMP-dependent protein kinase, *Proc Natl Acad Sci U S A 109*, E1221-1229.

[78] Owen, G. R., Stoychev, S., Achilonu, I., and Dirr, H. W. (2014) Phosphorylation- and nucleotide-binding-induced changes to the stability and hydrogen exchange patterns of JNK1β1 provide insight into its mechanisms of activation, *J Mol Biol 426*, 3569-3589.

[79] Narayana, N., Cox, S., Nguyen-huu, X., Ten Eyck, L. F., and Taylor, S. S. (1997) A binary complex of the catalytic subunit of cAMP-dependent protein kinase and adenosine further defines conformational flexibility, *Structure 5*, 921-935.

[80] Tsigelny, I., Greenberg, J. P., Cox, S., Nichols, W. L., Taylor, S. S., and Ten Eyck, L. F. (1999) 600 ps molecular dynamics reveals stable substructures and flexible hinge points in cAMP dependent protein kinase, *Biopolymers 50*, 513-524.

[81] Akamine, P., Madhusudan, Wu, J., Xuong, N. H., Ten Eyck, L. F., and Taylor, S. S. (2003) Dynamic features of cAMP-dependent protein kinase revealed by apoenzyme crystal structure, *J Mol Biol 327*, 159-171.

[82] Zheng, J., Knighton, D. R., ten Eyck, L. F., Karlsson, R., Xuong, N., Taylor, S. S., and Sowadski, J. M. (1993) Crystal structure of the catalytic subunit of cAMP-dependent protein kinase complexed with MgATP and peptide inhibitor, *Biochemistry 32*, 2154-2161.

[83] Taylor, S. S., Yang, J., Wu, J., Haste, N. M., Radzio-Andzelm, E., and Anand, G. (2004) PKA: a portrait of protein kinase dynamics, *Biochim Biophys Acta 11*, 1-2.

[84] Madhusudan, Akamine, P., Xuong, N. H., and Taylor, S. S. (2002) Crystal structure of a transition state mimic of the catalytic subunit of cAMP-dependent protein kinase, *Nat Struct Biol 9*, 273-277.

[85] Guex, N., and Peitsch, M. C. (1997) SWISS-MODEL and the Swiss-PdbViewer: an environment for comparative protein modeling, *Electrophoresis 18*, 2714-2723.

[86] Figuera-Losada, M., and LoGrasso, P. V. (2012) Enzyme kinetics and interaction studies for human JNK1β1 and substrates activating transcription factor 2 (ATF2) and c-Jun N-terminal kinase (c-Jun), *J Biol Chem 287*, 13291-13302.

[87] Kohen, A., Jonsson, T., and Klinman, J. P. (1997) Effects of protein glycosylation on catalysis: changes in hydrogen tunneling and enthalpy of activation in the glucose oxidase reaction, *Biochemistry 36*, 2603-2611.

[88] Gekko, K., Tamura, Y., Ohmae, E., Hayashi, H., Kagamiyama, H., and Ueno, H. (1996) A large compressibility change of protein induced by a single amino acid substitution, *Protein Sci 5*, 542-545.